

Experimental and numerical validation of an innovative OSD strengthening with a bonded and bolted plate

K. Slingerland



Experimental and numerical validation of an innovative OSD strengthening with a bonded and bolted plate

By

Kylian Slingerland

in partial fulfilment of the requirements for the degree of

Master of Science
in Civil Engineering

at the Delft University of Technology,
to be defended publicly on Tuesday May 9, 2022 at 14:00

Supervisor:	Prof. Dr. ir. M. Veljkovic, TU Delft
Thesis committee:	Ir. P.A. de Vries, TU Delft
	Dr. A.A. Mehrotra, TU Delft
	Ir. F. Csillag, Arup

An electronic version of this thesis is available at <http://repository.tudelft.nl/>.

Preface

This report is the final product of my time as a student at the TU Delft. Despite the sometimes difficult circumstances I have learned a tremendous amount along the way and I am happy and proud of the end result.

I would like to thank everyone in my assessment committee from the TU Delft: M. Veljkovic, P.A. de Vries and A.A. Mehrotra. Their critical remarks and guidance have helped me get this report to where it is now. I would like to provide as special thanks to Fred Schilperoort for his help and flexibility that made it possible to do the required testing and monitoring.

Secondly, I would like to thank Arup for providing me with the opportunity of doing this research and making me feel at home. I would like to say a special thanks to Maarten Rikken for helping me come up with this interesting topic, as well providing guidance with endless enthusiasm. Furthermore I would like the entire Suurhoff project team for their help and guidance where needed, as well as for their support and hospitality. A special thanks to Charlotte Murhpy for her support with the organisational side of the testing and monitoring. Lastly I would like to thank Fruszina Csillag, my supervisor at Arup, for her continual help, support and useful insights whenever I needed it.

I would also like to provide a special thanks to my parents and my girlfriend for their continual support whenever I needed it.

*Kylian Slingerland
Nieuwkoop, April 2022*

Abstract

For the renovation of the Suurhoff bridge, Arup decided to design and propose a new, innovative strengthening scheme, which improves the fatigue performance of the bridge deck and extends the design life of the bridge by at least 15 years. In this strengthening scheme, a steel plate is placed on top of the existing deck plate with a layer of epoxy in between. Preloaded injection bolts are also used to connect the strengthening plate with the deck plate. This strengthening techniques has clear advantages over the current alternatives with regard to weight, execution time, risks and flexibility in the design.

In order to better understand the behaviour of the renovated bridge deck, verify the effectiveness of the strengthening scheme and check the accuracy of the numerical models, a monitoring scheme is desirable. This is an important step in the development and optimisation of the strengthening approach, especially when the goal is to apply the scheme more often on future bridge renovation projects. To achieve this, the two research questions of this thesis are formulated as follows:

- **What is the effectiveness of strengthening an orthotropic steel deck with a bonded & bolted strengthening plate?**
- **How can the behaviour of the bridge be numerically modelled to accurately capture the improved fatigue resistance?**

This question will be answered through a combination of monitoring and finite element modelling. First, a monitoring scheme is set up with 16 strain gauges that are installed on the deck plate, troughs and cross girder. Quasi-static load tests are executed using a truck with known weight, both before and after the application of the strengthening scheme.

The load tests were successfully and accurately carried out and the results show a large reduction in the stress cycle. Stresses in the troughs are alleviated by 45-55% and stresses in the deck plate are reduced by 85-90%. This is largely in line with what was expected during the design.

Furthermore, the used FE models are validated so that more confidence can be gained in the design decisions. The full influence line is simulated, with the truck positioned at more than 120 longitudinal locations. The numerical modelling was able to accurately predict the shape and magnitude of the influence line generated by the truck loading. A difference in peak value between experimental and numerical results of no more than 25% was observed. The largest differences are observed for local bending in the deck plate of the unstrengthened bridge, but this is largely explained by the large sensitivity to the exact wheel position. For the strengthened bridge, a very good match is obtained in almost all locations. A difference between numerical and experimental results of no more than 10% is observed when not considering the area close to the bolts.

Close to the bolted connection (± 200 mm), no accurate results can be obtained with a simplified modelling approach that uses shear springs to model the bolts. However, the obtained numerical results are conservative compared to the experimental results. Some simple modelling adjustments have been applied but are unable to significantly improve the results. A detailed modelling approach has successfully been applied in which the bolt has been modelled fully in solid elements. The preload is implemented through a dynamic relaxation phase, so the bolt force is transferred through friction of the plates without any relevant increase in computation time. Therefore, this modelling technique can relatively easily be applied in a global FE model. This modelling technique is more accurate, and analyses have successfully managed to reduce the error by 50%. However, stresses close to the bolt are still overestimated even with this advanced modelling approach and more research is needed for a complete match in this area.

In conclusion, the largely matching results reinforce the decisions from the design report. More confidence is gained in the static and fatigue design life, acknowledging the potential of this new strengthening scheme for future applications.

As recommendations for future research, more testing and design work could be carried out to further optimise the design of the strengthening scheme. Furthermore, the temperature loading can be investigated through testing and monitoring in order to reduce this critical load case. Lastly, more detailed local FE modelling around the bolted connection can help understand the behaviour in this area. This can further increase the potential of the strengthening scheme when bolts are applied in close proximity of critical fatigue details.

Table of Contents

Preface	v
Abstract	vii
Table of Contents	ix
List of Figures	xi
List of Tables	xiv
1. Introduction.....	1
1.1. Problem definition.....	1
1.2. Research question and methodology.....	2
1.3. Outline.....	2
2. Literature Review.....	3
2.1. Introduction to Orthotropic Steel Decks.....	3
2.2. Fatigue in Orthotropic Steel Decks	9
2.3. Monitoring techniques.....	16
2.4. Inspection techniques.....	18
2.5. Reparation techniques.....	19
2.6. Renovation techniques	24
2.7. Preloaded injection bolts.....	26
3. Strengthening design.....	38
3.1. Background renovation technique.....	38
3.2. Strengthening elements.....	40
3.3. Preloaded injection bolts.....	41
3.4. Epoxy	42
3.5. Fatigue	44
3.6. Future design optimisation.....	49
4. Monitoring & load test description	52
4.1. Monitoring scheme	52
4.2. Load test description.....	55
5. Results load tests	58
5.1. Post-processing information	58
5.2. Cross girder.....	59
5.3. Deck plate	61
5.4. Troughs	72
5.5. Summary.....	77
6. FE modelling.....	78
6.1. Software	78
6.2. Unstrengthened model	78
6.3. Strengthened model	81
6.4. Load generation.....	82
7. Results FE modelling.....	84
7.1. Unstrengthened FE model load tests.....	84
7.2. Strengthened FE model load tests.....	89
7.3. Uncertainties	96
7.4. Fatigue implications.....	97
8. Bolt modelling.....	100
8.1. Mesh refinement.....	100
8.2. Spring stiffness.....	102
8.3. Spring with rotational restraints.....	103
8.4. Detailed modelling	105
9. Conclusions & recommendations.....	112
9.1. Conclusions.....	112
9.2. Recommendations.....	113
Bibliography.....	114
Annex A: Reduced input file with analysis details.....	119
Annex B: Python code for data analysis.....	120

List of Figures

Figure 1: Overview strengthening solutions moveable Suurhoff bridge (MC Renovatie Bruggen, 2021).	1
Figure 2: Components of an OSD system.....	3
Figure 3: Typical wearing surface for a steel bridge deck in The Netherlands (Medani, 2006)	4
Figure 4: Different types of longitudinal stiffeners (de Backer, 2015).....	5
Figure 5: Typical trapezoidal stiffener design (Lebet & Hirt, 2013)	6
Figure 6: Trough dimensions with Haibach-type cope hole (Rijkswaterstaat, 2021)	6
Figure 7: Feasible span ranges of different structural systems (Lebet & Hirt, 2013).....	7
Figure 8: Steel battle deck floor (European Steel Design Education Programme, 2021)	8
Figure 9: Crack initiation process (Schijve, 2009)	10
Figure 10: Definition of the stress range and stress cycle (Nussbaumer, Borges, & Davaine, 2011), adjusted from (Hirt, Bez, & Nussbaumer, 2006)	11
Figure 11: (a): Definition of the stress cycle in variable amplitude loading (European Convention for Constructional Steelwork, 2000), (b): Example of a stress range histogram (Schumacher & Blanc, 1999)..	11
Figure 12: Fatigue test results of structural steel members under constant amplitude loading (Nussbaumer, Borges, & Davaine, 2011), adjusted from (Hirt, Bez, & Nussbaumer, 2006).....	13
Figure 13: Fatigue design curves (European Committee for Standardization, 2005).....	13
Figure 14: Possible deck to trough fatigue cracks (European Committee for Standardization, 2011)	14
Figure 15: Trough splice fatigue detail. (a): EN1993-2/NB, (b) & (c): EN 1993-1-9 (European Committee for Standardization, 2005).....	15
Figure 16: Trough to cross girder detail, crack in trough bottom (European Committee for Standardization, 2011)	15
Figure 17: Trough to cross girder detail, crack in cross girder (European Committee for Standardization, 2011)	15
Figure 18: Goals of different monitoring programs found in literature (Webb, Vardanega, & Middleton, 2015)	16
Figure 19: Sensor types used in 31 bridge monitoring installations (Vardanega, Webb, Ricles, & Middleton, 2015), with data taken from (Webb & Middleton, 2014).....	17
Figure 20: Elements of a typical strain gauge (Michigan Scientific Corporation, 2021).....	17
Figure 21: Different inspection techniques (van Dooren, 2018).....	19
Figure 22: Repairation of deck weld crack with gouging and rewelding and UIT treatment (TNO, 2010)	20
Figure 23: Two covering plates installed during a reparation (van Dooren, 2018)	21
Figure 24: Installation of a 'kram' over the deck plate (TNO, 2010)	22
Figure 25: Different weld detail for installing a replacement part (TNO, 2010).....	23
Figure 26: Repair of a trough to cross girder connection with a 'kano'	23
Figure 27: OSD renovation using HSC with (a) an epoxy/bauxite connection (van Dooren, 2018), (b) Shear studs (Yuan, Wu, & Jiang, 2019)	25
Figure 28: Cross-section of the epoxy bonded plate solution (de Freitas, Kolstein, & Bijlaard, 2017).....	25
Figure 29: Different SPS strengthening applications. (a): Highway bridge in China (Wang, Ke, Gao, & Zhang, 2019). (b): Krefeld bridge in Germany (Matuschek, Stihl, & Bild, 2007).....	26
Figure 30: Load transfer through friction in a preloaded double lap shear connection (ESDEP).....	27
Figure 31: Method for determining slip load from test (European Research Commission, 2018).....	28
Figure 32: Influence of coating system on load-displacement behaviour (European Research Commission, 2018).	29
Figure 33: Visualisation bearing stress transfer (European Committee for Standardization, 2011)	30
Figure 34: Bearing stress distribution in long bolts (European Convention for Constructional Steelwork, 1994)	31
Figure 35: Force-displacement behaviour injection bolted connection left: (Nijgh M. , 2017), right: (Koper, 2017)	32
Figure 36: Ultimate failure tests injected bolts (Nijgh M. , 2017).....	33
Figure 37: Slip tests comparing preloaded, injected and preloaded injected connection. Test setup according to EN1090-2, $\mu = 0.33$. (Gresnigt, Beg, & Bijlaard, 2012)	34
Figure 38: Spring model double-lap preloaded bolt (TNO, 2017)	35

Figure 39: Comparison of spring model with test results (test results from (European Research Commission, 2018))	36
Figure 40: Overview strengthening solution	38
Figure 41: Overview strengthening interventions Suurhoff bridge (Rijkswaterstaat, 2021)	39
Figure 42: Strengthening plate welded splice (MC Renovatie Bruggen, 2021)	41
Figure 43: Profile of the temperature loading governing for shear force in the bolts (MC Renovatie Bruggen, 2021)	42
Figure 44: S-N curves for GreenPoxy with and without runout based on the maximum shear stress (MC Renovatie Bruggen, 2021)	44
Figure 45: Comparison of hot spot stresses in fatigue details with composite and non-composite plates	50
Figure 46: Impact of composite action on the stress distribution between troughs	50
Figure 47: Maximum shear force in original bolt configuration	51
Figure 48: Measuring equipment setup (picture taken after strengthening)	53
Figure 49: location of sensor TROU04, approximately 5 mm off-centre	53
Figure 50: Sensor locations	54
Figure 51: Unstrengthened load test	56
Figure 52: Truck weighing	56
Figure 53: Difference between the unfiltered data(left) and the filtered data(right)	58
Figure 54: Noise filter comparison	59
Figure 55: Results from the load test on the unstrengthened bridge, stresses in cross girder bottom flange	59
Figure 56: Results from the load test on the strengthened bridge, stresses in cross girder bottom flange	60
Figure 57: Results from the load test on the unstrengthened bridge, transverse bending of the deck plate at mid-bay	61
Figure 58: Results from the load test on the strengthened bridge, transverse bending of the deck plate at mid-bay	62
Figure 59: Comparison before and after strengthening, transverse bending of the deck plate at mid-bay	63
Figure 60: Comparison before and after strengthening, transverse bending of the deck plate at mid-bay	63
Figure 61: Overview results of Deck09, transverse bending of the deck plate at mid-bay	64
Figure 62: Overview results of Deck07, transverse bending of the deck plate at mid-bay	64
Figure 63: Results from the load test on the unstrengthened bridge, longitudinal bending of the deck plate at mid-bay	65
Figure 64: Results from the load test on the strengthened bridge, longitudinal bending of the deck plate at mid-bay	66
Figure 65: Comparison before and after strengthening, longitudinal bending of the deck plate at mid-bay	66
Figure 66: Overview results of Deck08, longitudinal bending of the deck plate at mid-bay	67
Figure 67: Comparison before and after strengthening, transverse bending of the deck plate at cross girder, sensor Deck01	68
Figure 68: Comparison before and after strengthening, transverse bending of the deck plate at cross girder, sensor Deck03	68
Figure 69: Overview results, transverse bending of the deck plate at cross girder	69
Figure 70: Comparison of transverse deck plate stresses at cross girder and mid bay, before strengthening, track 5	70
Figure 71: Comparison transverse stresses at cross girder and mid bay after strengthening, track 5	70
Figure 72: Comparison before and after strengthening, strain gauge Deck02, track 5	71
Figure 73: Overview results of Deck02	71
Figure 74: Results from the load test on the unstrengthened bride, trough at mid-bay	72
Figure 75: Results from the load test on the strengthened bride, trough at mid-bay	73
Figure 76: Comparison before and after strengthening, trough at mid-bay	74
Figure 77: Overview results of trough at mid-bay	74
Figure 78: Results from the load test on the unstrengthened bride, trough at cross-girder	75
Figure 79: Results from the load test on the strengthened bride, trough at cross-girder	75
Figure 80: Comparison before and after strengthened bridge, trough at cross-girder	76
Figure 81: Overview results of trough at cross-girder	76
Figure 82: Unstrengthened FE model	79
Figure 83: Close up of the detailed mesh with the elements used for the hot spot stress calculation	79
Figure 84: Belytschko-Lin-Tsay element formulation (left) and fully integrated shell formulation (right) (Haufe & Schweizerhof, 2013)	80

Figure 85: Local of boundary conditions of FE model	80
Figure 86: Overview of strengthened FE model components	81
Figure 87: Illustration of a mortar segment to segment contact (Livermore Software Technology Corporation, 2018)	82
Figure 88: Unstrengthened load test – FE comparison, stresses in cross girder bottom flange	85
Figure 89: Unstrengthened load test – FE comparison, transverse deck plate bending at cross girder	85
Figure 90: Unstrengthened load test – FE comparison, longitudinal deck plate bending at cross girder	86
Figure 91: Unstrengthened load test – FE comparison, transverse deck plate bending at mid bay	87
Figure 92: Unstrengthened load test – FE comparison, longitudinal deck plate bending at mid bay	88
Figure 93: Unstrengthened load test – FE comparison, stresses in the trough bottom at mid bay	88
Figure 94: Unstrengthened load test – FE comparison, stresses in the trough bottom at cross girder	89
Figure 95: Strengthened load test – FE comparison, stresses in cross girder bottom flange	90
Figure 96: Strengthened load test – FE comparison, transverse deck plate bending at cross girder (Deck03)	91
Figure 97: Strengthened load test – FE comparison, transverse deck plate bending at cross girder (Deck04)	91
Figure 98: Strengthened load test – FE comparison, transverse deck plate bending at cross girder (Deck05)	92
Figure 99: Strengthened load test – FE comparison, longitudinal deck plate bending at cross girder	93
Figure 100: Strengthened load test – FE comparison, transverse deck plate bending at mid bay	93
Figure 101: Strengthened load test – FE comparison, longitudinal deck plate bending at mid bay	94
Figure 102: Strengthened load test – FE comparison, stresses in the trough bottom at mid bay	95
Figure 103: Strengthened load test – FE comparison, stresses in the trough bottom at cross girder	95
Figure 104: Transverse influence line for deck plate bending close to the cross girder	96
Figure 105: Influence of tyre length on the observed deck plate stress	97
Figure 106: Stress reduction factor in fatigue detail 1a	98
Figure 107: Stress reduction factor in fatigue detail 1b	98
Figure 108: Stress reduction factor in fatigue detail 2	99
Figure 109: Stress reduction factor in fatigue detail 3	99
Figure 110: Top view of the refined FE model	100
Figure 111: Isometric view of the detailed area showing all refined components.	101
Figure 112: Tensile transverse stress distribution in the deck plate, before refinement (a) and after refinement (b) (stresses in MPa)	101
Figure 113: Refined model results with bolts included (a) and bolt excluded (b) (stresses in MPa)	102
Figure 114: Comparison between normal bolt stiffness (a) and high bolt stiffness (x1000) (b) (stresses in MPa)	103
Figure 115: Comparison of the impact of rotational restraint around bolt area. Comparison between no restraints (a) with a restrained area of 2x2 (b), 4x4 (c) and 6x6 (d) elements. (stresses in MPa)	104
Figure 116: Meshed bolt hole	105
Figure 117: Fully solid mesh of the bolt	106
Figure 118: Solid part of the deck plate	106
Figure 119: Transverse stresses after preloading (a) and during loading (b), fully solid bolt (stresses in MPa)	107
Figure 120: Comparison of deck plate results close to the bolted connection	108
Figure 121: Packer plate seen from the bottom of the deck plate	109
Figure 122: Transverse stresses after preloading (a) and during loading (b), added packer plate (stresses in MPa)	109
Figure 123: Geometry of the fully solid deck plate in the detailed region	110
Figure 124: Comparison of Z-stress distribution between model with small solid region (a) and more extensive solid region (b)	110
Figure 125: Transverse stresses after preloading (a) and during loading (b), solid deck plate (stresses in MPa)	111

List of Tables

Table 1: Some commonly applied surface treatments and corresponding friction class (European Committee for Standardization, 2018).....	28
Table 2: Excerpt risk register	40
Table 3: GreenPoxy temperature dependent stiffness	43
Table 4: Detail classifications in the existing deck structure (MC Renovatie Bruggen, 2021)	44
Table 5: Predicted fatigue damage in deck details 1a and 1b	47
Table 6: Predicted fatigue damage in deck details 2 and 3a	47
Table 7: Fatigue details in added strengthening steel and bolts (MC Renovatie Bruggen, 2021)	48
Table 8: Peak stress values from relevant trucks	49
Table 9: Predicted damage of strengthening steel plate details	49
Table 10: Truck weight measurements	56
Table 11: Summary of observed stress reduction in strain gauge locations	77
Table 12: Material properties used in the unstrengthened FE model.....	80
Table 13: FE model constraints	80
Table 14: Description different components of the strengthened FE model.....	81
Table 15: Material properties used in strengthened finite element model.....	82
Table 16: Description different components of the strengthened FE model (similar to Table 14)	101
Table 17: Comparison of transverse stresses in strain gauge location Deck03.....	104
Table 18: Overview of different modelling results.....	111

1. Introduction

1.1. Problem definition

A lot of bridges that were built after the Second World War are currently approaching the end of their lifespan. Furthermore, the amount of heavy traffic and their corresponding axle loads has increased more than was expected and designed for. Because of this, many other bridges are not able to reach their intended lifespan. Especially bridges with a steel deck are heavily affected, as these increased cyclic loads have caused unforeseen fatigue problems (Rijkswaterstaat, 2007).

Replacing bridges is a very difficult and expensive operation, often causing long disruptions to the traffic network. Moreover, replacing bridges is not always the most sustainable option, since only certain parts of the old bridge may not fulfil the requirements anymore. A possibly more sustainable alternative, in which a lot of the material can be reused, may be to renovate the bridge. Recent projects, such as the renovation of the 2nd Van Brienoord bridge, have shown that it is even possible to extend the lifespan by 100 years in this way (Arup, 2021).

Because of Rijkswaterstaat's large portfolio of bridges that need strengthening before 2030 and the limited resources available, some bridge interventions are designed to extend the lifespan by only 15 or 30 years. This intervention is seen as a temporary solution, which is deemed necessary because there are simply not enough resources to tackle the entire portfolio simultaneously (Rijkswaterstaat, 2021).

The movable part of the existing Suurhoff bridge, one of the bridges in Rijkswaterstaat's portfolio, has developed fatigue damage in the orthotropic deck structure. However, the renovation methods that Rijkswaterstaat has experience with are undesirable for this application, due to weight and size limitations. Therefore, Arup decided to design and propose a new, innovative strengthening scheme, which improves the fatigue performance of the bridge deck and extends the design life of the bridge by at least 15 years. In this strengthening scheme, a steel strengthening plate is placed on top of the existing deck plate with a layer of epoxy in between. Preloaded injection bolts are also used to connect the strengthening plate with the deck plate. This is a lightweight solution that can be swiftly executed, which makes it an attractive alternative to the current strengthening schemes used by Rijkswaterstaat. Furthermore, using bolts alongside the epoxy layer reduces execution and durability risks. For this pilot application, risks are further reduced as composite interaction is not necessary to guarantee the extended design life of the renovated bridge. An impression of the strengthening approach can be seen in Figure 1.

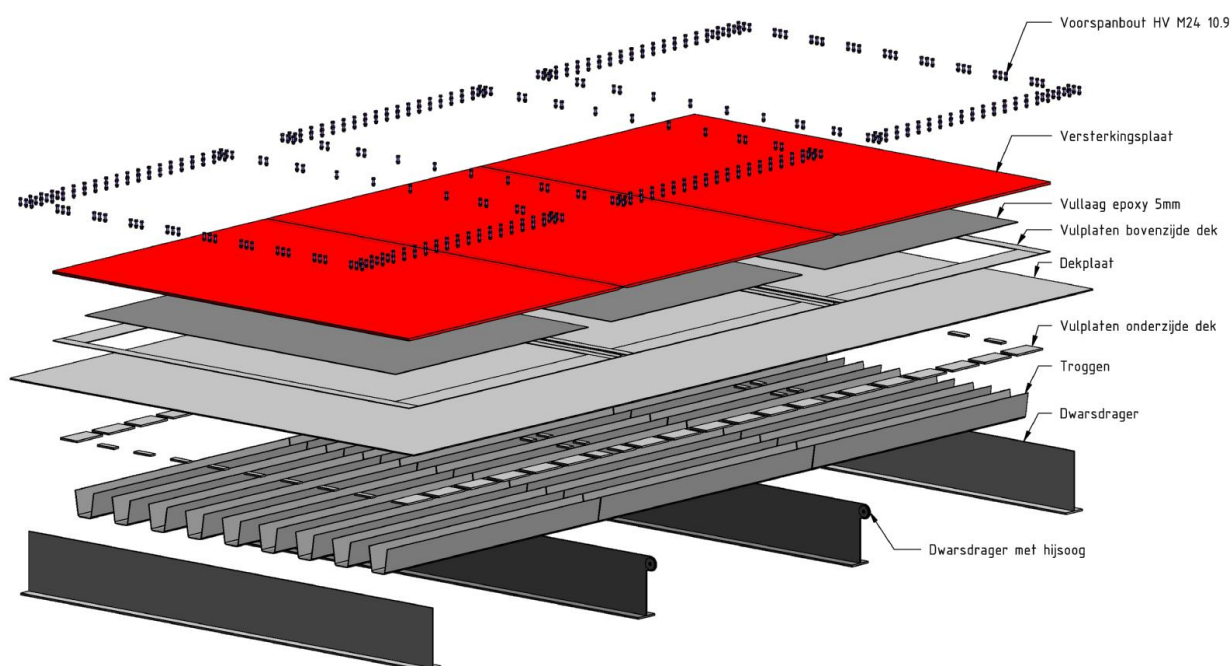


Figure 1: Overview strengthening solutions moveable Suurhoff bridge (MC Renovatie Bruggen, 2021).

1.2. Research question and methodology

In order to better understand the behaviour of the renovated bridge deck, verify the effectiveness of the strengthening scheme and check the accuracy of the numerical models, a monitoring scheme is desirable. This is an important step in the development and optimisation of the strengthening approach, especially when the goal is to apply the scheme more often on future bridge renovation projects.

To this end, the research questions of this thesis are formulated as follows:

- **What is the effectiveness of strengthening an orthotropic steel deck with a bonded & bolted strengthening plate?**
- **How can the behaviour of the bridge be numerically modelled to accurately capture the improved fatigue resistance?**

This question will be answered through a combination of monitoring and finite element modelling. The monitoring scheme consists of 16 strain gauges that are installed on the deck, troughs, and cross-girder of the bridge deck. A load test is carried out both before and after the strengthening, in which a truck with known weight will drive over specified locations of the bridge. This will provide valuable data on the reduction of the stress cycles experienced by various elements in the structure.

An FE model of the unstrengthened and the strengthened movable bridge has been provided by Arup as a starting point for this thesis. The results from the load tests will first be used to assess the accuracy of the numerical models and validity of modelling choices. Furthermore, sensitivity studies are carried out to understand the impact of important variables and modelling choices. Lastly, a detailed FE model is made of the bolted connection in order to further improve the current models.

1.3. Outline

This thesis is structured as follows. Chapter 2 first provides a literary review of relevant topics concerning bridge renovation and fatigue. Chapter 3 then provides an overview of the innovative strengthening approach, including relevant literary background information on relevant topics such as preloaded injection bolts and epoxy material properties. After this, chapter 4 will describe and justify the methods used in this research. Chapter 5 will then present and discuss the results from the load tests, comparing the results from before and after the strengthening. Consequently, chapter 6 will discuss the FE models, load setup and the analyses that are carried out in this thesis. Chapter 7 will then discuss the results from the analyses. This is also where the comparison between the FE models and the load tests is made and sensitivity studies are carried out. In chapter 8, the behaviour bolted connection is discussed and modelled in more detail. Finally, chapter 9 will present the conclusions and recommendations of the thesis.

2. Literature Review

This section will present an overview of background literature and state of the art research. First, sections 2.1 and 2.2 will present an introduction to orthotropic steel decks and an overview of fatigue in orthotropic steel decks. Section 2.3 will then present an overview of monitoring techniques and equipment, after which section 2.4 will give an overview of the inspection techniques that can be used for spotting the extent of damage in an OSD. Consequently, section 2.5 will present an overview of current repair techniques. Section 2.6 will present the renovation techniques that are currently being applied on OSD's. Lastly, section 2.7 presents a state-of-the-art overview of preloaded injection bolts, which will play an important role understanding the behaviour of the strengthening scheme and the corresponding FE models.

2.1. Introduction to Orthotropic Steel Decks

This section aims to give a general introduction to the orthotropic steel deck, hereafter referred to as the OSD. Unless explicitly stated, information and specific guidelines and design practises focus on the situation in The Netherlands. First, in section 2.1.1, the OSD system is described and explained, after which section 2.1.2 will explain the force transfer through the OSD. In section 2.1.3, the historical development of the OSD will shortly be presented, after which section 2.1.4 will shortly discuss the advantages and disadvantages of the system.

2.1.1. Overview

An orthotropic steel deck system consists of a steel deck plate which is stiffened in both directions. It is the different stiffness in longitudinal and transverse directions that gives the system orthogonally anisotropic, also called orthotropic, properties. This makes it an efficient and lightweight solution, but it is not without drawbacks either. Within the system, the following components can be distinguished, also visualised in Figure 2:

1. Wearing surface
2. Deck plate
3. Longitudinal stiffeners (troughs)
4. Cross girder
5. Main girder

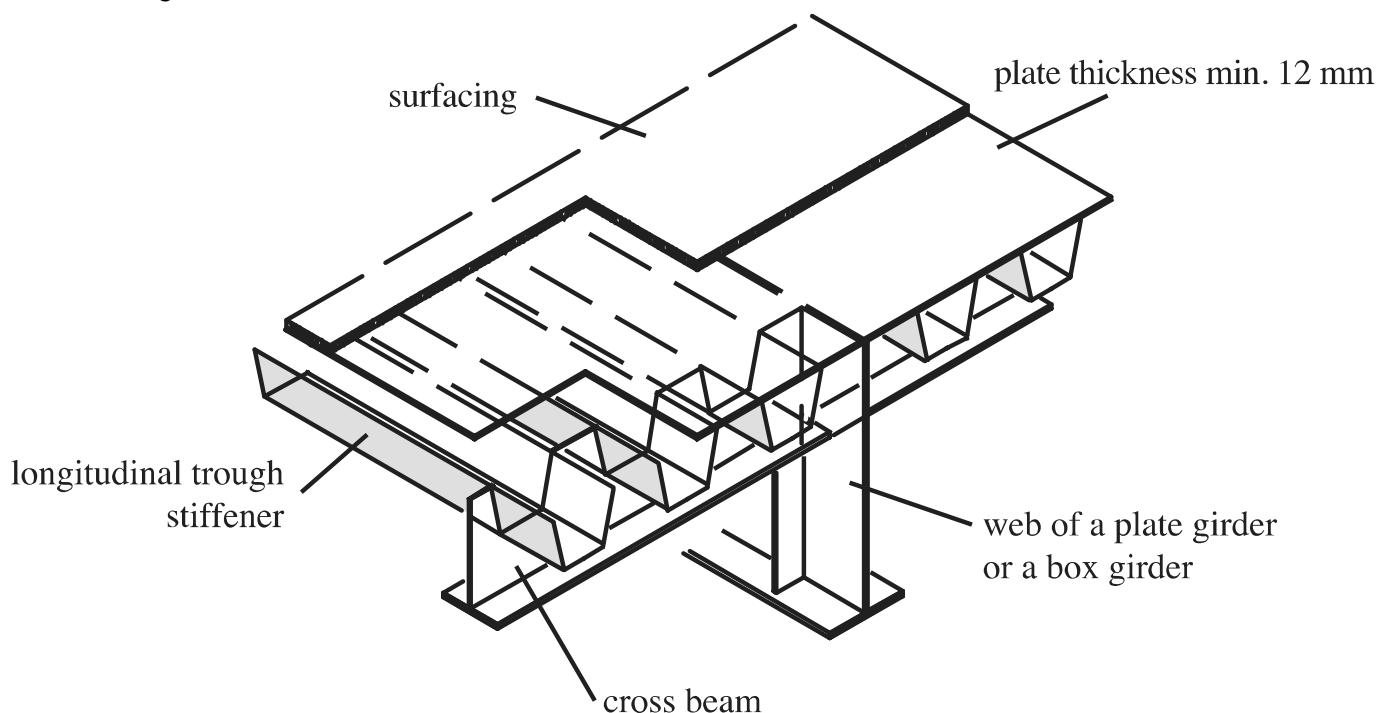


Figure 2: Components of an OSD system

Wearing surface

The wearing surface is the top-most layer of the deck system over which the traffic drives. Its main function is to provide a smooth, flat, running surface with an appropriate skid resistance which allows the traffic to pass over in a safe and preferably quiet way (Gurney, 1992). Furthermore, the surface needs to have minimal wear and also provide a waterproofing layer to protect the steel deck plate.

There are different solutions for the wearing surface for steel bridge decks, depending on the application. The two most relevant solutions, for fixed and for movable bridges, will shortly be discussed below.

Fixed bridges

For fixed bridges, the wearing surface usually consists of several layers with different materials. Firstly, there is a bonding layer that ensures there is a good bond between the deck plate and the rest of the wearing surface, usually in the form of an epoxy product (Medani, 2006). Second, there is an isolation layer which protects the steel from corrosion by preventing the ingress of water and salts. It also has to be fatigue resistant and bond to the asphalt above. In the Netherlands, this is usually done through an epoxy layer with grit or bauxite spread over the top.

Above this is a two layered asphalt construction. In the Netherlands, the bottom layer is usually executed with mastic asphalt ('gietasfalt'). Mastic asphalt has a very low void content which makes it almost impermeable, but it does require a layer of fine aggregates on its surface to increase the skid resistance. Historically, the top asphalt layer was also executed in mastic asphalt, completing the typical cross-section as shown in Figure 3 (Medani, 2006). However, due to the increased traffic intensity over the past decades the Dutch government prefers the use of Porous Asphalt (ZOAB) on bridge decks. PA has a very high void ratio, which reduces noise, standing water and rutting of the asphalt. In order to improve the structural behaviour and lifespan of the PA layer, a membrane with proper bonding should be applied between the different asphalt layers (Huurman, Voskuilen, van Dijk, & Molenaar, 2008).

Alternative solutions include Epoxy Asphalt (EA), which is relatively new in The Netherlands but has been reported to have a much larger fatigue resistance and service life, as well as better thermal properties. Applications include the San Francisco–Oakland Bay Bridge, where the wearing surface has been in service for almost 50 years and is still reported to be in good shape (Lu & Bors, 2015; Apostolidis, Liu, Erkens, & Scarpas, 2020)

The thickness of the asphalt package has to be at least 60mm according to the Dutch national annex of EN1993-2 (European Committee for Standardization, 2011). An advantage of this relatively thick package is that it contributes to the stiffness of the deck and therefore reduces the (local) bending deformations in the deck plate. This helps spread the local wheel loading over a larger surface, thereby reducing the stresses in some relevant fatigue details that will be discussed later (Cui, Zhang, Hao, Li, & Bu, 2018).

Even though considerable research is being done on incorporating the effect of the wearing surface (e.g. (Pouget, Sauzéat, Benedetto, & Olard, 2012)), the Dutch national annex to EN1993-2 only allows for the load spreading effect to be considered and it does not allow any interaction to be taken into account in any verification (European Committee for Standardization, 2011). The main issues with describing the behaviour properly are the not fully bonded behaviour of the surface structure, the non-linear stress distribution along the depth, and the large temperature dependence of the asphalt (Li, Liu, Scarpas, & Tzimiris, 2013).

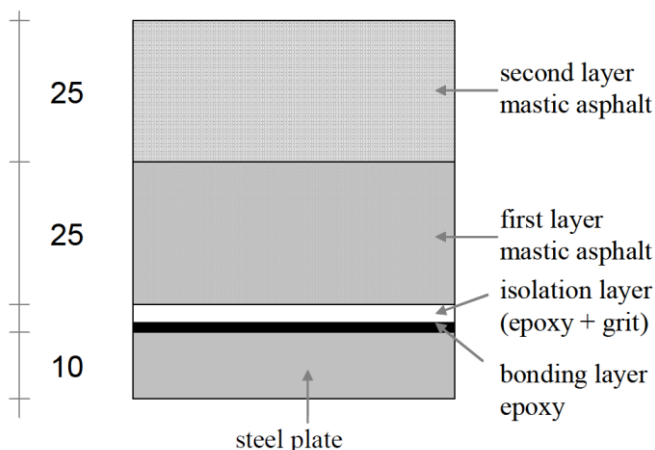


Figure 3: Typical wearing surface for a steel bridge deck in The Netherlands (Medani, 2006)

Movable bridges

For movable bridges, keeping the weight of the construction as low as possible is so important that the approach used for fixed bridges is not feasible. Instead, the wearing surface consists solely of an epoxy layer with an anti-skid finish. A thickness of 8mm is required according to the Dutch national annex to NEN-EN1993-2 (European Committee for Standardization, 2011). This is a considerably thinner solution than for fixed bridges which makes it a lot lighter, but it does not spread the load as much as the asphalt does, causing larger stresses in the deck plate due to local wheel loading.

Deck plate

Beneath the wearing surface is the deck plate. The current Dutch annex prescribes a minimal thickness between 14 and 22mm, depending on the type of bridge and the function of the bridge. For example, the ROK 2.0 prescribes a minimum deck plate thickness of 14 mm for fixed bridges on road with little heavy traffic, 18 mm for fixed bridges on major highways, and 22 mm for moveable bridges on major highways (Rijkswaterstaat, 2021). Due to the lack of asphalt and therefore load spreading on moveable bridges, these generally require thicker deck plates than fixed bridges.

Besides providing the surface for the traffic to drive over, the deck also contributes to the load bearing structure. It can transfer loads in both directions and it usually acts as the top flange for the rest of the load bearing structure (de Backer, 2015).

Longitudinal stiffeners (troughs)

The longitudinal stiffeners, also called troughs, add strength and stiffness to the deck plate. Roughly two different types of stiffeners can be distinguished: Open and closed stiffeners. Initially, open stiffeners were more popular because of the simpler analysis and welding involved. However, they have nearly no torsional rigidity and therefore limited force distribution along the transverse direction of the deck (de Backer, 2015). Nowadays, closed trapezoidal stiffeners are seen as the most efficient solution and these are most widely used.

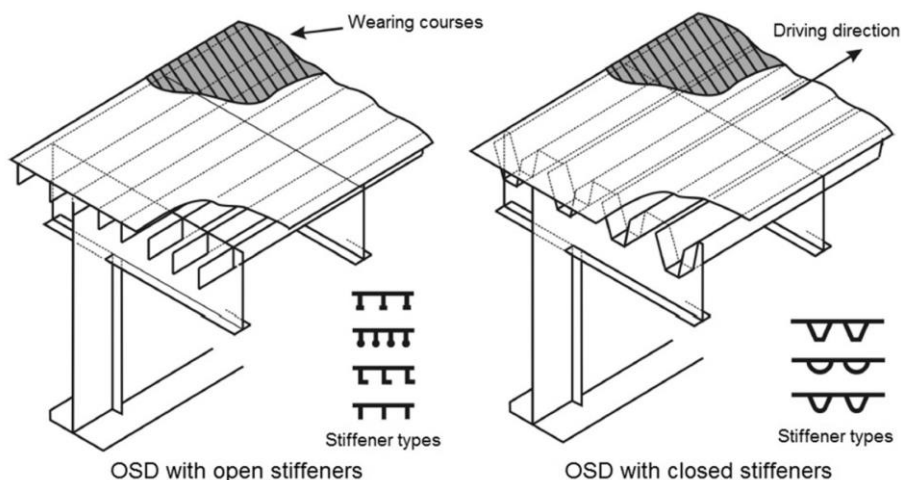


Figure 4: Different types of longitudinal stiffeners (de Backer, 2015)

A typical trapezoidal stiffener design is shown in Figure 5. The thickness of the stiffener is typically 6 or 8mm, and the spacings between the legs at the deck 300mm. The height of the trough is usually also around 300mm, and the width of the bottom side is 100 to 150 mm. The trough legs are welded to the deck plate as shown in Figure 5. It has to be noted that a lot of these values are based on historical practises and are not necessarily an optimized design. Parametric optimisation has indicated that troughs with a smaller spacing at the top may perform better in fatigue and result in a lighter solution than most current designs (van der Laan, 2021). These will however require more welding, and the smaller spacing decreases workability and ease of inspection.

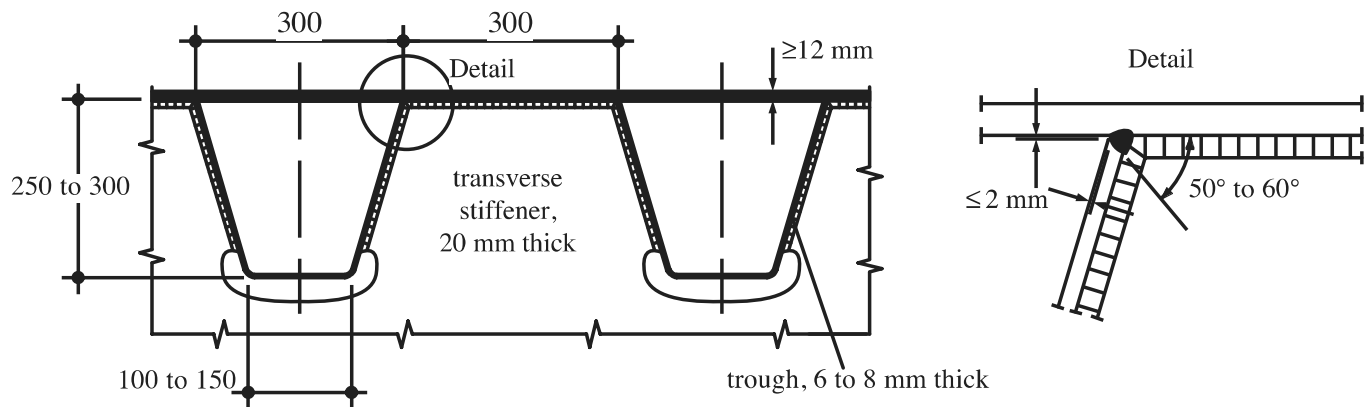


Figure 5: Typical trapezoidal stiffener design (Lebet & Hirt, 2013)

Cross girder

The deck and the troughs are supported by the cross girders, which are transverse stiffeners that support the deck along the width of the deck. These are present over the length of the bridge with a spacing of around 3-4m. They are usually built-up I sections, with the deck plate acting as the top flange. At the connection of the trough to the cross-girder (transverse stiffener), the troughs can be either continuous (with the cross-girder welded to the troughs) or discontinuous (with both sides of the trough welded to the cross-girder). This will result in different fatigue details. The choice to make the troughs continuous and weld the cross girder to the troughs is most commonly found on OSDs in The Netherlands.

In combination with continuous troughs, the ROK 2.0 allows for Haibach-type “cope holes” around the bottom side of the trough (Rijkswaterstaat, 2021). These are essentially cut-outs in the cross-girder around the bottom side of the troughs, as is shown in Figure 6 (Haibach & Plasil, 1983). This cut-out is to prevent fatigue problems in connection of the bottom side of the trough to the cross-girder, since this area usually experiences large stress concentrations.

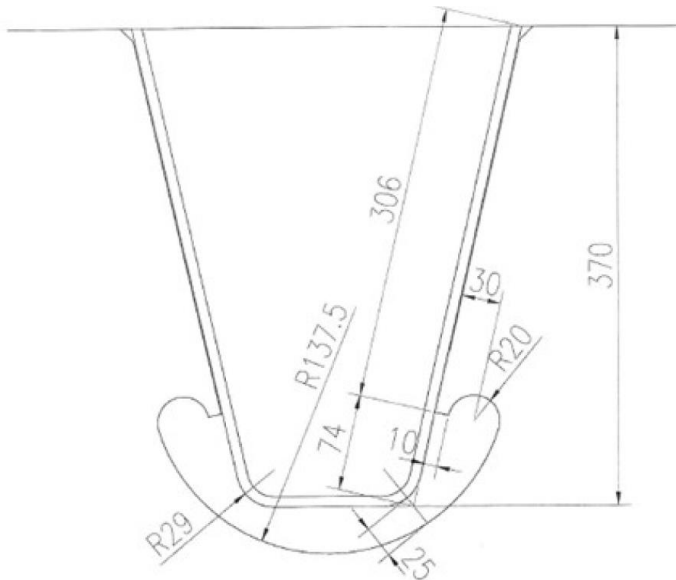


Figure 6: Trough dimensions with Haibach-type cope hole (Rijkswaterstaat, 2021)

Main girder

The final part of the load-bearing structure is responsible for transferring the loads to the foundation. Depending on the terrain, span, and location of the bridge, this can be done through a multitude of solutions. In the Netherlands, it is usually done through so-called main girders. These are large built-up sections that support the bridge deck at two or more locations along the length of the bridge. For relatively short spans, these can be I-shaped sections, whereas for longer spans box sections are preferred due to their torsional stability. These options are shown in

Alternatively, for very long spans, a box cell system can be used, which is essentially a very large box girder with the deck as the top flange. In this case, no clear main girder can be identified.

Furthermore, for longer span bridges, the main girders can be supported by a secondary load transfer system such as a truss, or by cables through an arch, cable stayed or suspension bridge. Depending on the

span of the bridge, a rough overview of the most optimal solution can be seen in Figure 7. These solutions will offer intermediate support locations for the bridge deck throughout the span, reducing the stresses and deformations of the structure.

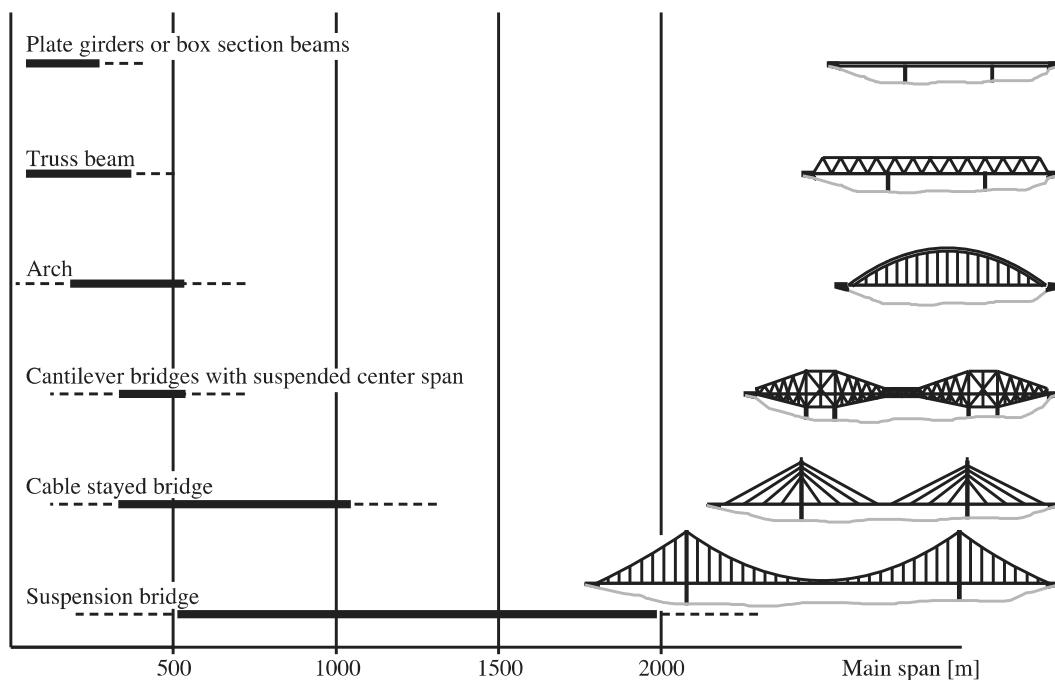


Figure 7: Feasible span ranges of different structural systems (Lebet & Hirt, 2013)

2.1.2. Force transfer

Understanding the force transfer mechanism is important for understanding the behaviour of the system and is closely related to the stiffness of the structural components. This section will shortly describe the force transfer through the OSD system when subjected to traffic loads.

When a wheel load travels over the bridge in longitudinal direction, it will exert a pressure on the wearing surface. This will be spread over a certain angle (usually 45 degrees is assumed) to the deck plate. The force is then transferred in transverse direction to the adjacent troughs through local bending of the deck plate. Through longitudinal bending of the troughs and part of the deck plate in longitudinal direction, the force is then transferred in longitudinal directions to the adjacent cross-girders. The cross girder, combined with part of the deck plate acting as the top flange, then transfers this load in transverse direction to the main girder. Finally, the main girders, again with the deck plate acting as a top flange, transfers the load in longitudinal direction to the support (piers, intermediate supports, cables, etc.).

2.1.3. Historical development

The development of steel bridge decks started in the 1930s, with the so-called 'battle deck floors' (de Backer, 2015). This was a layered steel construction as shown in Figure 8. The system is fairly similar to current OSD decks, with the main difference being that the steel deck plate was not yet part of the structural system and only acted as a load spreader to the rest of the structure. Therefore, the cross and main girders had their own top flanges, and I-type stiffeners were used to support the deck longitudinally. One of the first applications of this system was the Salt River Bridge in Michigan in 1932. From 1934 onwards, this system was also applied on many bridges in the Autobahn network in Germany (de Backer, 2015).

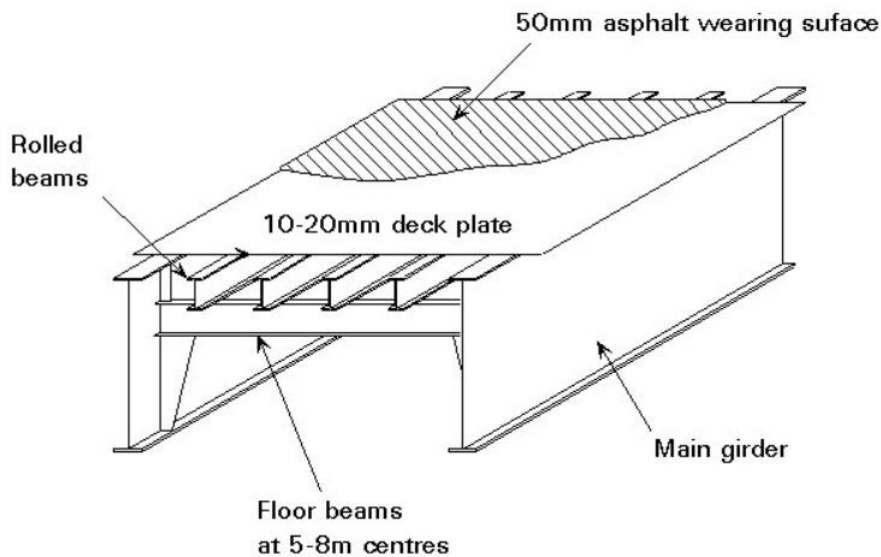


Figure 8: Steel battle deck floor (European Steel Design Education Programme, 2021)

Innovation and development of the OSD system peaked during the reconstruction after the second world war due to the massive amount of infrastructure projects in this period. In Germany, thousands of bridges were destroyed or damaged and needed reparation or replacement (Partov, Pasternak, Petkov, Nikolov, & Dimitrova, 2018). The scarcity of building materials in this period caused a search for the most efficient structural systems and the first application of the closed stiffener followed in Germany in 1954 (de Backer, 2015). Furthermore, the fatigue problems were not yet understood and the large increase in traffic loading was not anticipated, meaning that steel decks with very thin deck plates were built during this period. In The Netherlands, the first application of the OSD was a plate girder bridge over the Rhine near Rhenen in 1957. The construction was optimised to reach a self-weight of 375 kg/m^2 for the deck construction (475 kg/m^2 with the asphalt layer) (Romeijn, 2006). After this first application in The Netherlands, other bridges followed quickly. Many of the current large steel bridges (now nearing the end of their lifespan with fatigue problems) were built between the 1950s and 1980s (van Dooren, et al., 2010).

2.1.4. Advantages and Disadvantages

This section aims to give a brief summary of the advantages and disadvantages of the OSD deck system, which will help build an understanding of when an OSD deck is a suitable and feasible design choice.

First of all, it is clear that in an OSD system, the deck is more than just the driving surface. It contributes as the top flange for the troughs, cross girders and main girders, which results in a very lightweight and material efficient solution. This is a large advantage when the span of the bridge increases, i.e., when the self-weight of the bridge becomes a larger and larger part of the overall forces that the structure has to resist. Movable bridges is the other category where a lightweight structure is very desirable, and thus, where the OSD system is often applied.

Besides this main point, another advantage of the OSD is its quick erection speed. Due to the high level of prefabrication, the construction and transportation is relatively easy compared to a concrete alternative. Furthermore, an OSD solution can result in a very slender solution which can be desirable for aesthetic purposes but also results in a larger clearance. Steel also has a lot of deformation capacity and no creep and shrinkage problems. A high-quality guarantee can be obtained, resulting in a lot of confidence in the material and the structure.

Of course, the OSD system is not without its drawbacks either. The main drawback of the system, which has caused many problems over the years, is the fatigue problems that can occur. This is such an elaborate topic that this will be fully discussed in section 2.2. Besides this, the fabrication costs of an OSD deck can be significantly higher than a concrete alternative, which is one of the main reasons why it is not the most common deck type for shorter spans. Furthermore, the steel needs to be protected against corrosion with a paint layer, which will require occasional maintenance.

2.2. Fatigue in Orthotropic Steel Decks

This section will tackle the fatigue phenomenon in steel bridges. First, section 2.2.1 will lay out the historical development knowledge regarding fatigue. Section 2.2.2 will then present general information about the fatigue phenomena. Section 2.2.3 covers the fatigue loading on bridges, after which section 2.2.4 will tackle the fatigue assessment

2.2.1. Historical development of knowledge

The fatigue phenomenon became known during the industrial revolution when metallic structures such as steam engines, locomotives, wheel axles and pumps occasionally seemed to fail without giving any warning. The cause of the phenomenon was unclear and mysterious at the time, and fatigue has therefore been the cause of many lethal accidents in the aerospace, railway, and civil engineering industries (Schijve, 2003).

In the 19th century, the German engineer August Wöhler conducted a lot of research on fatigue and concluded that structures were breaking down when subjected to repeated loads that do not cause failure on a single load cycle. He also concluded that notched specimen required special attention, he argued for the design for fatigue life and he even commented on the crack propagation he observed in (cast) steel (Schütz, 1996). He presented his test results as tables, which were converted into log-log S-N curves in 1910 by Basquin that are still being used today.

In the period between 1920-1945, a lot of progress was booked on the topic of fatigue, mainly by the Germans. In particular, the importance of variable amplitude loading, further investigation of the effect of notches, the linear damage accumulation hypotheses currently known as the Palmgren-Miner rule (Palmgren, 1924) (Miner, 1945), and the development of fracture mechanics (Schütz, 1996).

During the design process of the first steel bridges, people were thus aware of the existence of the fatigue phenomenon. However, it was either left as a subject for further study or it was concluded that the verification of the static strength was sufficient to prove a sufficient fatigue capacity (Pelikan & Eßlinger, 1957).

2.2.2. Explanation of the fatigue phenomenon

Understanding the fatigue phenomenon is important in order to understand which conditions and aspects affect the fatigue life of a structure. In order to properly predict and discuss the process of fatigue, distinction is made between the crack initiation period and the crack growth period (Schijve, 2009). These two phases both have their own influencing parameters and characteristics and will be discussed separately.

Crack initiation

The initiation of a fatigue crack is due to the cyclic slip that happens at stress amplitudes well below the yield stress. As is shown in Figure 9, the microplasticity likely occurs in grains at a free surface since this has a lower slip constraint than grains constrained on all sides. This slip tends to occur at positions in the material with an inhomogeneous stress distribution, for example near notches, geometric discontinuities, or corrosion pits, since here the stress cycle experienced by the grains is largest. It is important to note that in any case, the crack initiation is a material surface phenomenon (Schijve, 2009).

When a slip plane occurs due to the cyclic loading, two phenomena occur that result in fatigue not being a reversible process. Firstly, an oxide layer is formed on the newly formed surface in the slip plane, which is not easily removed. Secondly, some strain hardening occurs in the slip band during the load cycle. This means that during unloading, a larger shear stress will act on the slip band and the reversed slip will occur on adjacent slip planes, which is shown in Figure 9 (b).

In many cases, the crack initiation period is much slower than the crack growth and a large portion of the fatigue life is thus spent in the crack initiation period.

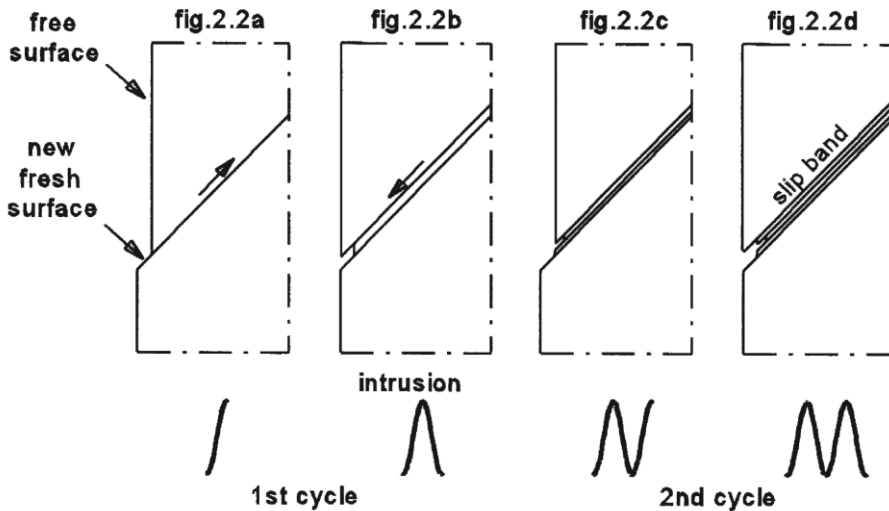


Figure 9: Crack initiation process (Schijve, 2009)

Crack growth

Once a crack is present in the material, there will be an inhomogeneous stress distribution on a microlevel around the crack, with a stress concentration around the tip of the microcrack. Once the crack is growing into adjacent grains, additional constraints on the slip displacement will make it more difficult for the crack to grow in just one slip plane and the crack is likely to grow perpendicular to the main principal stress.

The transition from the crack initiation to the crack growth phase can be defined as the point when the crack growth is no longer dependent on the surface conditions but rather on the material properties. At this point, fatigue is no longer a surface phenomenon and instead the crack growth is depending on the material as a bulk property (Schijve, 2009). Furthermore, as the crack grows in size, the stress concentration around the crack tip will also increase, making the crack growth a process that accelerates in speed due to this feedback mechanism.

During the crack growth phase, the effective cross-section that is left to withstand external loading continuously decreases. The final failure of the material is defined as the point when the final cross-section becomes too small to resist the loading. A fatigue failure can be clearly seen due to the so-called beach marks it leaves on the fractured cross-section, which show the crack growth through the load cycles.

Another important thing to note is that for several reasons, not all microcracks transition into the crack growth phase but stop growing after reaching a certain length (a few grain diameters). This occurs for example in notched specimen, where the initially high stress concentration at the surface causes the initiation of the crack, but where the stress cycle is too small to maintain a crack growth. In unnotched specimen, this can also occur when grain boundaries form a barrier to the microcrack and halt its growth. All these non-growing cracks occur beneath the so-called fatigue-limit. The fatigue limit is thus defined as the threshold for the growth of small cracks and not as the threshold for crack initiation (Schijve, 2009).

For steel members that are properly protected against environmental influences, the fatigue life (which is largely based on the crack initiation period) is determined by two factors: The fatigue strength and the fatigue loading. These aspects will now separately be discussed.

2.2.3. Fatigue loading on bridges

For the majority of bridges the main source of fatigue loading is the traffic. Depending on the chosen level of complexity, defining the fatigue loading on a bridge is an extensive and complicated process. This chapter aims to give a short overview of the process of defining fatigue loading on bridges according to the appropriate guidelines in The Netherlands. Furthermore, relevant terms and methods are shortly presented and discussed.

The stress cycle

Given a certain (welded) detail, fatigue tests have shown that main factor that influences the fatigue live is the stress range that the detail is subject to. The stress range can be defined as the difference between the maximum and minimum stress in a stress cycle (Nussbaumer, Borges, & Davaine, 2011). This can be seen in Figure 10.

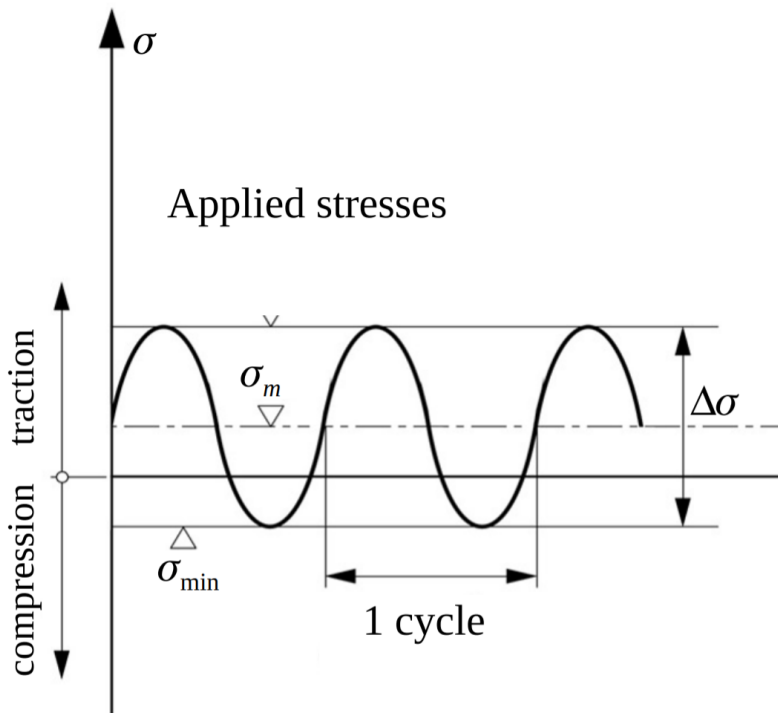


Figure 10: Definition of the stress range and stress cycle (Nussbaumer, Borges, & Davaine, 2011), adjusted from (Hirt, Bez, & Nussbaumer, 2006)

It is known other factors such as the average stress value, the ratio between the maximum and minimum stress and the cycle frequency also influence the fatigue life, but this is usually neglected in the design of welded details. This is mainly because of the residuals stresses that are introduced in the material because of the welding process. These tensile residual stresses remove any potentially positive effect from a (partially) compressive stress cycle or from the value of the average stress (Nussbaumer, Borges, & Davaine, 2011).

Variable amplitude loading and cycle counting

In reality, during the service life of a bridge, the stress cycle will not be as distinctly visible as in theory. Different truck locations, axle weights, layouts and combinations will all interact and result in a variable amplitude loading that will look more like Figure 11.

This data will need to be processed in order to obtain the proper stress cycles. There are multiple ways to do this, the most well-known being the rain-flow and the reservoir method. These methods both analyse the stress history in such a way that a stress range histogram can be obtained from them. If used properly, both methods will provide the same results.

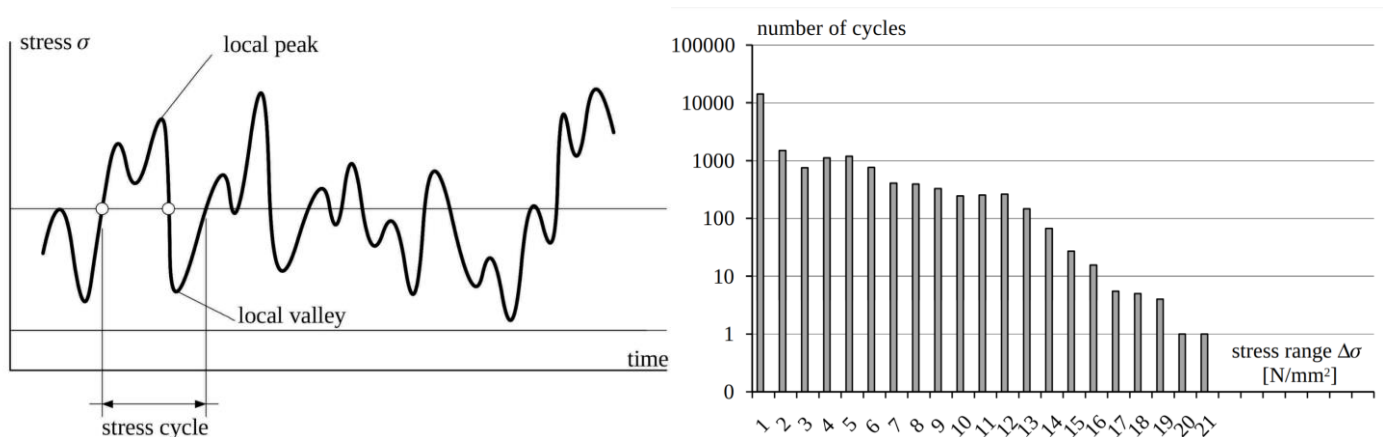


Figure 11: (a): Definition of the stress cycle in variable amplitude loading (European Convention for Constructional Steelwork, 2000), (b): Example of a stress range histogram (Schumacher & Blanc, 1999)

Fatigue loading according to the norms and guidelines

Calculation of fatigue loading for bridges in the Netherlands is done according to the Eurocode NEN-EN1991-2, supplemented with the national annex NEN-EN1991-2/NB. Different fatigue load models exist based on the application and desired accuracy. Furthermore, most large bridges in the Netherlands are owned by Rijkswaterstaat, which means the ROK (Richtlijnen Ontwerp Kunstwerken) also needs to be adhered to. In these norms, rules and guidelines are laid out that specify the distribution of different truck and axle types, as well as future traffic densities.

2.2.4. Fatigue assessment

Determining the fatigue strength of a new connection is a laborious and expensive task. Luckily, the fatigue strength for most connections has already determined and prescribed in relevant codes and does not need to be redone for every project. This section will focus on fatigue due to direct (normal) stresses as these are most common and relevant for the current subject.

The fatigue strength assessment of a connection is done by a comparison of stresses with their critical values (which are defined in the relevant codes) which cause a defined damage. This can be done through a number of different approaches with different complexities. The different methods of determining the fatigue strength, with increasing complexity, are very shortly presented below.

- **Nominal stress approach**

In certain standard connections the nominal stress method can be used, which is based on the stress calculated from the simple elastic strength of material theory. This will usually provide very conservative results.

- **Modified nominal stress approach**

Uses the stress determined from the nominal stress method, but includes an additional stress concentration factor (SCF) which account for 'macro' geometric effects such as openings, beam curvature and eccentricities.

- **Hot spot stress approach**

The hot spot stress approach determines the stress in the connection by evaluation the stresses at certain specified distances from the relevant connection. The exact distances are prescribed in the codes and depend on the type of stress and fatigue detail. These stresses are usually obtained from FE analyses and should be extrapolated to the weld toe to obtain the hot spot stress.

- **Effective notch stress approach**

The notch stress is an even more detailed approach which also takes the local geometry of the notch/weld into account. This requires advanced FE modelling and is not very suitable for standards/guidelines. It does not see many applications outside of academic studies.

These methods are used to determine the stress cycles that are experienced by the connection due to the fatigue loading. These can then be compared to the fatigue strength of the connection. The fatigue strength of a steel member or connection is presented by a so-called S-N curve, which expresses the fatigue failure as a function of the stress range and the number of stress cycles. This S-N curve is the result of numerous fatigue tests at different load levels and presents the relation between the number of cycles N to failure (or a defined size of the crack) with the stress range $\Delta\sigma$. An example of an S-N curve of fatigue test results is presented in Figure 12. The S-N curve is usually plotted using a double logarithmic scale so the results will lie on a straight line, which corresponds with the following relation:

$$\log(N) = \log(A) - m \log(\Delta\sigma)$$

Where:

- A - A parameter based on the specific detail in question
- N - The number of stress cycles
- m - Coefficient representing the slope of the S-N curve, usually equal to 3
- $\Delta\sigma$ - The constant amplitude stress range

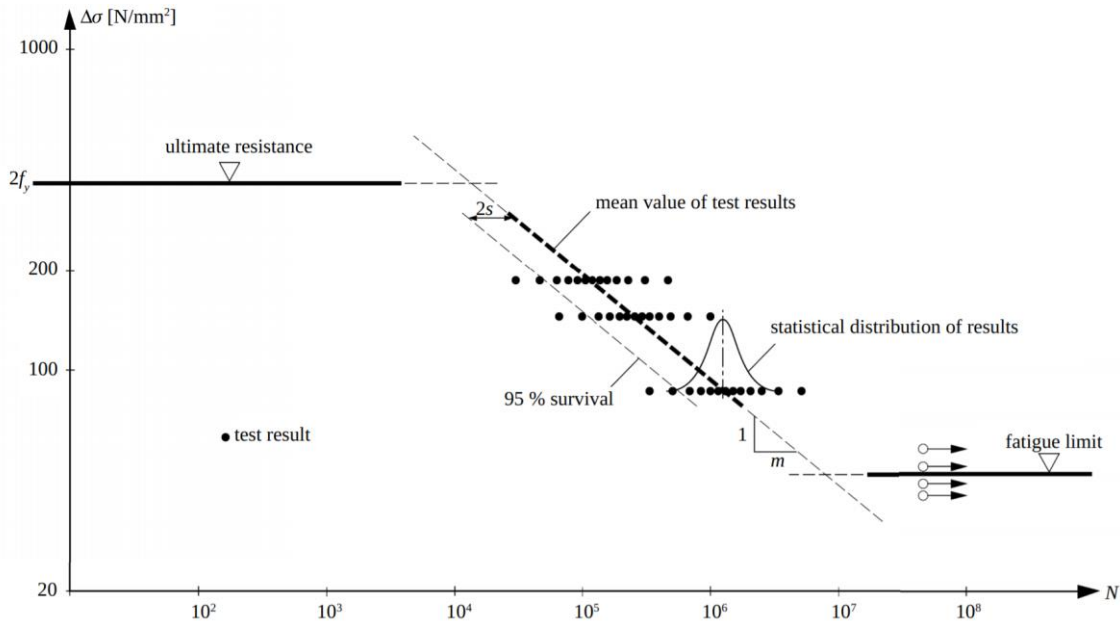


Figure 12: Fatigue test results of structural steel members under constant amplitude loading (Nussbaumer, Borges, & Davaine, 2011), adjusted from (Hirt, Bez, & Nussbaumer, 2006)

On the high end of this curve is the ultimate resistance, corresponding to twice the ultimate static strength of the material. This end of the spectrum, up to around 10^4 cycles, is called low-cycle fatigue and is only relevant in case of earthquakes or specific buildings (Nussbaumer, Borges, & Davaine, 2011). On the low end of the curve is the constant amplitude fatigue limit (CAFL). This is the limit beneath which stress cycles do not initiate fatigue damage to the steel member anymore. In case of variable amplitude loading, the CAFL can not simply be implemented since stress ranges under the CAFL may still impose fatigue damage once the crack reaches a certain size. Therefore, a resistance curve with a slope of $k=m+2$ below the CAFL is often used. A cut-off limit, beneath which stress cycles do not impose any damage at all, is often implemented at 10^8 cycles. The final S-N curves often used for design are shown in Figure 13.

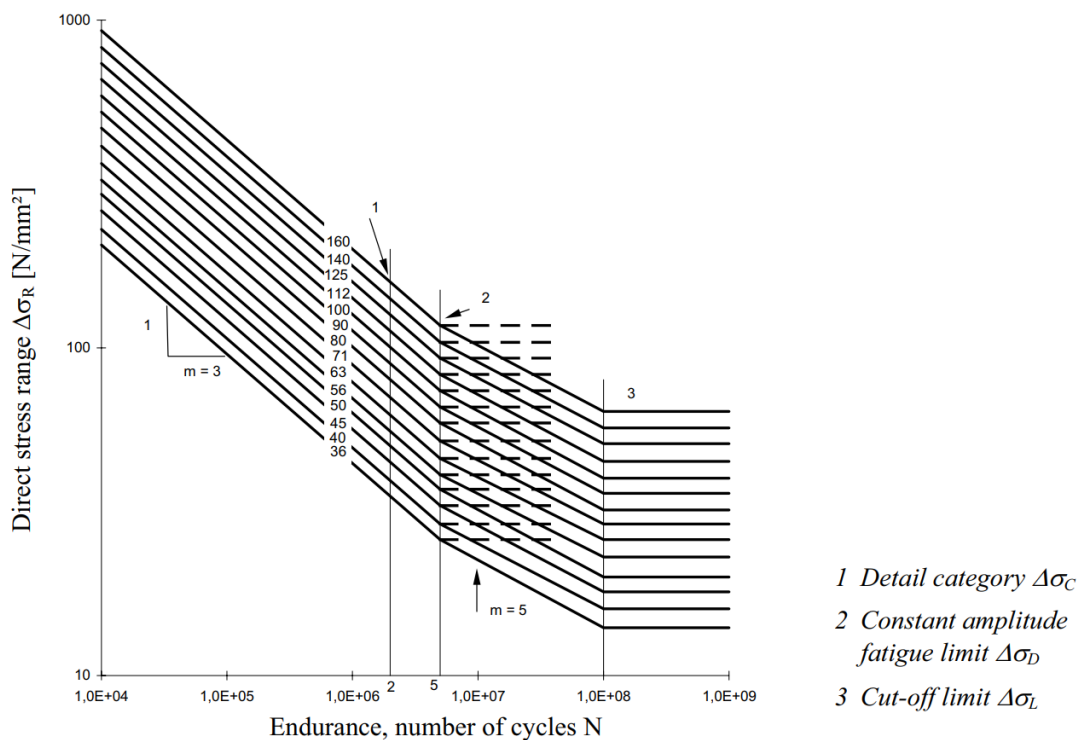


Figure 13: Fatigue design curves (European Committee for Standardization, 2005)

Fatigue details

The methods and theory described above are ways of obtained the stress cycles experienced by the connection and rest on the fact that the connection is already classified in a certain detail class. Detail classes are groups of connections that have a similar fatigue strength and are classified by a certain number, e.g. 125. This 125 corresponds to the stress cycle that the connection can withstand for 2 million times. This is illustrated by the number 1 in Figure 13. All detail classes are tabulated in EN 1993-1-9 (European Committee for Standardization, 2005) and EN1993-2.

When assessing a structure for fatigue, one first has to identify the critical fatigue details. Fatigue cracks often originate from a weld, as the welding process introduces a lot of heat in the material, which causes micro imperfections when the steel cools and shrinks. These imperfections can act as the starting point of a fatigue crack and can shorten the fatigue life, and specifically the crack initiation period, of the material significantly.

Furthermore, fatigue sensitive details can often be characterized by an abrupt change in stiffness. Areas with a sudden change in stiffness are usually accompanied by large stress concentration factors, that magnify any loading, which will be shown in section 2.2.3 to also have a large impact of the fatigue life.

The main fatigue problems occur when a sensitive fatigue detail is also subjected to relatively large stress cycles. For an OSD system, the large stress cycles are usually caused by the wheel loading on the deck plate. Therefore, most of the sensitive fatigue details are located in the connections between the deck, trough, and cross-girder. Below, a table is given with the most critical fatigue details, combined with their 'detail class'. The detail class is prescribed by the Eurocode and is used in the assessment of the fatigue detail. Only a quick overview is given, for the full requirements the relevant norms should be consulted.

- *Trough to Deck Plate*

The trough to deck plate cracks can propagate either through the deck plate or through the weld as shown in Figure 14. A detail category of 125 is allowed if the connection satisfies the requirements laid out in table NB.7 from EN1993-2/NB.

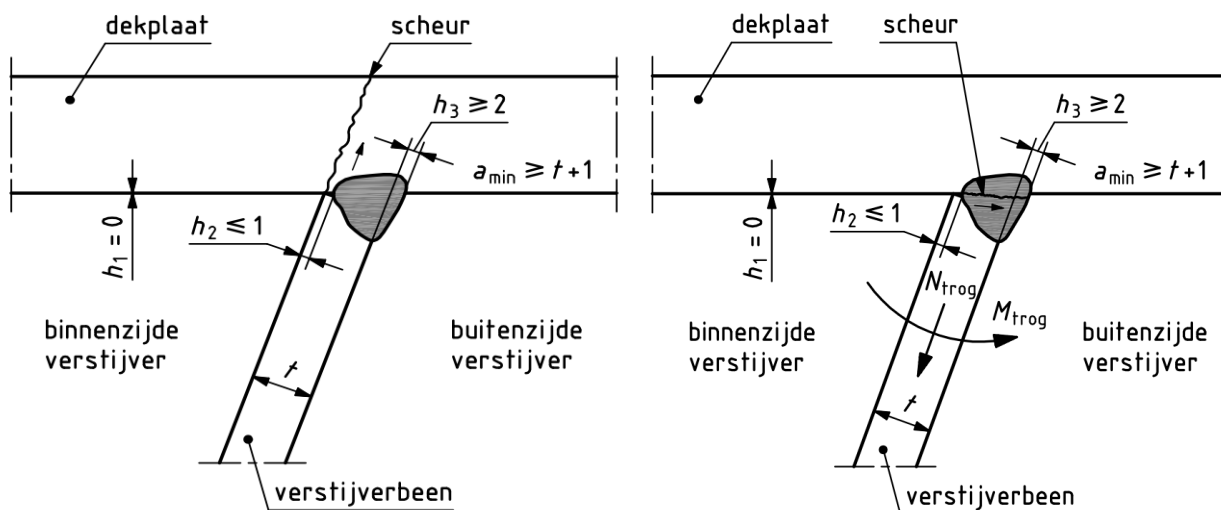


Figure 14: Possible deck to trough fatigue cracks (European Committee for Standardization, 2011)

- *Trough splice*

The detail category for the trough splice depends on the type and execution of the weld. The detail category can be 80 (Figure 15 (a)), 90 (b) or 112 (c) depending on the weld execution. Alternatively, a backing strip can be used to weld the troughs together, which results in a fatigue detail of class 100 (European Committee for Standardization, 2011).

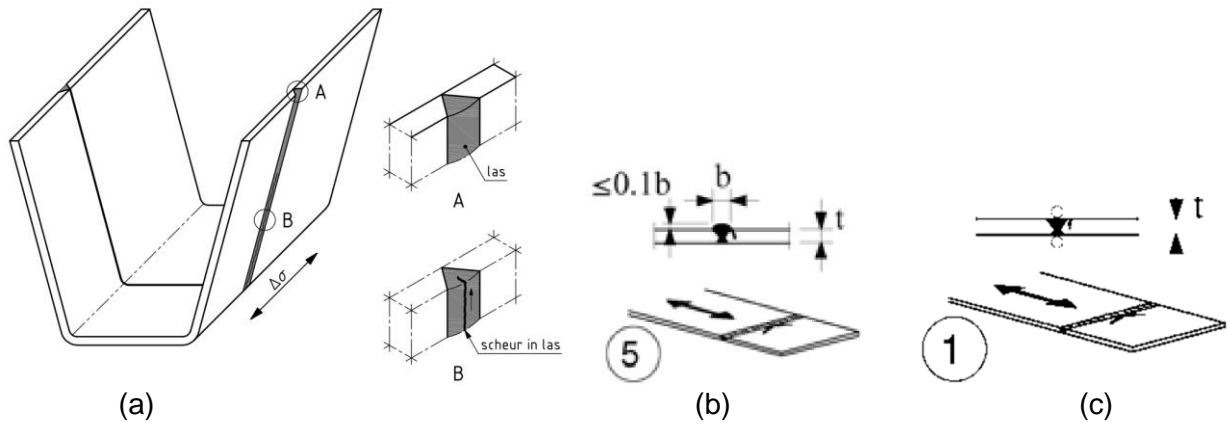


Figure 15: Trough splice fatigue detail. (a): EN1993-2/NB, (b) & (c): EN 1993-1-9 (European Committee for Standardization, 2005)

- *Trough to CG*

For the trough to cross girder connection, the fatigue detail again depends on the structural layout and the weld execution. Two different cracks can form in this detail, either in the cross girder or trough, as shown in Figure 16. For the crack in the trough, a detail class of 56 is achieved in case of discontinuous troughs. For continuous troughs, the detail class can vary between 80 and 125, depending on the thickness of the cross girder web and the method of determining the stresses. This exemplifies the benefit of using continuous trough to improve the fatigue life of a bridge.

For the crack in the cross girder, the detail category is equal to 80 both for continuous and discontinuous troughs. These cracks can be seen in Figure 17. In the case of cross-girders with cut-outs, a fatigue detail in the web of the cross will also need to be considered, given in table 8.8 of EN1993-1-9.

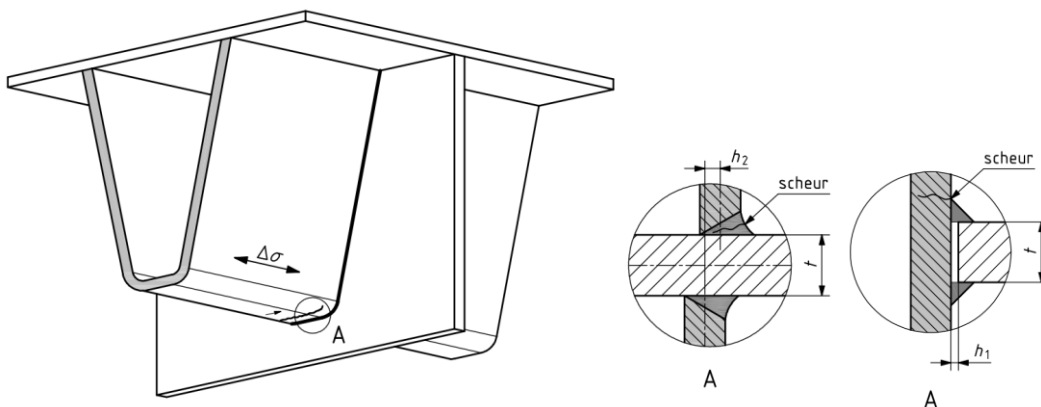


Figure 16: Trough to cross girder detail, crack in trough bottom (European Committee for Standardization, 2011)

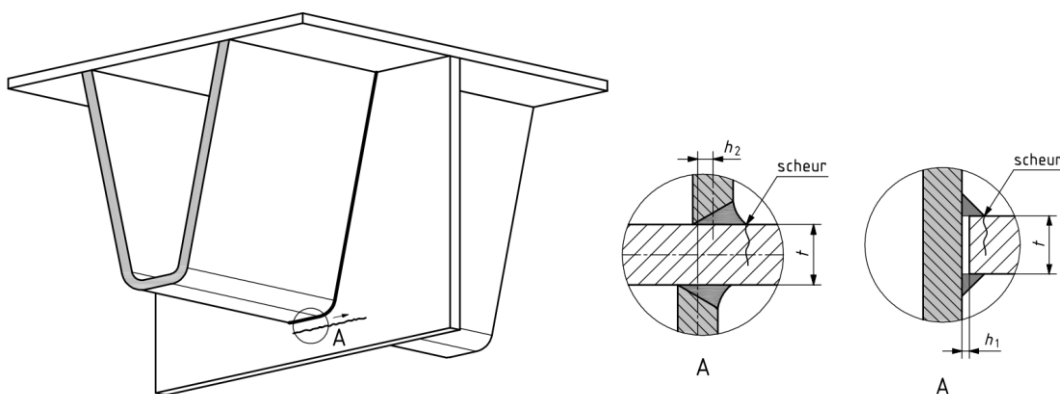


Figure 17: Trough to cross girder detail, crack in cross girder (European Committee for Standardization, 2011)

2.3. Monitoring techniques

Monitoring of bridges provides useful and important information on the behaviour of the structure, both for old and new built bridges. There are lots of possible purposes for applying some sort of monitoring. Validating the structural response and integrity of ageing infrastructure is a common and valid cause for monitoring. Furthermore, as is the case in this thesis, gaining confidence in the behaviour of (innovative) renovation measures is also a reason to monitor the structure. Verifying the safety and/or extending the service-life of a structure is also within the realm of possibilities (DeWolf, Lauzon, & Culmo, 2002). Other monitoring systems can aim to detect damage or simply check measurements against certain a certain threshold and warn the user in case of potential problems (Vardanega, Webb, Ricles, & Middleton, 2015).

In Figure 18, an overview the most common goals for structural health monitoring systems in literature is shown. This could however be quite a distorted view, since for example projects with new advanced modelling techniques are more likely to results in literary publications and attention, while simple damage monitoring investigations do not always result in literary publications and are thus underreported.

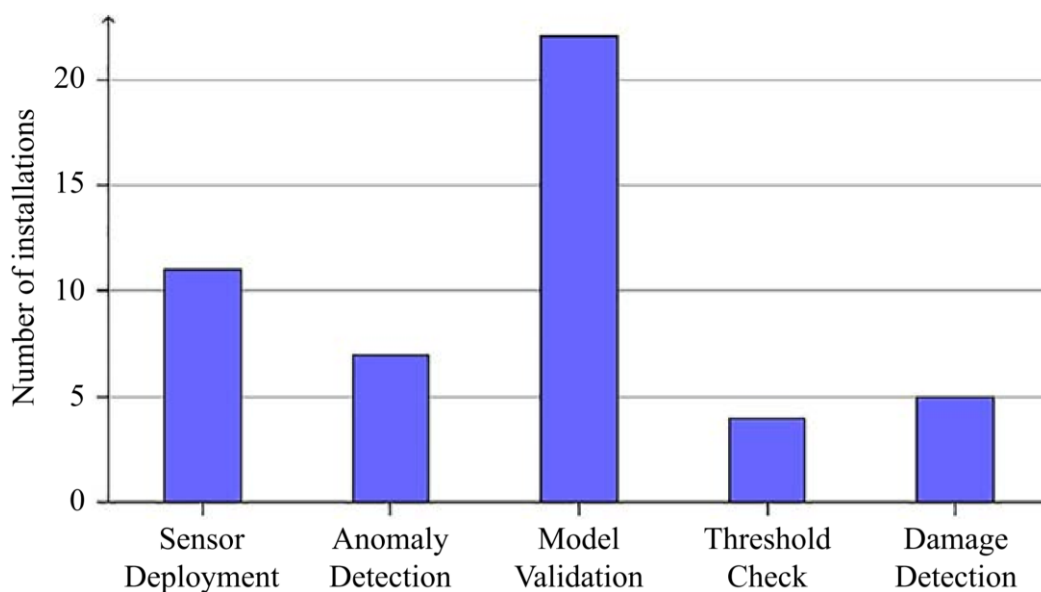


Figure 18: Goals of different monitoring programs found in literature (Webb, Vardanega, & Middleton, 2015)

Depending on the goals, scope, and size of the monitoring scheme there are many different types of sensors that can be applied. It is noted in (Vardanega, Webb, Ricles, & Middleton, 2015) that structural health monitoring projects often do not result in the desired insights because clear goals and objectives were missing when designing the system. With the wide range of available monitoring options available nowadays, designing a (cost) effective monitoring system is not so straightforward. It is therefore important that before a monitoring system is designed, the objectives are clear. Especially important is to think about what and how much information is needed in order to reach the desired goals.

In (Webb & Middleton, 2014), 31 bridge monitor projects were analysed and the different types of sensors used are shown in Figure 19. A monitoring programme is not limited to one type of sensor and usually consists of any combination of strain, temperature, and vibration measurements on the bridge.

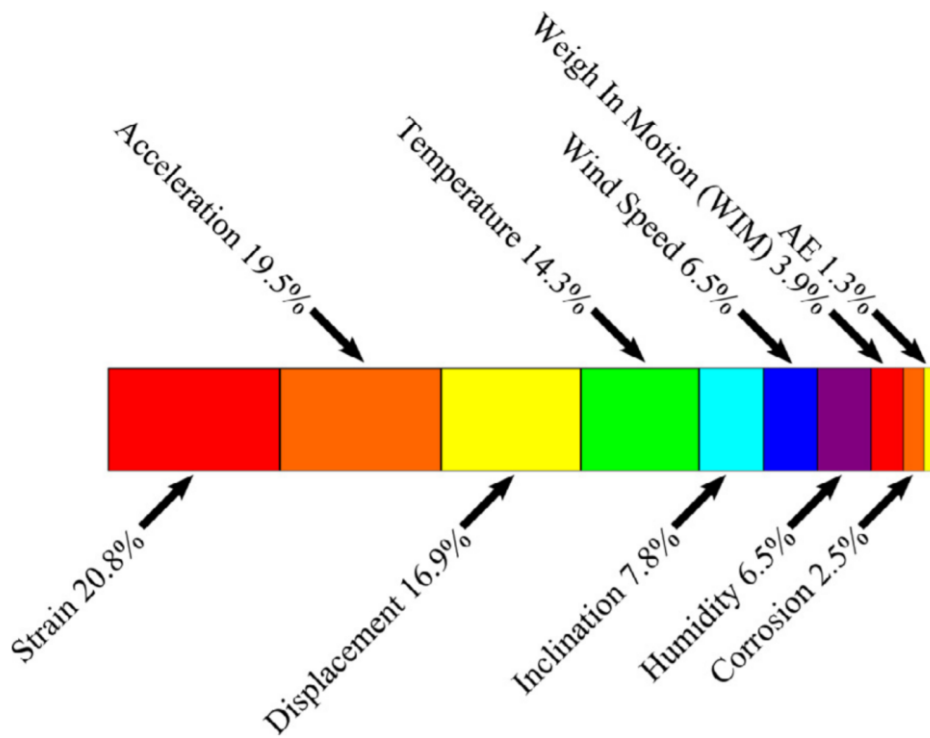


Figure 19: Sensor types used in 31 bridge monitoring installations (Vardanega, Webb, Ridles, & Middleton, 2015), with data taken from (Webb & Middleton, 2014)

The strain gauge, which is also used as the monitoring sensor for this thesis, is the most commonly applied sensor. It typically uses electrical resistance, but there are also strain gauges that utilise piezoelectric transducers and vibrating wires. In an electrical strain gauge, the strain is measured by the change in resistance that is observed at the ends of the electrical wires. An overview of a typical strain gauge is shown in Figure 20. These are typically single use and fairly cheap. They can be glued to the clean steel member, so only the coating system needs to locally be removed. Due to their ease of application, versatility and accuracy, strain gauges are widely used in structural health monitoring. As with most monitoring techniques, a constant and clean power supply is needed to obtain the cleanest measurements. Also, the strain gauge only measures strain in one direction at one specific point in the structure. Care needs to be taken in areas with large stress gradients or complicated stress states.

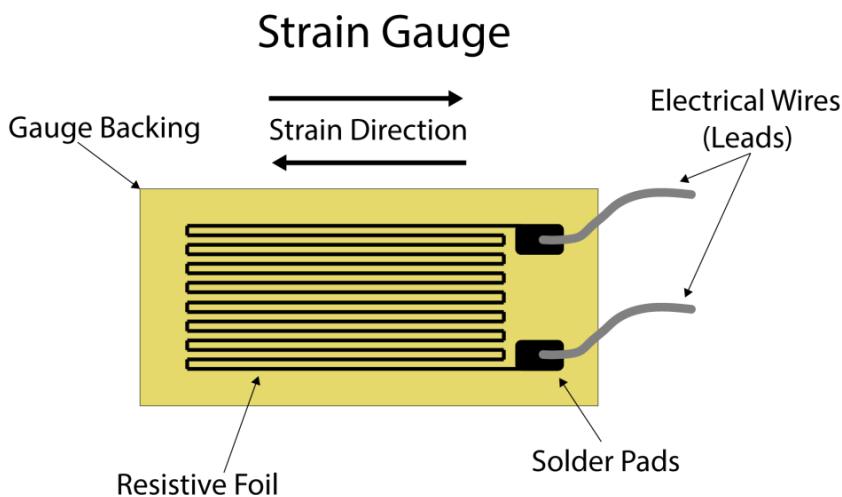


Figure 20: Elements of a typical strain gauge (Michigan Scientific Corporation, 2021)

Many other types of sensors exist, but for brevity's sake these will not be discussed in this thesis. The last point to stress is the upcoming popularity of cloud services. There are several cloud service providers (Amazon Web Services, Microsoft Azure, etc) that allow for the use of high computing power and storage capabilities for a wide audience. This allows for the storage and processing of large quantities of data, and more sophisticated and automated monitoring systems and services are being developed using these new tools.

2.4. Inspection techniques

This section will shortly discuss the main inspection techniques for bridge decks that are being used in The Netherlands. In order for an inspection technique to be viable for this purpose, a few criteria should be fulfilled. First of all, fatigue is a phenomenon subject to a lot of uncertainty. Spread of results are so large that two details subject to the same loading can show very different levels of fatigue damage. During inspection of steel bridge decks, it is therefore insufficient to thoroughly inspect a few details and make conclusions for the rest of the bridge based on this. An inspection technique needs to be applicable on a large scale in order to cover a lot of ground.

Other important considerations are that the inspection of the bridge has to cause minimal hindrance to traffic and has to be executable under all weather conditions. Also, in order to inspect deck plate cracks, it is very desirable that the inspection technique is able to either look through the steel (when inspecting from the bottom) or look through the topping layer (when inspecting from the top) (TNO, 2010). Based on technical limitations and these beforementioned aspects, the three most applied inspection methods are the Crack-PEC, TOFD and visual inspection. These will now be discussed in some more detail:

2.4.1. CrackPEC:

The CrackPEC system, also referred to as the 'insPECteur', is a system that uses Pulsed Eddy Current (PEC) for inspection (van Dooren, 2018). This is an electromagnetic technique that uses a magnetic field which penetrates through any non-conductive layer such as concrete or asphalt. When the emission of the current is cut off, eddy currents are generated within the steel which are captured and recorded. Using the decay rate and data processing techniques, the thickness of the steel layer is determined (MISTRAS, 2021).

This technique can also be used to detect cracks, but only cracks that have penetrated through the deck plate and have a length of at least 100mm. The inspection can be carried out from a modified trailer shown in Figure 21 which can inspect a lane of around 300-400m in one night. Combined with the fact that no asphalt has to be removed, this inspection technique causes very minimum hindrance to the traffic, making it an attractive inspection technique (van Dooren, 2018).

2.4.2. TOFD

When more accuracy is required and smaller cracks need to be detected, TOFD is the most widely used technique. TOFD, which stands for Time-of-Flight Diffraction, is a technique based on ultrasound (US) used to inspect welds. When inspecting a weld, transducers are located on both sides of the weld, one as a transponder and the other as a receiver. A soundwave is transmitted, which will diffract and reflect if it bounces off a crack. This inspection can be done using a small device shown in Figure 21 which can be moved along the length the weld. The process automatically converts the signals into plots of longitudinal and transverse cross-sections of the weld, usually in greyscale, that can quickly be used to assess any cracks (Infra Inspectie B.V., 2021). The big advantage of this technique is that it can quickly and accurately detect cracks from a length of 3 mm, even when the cracks have not yet propagated through the entire deck. It does however require the removal of the surface layer, which limits its use for in-service bridges (van Dooren, 2018).

2.4.3. Visual inspection

In some scenario's, such as the inspection of an entire bridge, these options are not feasible. The alternative then is to do a visual inspection. This means that a team of experts has to inspect every member of the bridge to check for potential cracks, corrosion or other problems. For fatigue considerations, visual inspection is applied at the bottom side of the bridge deck. Especially for cracks in the connection of the trough and the cross girder and trough splices, there are not yet any good alternatives to a visual inspection to the authors knowledge. On the top side of the bridge deck, visual inspection is usually only applied as a quick first check to see if severe cracking is visible.

It is hard to make general remarks on the crack sizes that can be spotted through visual inspection, as this is dependent on a lot of factors and on the quality of the inspector. The ability to spot cracks increases when the crack deforms under traffic loading, when there are rust stains or when there are wet spots visible around the cracked area. Furthermore, thick coating layers can make spotting of the crack more difficult. Even the colour of the coating can impact visibility, and due to this the municipality of Rotterdam only tends to use light coloured coatings on new bridges (TNO, 2010). On the bottom side of the bridge deck, a rough rule of thumb is that cracks from around 50-75 mm can be spotted using visual inspection (de Jong, 2006). The presence of through thickness deck plate cracks can also be tested by knocking on the troughs. If this does not sound hollow this means water has ingresses into the trough, indicating a crack through the deck plate.

Another advantage of visual inspection on the bottom side of the bridge is that traffic is not hindered. Depending on the site characteristics, hinder to train or maritime shipping underneath the bridge will occur.



(a) CrackPEC inspection



(b) TOFD inspection

Figure 21: Different inspection techniques (van Dooren, 2018)

2.5. [Reparation techniques](#)

Just as with monitoring or inspection techniques, there are numerous options and solutions available for repairing orthotropic steel decks. This section will shortly describe the arguments that are considered when choosing an appropriate reparation technique, and the most used reparation techniques will be presented.

Due to the large economic and societal impact of road closures, one of the main driving factors of a reparation is the closure time of the bridge. Often this is even considered as a boundary condition (e.g., the bridge can only be closed for a few hours at night). Other factors to take into account is the increase of service life, preventing brittle material behaviour, preventing large residual stresses, ease of application, costs, and more (TNO, 2010). Some of the most common reparation techniques will be presented in some detail:

2.5.1. [Gouging and rewelding of the crack](#)

A possible repair for a deck plate crack is through gouging out the crack and rewelding. This technique is based on the idea of repairing the deck plate by rewelding the crack. However, when welding a crack that is only partially penetrated through the deck plate, a poor fatigue detail is created. Therefore, before the welding, the crack will be gauged out through almost the full deck plate thickness so that the weld will fully penetrate the deck plate. The procedure is shown in Figure 22. When applying this technique, some important things to consider are:

- It needs to be verified, often through magnetic inspection, whether the procedure has been successful and whether the crack has not bent into the deck plate
- If the steel of the deck plate has a large carbon percentage, the area around the weld will have to be heated appropriately to prevent brittle behaviour of the weld. Since the chemical composition of the steel is not always known in advance, this is often standard procedure.
- The weld area needs to be properly protected from water ingress.
- Shrinkage around the weld can result in large residual stresses. If the repair area is too large, this can even result in new cracks emerging in adjacent troughs due to the reparation. To reduce shrinkage, Ultrasonic Impact Treatment (UIT) can be applied after the strengthening. Research has shown that this can reduce the strain due to shrinkage by around 40% (Stam, 2008). Furthermore, UIT also improves the microstructure of the material and makes for a smoother transition between weld and plate material. This UIT should be carried out after every weld pass.

- The top of the weld can be ground flush with the deck plate after completing this repair. This will slightly increase the fatigue performance of the detail. Even though this is done in many countries, in the Netherlands this is often skipped since it is relatively expensive and the improvement in fatigue life is still insufficient to act a permanent repair method. (TNO, 2010)

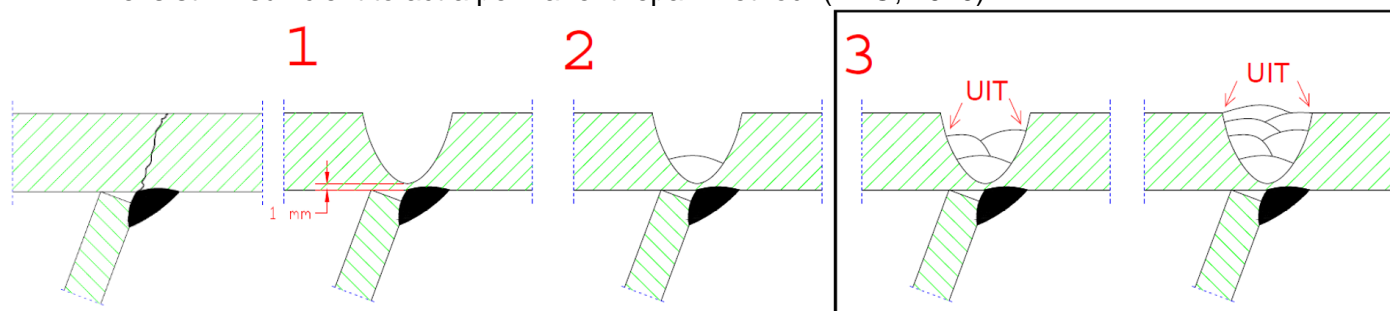


Figure 22: Reparation of deck weld crack with gouging and rewelding and UIT treatment (TNO, 2010)

Even when properly applied, the obtained detail will still have a lower fatigue life than the original detail. Considering the original detail falling in detail class 125 or 147 N/mm², the repaired detail is expected to be of a detail category between 90 N/mm² and the original detail. Furthermore, due to the shrinkage problems and the limited fatigue improvement, only cracks to around 500mm are repaired using this technique. Even though this repair technique is not the most effective, it is very easy to carry out. It is therefore a very viable solution as a temporary repair. It is a quick solution of which multiple can be carried out during a single night closure.

2.5.2. Covering plate

For bridges with an asphalt covering and deck plate cracking, a possible temporary solution is the application of covering plates. This is especially relevant when two adjacent trough legs show deck plate cracking since this can potentially result in a dangerous situation and requires a robust reparation technique. It can also be used for long cracks (>500mm) or when cracks re-emerge in a location that was already previously repaired (for example through gouging and rewelding) (TNO, 2010).

In this reparation technique the asphalt layer is taken out and over the cracked area a covering plate is welded on top of the existing deck plate (van Dooren, 2018). The cracks in the deck plate are not first repaired. The width of the covering plate is 400mm, so it can cover two trough legs (300 mm spacing) with 50 mm extra space to prevent welding on top of the sensitive connection. Furthermore, the 400mm is slightly smaller than the replacement part (which will be discussed in section 2.5.3) that can be installed as a permanent solution. The cover plate is rounded off to avoid stress concentrations and sharp angles in the welds. In longitudinal direction, the chosen length of the covering plate is usually chosen as the length of the crack plus an overlap of 200-300 mm on each side. This is to cover possible crack growth after the application of the strengthening (TNO, 2010).

The thickness of the covering plate is usually equal to 12mm, the same as the thickness of most deck plates. This allows for the plate to carry the stresses that were in the deck plate without being too thick, which would result in possible problems with the asphalt due to the stiffness difference (TNO, 2010).

Depending on the number of trucks, this reparation technique will last around 2-4 years. It is more reliable compared to gouging and rewelding, and results in less shrinkage in the deck plate. Nonetheless, it is a temporary solution that is applied until a full renovation begins. Before the renovation of the Galecopper bridge, 170 of these covering plates were installed. After taking these back out a few years later, no additional crack growth in the deck plate was observed (TNO, 2010). The execution is slower than gouging and rewelding, but it still possible to apply around 3 covering plates in 1 night with 1 shift (van Dooren, 2018).



Figure 23: Two covering plates installed during a reparation (van Dooren, 2018)

2.5.3. Replacement part

Currently, a replacement part is seen as the only permanent reparation solution to fatigue cracks in the deck plate. Furthermore, it can be applied both in movable and fixed bridges. This solution is chosen when the deck plate at two adjacent trough legs show cracking of significant length. It can also be used as a replacement of one of the other reparation techniques that were discussed. The disadvantage of this technique is that it is also the most laborious and expensive options.

Simply put, a reparation with a replacement part consists of removing part of the deck plate and replacing it with a new piece. The maximum length of a replacement part is 2000 mm in longitudinal direction due to execution and safety reasons. The width is regularly taken as 450 mm. The thickness of the replacement part is usually 16 mm, slightly thicker than most deck plates. The execution of a replacement part requires special attention due to a number of potential problems. First of all, weld shrinkage can again cause problems during the execution of the replacement part. Furthermore, the deck plate also acts as the top flange for the cross girder and the structural behaviour of the bridge is negatively impacted during the reparation.

A solution to these problems is to install so-called 'krammen' over the part of the deck plate that will be removed, as can be seen in Figure 24. This piece of strengthening has multiple functions; besides the beforementioned problems it also helps elevate vertical alignment issues between both sides of the hole. Normally, these steel sections are 40 mm thick and have a height of at least 400 mm. Depending on the length of the replacement part, 2 or more krammen can be necessary. They are welded to the deck at locations that are not sensitive to fatigue damage. Furthermore, the welds have a throat thickness of 15 mm and need to be inspected using TOFD to check for possible defects. This is prescribed to ensure a safe reparation without the need for extensive calculations (TNO, 2010).

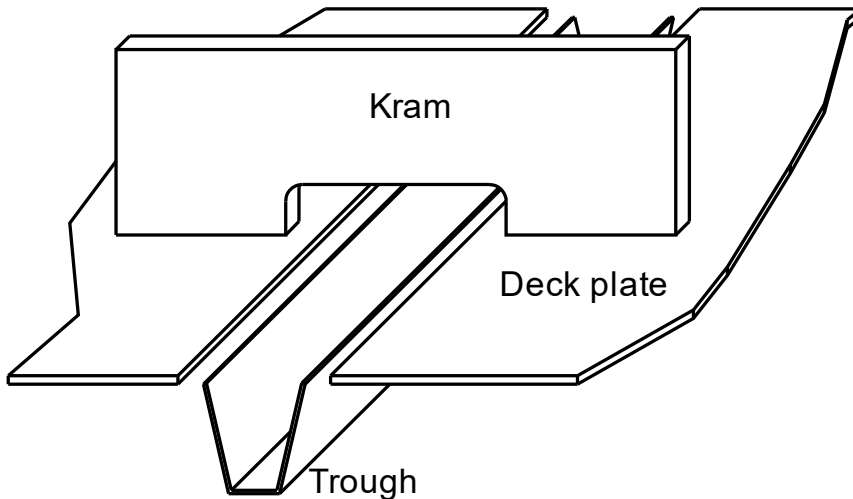


Figure 24: Installation of a 'kram' over the deck plate (TNO, 2010)

After installation of the kram, the cracked part of the deck plate has to be removed. A width of 448 mm is taken out, 2 mm smaller than the width of the replacement part to counteract the shrinkage in the welds. During this operation, the trough is first grinded off from the deck plate. The deck plate is then cut off from the cross girder, and finally the deck plate is removed. The trickiest part of this operation is the removal of the deck plate from the trough, since there is very limited space and little room for error. A small grinder has to be used due to the trough spacing, the work is above head level, and care needs to be taken that the cut is made in the correct location without damaging the trough leg (TNO, 2010).

After this is completed, the next tricky step is to place the new deck plate in the correct position and properly weld the different parts back together. The replacement part is slightly thicker than the original deck plate to counteract the material loss of the trough legs (besides for the reason that this reduces stresses in this new deck plate). At the sides of the replacement part, the plate is tapered to prevent a jump in thickness. All the different parts are connected using X- or V-welds as shown in Figure 25. Welds are regularly checked with magnetic or ultrasonic inspection to ensure a successful repair.

Due to all these steps and the necessary accuracy, reparation with a replacement part can take around 24 hours or more, depending on the experience of the contractor. This means the reparation cannot be done during a night closure and will often have to be carried out in the weekend (van Dooren, 2018).

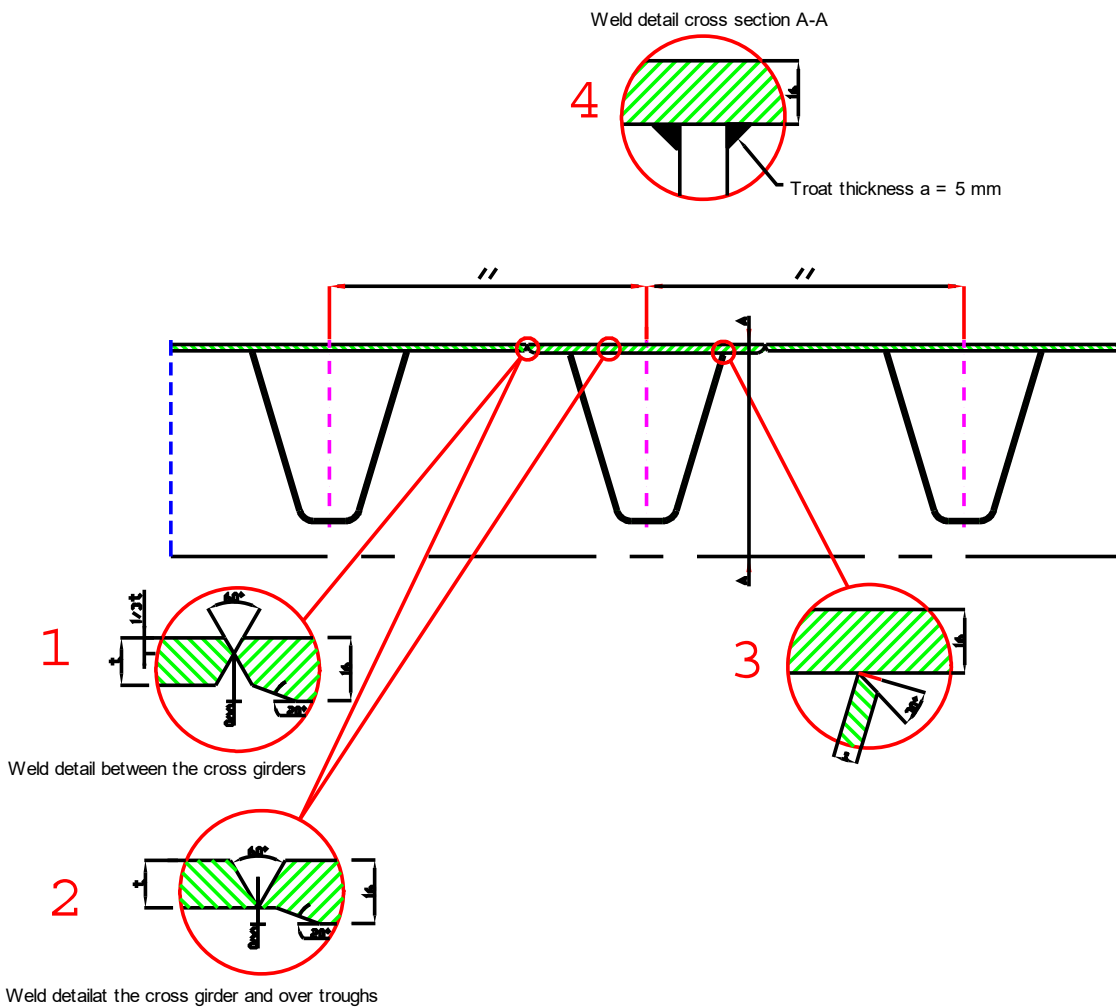


Figure 25: Different weld detail for installing a replacement part (TNO, 2010)

2.5.4. Kano

So far, all the discussed techniques were for the reparation of deck plate cracking. However, some bridges also have significant fatigue problems in the trough to cross girder connection where these techniques cannot be applied. A possible reparation technique is through a so-called 'kano'. This consists of steel strengthening elements that are welded to the trough bottom and bolted to the cross girder with the aim of reducing the stress concentrations in the original detail. A figure of a 'kano' is shown in Figure 26.



Figure 26: Repair of a trough to cross girder connection with a 'kano'

2.5.5. Relocation of trucks

Despite not theoretically being either a repair or a renovation technique but more of a mitigation measure, relocating the location of the slow lane on the bridge deck can be a very effective (temporary) solution to prevent further fatigue damage. Fatigue sensitive details, especially in the deck plate and trough connections, are due to very local wheel loading and generally do not occur much besides in a few trough widths around the slow lane. If possible, redesigning the road layout and placing the slow lane on a 'fresh' part of the bridge deck is a possible immediate solution to the fatigue problem. However, this is most of the time not possible without reducing the number of lanes and/or speed limit on the bridge and is thus only applied as a last ditch solution before a renovation commences.

2.6. Renovation techniques

Due to the aging infrastructure and insufficient fatigue capacity of many existing steel bridges, the renovation of orthotropic steel decks has attracted a lot of attention in recent years. This section aims to give a short overview of the different strengthening options that have been researched for both fixed and movable bridges, with a focus on the Netherlands.

Almost all strengthening techniques boil down to improving the stiffness of the deck structure, and thus lowering the stresses in the critical fatigue details, usually by adding a stiff layer on top of the existing deck. There are two different strengthening schemes for steel decks that Rijkswaterstaat has experience with: High Strength Concrete (HSC) and an epoxy bonded steel plate solution (MC Renovatie Bruggen, 2021). These will be discussed in section 2.6.1 and 2.6.2 respectively. Another option, not (yet) applied in the Netherlands, concerns the use of a sandwich plate system for bridge strengthening. This will be discussed in section 2.6.3.

2.6.1. High strength concrete

An effective and the most widely used strengthening method is the replacement of the asphalt surfacing with a high strength concrete layer. Depending on the concrete mix and application, the thickness of the layer can vary between around 30 mm for movable bridges and 50 - 90 mm for fixed bridges.

Different designs and alternatives have been designed and applied over the years. Applications in China have often applied a HSC/UHPC/RPC layer in combination with shear studs, which are welded to the deck plate using stud welding with a spacing of 300 mm (Wang, Ke, Gao, & Zhang, 2019; Yuan, Wu, & Jiang, 2019). In the Netherlands, the bond between the reinforced HSC and deck plate has been researched and it was found that pouring the HSC onto a hardened epoxy layer with bauxite particles showed the best results (Buitelaar, Braam, & Kaptijn, 2004). This bauxite epoxy solution is preferred in most applications in the Netherlands. A visualisation of this solution can be seen in Figure 27. On top of the concrete, either an epoxy topping layer or an asphalt layer is applied as the wearing surface. An epoxy is usually preferred, since an additional asphalt layer would increase the total weight of the structure after strengthening, which is undesirable.

Strain measurements and FE modelling have proven that HSC is very effective at reducing the stress in the deck plate and improving the fatigue performance of the structure. Measurements at the Caland bridge, which was one of the first applications in the Netherlands, have shown a stress reduction of 75-80% in the deck plate and 66-75% in the trough wall (Buitelaar, Braam, & Kaptijn, 2004; de Jong & Kolstein, Strengthening a Bridge Deck with High Performance Concrete, 2004). The layout of the concrete and reinforcement has been optimised over the years and test measurements taken of the Muiderbrug have shown a stress reduction at the underside of the deck plate at the trough to crossbeam intersection of 88% (Arup, 2012). This was in good agreement with finite element modelling of uncracked concrete.

Even though using HSC has proven to work very well, it is not applicable in all situations. In the case of fixed bridges, this concrete layer replaces the asphalt layer and therefore will not add significant weight to the total structure. For movable bridges however, this solution will add significant weight, making it not a suitable solution in most cases. Some studies have tried decreasing the thickness of the added layer by using very high strength concrete in combination with corrosion resistant reinforcement (Bouters, Braam, Kolstein, & Romeijn, 2009). This showed promising results (47-64 kg/m², 74% stress reduction in static bending tests), but to the author's knowledge this has not seen any applications.

Furthermore, the cast-in-situ nature of the solution causes lengthy traffic disruptions that can be problematic for important pieces of infrastructure (van Dooren, et al., 2010). This issue has also attracted

attention, and a solution of welded studs in combination with a prefabricated Ultra High Performance Fibre Reinforced Concrete (UHPFRP) has been proposed as an alternative with a faster execution time. This solution has been applied on a bridge in Pont de Illzach, in France, and has also been proposed as an alternative solution to the strengthening of the Ewijk bridge (Gibson, et al., 2014).

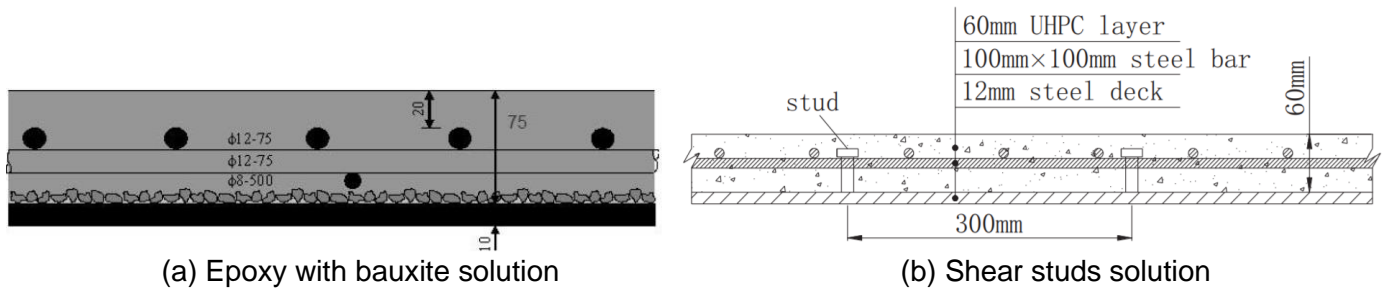


Figure 27: OSD renovation using HSC with (a) an epoxy/bauxite connection (van Dooren, 2018), (b) Shear studs (Yuan, Wu, & Jiang, 2019)

2.6.2. Bonded plate

When low self-weight is of importance, an alternative renovation solution is the application of a bonded plate. This technique is a lot lighter ($50-60 \text{ kg/m}^2$) and is therefore especially applicable to movable bridges (de Freitas S. , 2012). In this solution, a steel plate is installed on top of the deck plate, connected compositely through a layer of epoxy. A cross section of the solution is shown in Figure 28.

The development of the strengthening solution with bonded steel plates has been promising, and a pilot has been completed on the (movable) Scharsterrijn bridge. (de Freitas S. , 2012). This has yielded good results, and the scheme has been applied again on the Gideon bridge and the bridge over the Hartelkanaal (de Freitas, Kolstein, & Bijlaand, 2013; Voermans, Souren, & Bosselaar, 2018).

Experimental results using a 2 mm epoxy layer and a 6 mm plate showed a strain reduction of at least 45% over the cross-girder and at least 60% at midspan. This translates to a fatigue life increase of 6 to 15 times (de Freitas, Kolstein, & Bijlaand, 2013). Furthermore, the system was tested under fatigue loading and proved to have sufficient capacity (de Freitas, Kolstein, & Bijlaard, 2017)

Besides experimental results, the pilot application on the Scharsterrijn bridge also included a monitoring project. Short term results show a reduction of around 55% at the deck plate and 35% at the stiffener web, translating to an increase of fatigue life of 11 and 3.6 times respectively. The long-term measurements do not show significant changes in the stress level at the bridge deck during the year of monitoring (de Freitas, Kolstein, & Bijlaard, 2012).

However, this is still very innovative strengthening solution and therefore there are risks involved. Uncertainties exist especially regarding the long-term behaviour of the bonded plate, the structural behaviour under elevated temperatures, and the risk of debonding. These risks are manageable for a small surface area that is to be renovated but they increase for larger bridges.

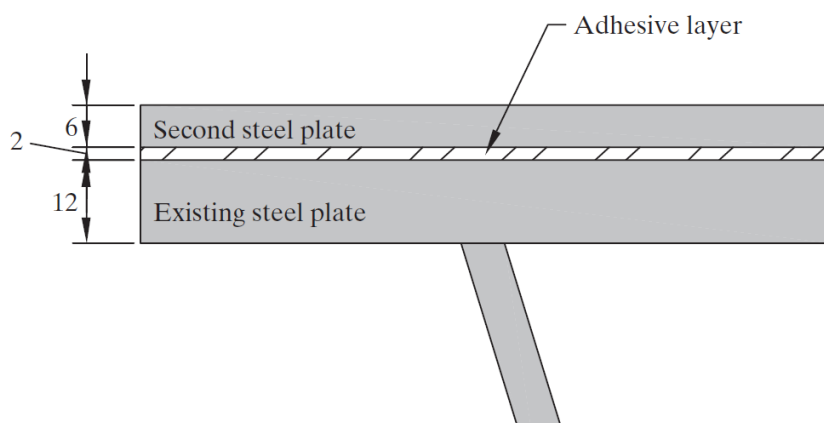


Figure 28: Cross-section of the epoxy bonded plate solution (de Freitas, Kolstein, & Bijlaard, 2017)

2.6.3. Sandwich plate system

Another option that has been explored and applied on various bridges is the use of a sandwich plate system. This solution is similar to the bonded plate strengthening in that a steel plate is connected on top of the deck plate. For the sandwich system however, a polyurethane (PU) core is used to connect the elements (Marzahn & Hamme, 2008). A cross-section of this can be seen in Figure 29.

This solution was originally designed for the repair and upgrade of ferry decks but after successful pilots has now seen various application in bridge strengthening (Vincent & Ferro, 2004; Feldmann, Sedlacek, & Geßler, 2007; Zhang, Li, & Cui, 2011; de Freitas, Kolstein, & Bijlaand, 2013). It has been applied on fixed bridges with an asphalt topping (Matuschek, Stihl, & Bild, 2007; Stihl, Chassard, & Feldmann, 2013; Wang, Ke, Gao, & Zhang, 2019), but it has also been proposed as a solution for movable bridges (de Freitas, Kolstein, & Bijlaand, 2010; de Freitas S. , 2012).

In order for application on movable bridges, a lightweight strengthening solution with a maximum weight between 50 and 80 kg/m^2 is desirable. To this end, SPS layups with different core and face thicknesses were designed and compared in an experimental study (de Freitas, Kolstein, & Bijlaand, 2010). In this study, it was found that a 30 mm PU core combined with a 5- or 6-mm upper face was about 10-5% more efficient than a 15- or 20-mm PU-core. However, the thicker core could potentially lead to height and clearance issues in some bridges.

The reduction of stresses in the deck plate due to the SPS strengthening has been predicted at around 60-95% (de Freitas, Kolstein, & Bijlaand, 2010), with a load test showed a reduction in deck plate stresses of 70%. The renovation of the Krefeld bridge in Germany using an SPS system was supposed to extend the fatigue life of the bridge by 32 times (van Dooren, 2018).

Another study showed that the SPS system performed worse (70% reduction) than a reactive powder concrete (RPC) alternative (which showed a 95% reduction) (Wang, Ke, Gao, & Zhang, 2019). It was also concluded in (de Freitas S. , 2012) that the SPS system performed worse than a bonded plate solution, especially close to welds. This is due to the fact that the bending performance of the SPS system decreases significantly when large shear forces also act on the system. Therefore, SPS systems also perform better between crossbeams compared to over crossbeams (de Freitas S. , 2012).

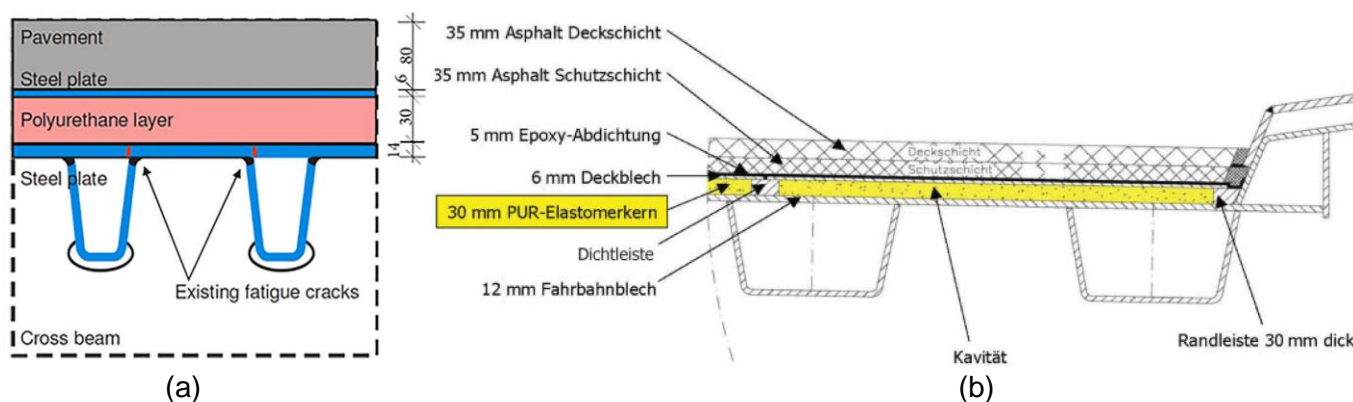


Figure 29: Different SPS strengthening applications. (a): Highway bridge in China (Wang, Ke, Gao, & Zhang, 2019). (b): Krefeld bridge in Germany (Matuschek, Stihl, & Bild, 2007)

2.7. Preloaded injection bolts

In the pilot application of the Suurhoff strengthening, the behaviour of the preloaded injection bolts is one of the main unknowns. This chapter will give an overview of the force transfer mechanisms in section 2.7.1. Section 2.7.2 will focus on the finite element modelling options and techniques that can be used to model preloaded bolted connections.

2.7.1. Theoretical force transfer mechanisms

In a preloaded injected bolt, the force is transferred by two mechanisms: bearing of the resin and friction between the plates due to the preloaded bolt. These mechanisms both have a certain stiffness and deformation capacity that are vital to understanding the behaviour of the connection. These mechanisms are first discussed individually, and then the interaction between the mechanisms is discussed.

Friction due to preloading

Preloaded bolts transfer the force through the friction between the plates that is introduced by the clamping force. The slip capacity is therefore mainly dependent on the friction coefficient of the relevant surfaces, as well as on the preload level. The load transfer principle is visualized in Figure 30. If this slip resistance is overcome, the connection will slip until the bolt shank comes in contact with the plates. The connection will then transfer the force through bearing just as a regular bolted connection. The ultimate capacity of a bearing connection is governed by either the shear capacity of the bolt or the bearing resistance of the plates (European Committee for Standardization, 2011).

Important parameters that govern the behaviour and capacity of the preloaded bolt are the slip load & displacement, the friction coefficient and preload level, and the connection stiffness. These topics will each be shortly addressed.

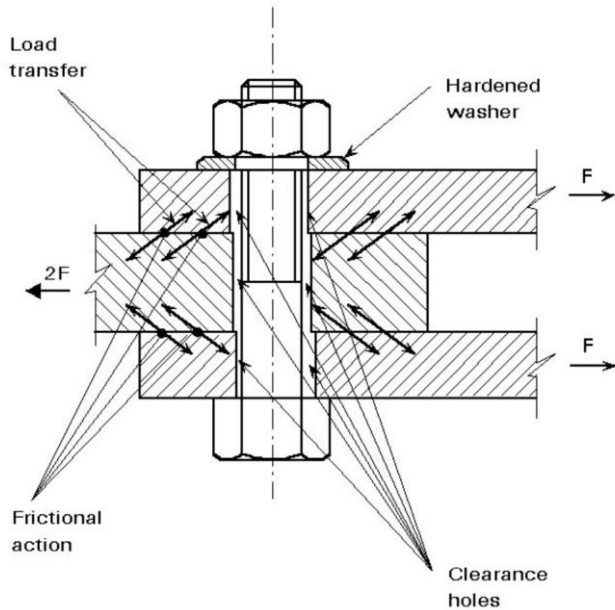


Figure 30: Load transfer through friction in a preloaded double lap shear connection (ESDEP)

Preload level and friction coefficient

The friction coefficient is defined as the ratio between the slipping force and the clamping force. It can be determined with the slip test, defined in EN1090-2 (European Committee for Standardization, 2018). As it directly relates the preload level with the slip capacity of the connection, it is an important property in preloaded connections, especially since the preload level is fixed by the design code. The friction coefficient depends mainly on the applied coating system and thickness. Some commonly applied coating systems and corresponding slip factors are given in Table 1.

Table 1: Some commonly applied surface treatments and corresponding friction class (European Committee for Standardization, 2018)

Surface treatment	Class ^a	Slip factor μ ^b
Surfaces blasted with shot or grit with loose rust removed, not pitted.	A	0,50
Surfaces hot dip galvanized to EN ISO 1461 and flash (sweep) blasted ^c and with alkali-zinc silicate paint with a nominal thickness of 60 μm ^d .	B	0,40
Surfaces blasted with shot or grit: a) coated with alkali-zinc silicate paint with a nominal thickness of 60 μm ^d ; b) thermally sprayed with aluminium or zinc or a combination of both to a nominal thickness not exceeding 80 μm .	B	0,40
Surfaces hot dip galvanized to EN ISO 1461 and flash (sweep) blasted (or equivalent abrasion method) ^c	C	0,35
Surfaces cleaned by wire-brushing or flame cleaning, with loose rust removed	C	0,30
Surfaces as rolled	D	0,20

^a Classes as given in G.6.
^b The potential loss of preloading force from its initial value is considered in these slip factor values.
^c Unless alternative equivalent abrasion process capability can be demonstrated, flash (sweep) blasting of hot dip galvanized surfaces shall be carried out according to the procedures and conditions set out in EN 15773. After flash (sweep) blasting the appearance of a matt surface indicates that a soft surface layer of un-alloyed zinc has been removed.
^d Dry thickness to be within 40 μm to 80 μm range.

The preload level is the other parameter directly linked to the slipping force as it determined the amount of clamping between the plates. The preload level is fixed by NEN-EN 1993-1-9. However, tests done in the SIROCO projects have also shown that the slip factor is dependent on the level of preload. It is theorized that the larger preload force could lead to more creep in the coating surface and more flattening of the plate surface, potentially reducing the friction coefficient (European Research Commission, 2018). This means that lower preload levels potentially result in higher friction coefficients, even though there is still a net decrease in capacity. This could prove valuable because limiting the preload to the elastic range opens up options for reuse.

Slip load and corresponding displacement

The slip load can be determined according to EN1993-1-8 or by means of the slip test as defined in EN1090-2. According to these codes, the slip load is defined as the maximum load before or the load at a slip of 0.15mm. The slip displacement is taken as the displacement where the slip load occurs, illustrated in Figure 31 (European Committee for Standardization, 2018).

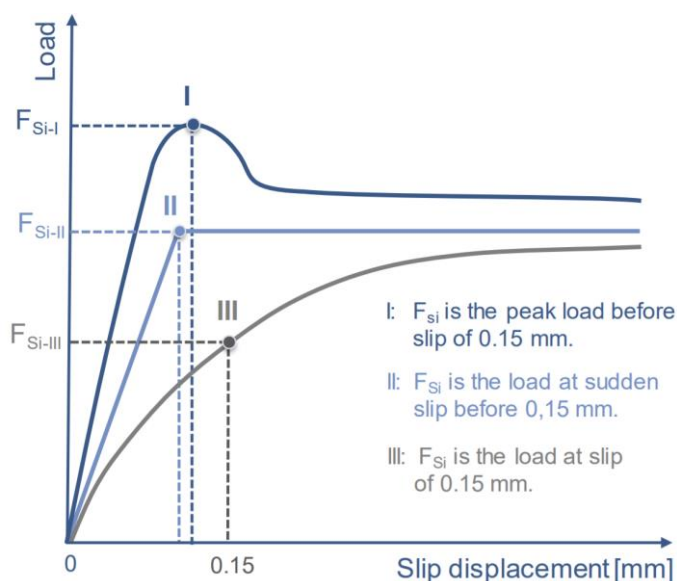


Figure 31: Method for determining slip load from test (European Research Commission, 2018)

This criterion can be questioned since this fixed value does not have any physical background. In fact, the load-displacement behaviour depends on the coating system that is applied and the size of the specimen. This is exemplified in Figure 32 (European Research Commission, 2018). Here it can be seen that some coating systems have already had their peak load before the 0.15mm, while other systems respond differently and only attain their maximum capacity at displacements in the range of 0.25-0.35 mm. The initial stiffnesses of the specimen also vary quite significantly depending on the coating system. No current design code or modelling technique available seems to make any distinction between coating systems except for their impact on the friction coefficient.

This simplification does not pose large problems in determining the resistance of the connection, but when the (pre-slip) force-displacement behaviour of the slip-resistant connection is being investigated it is clear that a distinction between different coating systems might very well be necessary.

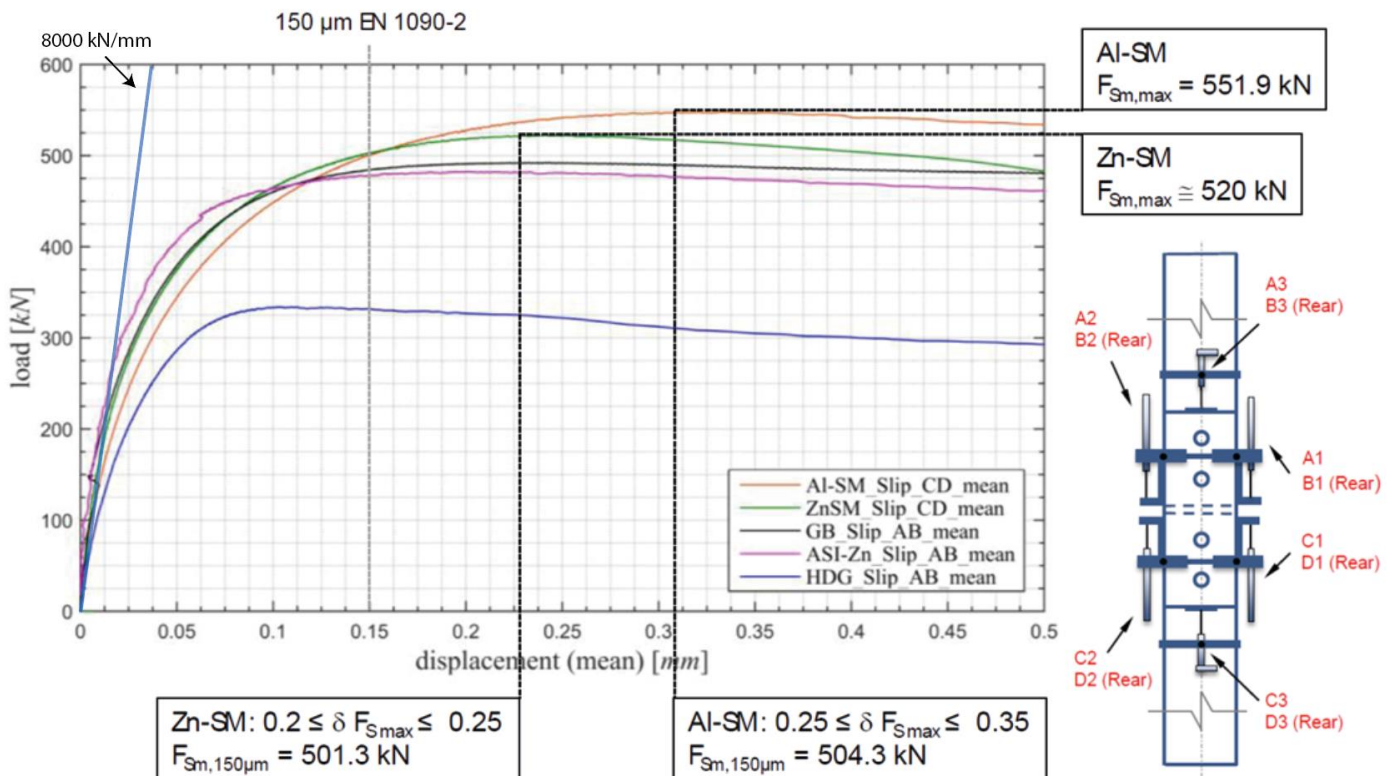


Figure 32: Influence of coating system on load-displacement behaviour (European Research Commission, 2018).

Connection stiffness

The connection stiffness is a topic that has not attracted extensive attention in research and norms. The design resistance of a category C connection (slip resistant in ULS) is simply found by multiplying the number of bolts by the design slip resistance of a bolt (European Committee for Standardization, 2011). Furthermore, the stiffness coefficient of preloaded bolts in shear is defined as infinite in EN1993-1-8 table 6.11.

Based on slip tests done on preloaded bolted assemblies, it can be seen that the stiffness is finite and non-linear. Shown in Figure 32 and already noted is the fact that the connection stiffness is dependent on the coating system. Despite the large non-linearity, it can be informative to estimate the stiffness at different displacement levels. Based on the force-displacement curves from the different coating systems, the initial stiffness of an M20 prestressed bolt in a double-lap connection is estimated as:

$$k_{ini} \approx \frac{400 \text{ kN}}{0.025 \text{ mm}} * \frac{1}{2} \approx 8000 \text{ kN/mm}$$

Where the factor $\frac{1}{2}$ originates from the assumption that the 2 bolts from the slip test contribute equally to the stiffness. With the same line of thinking, the stiffnesses at some other displacement levels can be very roughly estimated as $k_{0.01mm} \approx 4000 \text{ kN/mm}$, $k_{0.05mm} \approx 1000 \text{ kN/mm}$ and $k_{0.1mm} \approx 0 - 100 \text{ kN/mm}$ (depending on the coating system).

Ultimate capacity

When the slip capacity of a preloaded bolt is reached, the connection will slip and turn into a bearing type connection. Once the bearing mechanisms starts, load will be transferred through the contact between the bolt shank and the plate. This causes very high compressive stresses close to the contact area, as well as a tensile arc that forms in the plate in order to resist this tensile stress. Final failure may either be at the edges of this arc, in the bolt or in the net cross-section (Može, 2018). Bearing failure is a complex phenomenon dependent on many aspects such as the plate geometry, edge spacing, bolt spacing and the steel quality (Može & Beg, 2011). Furthermore, by the time joint failure occurs, almost all of the initial clamping force has dissipated due to the shear deformation in the bolt and plate yielding (Kulak, Fisher, & Struik, 2001). It is thus stated that the ultimate shear strength of the bolt is not dependent on the amount of preload.

Bearing through the resin layer

Bearing of the resin is the other type of force transfer that can be expected. Due to the fact that there is no cavity between the bolt and the plates, the plates will have to compress the resin in order to move relative to each other. This is visualized in Figure 33. The behaviour of the injection bolted connections is highly dependent on the bearing stresses in that occur in the resin, but the stress distribution and behaviour of the resin layer is not well understood (Koper, 2017).

From 2014-17 the RFCS project SIROCO carried out a lot of research regarding slip-resistant connections (European Research Commission, 2018). Task 3.2 of the project concerned the use of injection bolts but focussed mainly on non-preloaded bolts. It was found that there is a poor correlation between the mechanical properties of a resin and its performance in injection bolts. Instead, the pot life and viscosity of the resin are the most important parameters of a resin, and a proper injection procedure is the most important aspect for a successful application (European Research Commission, 2018).

This review will focus on the product RenGel SW 404 + HY2404, since it is the most often used resin and shows a good behaviour compared to other products (Koper, 2017). It is also the resin that has been applied for the Suurhoff strengthening. This section will give a short overview of the topics relevant to the bearing force transfer: The Young's modulus, bearing strength, and the force-displacement behaviour.

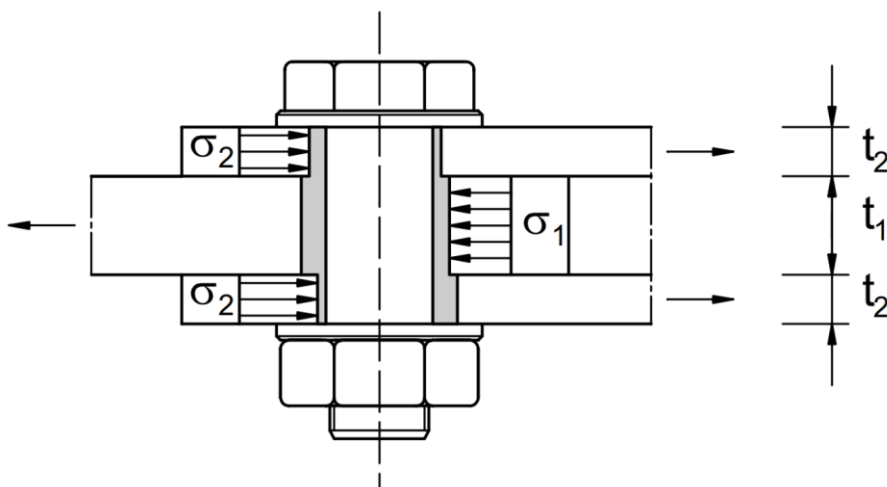


Figure 33: Visualisation bearing stress transfer (European Committee for Standardization, 2011)

Young's modulus

According to the product sheet, the Young's modulus for the resin is equal to 9.0-9.5 GPa (Inter-Composite, 2021). The Poisson's ratio is usually assumed around 0.3 (Epotek, 2011). However, tests and modelling work have shown that the Young's modulus can differ from this value significantly.

Quasi-static uniaxial compression tests done in (Nijgh, Xin, & Veljkovic, 2019) found a Young's modulus of 5.64 GPa, quite different from the product specifications. Research by (Koper, 2017) has calibrated analytical experiments to fit test data, focussing on different L/d bolt ratios. The analytical model uses a Timoshenko beam to represent the bolt and distributed springs to represent the resin. A Young's modulus of 7.5 GPa was found as a best fit. In (Nijgh M., 2017), a FEM model is made to verify double shear-lap tests on injected bolts, and he found a Young's modulus of 4.25 GPa as a best fit. In research by (Kortis, 2011), a Young's modulus of around 5 GPa is reported.

From these examples it becomes clear that estimating the material properties of the resin is not a trivial task. Discrepancies in the found material properties between authors can be due to differences in modelling, geometry, boundary conditions or other factors.

Bearing strength

According to the RenGel SW 404 + HY2304 product sheet, the uniaxial compressive strength is equal to 110-125 MPa (Inter-Composite, 2021). A similar value was found in quasi-static uniaxial compressive tests from (Nijgh, Xin, & Veljkovic, 2019). In (Nijgh M. , 2021), an ultimate compression strength of 170 MPa is found.

In preloaded injection bolts, the resin is confined between the bolt and the plates which has a large impact on the behaviour of the resin. To illustrate the impact of the confinement: A cylindrical confined resin sample tested in (Nijgh M. , 2017) showed a compressive strength of 412 MPa; significantly larger the 110-125 MPa that is stated in the product sheet. It is clear that the confinement causes a large increase in compressive strength compared to the uniaxial compressive strength.

Besides the ultimate bearing strength, the distribution of the bearing stresses is also of importance. For connections with $L/d < 3$, the bending deformation of the bolt is assumed small enough to neglect and the bearing stress is assumed uniform (European Convention for Constructural Steelwork, 1994). The distribution of bearing stresses in long bolts is shown in Figure 34. (Koper, 2017) has shown, using the analytical Timoshenko beam model, that even for an l/d ratio of 3 the peak stress in the resin layer is 33% larger than the average stress. This average stress is simply found trough the following relation:

$$\sigma_b = \frac{F_{ext}}{t_p * d_b}$$

Where:

F_{ext}	=	External force applied on the specimen	[N/mm ²]
t_p	=	Plate thickness	[mm]
d_b	=	Bolt diameter	[mm]

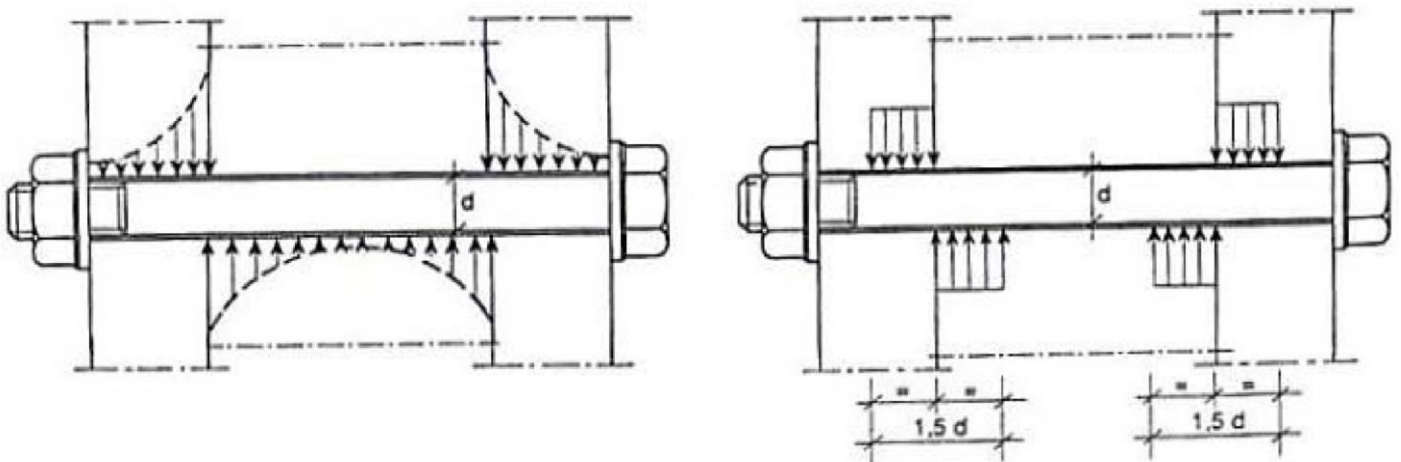


Figure 34: Bearing stress distribution in long bolts (European Convention for Constructural Steelwork, 1994)

The (average) bearing strength of resin has been the focus of multiple studies, with long-term values ranging from 175 MPa (European Research Commission, 2018) to 200 MPa (Gresnigt, Beg, & Bijlaard, 2012). It also has to be noted that there are significant differences between the long-term and short-term bearing strength, with the latter being closer to 280 MPa according to (Gresnigt, Beg, & Bijlaard, 2012). This bearing strength is usually defined as the bearing stress that is activated at a 0.15mm displacement as this defines the slip resistance.

Force-displacement behaviour

Now that the Young's modulus and bearing strength are discussed, it is also interesting to look into the more general force-displacement behaviour of the connection. Two force-displacement graphs of a slip tests on injected bolted specimens from literature can be seen in Figure 35.

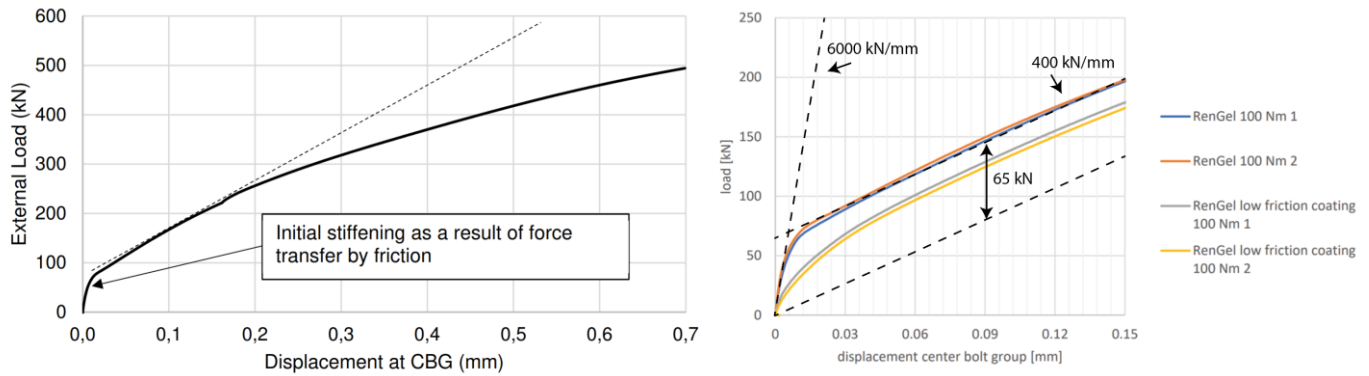


Figure 35: Force-displacement behaviour injection bolted connection left: (Nijgh M. , 2017), right: (Koper, 2017)

Even without preloading, there seems to be a large initial stiffness due to force transfer by friction. This can clearly be seen in the right graph, where a low-friction coating is applied as a comparison. This causes the effect of the friction force transfer to be much less and isolates the force transfer through bearing of the resin.

It can also be noted that even in injected connections, friction between the plates contributes significantly to the slip resistance at 0.15. From the right graph Figure 35 it can be seen that when fastening the bolts with a torque of 100 Nm ($F_{p,c} \approx \frac{T}{Kd} \approx 25kN$ (Crocco, de Agostinis, & Vincenzi, 2011)), the friction of the plates increases the resistance by about 60 kN, which is almost 1/3rd of the slip resistance of 200 kN at 0.15mm. Guidelines therefore prescribe tightening the bolts to a torque of 30Nm, stating that at this level the friction resistance can be neglected (European Convention for Constructural Steelwork, 1994).

After this initial stiff response due to friction, the stiffness response seems far more linear than for preloaded connections, and the connection stiffness can be estimated between 0.05 - 0.15 mm. Authors report a stiffness around $k = 1000 kN/mm$ (Nijgh M. , 2017) (Koper, 2017) using the EN1090-2 test setup (2 bolts). Furthermore, the impact of the location of the bolt in the hole has been addressed by (Nijgh M. , 2017). He has found that, for regular hole clearances, the stiffness is 22% lower when the bolts are located in the most onerous position (maximum resin thickness) compared to when the bolts are randomly placed in the holes. This reduced the stiffness to $k = 770 kN/mm$. (Gresnigt, Beg, & Bijlaard, 2012) report a 14% decrease in capacity at 0.15mm when placing the bolts in the most eccentric position. Moreover, (Koper, 2017) examined the influence of the bolt l/d ratio, showing that for an l/d ratio of 3 and 4, the stiffness is significantly lower at around $k = 600 kN/mm$, while also having the bolt in the most onerous position. Research by (Nijgh M. , 2017) showed that the bolt hole clearance also has a significant influence on the stiffness, with oversized and slotted holes showing a lower stiffness.

Small air inclusions or improper execution of the injection procedure can also result in jumps in the force-displacement behaviour (Koper, 2017). This stresses the importance and necessity of proper execution that is needed in order to gain confidence in the behaviour of the connection.

It also has to be noted that these connection stiffnesses are again obtained using the EN1090-2 test setup, which means that the response is the result of two bolts. The stiffness of a single bolt can be assumed to be half of this, thus in the range of $k \approx 300 - 500 kN/mm$.

Ultimate capacity

What can also be seen in Figure 35 is that contrary to prestressed connections, injected connections do not reach their capacity around 0.15mm and show much more deformation capacity. They also have no clear slip plateau due to the presence of the resin. To illustrate this point, (Nijgh M. , 2017) conducted testing on specimen with geometry according to EN1090-2 but with only 1 bolt in the end-hole of the centre plate (due to limitations of the testing rig). The specimen were loaded up to failure, and the force-displacement can be seen in Figure 36. The specimen with normal hole clearance fails in a combination of bearing and cleavage and is thus governed by the resistance of the plate and not of the bolt. It can be seen that there is no slip plateau and a lot of deformation capacity in the development of this failure mode.

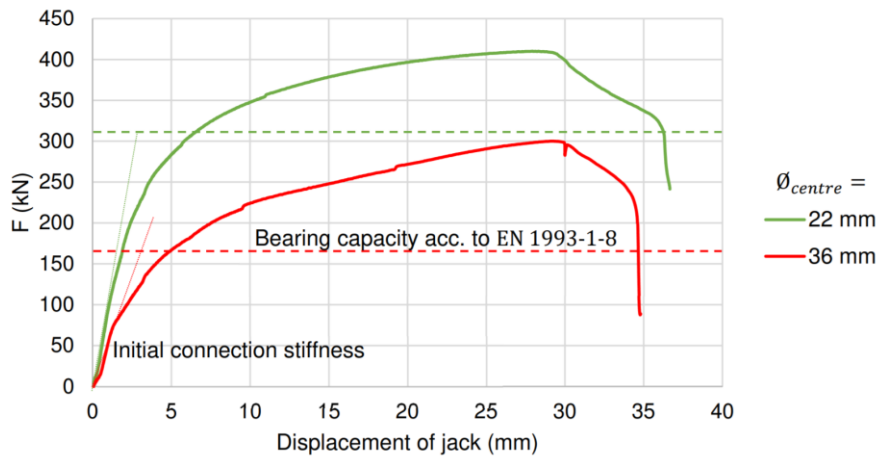


Figure 36: Ultimate failure tests injected bolts (Nijgh M. , 2017)

It can be theorized that the 0.15mm displacement that determines the resistance of the slip-resistant connection is based solely on preloaded bolted connections (European Committee for Standardization, 2018). It does not conform with the force-displacement behaviour of injection bolts, for which the 0.15mm limit seems very arbitrary. Depending on the deformation limits and fatigue considerations for the specific application, assessment of the capacity of injected bolted connections could very well be improved and the design resistance increased.

Interaction between the mechanisms

In preloaded injection bolts, the force is transferred by both of the previously described mechanisms. However, relatively little research is carried out about the exact interaction between the mechanisms. This section will present an overview of the literature available and a reflection on the knowledge gaps that still exist.

Force-displacement behaviour

Even though there are very little tests done on preloaded injection bolts, a number of authors have commented on the behaviour. There seems to be a consensus among authors (e.g. (Pedrosa, Correia, Rebelo, Veljkovic, & Gervásio, 2021) that in preloaded connections, the force transfer will initially be through friction of the bolt. The bearing of the resin is reportedly only activated once the friction resistance is overcome (Nijgh M. , 2021). None of the authors seem to give a physical explanation for this. Perhaps this is based on observations from tests on injected bolts, as shown in Figure 35, that clearly show that there is a stiff initial response due to friction even when the bolts are not preloaded.

The only comparisons in literature to the author's knowledge are from tests done at the university of Ljubljana (Rugelj, 2008) (Gresnigt, Beg, & Bijlaard, 2012). Tests are done on preloaded connections, injected connections, and preloaded injected connections. The results are shown in Figure 37.

It can be seen that for the first 0.05mm, the preloaded connection has a nearly identical response to the preloaded injected connection. The curves then start to diverge, and around 0.1-0.15mm the curves of the injected bolted connection and the preloaded injected bolted connection seem almost parallel.

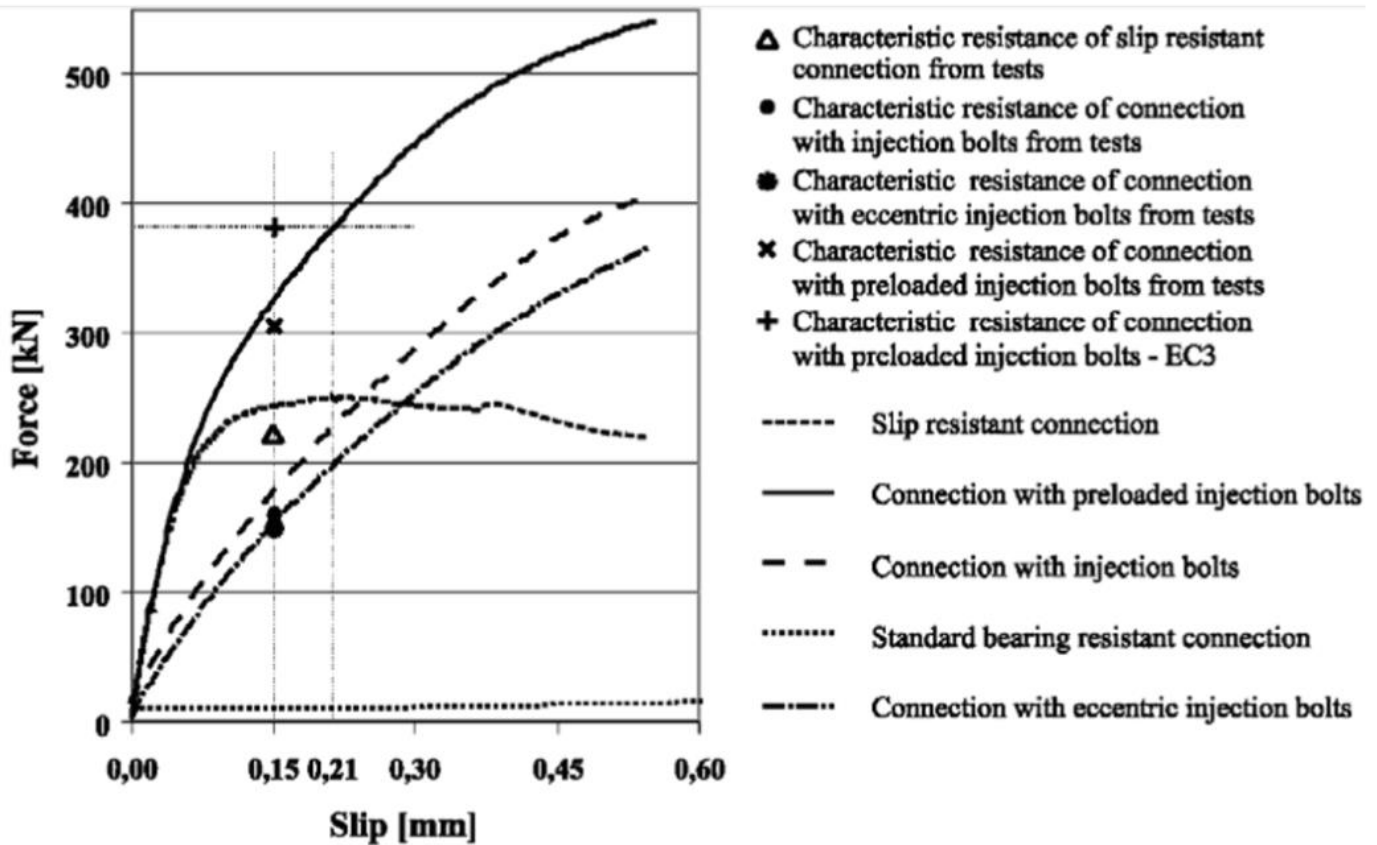


Figure 37: Slip tests comparing preloaded, injected and preloaded injected connection. Test setup according to EN1090-2, $\mu = 0.33$. (Gresnigt, Beg, & Bijlaard, 2012)

As can be seen in Figure 37, one of the conclusions made in the study was that it seems that the summed resistances of the preloaded and the injected bolts is larger than the resistance of the preloaded injection bolt (Gresnigt, Beg, & Bijlaard, 2012). The authors do not seem to have any explanation for this.

The discrepancy could be explained by the fact that when testing injected connections, as was shown in Figure 35, it is impossible to eliminate the friction force transfer mechanism and it can contribute a significant amount to the resistance. When summing the test results the resistance can thus be overestimated as the contribution by friction in the injected bolted connection should not be counted. The authors do not state the amount of torque applied when tightening the injection bolts.

When assessing the results shown in Figure 37, this effect does seem to exist, but to a lesser extent than in Figure 35, which could imply that a small torque is used. The friction in Figure 37 seems to account for only around 10% of the slip resistance of the injection bolt, indicating a proper torque of 30Nm.

Another possible reason for the discrepancy could be a loss of prestress due to the shear deformation in the bolt. Preloaded connections lose their prestress when the force starts to transfer through bearing. Because in preloaded injection bolts the bearing already occurs from the very start, it could be theorised that this leads to prestress losses due to shear deformation in the bolt shank. This would also explain a possible overestimation of the slip capacity when summing the individual resistances. This shear deformation would however be difficult to measure during testing and requires a very detailed FE model to simulate. To the author's knowledge, no literature has addresses or identified this issue in preloaded injection bolts.

Ultimate capacity

To the author's knowledge, no research has been done on the ultimate capacity of preloaded injection bolts. However, based on the knowledge of preloaded and injected bolts, one could argue that the ultimate capacity is governed by the same failure mechanisms as the preloaded and the injected bolt; either shear failure in the bolt or bearing failure in the plate. Since the ultimate shear capacity of the bolt is independent of the preload force, the ultimate capacity for preloaded injection bolts can be assumed similar to that of non-preloaded injection bolts.

2.7.2. Finite element modelling of preloaded injection bolts

Finite element modelling of bolts can be done using a wide array of options. This ranges from simple spring models to bolts modelled in solid elements. This section will first cover the spring model, after which more advanced modelling methods are discussed.

Spring models

Proper modelling of a bolted connection can be very laborious and require a lot of computing power. This is not feasible for example in a global FEM model containing a lot of connections. The most common solution is then either to make a rigid restraint or to simplify the connection as one or more springs. Especially in connection with multiple bolts, having a rigid restraint will cause a very unfavourable load distribution between the bolts, and a spring model is much preferred. This section will therefore focus on the application of spring models for preloaded injection bolts.

When looking back at the force-displacement behaviour that was discussed in section 2.7.1, it can be seen that determining a linear spring stiffness will be very difficult as the response is very non-linear. A good estimate is only possible when the deformations can be predicted accurately. Otherwise, it is important to realise whether a stiff or flexible spring is the most onerous (or perhaps both for different components) and take a conservative value.

Increasing the complexity, a non-linear spring model can be used. This can predict the force-displacement behaviour a lot more accurately, but it can pose problems with computing power in large FEM models. It is nonetheless valuable in smaller scale models to approximate the force-displacement behaviour. The models will need to be validated and calibrated by tests in order to gain confidence in the results.

The main issue with these models is that because the force-displacement behaviour is completely determined by the user input, the behaviour needs to be very well known in advance in order to be confident in the results. The impact of important influencing parameters needs to be known and put in the spring model in order to be able to accurately apply it on situations other than the one it was calibrated for.

For preloaded connections, some of these models do exist. One of these is the spring model proposed in the preliminary NEN8703, given in Figure 38. The force-displacement behaviour in the first 0.125 mm is given by:

$$\delta = 0.1 * \left(\frac{F}{F_{slip}} \right)^4 + 0.025 * \frac{F}{F_{slip}}$$

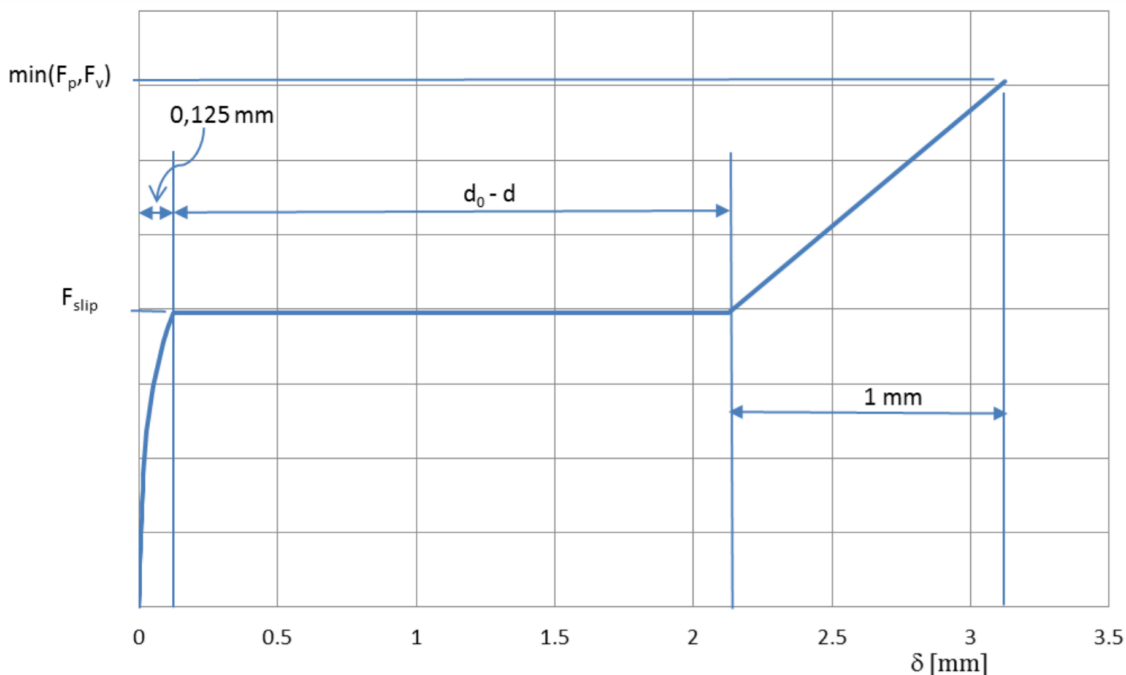


Figure 38: Spring model double-lap preloaded bolt (TNO, 2017)

In general, the behaviour seems to match test results with a large initial stiffness. The initial stiffness of the model is equal to 8000 kN/mm for a slip capacity of 200 kN per bolt. However, this equation does not consider any influence of important parameters such as the type of coating system. The bolt is assumed to be in the most onerous position and the deformation capacity from the initiation of bearing is only 1 mm whilst a bearing failure has significantly more deformation capacity.

In Figure 39, the first 0.125mm according to the spring model is overlaid on test results on different coating systems (Note that the slip tests have 2 bolts per connection while the spring models covers 1 bolt, so the results have been scaled by 2). For most coating systems, the curve approximates the behaviour well. However, for some, most notably the ASI and ESI coating systems, the curve does not match the test results very well and the stiffness of the connection is considerably underestimated at larger displacements. Furthermore, a lot of literature has also pointed out that in practise, the slip will be significantly lower than the maximum possible value (Kulak, Fisher, & Struik, 2001).

Care also has to be taken when combining this spring model with the EC guidelines. When taking the slip capacity according to the Eurocode instead of the characteristic value from test results, the stiffness will be significantly underestimated.

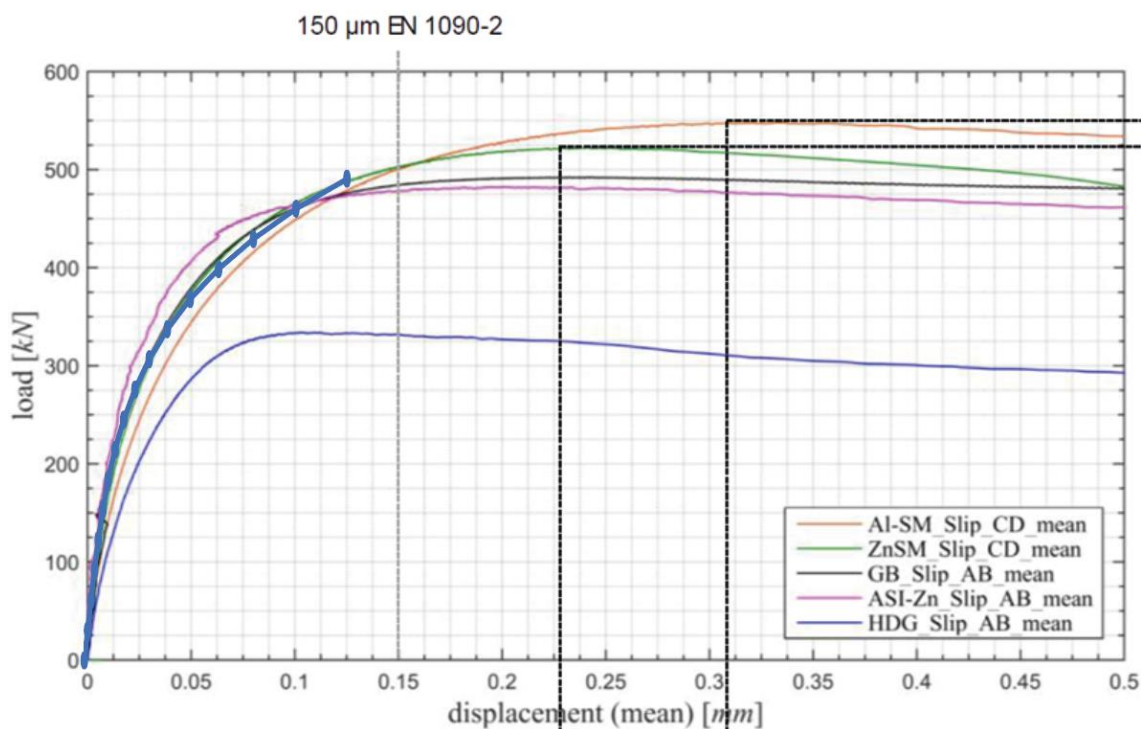


Figure 39: Comparison of spring model with test results (test results from (European Research Commission, 2018))

For injected connections, linear spring modelling is already quite accurate since the force-displacement behaviour is a lot more linear, at least for displacements below the slip capacity.

FE modelling

In order to gain the most insight into the behaviour of the connection, advanced finite element modelling remains the most accurate modelling approach. This can provide much more detailed information into the stress distribution, deformations and even failure mechanisms.

The flipside is that in order to get accurate results, detailed models that require a lot more computational power are required. Such complicated analysis can also lead to numerical problems such as singularities, negative eigenvalues, rigid body motion or extensive elongation of bolts after pretension (Krolo, Grandić, & Bulić, 2016).

Advanced bolt modelling has been implemented in various research in the past. A lot of powerful software packages are available such as Abaqus and LS-DYNA. Both offer various implicit and explicit solvers and option for dynamic and non-linear simulations. Because of Arup's affinity with LS-DYNA and due to licensing reasons, this thesis will focus on modelling in LS-DYNA. Since there is very limited research done on preloaded injection bolts, the following paragraphs will mostly focus on preloaded bolts and injection bolts separately.

Different FE modelling approaches exist for the modelling of preloaded bolts. There are simplified approaches that try to model the bolt shank with beam elements, the bolt head and nut with rigid shells, and use discrete spring elements to connect the bolt to the plates. More detailed modelling uses solid elements for the bolt shank and contact interaction to simulate the interaction with the plates (Narkhede, Lokhande, & Gaddekar, 2010). For the modelling of contact interfaces, a surface-to-surface discretization method minimises errors since it considers the shape functions of both the slave and the master surfaces (Abaqus FEA, 2021).

An intermediate approach is to simulate the shank with beam elements which are attached to radially arranged beam elements representing the bolt head and nut, also known as a spider mesh. This eliminates the need for contact interfaces but cannot model failure modes that require accurate representation of the bearing stresses (Hadjiannou, Stevens, & Barsotti, 2016). Still another approach that tries to combine the advantages of the beam spider connection with proper bearing stress representation is to model the bolt head with shell elements that are connected to beam elements representing the bolt shank. This shank can then interact with the bolt hole through null beams (Sonnenschein, 2008). This model however is still not capable of properly capturing failure modes.

A lot of preloaded bolt modelling in LS-DYNA is related to crash tests, in which large deformations and failure mechanisms are of big importance. These often use advanced material models such as the Johnson-Cook model, a temperature and strain-rate dependent flow-stress model, to describe the evolution of the yield surface (Johnson & Cook, 1983). Alternative, simpler options include the LS_DYNA cards *MAT_PIECEWISE_PLASTICITY or *MAT_PLASTIC_KINEMATIC that can also properly describe material behaviour (Narkhede, Lokhande, & Gaddekar, 2010) (Karajan, Schenke, Borrvall, & Pydimarry, 2018).

A big advantage of using solid elements compared to simplified approaches is such that advanced material models can be used to predict damage (Stopel, Cichański, & Skibicki, 2017). However, prediction of fracture in steel components, especially in high strength steels such as bolts, is not straightforward. Fracture initiation can generally be modelled in two ways; either by relating failure to the stress and/or strain levels in the bolt, or by incorporating the fracture initiation criterion and damage evolution laws directly into the model (Hedayat, Afzadi, & Iranpour, 2017). These modelling approaches however go beyond the scope of this thesis and will not be discussed in more detail here.

The introduction of the prestress for solid elements can be done through the *INITIAL_STRESS_SECTION option in LS-DYNA (DYNAmore GmbH, 2021). This implicitly captures any loss of prestress due to shear deformation and plate yielding. Models on preloaded bolts seem to almost always neglect the bolt thread since it is not in the shear plane.

FE modelling of injection bolts has attracted much less attention compared to preloaded bolts. In (Nijgh M. , 2021), FEA on resin injected connections was done in Abaqus using solid elements. All features of the connections were modelled, even the threads of the bolt. This could be necessary to properly model the contact interactions and the failure mechanisms (Pavlovic, Markovic, Veljkovic, & Budevac, 2013). The modelling of the thread is more important in injected bolts since this is the area where most of the load-transfer takes place, as opposed to preloaded connections where the load-transfer is mainly through friction, and the failure takes place in the shear plane that usually does not have a thread. For the epoxy resin, the Drucker-Prager material model, describing a pressure dependent yield surface, is used (Nijgh M. , 2021). This model seems to correspond fairly well with experimental results.

3. Strengthening design

Arup has designed an innovative strengthening scheme which improves the fatigue performance of the bridge deck and extends the design life of the bridge by at least 15 years.

This chapter will present the new strengthening scheme that will be applied. Chapter 3.1 will cover the general info regarding the strengthening scheme and section 3.2 will present the different elements of the scheme. The subsequent subchapters will each cover an important aspect of the strengthening design. Chapter 3.3 discusses the preloaded injection bolts and 3.4 will cover the epoxy layer. Chapter 3.5 will cover the fatigue design. Lastly, chapter 3.6 discusses the future design optimisations.

3.1. Background renovation technique

In an attempt to preserve the advantages and reduce some of the associated risks, this strengthening scheme builds upon the existing strengthening method of a bonded plate, which was discussed in section 2.5. As with the bonded plate solution, a steel strengthening plate is placed on top of the existing deck plate with a layer of epoxy in between. However, preloaded injection bolts are also used to connect the strengthening plate with the deck plate and help with the transfer of shear forces. Using bolts alongside with the epoxy layer reduces execution and durability risks and improves the resistance against shear loading between the plates.

In contrast to the bonded plate solution, vacuum injection is not the preferred solution for this scheme because of the added bolt holes and the relatively slow execution speed of this solution. Pressure injection is instead the preferred technique. Due to the risks associated with such an innovative renovation, the design was made so that composite interaction is not necessary to reach the desired design life. This means that a relatively thick strengthening plate was needed for this pilot (30 mm). Nonetheless, this is a lightweight solution that can also be swiftly executed, which makes it an attractive alternative to the current strengthening schemes used by Rijkswaterstaat (HSC and a bonded plate). An impression of the strengthening approach can be seen in Figure 40.

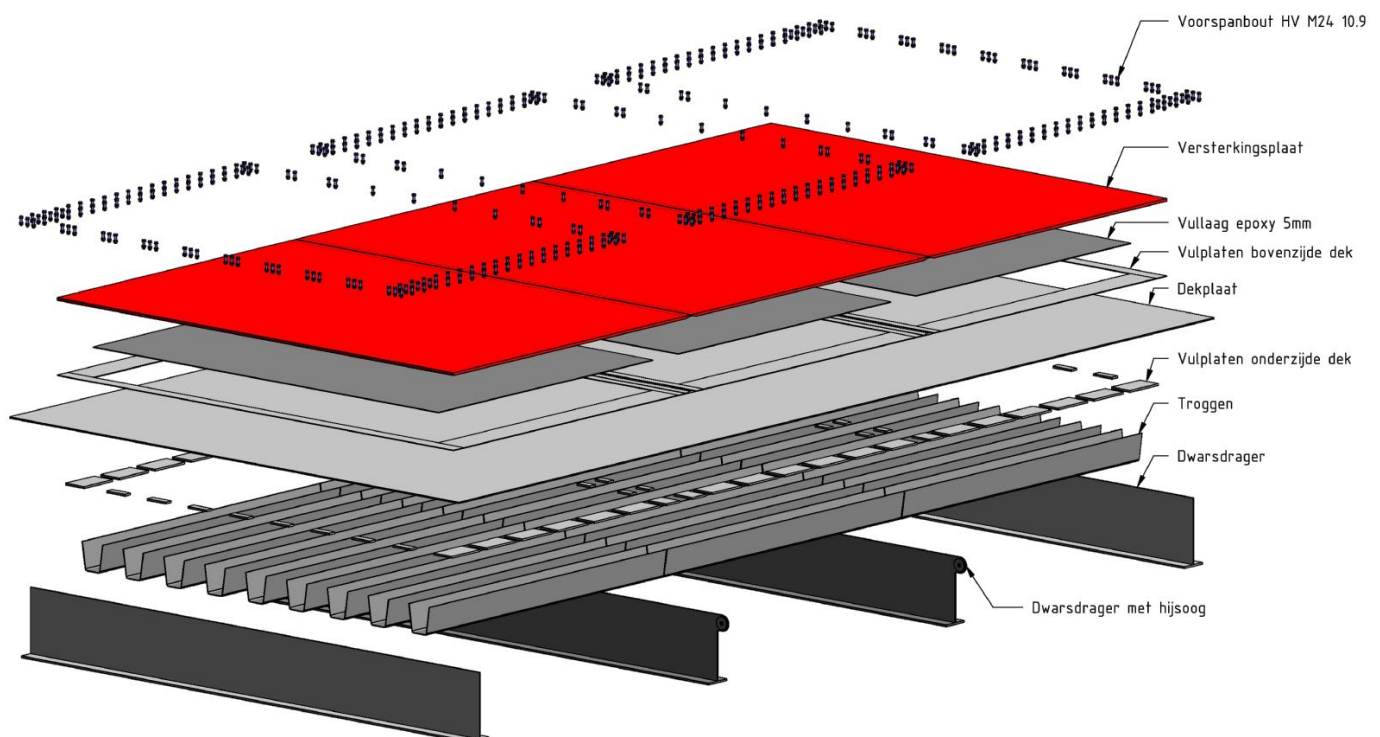


Figure 40: Overview strengthening solution

This strengthening scheme was initially designed by Arup as one of the strengthening options for the 2nd Van Brieneoord bridge. Considering the risks of a new strengthening approach and the importance of the Van Brieneoord bridge connection, Rijkswaterstaat decided not to apply it on that project. It did however acknowledge the potential and encouraged further research in order to apply the scheme in a smaller project.

During a routine inspection in 2018, it was found that the movable part of the existing Suurhoff bridge developed fatigue damage in the orthotropic deck structure. In the summer of 2020, it was decided that the movable Suurhoff bridge needed strengthening, and Arup decided to propose the new strengthening solution again. This time Rijkswaterstaat agreed with the proposal and decided that the strengthening needed to happen at the same time as the fixed bridge renovation in the summer of 2021.

The Suurhoff bridge provides access to the Maasvlakte and is therefore an important piece of infrastructure in the port of Rotterdam. The bridge over the Hartelkanaal is part of the A15 and before the renovation consisted of two traffic lanes in both directions. Furthermore, there is a train connection next to the traffic bridge. The traffic bridge was constructed in 1972 and is experiencing significant fatigue damage in the deck structure.

The Suurhoff bridge has an orthotropic deck plate with discontinuous troughs. This means that the damage in the deck plate and the development of fatigue cracks is hard to predict compared to a bridge with continuous troughs (MC Renovatie Bruggen, 2021). Rijkswaterstaat decided that the bridge will be replaced around 2030, and that a strengthening is needed in order to elongate the service life of the bridge by 15 years. To this end, as is shown in Figure 41, a number of interventions are carried out, among which the placement of an extra arch bridge that will elevate the current bridge of half of its traffic load. Furthermore, the current bridge is repaired. The focus of this thesis however is on the bascule bridge, which will be renovated by the aforementioned technique.



Figure 41: Overview strengthening interventions Suurhoff bridge (Rijkswaterstaat, 2021)

In order to mitigate risks as much as possible, a risk-based design approach was adopted. In collaboration with the client (Rijkswaterstaat), all risks associated with the design and execution of the renovation were collected, documented, and shared from an early stage. This risk register forms the basis of the design, which will aim to reduce the risk level as much as possible. An excerpt of this risk register is presented in Table 2. This transparent and collaborative way of designing was very beneficial with convincing the client of the safety and advantages of the innovative design.

Table 2: Excerpt risk register

Risk Description	Initial risk	Updated risk	Mitigation measures	Type of measure	Section design report	Status
Debonding due to traffic loading resulting in no composite action and possible fatigue of epoxy	High	Low	Consequence of debonding is small since bolts are designed to take full shear load	Design report	3.1	Complete
			Use application method that results in good execution quality	Small scale test	6.3.1	Complete
			Use appropriate surface prepare and paint system	Small scale test	6.3.1	Open
			Verify installation quality on small scale testing using: <ul style="list-style-type: none"> • UT scans • Destructive testing 	Small scale test	6.3.1	Complete
			Verify installation quality on yard test using: <ul style="list-style-type: none"> • UT scans • Destructive testing 	Yard test	7.4	Complete

3.2. Strengthening elements

This section will shortly go over all the important strengthening elements in some more detail. A 30 mm strengthening plate is placed on top of the 14 mm deck plate in order to stiffen the deck. A 5 mm epoxy layer is injected in between these steel plates to eliminate any unwanted effects from out-of-flatness of the steel elements. Furthermore, it provides the vertical load transfer between the strengthening plate and the deck plate. In future applications this epoxy layer can also help with the transfer of shear forces but to reduce risks this shear transfer is not accounted for in the verification of the steel elements during this renovation. A product called GreenPoxy is chosen as the epoxy of choice, based on a testing programme which will be discussed in section 3.4. An Edilon primer is chosen for the bond between the adhesive and the steel. The epoxy layer is present everywhere except over the cross-girders and on the edges of the bascule bridge. Here, steel filler plates are used to prevent huge prestress losses in the preloaded injection bolts which are located at these locations. The filler plate and the deck plate in the vicinity of the bolts are prepared using Thermally sprayed Aluminium (TSA). This results in a slip factor of 0.4 according to EN1090-2 (European Committee for Standardization, 2018), but larger slip coefficient have been observed using this technique (European Research Commission, 2018). The bolts are countersunk since there is no asphalt layer on the bascule bridge. S355 steel is used for all components, and HV M24 10.9 bolts are applied in combination with Araldite injection material. Over the cross-girders, the strengthening plate splices are located. Here, a backing strip is applied, and the strengthening plates are welded together as can be seen in Figure 42. Finally, an epoxy wearing surface is applied over the bridge.

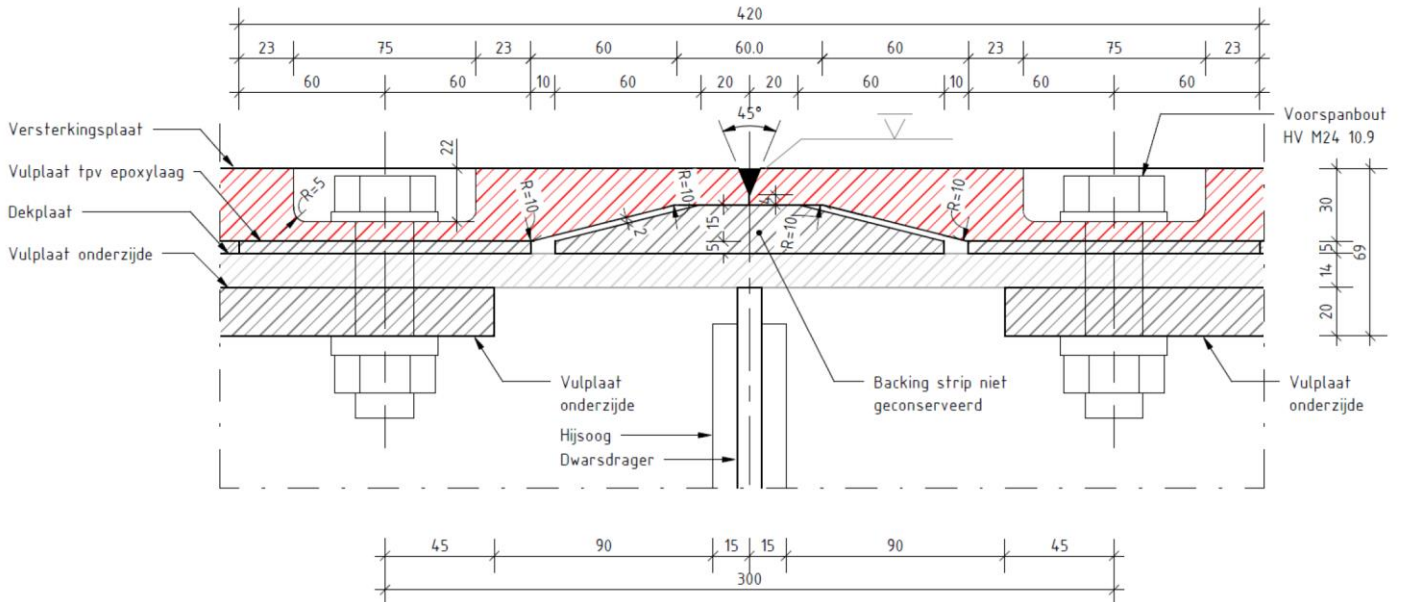


Figure 42: Strengthening plate welded splice (MC Renovatie Bruggen, 2021)

3.3. Preloaded injection bolts

In the strengthening scheme, a total of 1870 preloaded injection bolts are applied to tie the deck plate and the strengthening plate together. These are conservatively designed in order to take up all shear forces, i.e. no shear transfer through the epoxy is accounted for in the verification of the bolts and steel. Furthermore, since the bolts are highly utilised, any prestress loss was not deemed acceptable, and the bolts were elongated to limit any prestress loss.

This section will now shortly focus on the static strength verifications of the bolts.

First, the ULS capacity of the M24 bolts was determined based on NEN-EN1993-1-8, meaning that the capacity of the preloaded injection bolt is taken as the sum of the capacities of the preloaded bolt and the slip strength of an injected bolt. Despite a TSA friction being classified as in class B (friction coefficient 0.4 according to NEN-EN 1090-2), several studies have shown that a significantly higher friction coefficient can be achieved. Therefore, in accordance with the new tentative NEN8703, a friction coefficient of 0.5 has been assumed. For the bearing strength of the Araldite injection, a value of 200 MPa has been taken. It is assumed that temperature loading falls somewhere between short-term and long-term loading, for which values of 225 and 150 MPa can be assumed according to NEN6788:1995 clause 20.3.6.2. The constant k_t is taken as 1.2 for short term loading (ULS). The slip resistance was then calculated according to NEN-EN1993-1-8 clause 3.6.2.2 (5) as:

$$F_{b,resin} = \frac{k_t k_s d t_{b,resin} f \beta_f f_{b,resin}}{\gamma_{M4}} = \frac{1.2 * 1 * 24 * 8 * 1 * 200}{1} = 46.08 \text{ kN}$$

$$F_{p,Rd} = \frac{k_s * \mu}{\gamma_{M3}} * 0.7 f_{ub} * A_s = \frac{1 * 0.5}{1.25} * 0.7 * 1000 * 353 = 98.84 \text{ kN}$$

$$F_s = F_{b,resin} * f_{p,Rd} = 144.92 \text{ kN}$$

The forces transferred through the bolts are largest due to temperature loading. These forces generated due to the temperature loading are high because of the insulating function of the epoxy layer between the two steel plates. Since the temperature profile is not exactly known, a very conservative temperature distribution was assumed. In line with NEN-EN 1991-1-5, NEN 6786-1 and NEN 8701, the most onerous temperature load case for the bolt design was determined. In discussion with Rijkswaterstaat, a conservative 20-degree Celsius jump at the epoxy layer was taken. The temperature profile resulting in maximum bolt shear forces is shown in Figure 43.

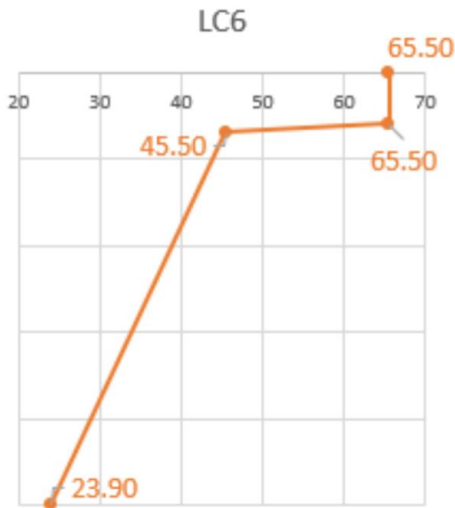


Figure 43: Profile of the temperature loading governing for shear force in the bolts (MC Renovatie Bruggen, 2021)

The next step is to determine the force distribution between the bolts. This has to be done through finite element simulation. In an early design stage, it was found that using the logic used in the design codes, prescribing an infinite stiffness to preloaded bolts in shear, results in unrealistically high forces in the bolts. It was therefore determined that the bolts need to be modelled slightly more sophisticatedly. To this end, shear springs in x and y direction are used to simulate the bolted connection. To determine the proper stiffness of the springs, the following steps were taken.

First of all, lab tests were used to assess the structural response and slip capacity of the preloaded injection bolts. Tests were done both on preloaded and preloaded injected specimens. It was found that using LVDT measurements, the injection provided a 25% increase in stiffness in the response. To then determine the shear stiffness, it is assumed that the injection and the friction act simultaneously, and slip is assumed to occur at 0.1mm. The stiffness is then simply taken as the secant stiffness, ignoring the non-linear response, as $144.92 \text{ kN} / 0.1 \text{ mm} = 1449 \text{ kN/mm}$. Furthermore, to investigate the influence of the stiffness on the maximum bolt force, a second analysis is done using a stiffness of around 16% less, 1220 kN/mm.

The maximum shear force found using ULS temperature loading with these springs was determined as 115.2 kN. Using the slightly lower stiffness of 1220 kN/mm, a maximum shear of 113.9 kN was found instead. This amounts to an increase of around 1% for an increase in spring stiffness of 16%. It is however hard to determine the relation between the increase in maximum bolt force and bolt stiffness without doing a more detailed sensitivity study.

3.4. Epoxy

Between the two steel plates, an epoxy product is injected in order to negate out of flatness effects. As was already discussed, for the design of all steel parts, this epoxy is not expected to transfer shear forces. Nonetheless, it would be beneficial if it did so as this would make for a much more optimised design. To this end, during the design, a lot of effort has gone into understanding the behaviour of the epoxy. To prove composite action will occur during the design life of the structure, it needs to be proven that no debonding will occur anywhere in the epoxy layer. Tests have been carried out in order to accurately determine the epoxy material properties, the results of which will be shortly discussed now.

Epoxy is a family of thermosetting plastics that is widely used in many applications as a coating, adhesive or part of a composite material. In the current application, the epoxy has the function of an adhesive and has to satisfy a few requirements. The viscosity of the chosen epoxy needs to be low enough so it can be injected properly in between the plates without any air gaps. Furthermore, it needs to have sufficient static and fatigue strength to prevent debonding of the plates for its service life. A large testing programme has been set up in order to choose an appropriate product and determine its material properties.

First of all, six products were initially selected as potential adhesives. Small execution tests were done on these products to check whether the texture and viscosity are acceptable. Due to reasons such as bad workability, foam development and a large pressure needed during injection, two of the six products were

rejected. Next, dolly tests, thermal cycle tests and three point bending tests were carried out to investigate the material properties. The chosen product, GreenPoxy, was chosen due to the following reasons:

- GreenPoxy has a low viscosity and a workable texture which is expected to result in a good execution quality
- GreenPoxy has a relatively large stiffness compared to the other products and therefore enables a greater stress reduction in the existing deck
- GreenPoxy does not require an elevated temperature to cure, resulting in an easier execution and less uncertainty in the final quality
- GreenPoxy is expected to have sufficient static and fatigue capacity based on the product sheet, but this will be further investigated

After choosing the adhesive product, more detailed testing is done to verify the material properties. The stiffness, Poisson's ratio, ultimate tensile strength and rupture strain are determined based on tensile tests. Since the material properties are material dependent, tests are done at different temperatures. Results can be seen in Table 3. On top of this, the thermal expansion coefficient for the material is determined as this is important in a composite structure subject to temperature loading. Based on five thermal expansion tests, the design value of the thermal expansion coefficient, which is taken as the mean value plus two standard deviations, is equal to $66.7 * 10^{-6} 1/K$.

Table 3: GreenPoxy temperature dependent stiffness

Temperature [°C]	E-Modulus [MPa]	Poisson's ratio [-]	Rupture strain [%]	Ultimate tensile stress [MPa]
-20	3639	0.364	2.027	45.5
-10	3618	0.361	1.963	34.3
+23	3205	0.386	5.459	70.9
+50	2717	0.384	4.670	56.5

In the structure, the behaviour of the composite layer is not only determined by the properties of the steel and the epoxy. The primer that is applied on the steel is also of importance, as is the interface between the steel and the primer and the epoxy and the primer. To determine the strength of the adhesive layer, as well as the failure mechanism, additional three point bending tests were carried out to verify this interface strength and the failure mechanism that occurs in the composite package. In these tests, debonding at the interface of the primer was observed at the failure load. Using a Scanning Electron Microscope, it can be concluded that the most likely failure mechanism is a cohesive failure of the primer. This is advantageous because an adhesive failure is much more difficult to predict as it is very dependent on the execution quality and time-dependent effects.

These tests were replicated in FE software to provide insights on the stresses in this critical layer. The stress at the location of the crack was 19.1 MPa, only 26% of the ultimate tensile strength. By subtracting the standard deviations, a shear stress (YZ) of 13.0 MPa is taken as the shear capacity of the epoxy layer. This lower-bound capacity is taken as the maximum allowable stress in the epoxy layer during static design verifications.

Lastly, fatigue tests were carried out on specimen with the GreenPoxy product, including the primer. The occurrence of the first crack is determined for different load level and S-N curves are constructed. Based on 12 test specimens, mean and design S-N curves were regressed as shown in Figure 44. In the two largest cycle tests, no fatigue damage seemed to occur after 500 000 cycles. When taking this value as the run-out, a fatigue threshold for shear stresses of the epoxy is determined as 7.11 MPa. Without any fatigue threshold, 5.4 MPa and 4.3 MPa are found as the maximum allowable shear stresses at 10^7 and 10^8 load cycles respectively. It is noted that these fatigue results correspond well with research from (de Freitas S. , 2012).

Now that sufficient knowledge and understanding of the material is obtained, this can be applied to the global FEM results. After analysis of results of the major load cases, it can be concluded that the risk of debonding is governed by temperature loading, which causes 3-4x larger stresses in the epoxy layer compared to traffic loading. The maximum in plane shear stresses act during a warm temperature load case and imposes a stress of 4.57 MPa on the bond line, below the static strength of the bond line. Furthermore, the minimum and maximum principal stresses that act on the epoxy layer are 26.44 MPa and 9.27 MPa respectively. This is also well below the tensile and compressive strengths at the corresponding temperatures. A more elaborate

discussion on the impact of the angle of the principal stress on possible debonding is also presented in the design report, but this will not be discussed here for brevity's sake.

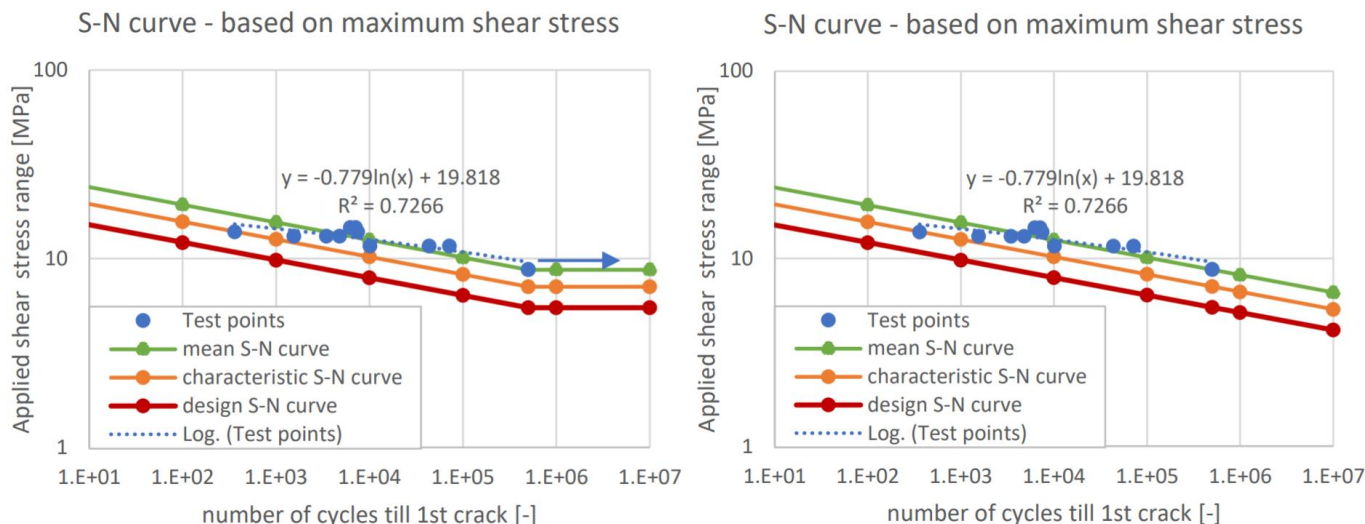


Figure 44: S-N curves for GreenPoxy with and without runout based on the maximum shear stress (MC Renovatie Bruggen, 2021)

To summarise, there were a lot of unknowns about the behaviour of the epoxy in the composite system. Throughout the design, extensive testing has significantly increased the understanding and confidence in the design. Furthermore, major steps have been taken to prove that no debonding will take place during the design life of the structure. If this will be accepted, then the design of the strengthening steel could be significantly optimised. This will be further discussed in section 3.6.

3.5. Fatigue

This section will describe the fatigue assessments that were done during the design of the strengthening scheme. The fatigue details of the existing deck plate are verified using the standard approach laid out in NEN-EN 1993-2-NB. An FE model is used to extract hot spot stresses in the proper locations. This is also done for the strengthening steel, which is checked according to NEN-EN1993-1-9.

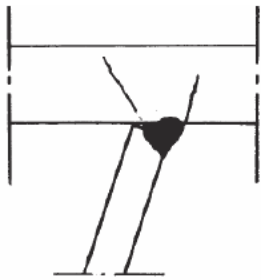
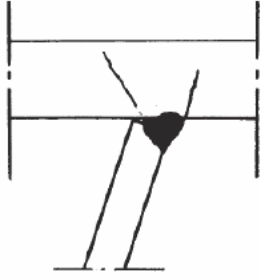
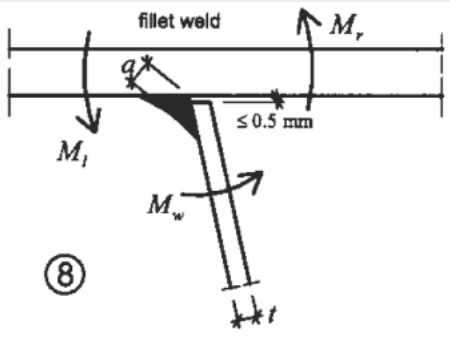
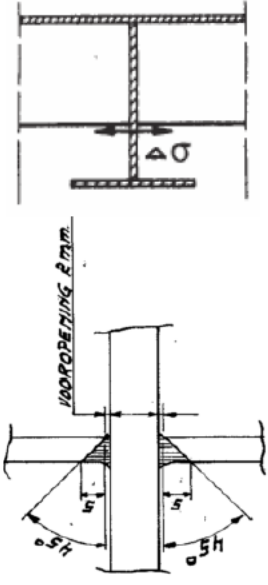
The fatigue capacity of the preloaded injection bolts are checked using physical testing as the FE model is not accurate enough in this aspect. The fatigue of the epoxy is also checked using scale testing for similar reasons.

Detail classification

To determine the detail classification of the fatigue details in the existing deck plate, lower detail classes are assumed to account for existing damages that were too small to repair during the renovation. Also, the fatigue capacity of the repaired detail might be worse than the as-welded condition. To this end, the following fatigue detail classifications have been used, based on previous MC projects, TNO research and recommendations in NEN-EN 1993-2 (TNO, 2017):

Table 4: Detail classifications in the existing deck structure (MC Renovatie Bruggen, 2021)

Detail	Weld	As-welded condition	Detail category	Historic damage/repairs	Notes
1a	Trough to deck plate joint: crack in deck plate outside trough. 5mm fillet weld.	125 MPa	56 MPa	Full damage reset to 0 due to all cracks > 3mm being repaired during renovation.	Stresses are extracted at 0.5 and 1.5 times the deck plate thickness from the toe of the weld, which is positioned at the weld length

	 <p>Deck plate crack</p>					from the plate intersection.
1b	<p>Trough to deck plate joint: crack in deck plate inside trough. 5mm fillet weld.</p>  <p>Deck plate crack</p>	125 MPa	56 MPa	Full damage reset to 0 due to all cracks > 3mm being repaired during renovation.	Stresses extracted at 0.4 times and 1.0 times the deck plate thickness from the heel of the weld, which is at the plate intersection.	
2	<p>Trough to deck plate joint: crack in weld starting at weld root. 5mm filler weld.</p>  <p>fillet weld</p> <p>M_r</p> <p>q^*</p> <p>M_1</p> <p>M_w</p> <p>$\leq 0.5 \text{ mm}$</p> <p>⑧</p>	71 MPa	50 MPa	Full damage reset to 0 as all visible cracks are repaired before renovation.	Stresses extrapolated at 0.5 times and 1.5 times the deck plate thickness from the toe of the weld, which is at the weld length from the plate intersection.	
3a	<p>Trough to trough support plate. A single-sided full penetration butt weld: crack in weld or trough.</p>  <p>$\Delta \sigma$</p> <p>100% OPENING 2mm</p> <p>s</p> <p>$5h$</p>	56 MPa	36 MPa	Full damage reset to 0 as all visible cracks are repaired before renovation	<p>Discontinuous trough to trough support plate joint welded all around with single sided butt weld.</p> <p>Stresses are extracted at 0.5 and 1.5 times the trough plate thickness from the toe of the weld, which is at the weld length from the plate intersection.</p>	

During the initial reassessment of the bridge, a crack in the cross girder at the connection with the trough has also been assessed. This could be named detail 3b, which is critical at the corner of the trough bottom and the trough leg. Analysis has shown that the stresses experienced in this detail are up to a factor 5 lower than in detail 3a. This is mainly due to the fact that these stresses are due to shear being transferred through the troughs, whereas the critical stresses for detail 3a are the larger longitudinal stresses. Furthermore, this crack has not been found in any maintenance work, increasing the confidence in the decision to not further investigate this detail during the renovation.

Other existing welds (i.e., deck plate splices, deck to cross beam joint) will not be verified because no fatigue damage was observed in these locations, the slow lane is shifted to a fresh part of the deck and because of the reduced change of future fatigue cracks due to the thick strengthening plate.

Fatigue performance

The expected fatigue performance will be assessed using both a theoretical framework, as well as with historic RISK data. For the theoretical framework, a simplified approach based on FLM5 (Annex A of NEN8701) is used. Therefore, no full stress spectrum or influence lines for different weaves are derived. Instead, the following steps are undertaken:

Existing deck:

Influences lines determined during a previously performed full fatigue assessment of the unstrengthened deck are scaled. A T1203A2 770 kN heavy truck from table A.3 in NEN8701 is placed in the most onerous position on the bridge. A stress factor will be used to scale the stresses from the full fatigue assessment to the current strengthened situation. Furthermore, a scale factor is applied the reservoir counted cycled data used in the full assessment to predict the future damages.

Strengthened steel:

A simplified but conservative fatigue assessment based on FLM5 from NEN8701 is used to assess the new steel components. The main purpose of this is to produce a conservative truck stress spectrum based on a minimal number of analyses. To this end, this method does not derive the full stress history with the full-length influence lines for different trucks and weaves. Instead, one stress range on the influence line is assumed, which is scaled based on the truck weight. The truck composition of FLM5 (NEN8701, annex A, Table A.3 3) is used for this analysis.

- First, the most onerous transverse location of a truck axle is determined by checking different transverse locations in combination with a few longitudinal positions. Then, a coarse influence line is constructed for the heaviest truck (T1203A2) in this transverse location. From this influence line, the peak stress as well as the largest stress range is extracted. Also, on the dominant longitudinal position that is found, analyses with the other 5 types of trucks are ran. Using the peak stresses found, the influence line is scaled to obtain the stress ranges for the other trucks. Combined with partial load factors and dynamic amplification, this provides a simplified stress spectrum of the fatigue detail, which can be considered conservative since every axle is assumed to cause a full peak fatigue cycle. Using the S-N curves according to EN 1993-1-9 and the Palmgren-Miner summation, the fatigue damage calculation is performed.

Epoxy

For the epoxy, a small-scale test program is set up to determine the fatigue threshold value or the cut-off limit. This is then compared to the stress data by using the heaviest truck in FLM5 (T1203A2) as a conservative assumption to easily verify the fatigue capacity

Assumptions and starting points

- Target fatigue life for both the new and old steel is 15 years. An inspection interval in combination with a repair strategy is possible as an alternative if the fatigue capacity cannot be guaranteed reliably.
- Future truck numbers are determined based on the extrapolation laid out in NEN8701 (Doubling of heavy traffic in 100 years).
- A dynamic amplification factor of 1.265 is used along the full length of the bridge to account for the effect of the expansion joint and general dynamic effects for the movable bridge.
- A partial safety factor of 1.15 is used for the existing steel and epoxy. A partial safety factor of 1.35 is conservatively used for the new steel components.

- Any effect of convoys, overtaking trucks, or trucks riding both directions simultaneously is not considered. All relevant influence lines are expected to be local not governed by multiple trucks being on the bridge simultaneously.

Analysis output

Existing deck

In order to evaluate the fatigue performance of the existing bridge, static analyses with the heaviest FLM5 truck load were performed. The key fatigue details, shown in Table 4, were re-assessed by extracting hot spot stress values. A stress factor was calculated that compared the stress in the strengthened bridge deck to the stress in the unstrengthened condition. Hot spot stresses are extracted at the location where peak expected damage was predicted in the fatigue assessment of the unstrengthened bridge. Using the cyclic stress data from this previous assessment and the stress factors, the new values of the expected fatigue damage in 2036 (15 years) of the strengthened bridge is determined using truck passage number provided by Rijkswaterstaat.

Table 5: Predicted fatigue damage in deck details 1a and 1b

Detail	Calculation	Unstrengthened bridge	Strengthened Bridge – No composite action
1a FAT 56 (125)	Hot spot Stress [MPa]	-71.43	-14.54
	Stress factor	1	0.20
	PD 2022-2036	61.9 (4.0)	0.1 (0.0)
1b FAT 56 (125)	Hot spot stress [MPa]	-74.73	-17.52
	Stress factor	1.00	0.23
	PD 2022-2036	83.4 (5.9)	0.3 (0.0)

In Table 5 it can be seen that the predicted fatigue damage for fatigue details 1a and 1b are well below 1 for the strengthened bridge, even without considering any composite action and lowering the fatigue detail classes. A stress reduction of around 80% is expected in the deck plate even without composite action. Table 6 presents similar results for deck detail 2 and 3a. In this case, the results are presented for a few different design assumptions to understand the sensitivity of the results to these assumptions.

Table 6: Predicted fatigue damage in deck details 2 and 3a

Detail	Calculation	Unstrengthened Bridge	Strengthened – No composite action	Strengthened – Full composite action, Epoxy E=0.1 GPa	Strengthened – Full composite action, Epoxy E=4.91 GPa
2 FAT 50 (71)	Hot spot Stress [MPa]	-85.77	-36.03	-29.73	-21.20
	Stress Factor	1.00	0.42	0.35	0.25
	PD 2022-2036	55.8 (18.7)	3.1 (0.7)	1.4 (0.3)	0.3 (0.0)
3a FAT (56)	Hot spot Stress [MPa]	-80.17	-46.02	-39.45	-27.30
	Stress Factor	1.00	0.57	0.49	0.34
	PD 2022-2036	69.9 (18.1)	12.3 (2.7)	7.4 (1.44)	1.9 (0.3)

It can be seen that for fatigue detail 2, the predicted damage is below 1 when considering composite interaction and a realistic epoxy stiffness. A stress reduction between 65% and 75% is expected for this detail. For fatigue detail 3a however, this simplified fatigue calculation does not guarantee a safe design life of 15 years, despite a stress reduction of around 50% - 65%.

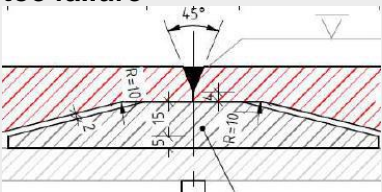
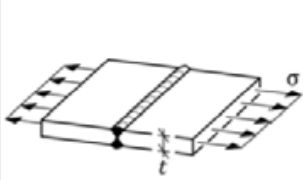
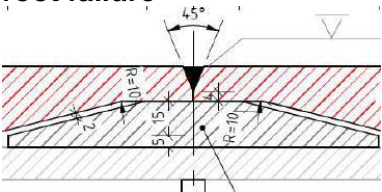
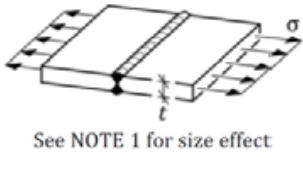
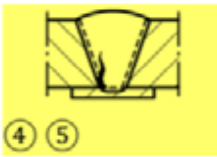
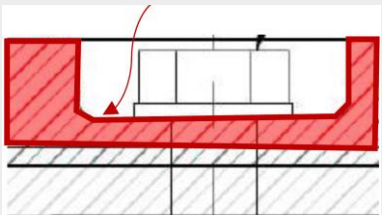
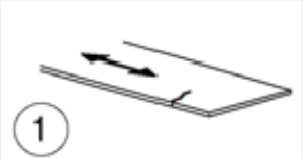
Because the possibility of fatigue cracks in the trough to cross-girder connection cannot be guaranteed using this simplified approach, two additional analyses are performed during the design. First of all, the future damage is predicted using historic RISK data. Second, a study on the effects of having a cracked trough to cross-girder study is performed. These will not be discussed here in detail, but the conclusions are summarised below:

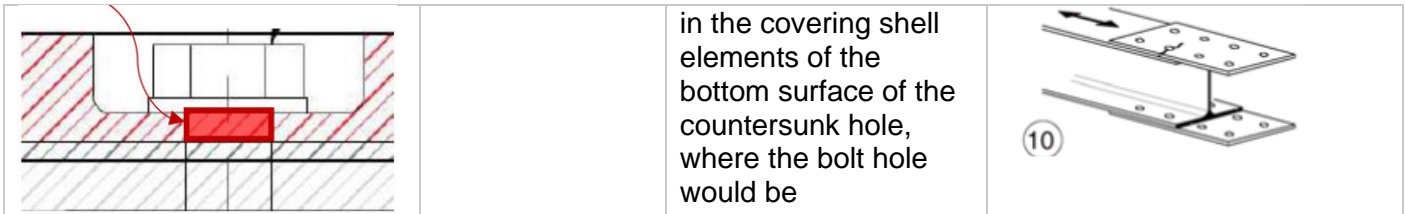
- The number of traffic cycles up to damage has been determined using historic RISK data and it is assumed that the future damage will occur after the same number of cycles
- Using the new traffic layout, the future traffic density, and the strengthening approach, it was concluded that no damage will occur before 2036.
- A trough detachment study shows that it takes a little over 6 years for a crack to grow from 210 mm (Initial crack length from the root of the weld at the bottom of the trough) to 700 mm (Maximum allowable crack length) in size.
- Based on this, two inspections during its service life (2024 and 2028) are advised. This provides enough time to find and repair any crack.

Strengthening steel & bolts

In Table 4, an overview is given of the fatigue details in the added strengthening plate and bolts that were identified and checked. A FE model with a detailed representation of the countersunk hole geometry is used to extract stresses for the fatigue assessment.

Table 7: Fatigue details in added strengthening steel and bolts (MC Renovatie Bruggen, 2021)

Detail	Detail category	Extracted stress	Reference
Strengthening plate splice toe failure 	112 MPa	Stress in deck in longitudinal (x) direction in the top covering shell elements	NEN-EN 1993-1-9:2020, Table 9.4, detail 1  See NOTE 1 for size effect 
Strengthening plate splice root failure 	71 MPa	Stress in deck in longitudinal (x) direction in the top covering shell elements	NEN-EN 1993-1-9:2020, Table 9.4, detail 4  See NOTE 1 for size effect 
Countersunk bolt detail 	160 MPa	The minimum and maximum principal stresses are read from the elements of the heel of the countersunk detail	NEN-EN 1993-1-9, Table 8.1, detail 1  
Bolt hole of the strengthening plate	90 MPa	Maximum and minimum principal stress in the elements	NEN-EN 1993-1-9, Table 8.1, detail 10



in the covering shell elements of the bottom surface of the countersunk hole, where the bolt hole would be

As was discussed, a simplified fatigue assessment as carried out. In Table 8, the peak stress values from all the trucks are presented.

Table 8: Peak stress values from relevant trucks

Loading truck	Splice toe	Splice root	Countersunk heel	Bolt hole
	σ_x [N/mm^2]	σ_x [N/mm^2]	$\sigma_{princ,min}$ [N/mm^2]	$\sigma_{princ,max}$ [N/mm^2]
V11	-12.6	6.9	-11.7	2.8
V12	-13.1	6.2	-24.1	6.8
T11O2	-16.5	8.5	-21.4	5.6
T11O3	-15.7	7.2	-28.9	6.2
V12A12	-21.5	9.7	-23.5	5.7
T12O3A2	-18	6.4	-36.5	6.6

With these peak forces and the strategy described earlier, the predicted damages are calculated and presented in Table 9. Note that the stress ranges $\Delta\sigma_{T12O3A2}$ here do not yet include the partial safety factor (1.35) and dynamic amplification factor (1.265).

Table 9: Predicted damage of strengthening steel plate details

Detail	$\Delta\sigma_c$ [N/mm^2]	$\Delta\sigma_L$ [N/mm^2]	$\Delta\sigma_{T12O3A2}$ [N/mm^2]	PD 2021-2036
Splice toe	112	45.32	27.31	0.11
Splice root	71	28.73	18.22	1.00
Countersunk heel	160	64.74	44.69	0.05
Bolt hole	90	36.42	12.35	0.00

It can be concluded that the fatigue capacity of all four details is sufficient even using this conservative approach. Furthermore, in the design report a more detailed study was carried out to prove the conservatism. Using a full influence line and assuming all trucks are of type T11O3, a predicted damage of 0.16 was found for the splice root detail, a factor of more than 6 lower than the simplified approach.

3.6. Future design optimisation

After the design and pilot application, Arup has put additional effort into proving the safety of the design and optimising the design for future implementations. This section will summarise some of the most relevant conclusions from these studies.

First of all, a lot of testing has been carried out on the strength of the epoxy layer, as was discussed in section 3.4. After discussion and consultation with TNO the conclusion was drawn that composite interaction between the steel plates can be assumed for the design life of 15 years. This is a very important conclusion which can result in a lot of design optimisations. Due to this, Arup has investigated the possible improvements of the bolt layout and the strengthening plate thickness. In Figure 45, the stress reduction factors of the hot spot stresses in the different fatigue details are presented. The current design is compared with a possible optimised design with a thinner strengthening plate with composite interaction.

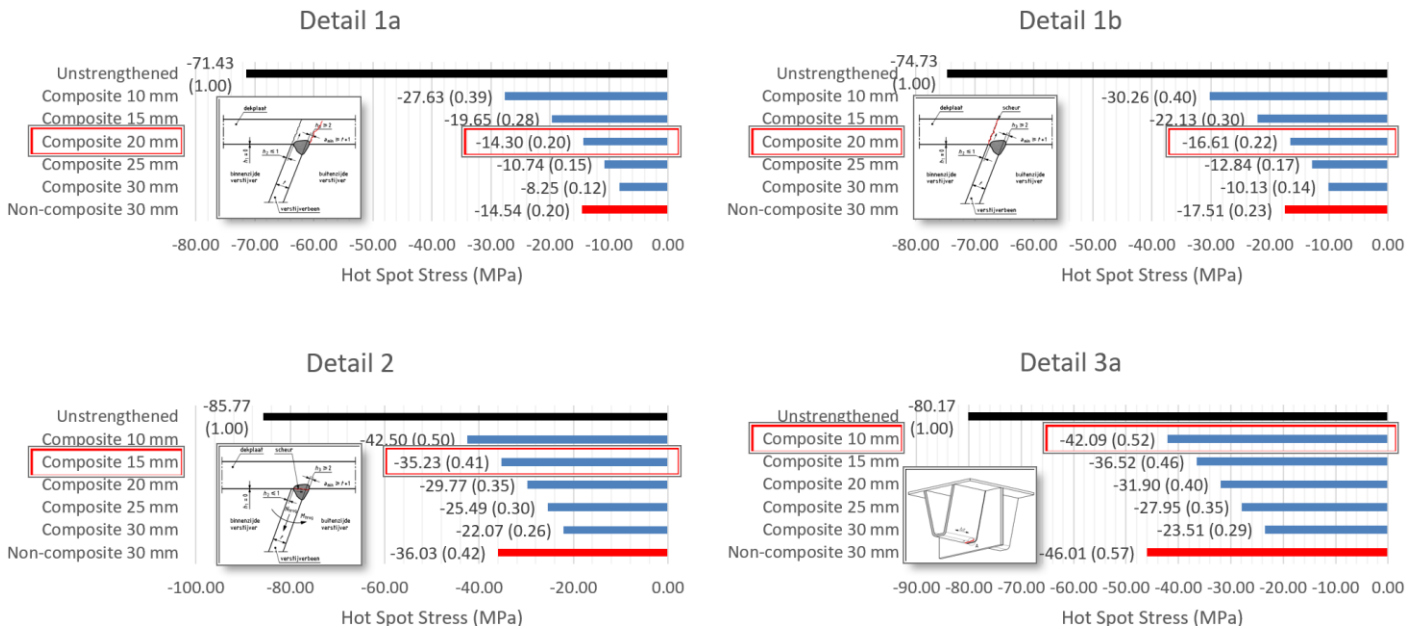


Figure 45: Comparison of hot spot stresses in fatigue details with composite and non-composite plates

From these results, it can be seen that the thickness strengthening plate can be reduced to at least 20 mm. A further reduction might be possible but also has practical limitations problems with the countersunk bolts will start occurring for a thinner strengthening plate. Interesting to note is that the composite interaction is more valuable for fatigue details located further away from the top of the strengthening plate. In Figure 46, the impact of the strengthening on the stresses in the troughs is visualised. Again, the benefit of the stiffening is clearly visible. Assuming composite action further increase the load spreading between the troughs and further optimises the design.

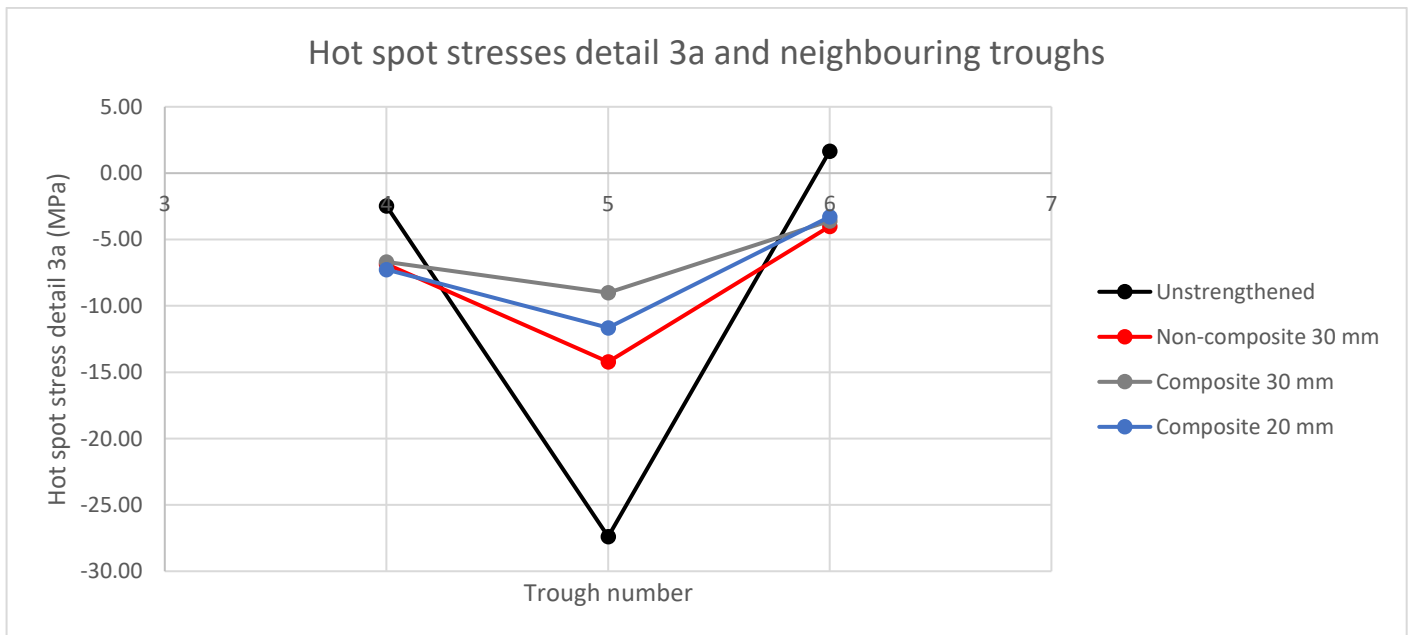


Figure 46: Impact of composite action on the stress distribution between troughs

All in all, these conclusions allow for a much lighter design when aiming for a similar stress reduction, as reducing the strengthening plate from 30 to 20 mm lowers the weight of the strengthening design by around 30%.

Lastly, being able to assume composite interaction has a large impact on the bolts. Since a large part of the shear force can now be transferred through the epoxy layer, the bolts are alleviated significantly, as shown in Figure 47. Shear forces in the bolts are almost cut in half, which allows for a redesign with fewer bolts, lowering the costs and execution time.

An initial study has shown that 50% of the bolts can easily be removed with this assumption. This is more of a practical minimum, since a single bolt is still needed between every trough to prevent tensile stresses in the epoxy. To get a UC of close to 1.0, bolt size can be reduced to M20 and a more practical Ethyl-zinc silicate can be applied instead of the TSA layer.

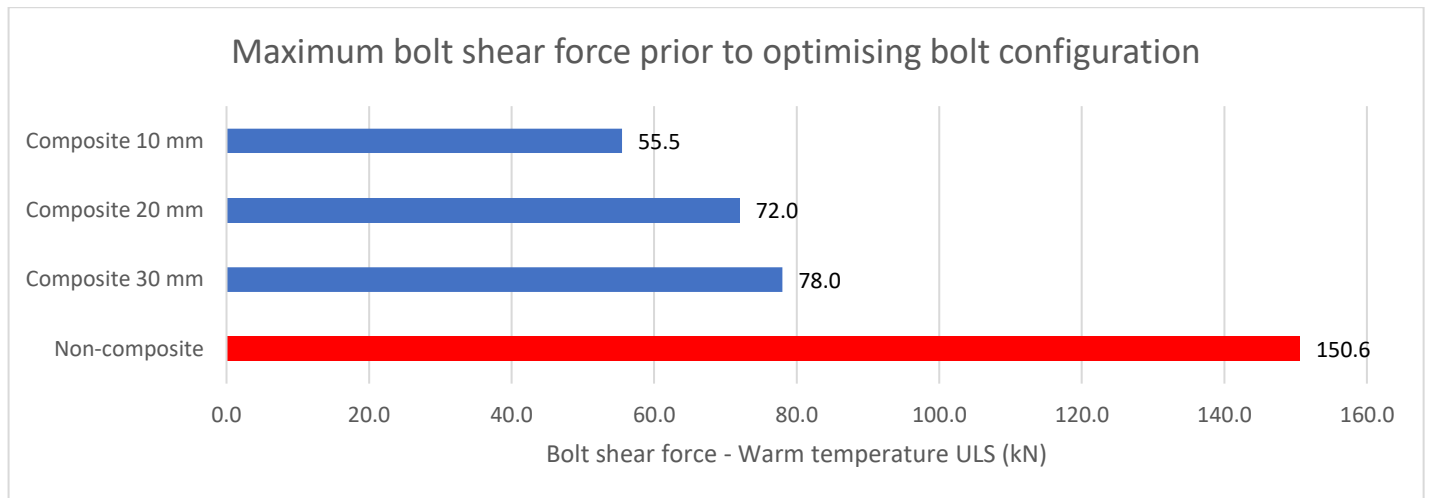


Figure 47: Maximum shear force in original bolt configuration

4. Monitoring & load test description

In this chapter, the methods that are used to answer the research question are described. Furthermore, choices in the methodology are discussed and justified. Section 4.1 describes the details of the monitoring scheme that is implemented. This includes the sensor locations and the way the sensors have been installed. Section 4.2 discusses the details of how the tests are carried out.

4.1. Monitoring scheme

During the design of an innovative project, it is important to have confidence in the effectiveness of the solution. Even though a lot of time and effort has gone into material testing and detailed FE modelling during the design of the strengthening scheme, questions regarding the actual behaviour of the bridge will always remain.

In such a pilot project, after the renovation has been carried out, it is very important to monitor the behaviour of the bridge. This will provide invaluable data that can be used to convince the client of the merit of the strengthening approach, but also to validate and improve the numerical models. In the end, the better understanding of the behaviour of the strengthening approach can lead to a more optimised design that can be used for future implementations.

As has been discussed in section 2.3, a wide range of monitoring techniques are available, and in order to execute a successful monitoring project it is important to have clear goals and objectives. In the case of this thesis, the goal of the monitoring scheme is to assess the behaviour of the structure both before and after strengthening. Furthermore, the data is used to validate the accuracy of FE models. Moreover, there is minimal funding, equipment and time is available, so it is important to have an efficient choice of monitoring equipment and locations. Finally, it is important to recognize any limitations, uncertainties, and errors in the chosen methodology so that proper confidence in the results can be obtained.

In order to best investigate the reduction in stresses, strain gauges are chosen as the most applicable solution. These are also relatively cheap and easy to install, making it possible to execute in the small window that was available. They are also accurate, have high polling rates and allow for measurements that can easily be compared to numerical models. To this end, in total 16 strain gauges are applied on the bridge:

- 11 strain gauges on the bottom of the deck plate (DECK01-DECK11) will provide data on the amount of strain in the deck plate, which is important for determining the efficiency of the strengthening scheme. Strain gauges at varying locations from the bolts and cross girders will provide information about the amount of composite interaction and about the way the forces are transferred through the structure.
- 4 strain gauges on the troughs (TROU01-TROU04) will measure strain at the bottom of the troughs, both at the cross-girder and in between two cross-girders. This will provide information about the behaviour of the bridge and the stress reduction at these locations, which is especially relevant for the poor fatigue detail at the connection of the trough and the cross-girder.
- 1 strain gauge is placed at the bottom of the cross girder (CGIR01) to assess more globally the accuracy of the numerical models and efficiency of the strengthening scheme.

All the sensors are positioned in an area where the tandem system will cause maximum global deflections. Furthermore, placing all sensors closely together has practical advantages, limits noise due to long wiring and limits the chance of wires or sensors being accidentally damaged as they are installed in an active work area. The positions are shown in Figure 50. The following steps are taken in the installation of the strain gauges:

- The locations are roughly marked up
- The surfaces are prepared according to NEN-EN ISO 8501-1 class St. 3 (Very thorough hand and power tool cleaning) (International Organization for Standardization, 2007)
- The location of the strain gauge is accurately marked up
- The location is smoothed with an angle grinder and p120 sandpaper

- Dust is removed and the surface is cleaned using acetone
- The strain gauge is glued to the surface
- A lacquer is applied on the strain gauge to prevent water ingress

After installation, the wires are taped to the deck and troughs to prevent any safety hazards and reduce the risk of anyone accidentally knocking them off. Despite the precautions, before the start of the second load test, it was seen that two sensor wires were unattached. However, these could easily be resoldered, and this did not pose any problems. Furthermore, the position of all sensors was verified and documented as shown in Figure 49. In general, the sensors were installed with an accuracy of around ± 10 mm.

All strain gauges are wired to the amplifier, which is connected to a laptop. A modem is installed next to the laptop so that the measurements can be started and read directly from the deck without needing access to the scaffolding beneath the deck. All the equipment is put in a box, which is connected with a magnet to the cross-girder. Furthermore, an ambient temperature sensor is installed which can measure the ambient temperature at the bottom side of the deck plate during strain measurements.



Figure 48: Measuring equipment setup (picture taken after strengthening)



Figure 49: location of sensor TROU07, approximately 5 mm off-centre

4.2. Load test description

To most accurately quantify the effect of the strengthening, it is important to have a good test setup that is executed identically both before and after strengthening. To this end, a truck with a known weight and axle geometry is driven over the length of the bridge. This is repeated multiple times with the truck in different positions in the width direction.

In total, the location of the truck in the width direction is varied by $8 \times 150\text{mm} = 1200\text{mm}$ (2 trough widths); from between trough 16-17 to between trough 18-19, as shown in Figure 50. With this setup it will drive over all the sensors and provide information about the behaviour of the bridge deck.

Some important notes on this test setup:

- The truck will pass the bridge 9 times, with the centreline of the wheel at tracks 1-9 as shown in Figure 50. The middle track 5 will be driven over thrice to get a better impression of the accuracy of the results and to get more data on the behaviour close to the bolts and cross-girder (see sensors DECK-DECK05).
- Guidelines will be marked on the bridge deck using coloured string and tape to ensure that the truck driver is in the correct position.
- The truck will drive at approximately 5 km/h, so that it can drive in a straight line as accurately as possible, if needed with the help of a person guiding the truck.
- With the polling rate of the strain gauges set at 1000Hz, this will result in a data point every 1.4 mm. This is deemed sufficient to accurately capture the maxima, since the influence lines are usually very 'spiky' in an OSD deck.
- The truck shall have a gross weight of at least 40 tonnes, to be recorded at a weighing station before or after the load tests. Furthermore, weighing plates are used to measure the weight of every wheel.
- The truck axle dimensions shall be recorded, and the position of the loading of the truck is recorded in order to load the truck in exactly the same way in both load tests.
- No other moving loads shall be on the bridge during the test. The load test is done while no other heavy moving machinery is present on the renovated portion of the bridge deck. However, one traffic lane was always open at the western cantilever of the bridge. This was an uncontrollable factor, but its influence is expected to be minimal and will be thoroughly checked.
- The ambient temperature shall be recorded.
- All load tests are recorded on camera to check the accuracy of the wheel relative to the marked track.

Truck weight & axle layout

For the load tests, the main contractor Hollandia B.V. agreed to assist us by supplying a truck with six axles, as depicted in Figure 51. The dimensions of the different axles were shown in Figure 50, and the nominal tyre pressure was 9 bar. Before the first load test, the truck went over a weighing station. Furthermore, before the second load test, the truck was both sent over the weighing station as well as driven over weighing plates to measure the weight of every individual wheel, as shown in Figure 52. Finally, the weight of axles 2 and 3 could be read from the truck itself as well. A summary of all measurements is given in Table 10.

From the measurements it can be seen that despite the identical loading, both the weighing station and the truck display show that the truck was around 2 tonnes heavier during the second load test. It is unknown where this discrepancy comes from, and its impact will have to be assessed during the finite element modelling.

Furthermore, when weighing the individual wheels, the total truck weight came out to around 4 tonnes more than was given from the weighing station. This is likely due to the fact that the weighing plates had a height of around 5 cm (see Figure 52), meaning that neighbouring axles would be slightly unloaded and the weighed axle a little extra loaded when the weighed axle was on the weighing plate. This would be most pronounced when the axles are closest together and it is not trivial to scale this back to get a more realistic weight. During the finite element modelling, a sensitivity study will be carried out to quantify the impact of a deviating wheel load. Furthermore, the impact of the length of the tyre print will have to be investigated as this proved hard to accurately measure.

Table 10: Truck weight measurements

Wheel no:	Weight (kg):	Other:	Weight (kg):
1	3905	Truck display 1:	
2	3930	Wheel 3 + 4	6100
3	3660	Wheel 5 + 6	6400
4	3985	Truck display 2:	
5	3405	Wheel 3 + 4	6200
6	3850	Wheel 5 + 6	6700
7	5055	Weighing station 1:	
8	5805	Total:	50 200
9	5235	Trailer	31 720
10	5880	Weighing station 2:	
11	5310	Total:	52 180
12	5995		
Total:	56 015		
Trailer (7-12):	33 280		



Figure 51: Unstrengthened load test



Figure 52: Truck weighing

4.2.1. Load test before strengthening

The first load test was carried after the removal of the topping layer and reparation of major cracks in the relevant troughs.

Unfortunately, due to a corona related isolation, the author was not able to oversee the execution of the first load test. Due to some error in the communication and/or setup of the load test, the truck paths were not set out as was intended, and therefore slightly different data was obtained as was intended. Instead of using tracks 1-9, with track 5 being done thrice, the truck drove on track 3-11, with track 7 being done thrice. Although this is unfortunate and provides a smaller number of useful results, it does not compromise the monitoring scheme and all conclusions can still be drawn from this data.

4.2.2. Load test after strengthening

The second load test was carried out right after application of the strengthening, and just before the application of the epoxy topping layer. There is thus no unwanted influence from any topping layer. Due to the error in the first test, it was decided to expand the second load test to cover tracks 1-11 instead of only doing track 1-9. Track 5 was done thrice as planned. Furthermore, the first try of track 6 was deemed too off-centre and was repeated in a more accurate way.

In general, based on observations and camera footage, it is estimated that the truck was able to drive over the tracks with an accuracy of around 30mm.

5. Results load tests

This section will present the results of the load tests. First, relevant information is laid out regarding the post-processing and handling of the data in section 5.1. After this, the results from the load tests will be given per sensor location, starting from the cross girder in section 5.2, followed by the deck plate in section 0. Finally, the trough locations are covered in section 5.4. In all these sections, the results before and after the strengthening are presented and compared. Also, a discussion and interpretation of the results is given in the sections.

5.1. Post-processing information

In order to better visualise the load test results, some post processing steps have been carried out on the raw data. This section will shortly list and discuss the actions that have been carried out. The results of the operations can be seen in Figure 53.

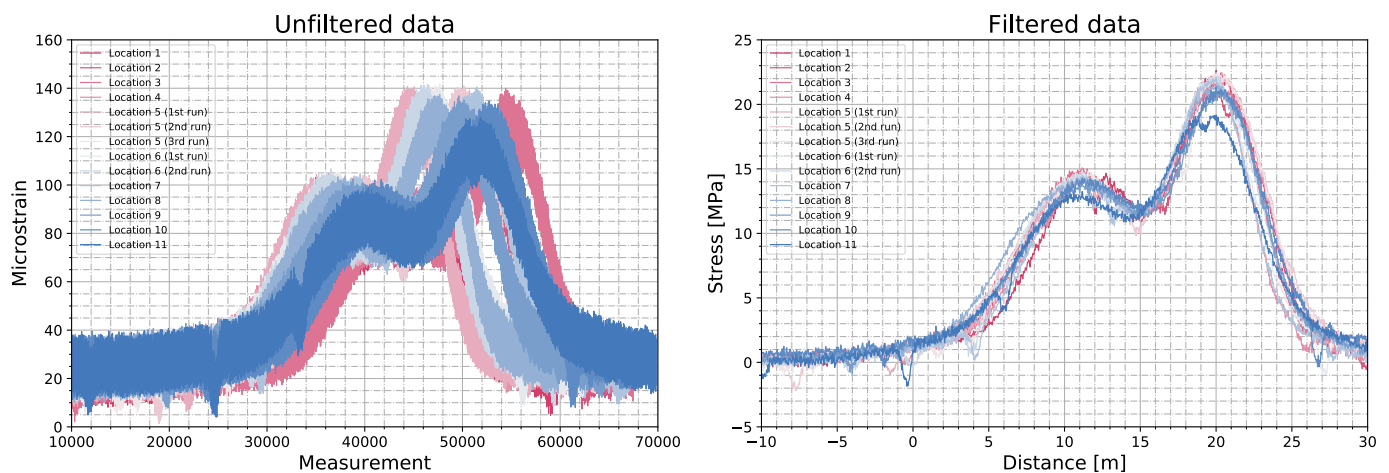


Figure 53: Difference between the unfiltered data(left) and the filtered data(right)

The following actions have been taken:

- The average strain of the first few seconds is set as the 0 mark for the duration of the test. This will isolate the strain cycle that the sensor experiences during the load test and make for easier comparisons between different tests.
- Since not every location was carried out with exactly the same speed and duration, the results are shifted so that the peaks coincide with each other. This again makes comparisons between different tests easier.
- The data on the x-axis is converted to distance so that the distance between the different axes is better visible and more intuitive.
- In order to eliminate unwanted electrical noise, the data is filtered. The main objective of this filter is to eliminate the excessive electrical noise present in the load test after strengthening.

Noise filter

A short discussion on the choice of noise filter will be presented here. When trying to filter out noise, it is important to realise the nature and characteristics of this noise. In this case, the noise is of electrical nature with a frequency of the noise is about 50Hz (also called the mains hum). Since there is no relevant data with such a high frequency, the chosen solution is to design a low-pass filter that will filter out data with frequencies above the specified cut-off. To this end, a low-pass 5th order Butterworth filter was used, with a cut-off frequency of 10 Hz. This was observed to provide the best noise filtering without impacting the peak values of the test results.

In Figure 54, the results of the Butterworth filter are visualised and compared to Savitzky-Golay filter, which does not take the frequency spectrum into account and filters noise on the basis of the running average of

the data. It can be seen in load test 1, the noise is limited and both filters are able to smoothen this out equally well. In load test 2 however, it is clearly visible that the Butterworth filter performs much better. It is able to smooth out the data completely, while the Savitzky-Golay filter cannot reduce the amplitude of the noise enough and the cyclic noise is still visible. Other filtering methods, such as Chebyshev type filters, could also be applicable. However, given the good fit of the Butterworth filter, these alternatives have not been investigated in the scope of this thesis.

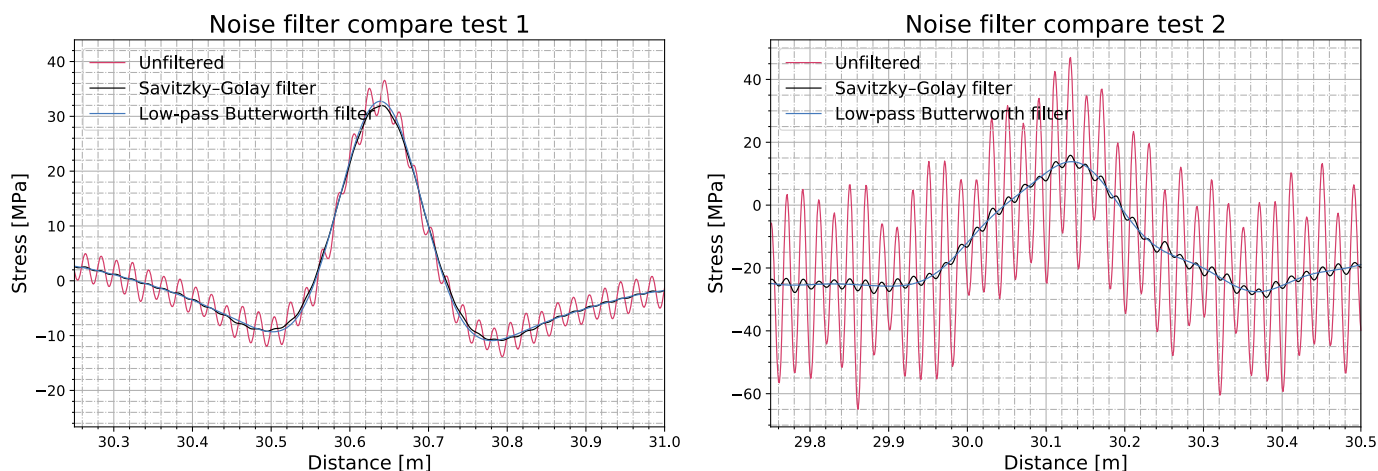


Figure 54: Noise filter comparison

5.2. Cross girder

Firstly, the results of the cross-girder sensor will be presented and discussed. The relevant sensor Cgir01 is located at the bottom of the bottom flange of the cross-girder. In Figure 55 and Figure 56 the results from load tests 1 and 2 are presented respectively.

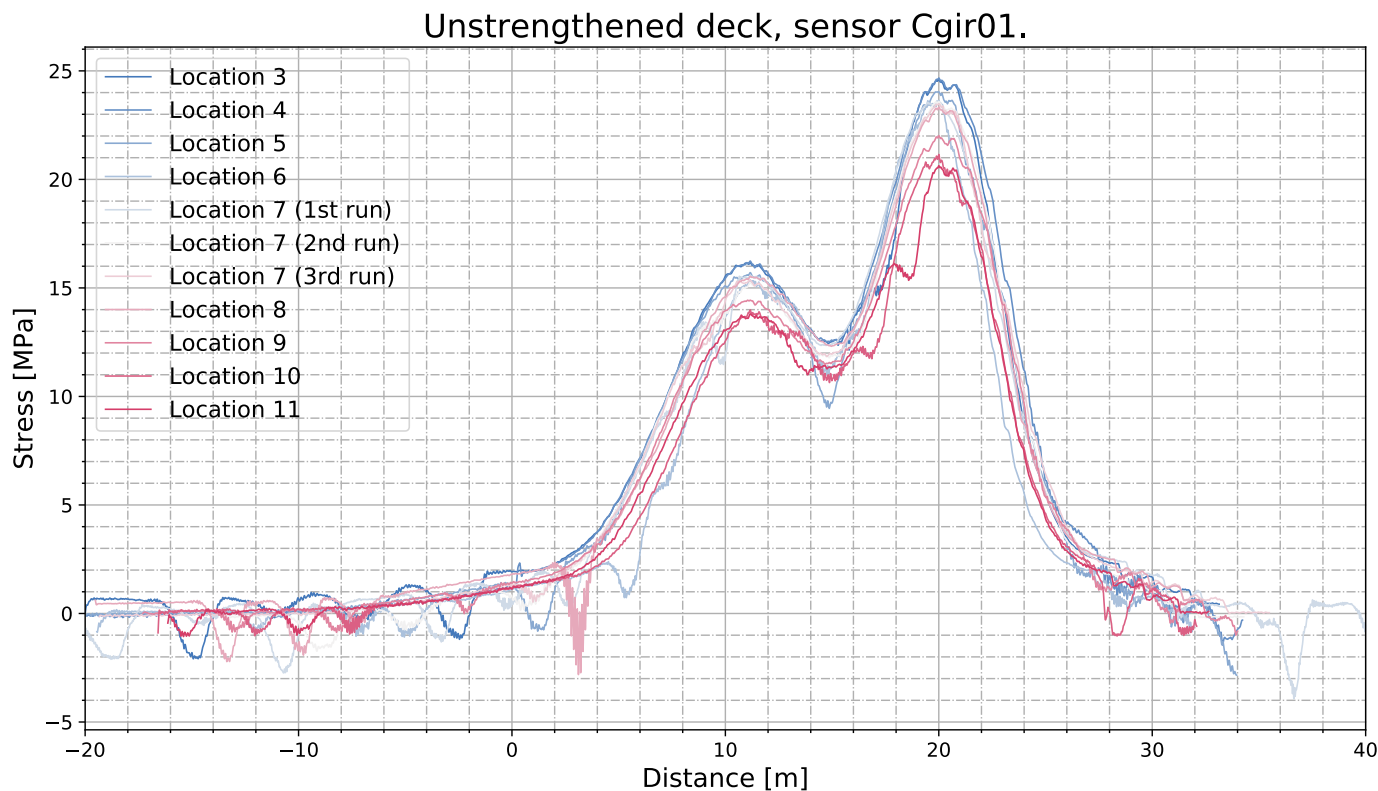


Figure 55: Results from the load test on the unstrengthened bridge, stresses in cross girder bottom flange

Strengthened deck, sensor Cgir01.

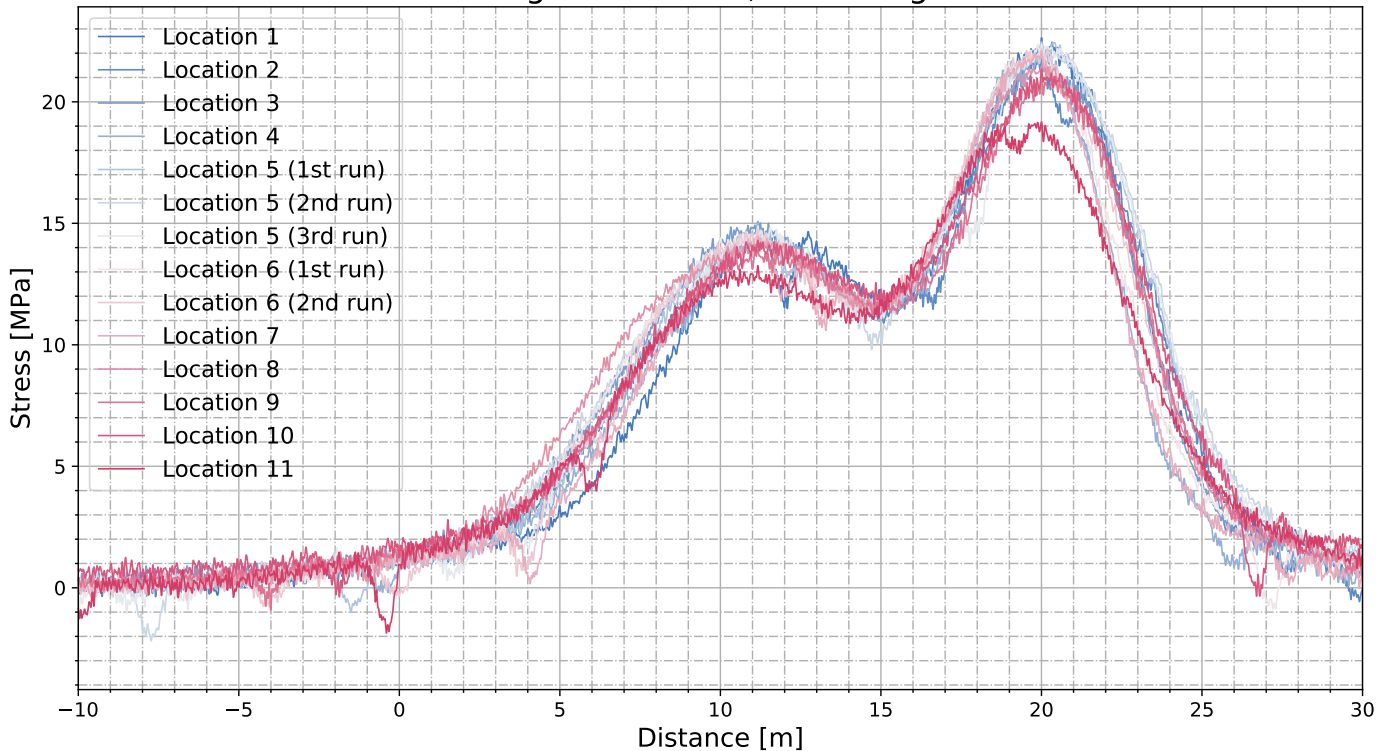


Figure 56: Results from the load test on the strengthened bridge, stresses in cross girder bottom flange

Some small dips in the stress are visible in Figure 55 and Figure 56, which correspond to traffic driving over the cantilever part of the bridge during the load test. The minimum stress that is used to determine the stress cycle for the cross girder is set to zero in order to eliminate any unwanted effect from passing traffic.

For the cross girder, the largest stress and stress cycle is experienced due to the heavier back three axles. The largest stress is between 20 and 25 MPa for the unstrengthened bridge depending on the truck location, whereas the maximum stress is around 21-23 MPa for the strengthening bridge. This amounts to a stress cycle decrease of around 10%.

Since the cross-girder sensor is located at the bottom of the bottom flange, the sensor mainly captures the global behaviour of the structure. Where most other sensors show 6 distinct peaks corresponding to the six axles, the cross-girder only shows two peaks at the times where the most weight is located on its bay. Since the results show the global deformation of the structure, the results do not differ significantly between the different tracks. The maximum stress measured by the strain gauge increases slightly as the truck is located more centrally between the main girders.

It is observed that the strengthening reduces the stresses at the cross-girder sensor location by about 10%. Since the sensor is located at the bottom of the bottom flange of the cross-girder, the stresses experienced in this location are not impacted significantly by the change in cross-section due to the strengthening. For the cross-girder, the strengthening essentially thickens and stiffens the top flange of the cross-section but compared to the height of the section this change is minimal and the change in the stress cycle is thus also limited.

On first sight, this reduction can be seen as very small considering the scope of the strengthening scheme. However, the limited improvement is not unexpected considering the location of the sensor. Strengthening of the deck plate is aimed mainly at stiffening the deck plate and improving fatigue details in the deck and troughs. This cross-girder sensor functions mainly as a check on the global behaviour and for comparison with the FE model. Thus, the results are no reason to worry and the stress reduction due to the strengthening seems realistic.

5.3. Deck plate

In total, 11 deck plate sensors were installed. The exact location of the sensors can be seen in Figure 50. The deck plate sensors are divided in four different categories for this section:

1. At mid bay, measuring transverse strain
2. At mid bay, measuring longitudinal strain
3. At the cross girder, measuring transverse strain
4. At the cross girder, measuring longitudinal strain

The results are presented and discussed based per sensor category.

5.3.1. At mid bay, measuring transverse strain

Three sensors were installed that measure transverse strain at mid-bay: Deck07, Deck09 and Deck11. However, because of the error during the execution of load test 1, no relevant data is obtained for Deck11, since it is located over track 1 which was not driven over before the strengthening.

The sensors in this first category measure the transverse strain of the deck plate. More specifically, they are located in the middle of the deck plate between two troughs, measuring the local bending of the deck plate due to local wheel loads. This area is expected to benefit a lot from the strengthening since the deck plate will be stiffened significantly. This, combined with the increased thickness of the package allows for better load distribution and thus smaller peak stresses due to local wheel loads. In Figure 57 and Figure 58, the results of Deck09 are shown. Figure 57 displays all weave locations to get an impression of the impact of the truck location. In Figure 58, only weave 5 is shown in order for the graph to remain readable.

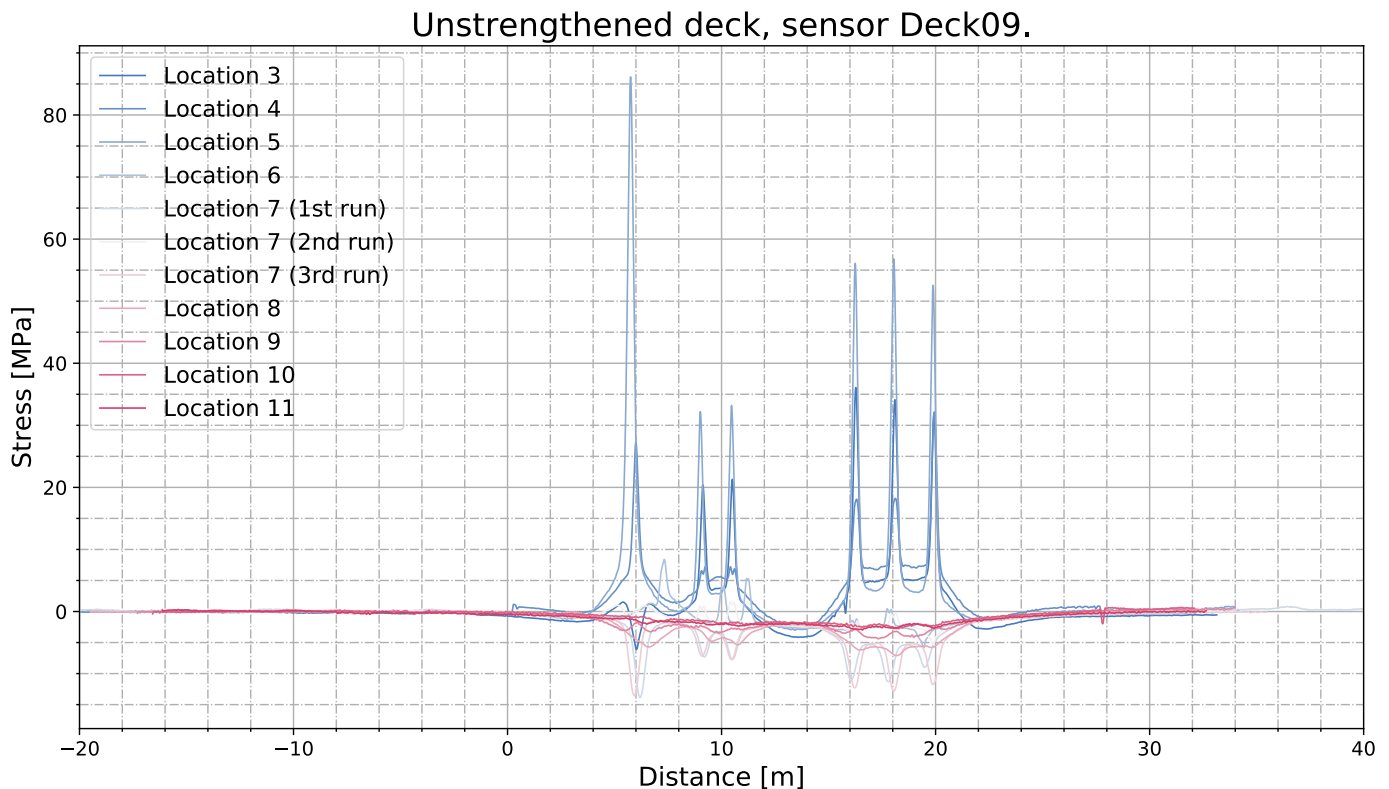


Figure 57: Results from the load test on the unstrengthened bridge, transverse bending of the deck plate at mid-bay

Strengthened deck, sensor Deck09.

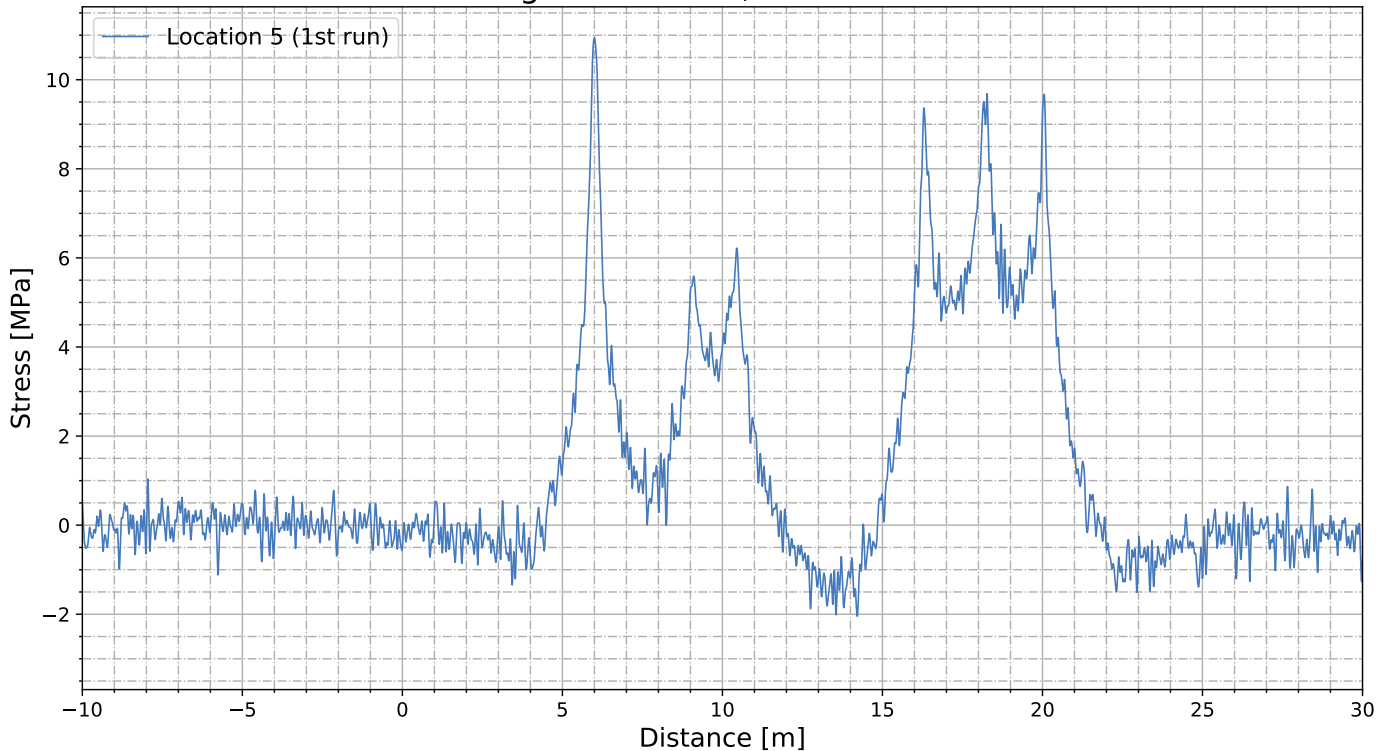


Figure 58: Results from the load test on the strengthened bridge, transverse bending of the deck plate at mid-bay

Firstly, it can be observed from Figure 57 and Figure 58 that the results of the unstrengthened and strengthened load tests follow expectations. Six distinct peaks are visible, especially before strengthening, corresponding to the six truck axles driving directly over the sensor. Even though the first axle is not the heaviest, it causes the largest stress cycle because the load is more concentrated between the troughs. After strengthening it can clearly be seen that the peaks are slightly less sharp and there is more stiffness in the structure, causing a larger part of the deck plate to be activated to take the axle loads. This can be observed by the larger stress values experienced by the sensor in between the peaks.

In Figure 59, the results of the unstrengthened and strengthened bridge are compared. The results are focused on track 5, when the truck drives directly over the sensor, causing the largest stress cycle.

In Figure 59, the large impact of the strengthening is visible. The peak stresses have decreased significantly. Notable also is Figure 60, which shows track 3 instead of track 5. In this truck location, the inner wheels of the double wheel axles are located over the sensor location. Furthermore, an overview of the results of all tracks is shown in Figure 61. In this graph, the maximum stress cycle of every track is calculated and plotted over the width of the bridge. The strengthened and unstrengthened bridge are compared in the same graph and the stress reduction is plotted on the right axis.

Load test results, track Location 5, sensor Deck09

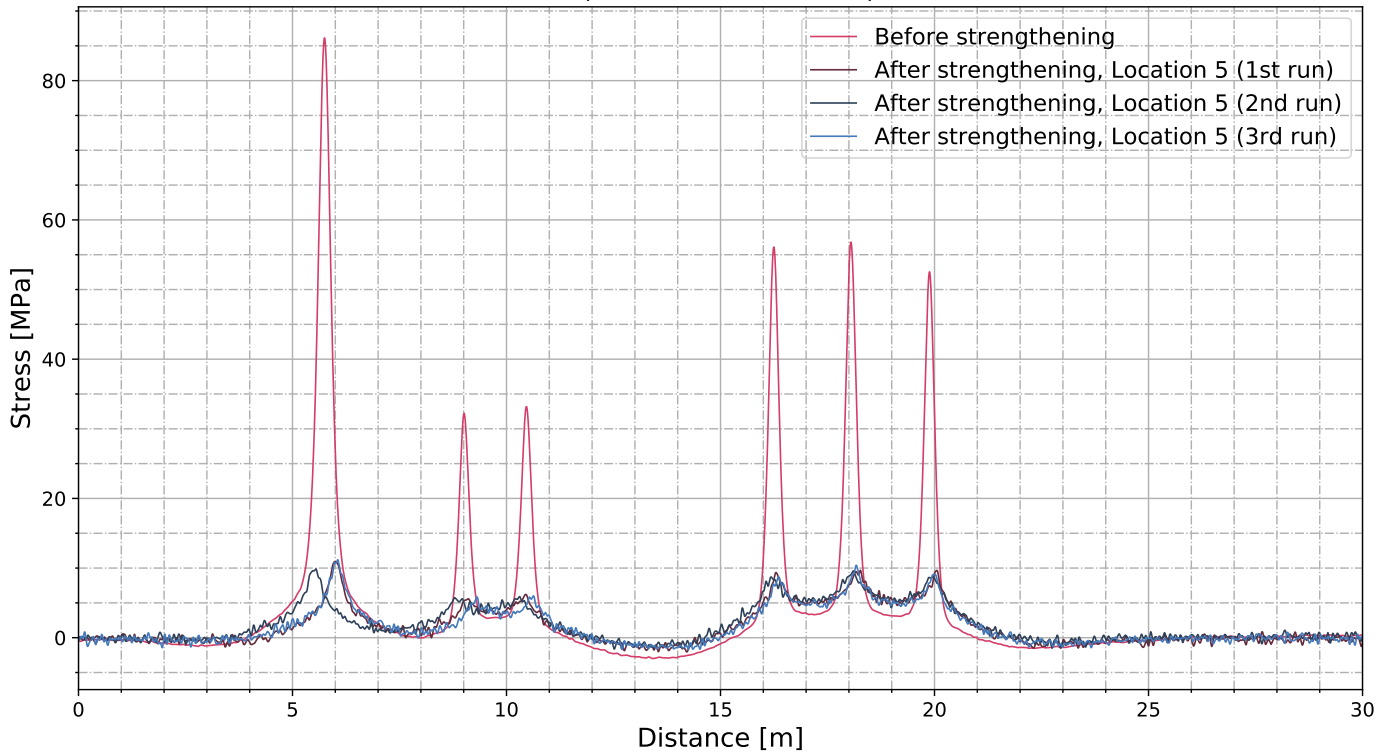


Figure 59: Comparison before and after strengthening, transverse bending of the deck plate at mid-bay

Load test results, track Location 3, sensor Deck09

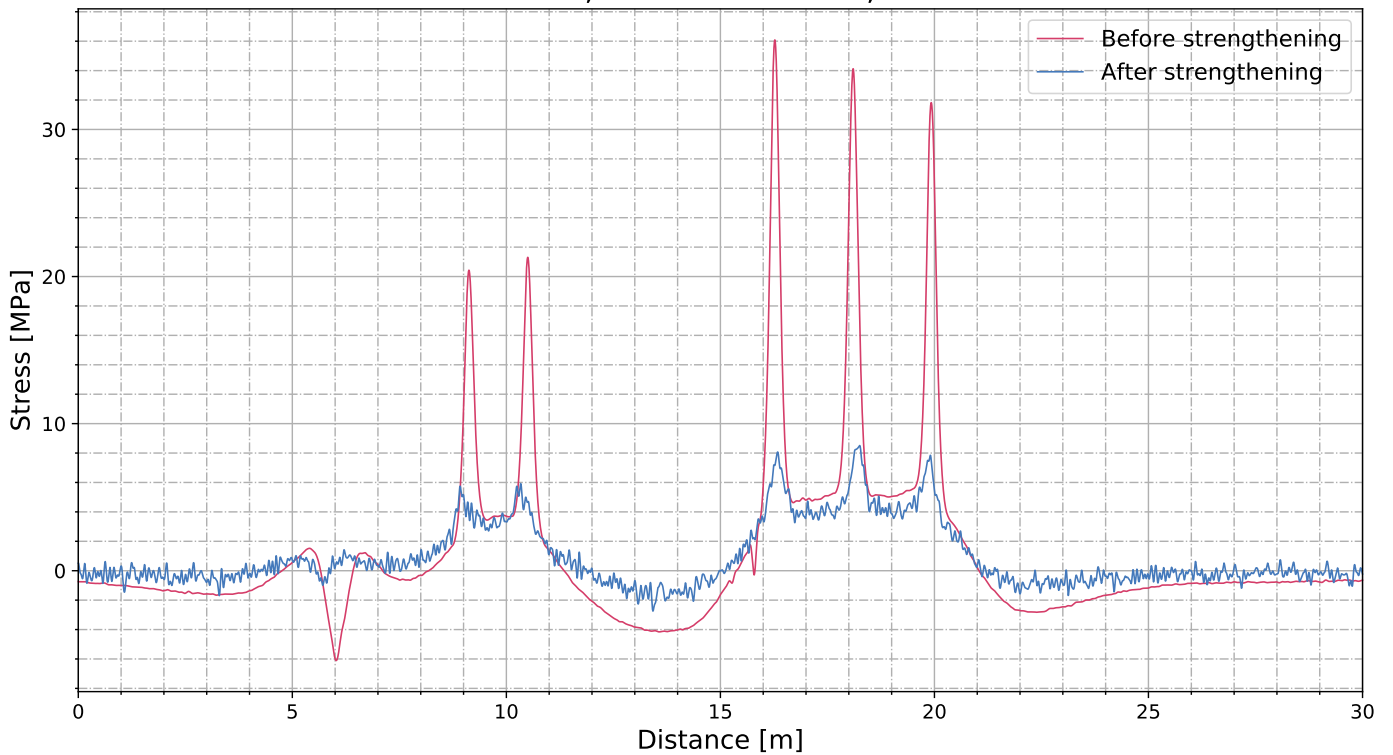


Figure 60: Comparison before and after strengthening, transverse bending of the deck plate at mid-bay

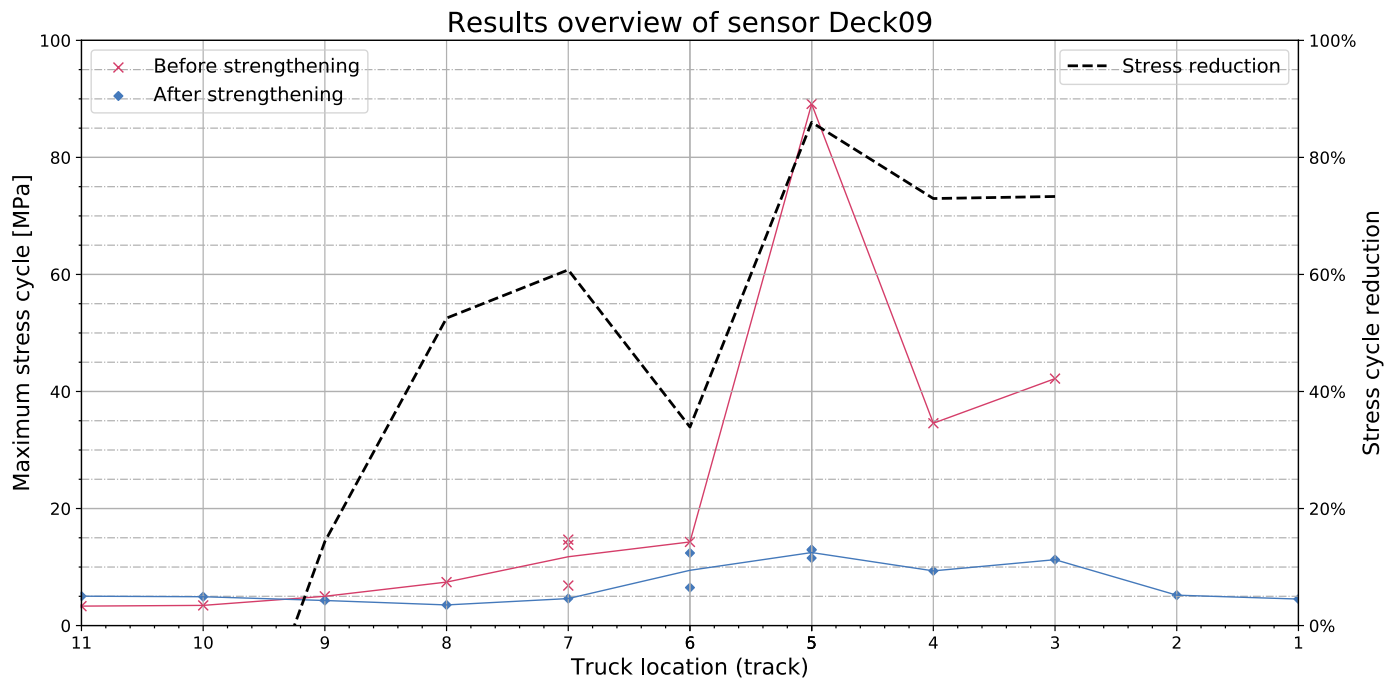


Figure 61: Overview results of Deck09, transverse bending of the deck plate at mid-bay

It can be seen that the strengthening is very effective for stresses in this location, reducing the stress cycle by almost 90% in this most onerous location as shown in Figure 61. As expected, the strengthened bridge spreads the load a lot better, which can be seen by the lack of a sharp peak in the influence line for the strengthened bridge. A consequence of this better load spreading is also that the strengthening is less effective away from the applied load, which is also visible in Figure 61. However, this is of minor importance since the stresses at these locations are lower and not relevant for fatigue issues.

This same behaviour can be observed when looking at sensor Deck07. This sensor also measured transverse strain in the deck plate but is located one trough over from sensor Deck09. For brevity's sake, not all graphs of this sensor will be shown, but the overview is shown in Figure 62.

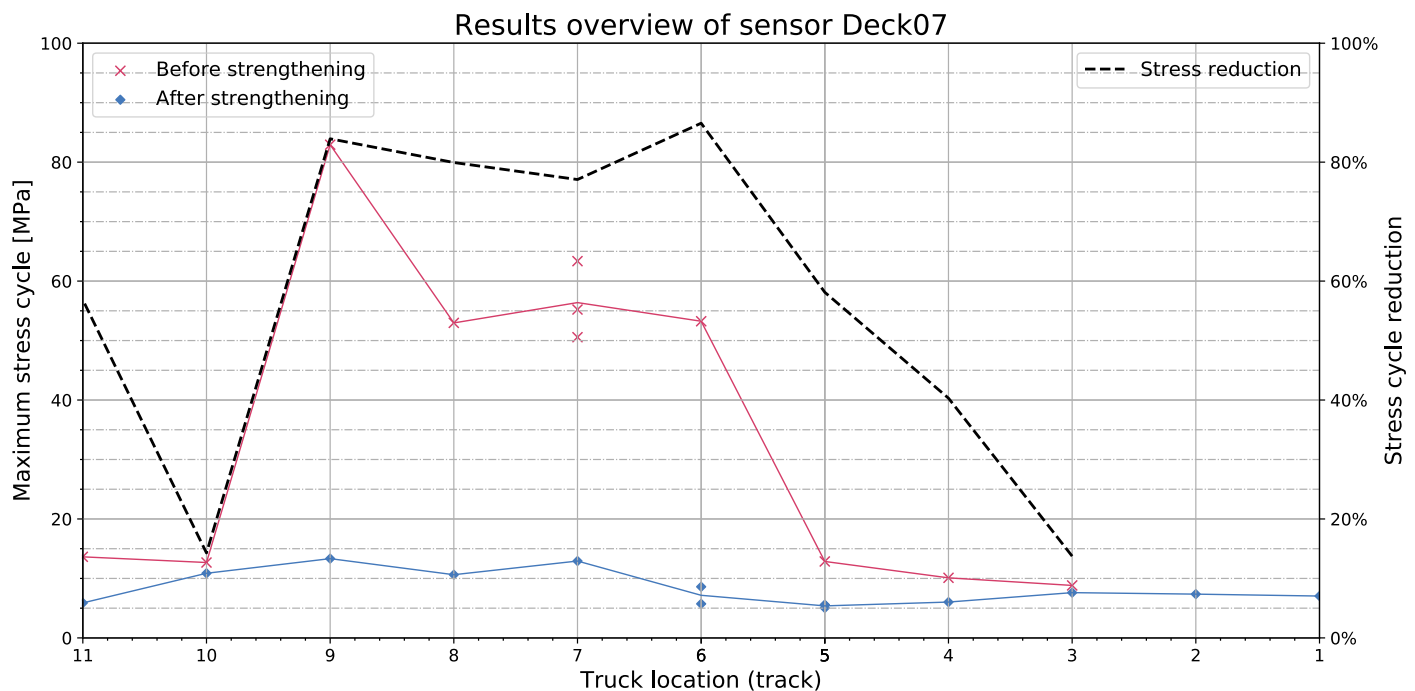


Figure 62: Overview results of Deck07, transverse bending of the deck plate at mid-bay

It can be seen that results of Deck09 and Deck07 are very similar. This is important since it indicates that the load test has been accurately performed since similar results are obtained for two different sensors, at different locations during different tests.

5.3.2. At mid bay, measuring longitudinal strain

Two sensors were installed that measure longitudinal strain at mid-bay: Deck08 and Deck10. However, because of the error during the execution of load test 1, no relevant data is obtained for Deck10, since it is located over track 1 which was not driven over before the strengthening.

In Figure 63, the results of Deck08 are shown for the unstrengthened deck.

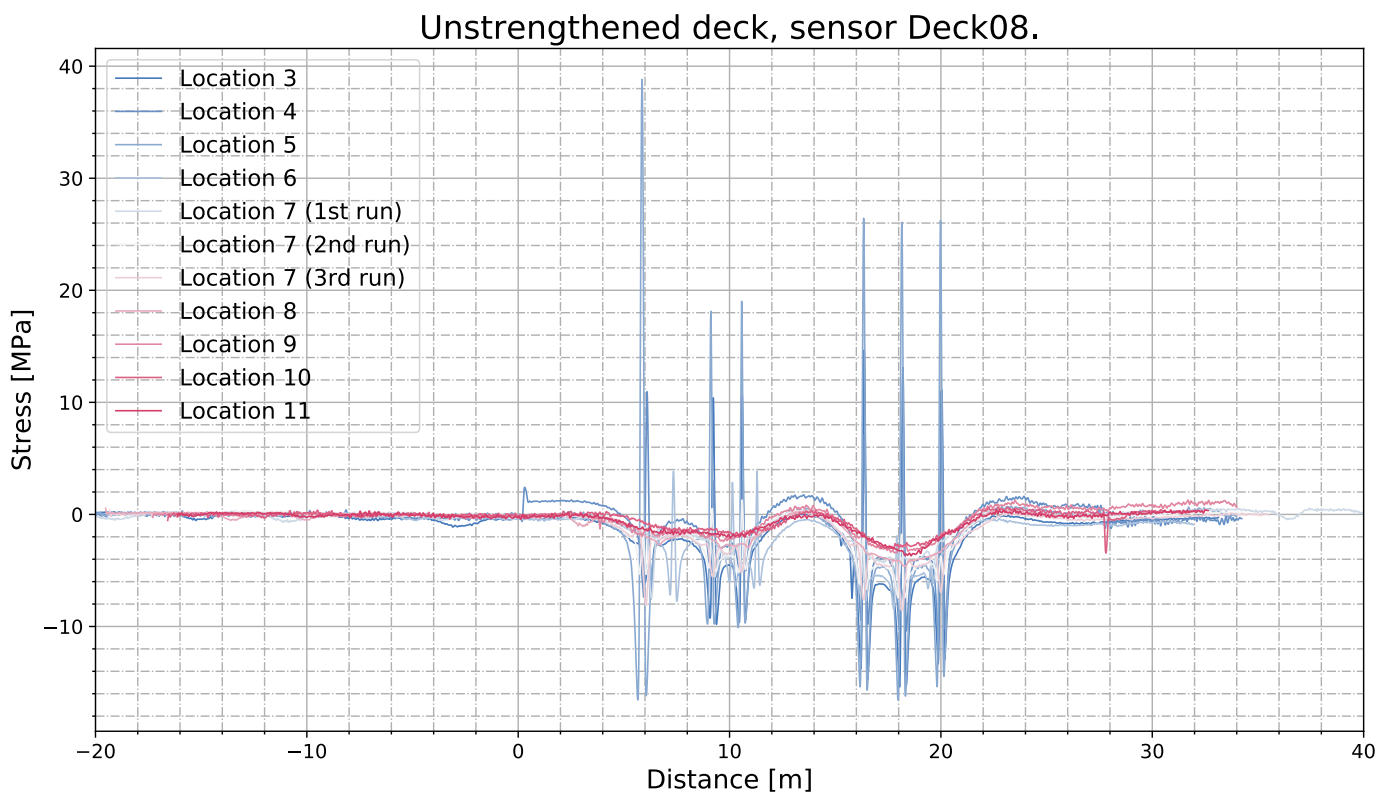


Figure 63: Results from the load test on the unstrengthened bridge, longitudinal bending of the deck plate at mid-bay

Since these sensors measure strain in the longitudinal direction rather than the transverse direction, this means that the longitudinal bending of the deck plate is measured instead of the bending between the troughs. This is also very local behaviour, as can be seen by the very peaky influence line of Figure 63. The individual wheels can clearly be distinguished, especially in the unstrengthened bridge. The deck structure is so flexible in the unstrengthened deck that longitudinal compressive stresses are observed in the bottom of the deck plate before and after the axles, indicating the deck plate is bending upwards.

The strengthening is expected to be very effective at this location since stresses in the deck plate due to local loads are highly dependent on the stiffness of the deck. The results of the strengthened deck are shown in Figure 64. For this once, all results are presented to visualise the stark contrast between the strengthened and unstrengthened bridge.

Strengthened deck, sensor Deck08.

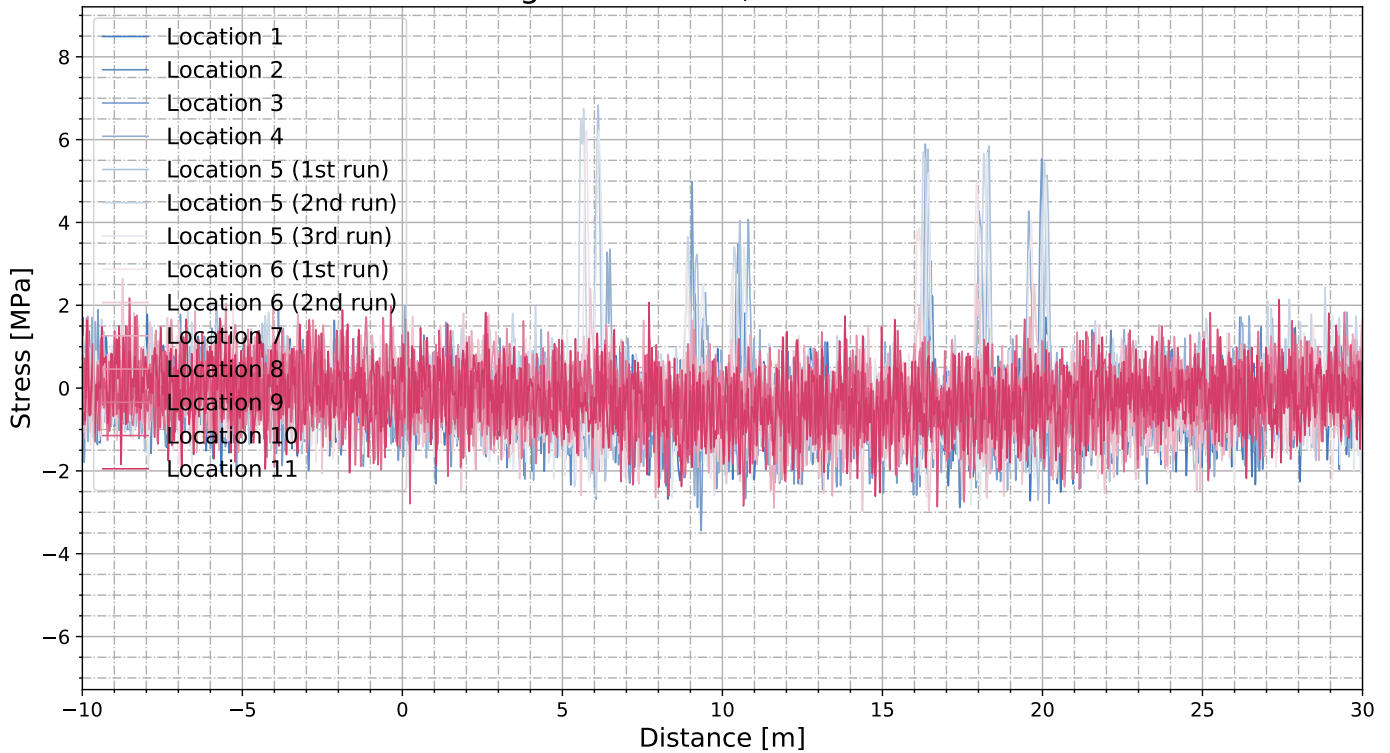


Figure 64: Results from the load test on the strengthened bridge, longitudinal bending of the deck plate at mid-bay

Load test results, track Location 5, sensor Deck08

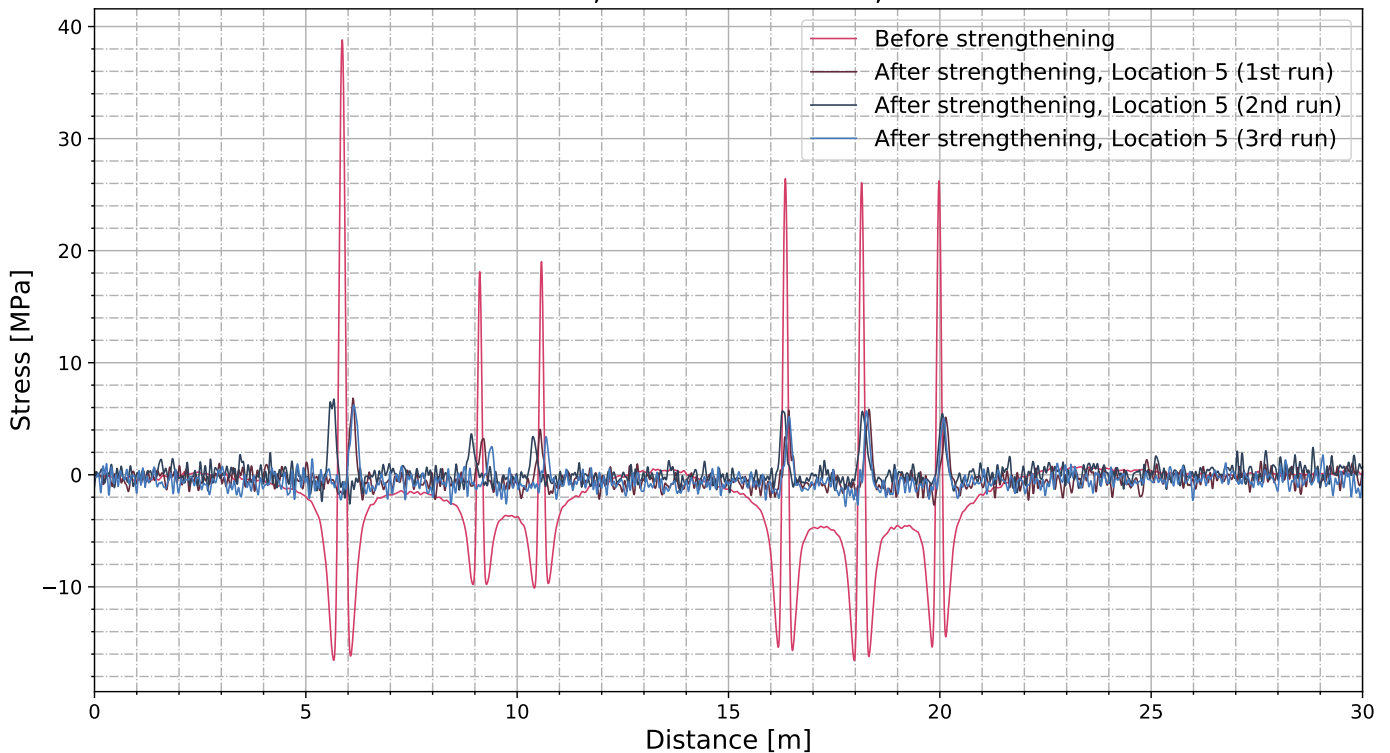


Figure 65: Comparison before and after strengthening, longitudinal bending of the deck plate at mid-bay

It can be seen that only some small peaks are observed after the strengthening in only a few weave locations. Furthermore, the negative stress peaks before and after the wheels are not discernible anymore. In Figure 65, the results from before and after the strengthening are compared. The results are again focused on track

5, which is when the truck drives directly over the sensor, causing the largest stress cycle. Furthermore, Figure 66 provides an overview of the results of all tracks.

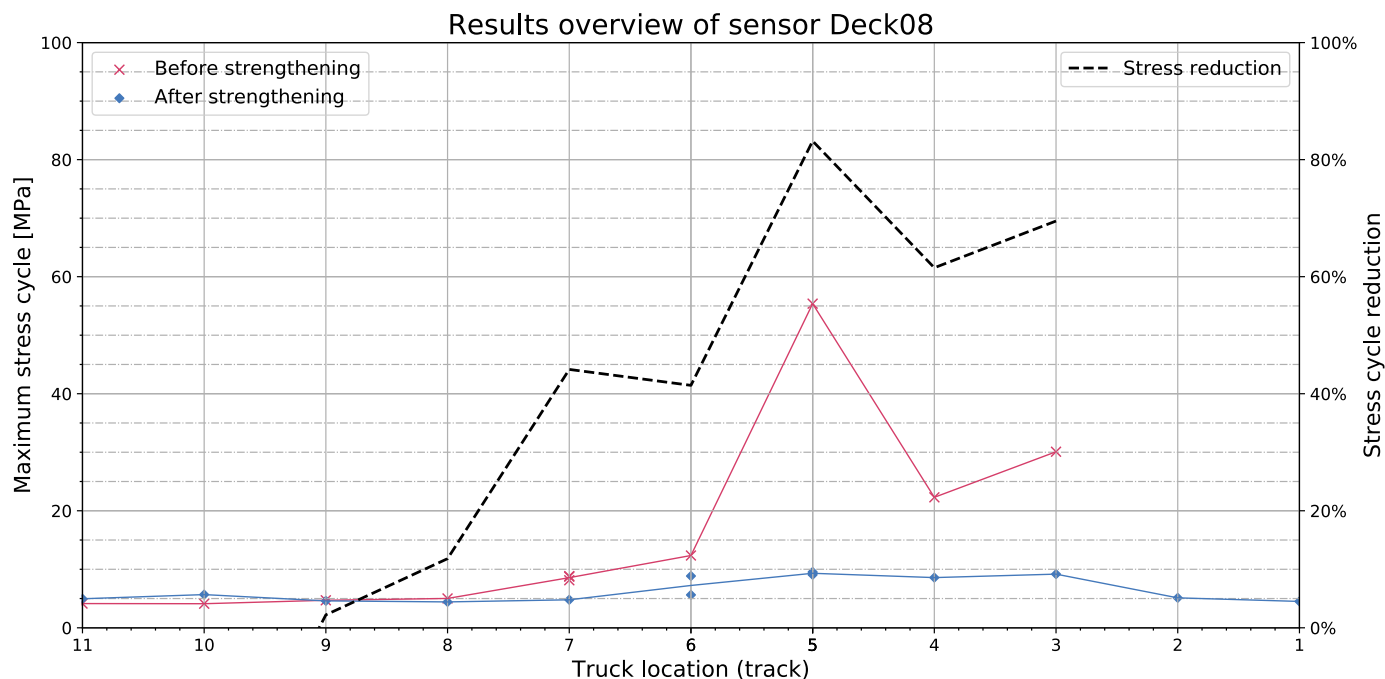


Figure 66: Overview results of Deck08, longitudinal bending of the deck plate at mid-bay

It can be seen that as was expected, the strengthening does a good job reducing the longitudinal stresses in the deck plate. Very limited stress cycles are observed after strengthening as the stiff deck plate restrains a lot of the local longitudinal bending.

From the transverse influence line in Figure 66 the stiffening the deck can clearly be seen. The largest stress cycle that was observed during the load test was reduced by around 83% for this sensor, with diminishing effectiveness away from the local stress peak.

5.3.3. At cross girder, measuring transverse strain

This type of sensor, measuring transverse strain in the bottom of the deck plate close to the cross girder, has been applied the most. Close to the cross girder, sensors Deck01 and Deck03 are installed to measure transverse strain. Furthermore, sensors Deck04 and Deck05 are installed close to Deck03 to investigate how the behaviour differs at different distances from the cross-girder and from the bolted connection that will be installed during the strengthening. Figure 50 can be reviewed for an overview of all sensor locations.

These sensors are of particular interest because they shed light on the behaviour of the strengthened bridge close to the bolted connection. The stresses at different distances from the bolted connection give a lot of information that can be used to verify the numerical models in the later chapters of this thesis.

Firstly, Figure 67 and Figure 68 show the results from sensors Deck01 and Deck03 for the relevant tracks. Furthermore, Figure 69 provides an overview of sensors Deck03, Deck04 and Deck05.

Load test results, track Location 9, sensor Deck01

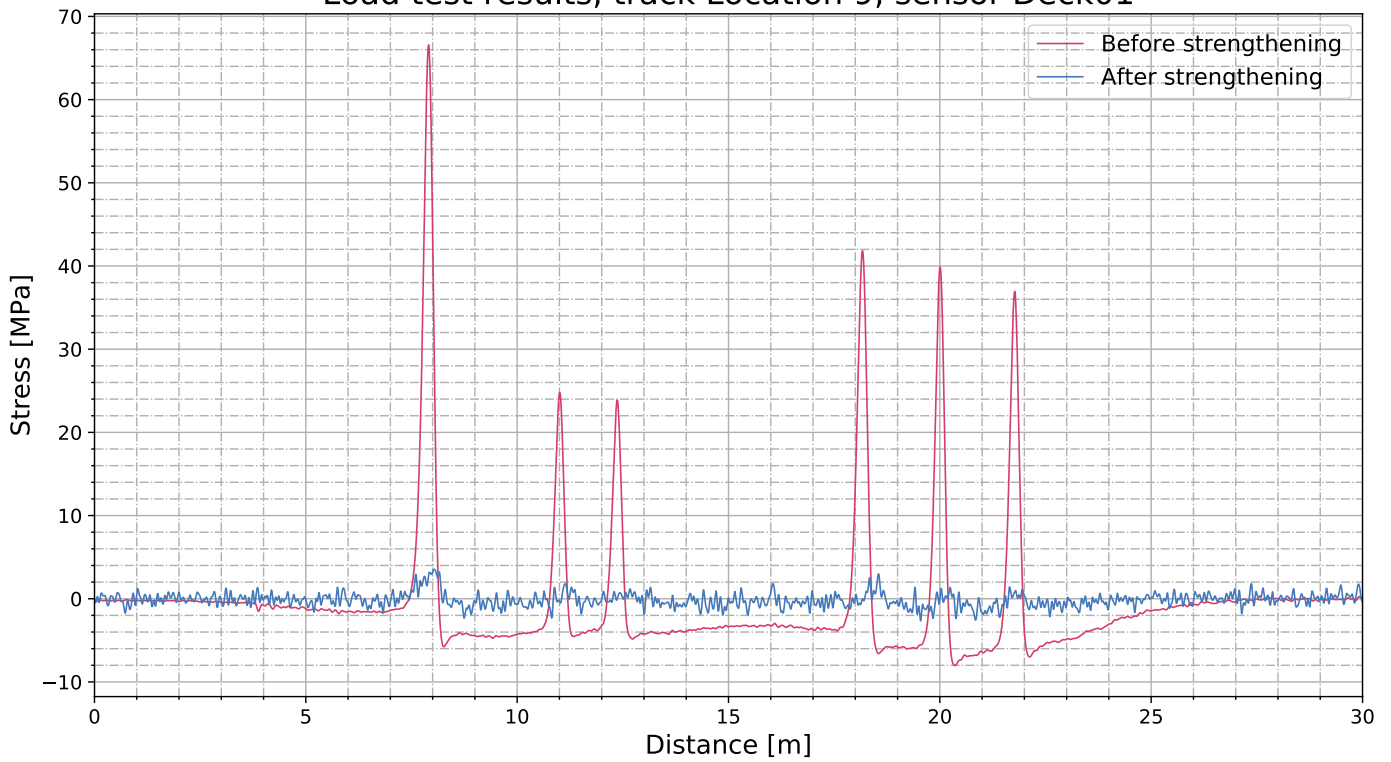


Figure 67: Comparison before and after strengthening, transverse bending of the deck plate at cross girder, sensor Deck01

Load test results, track Location 5, sensor Deck03

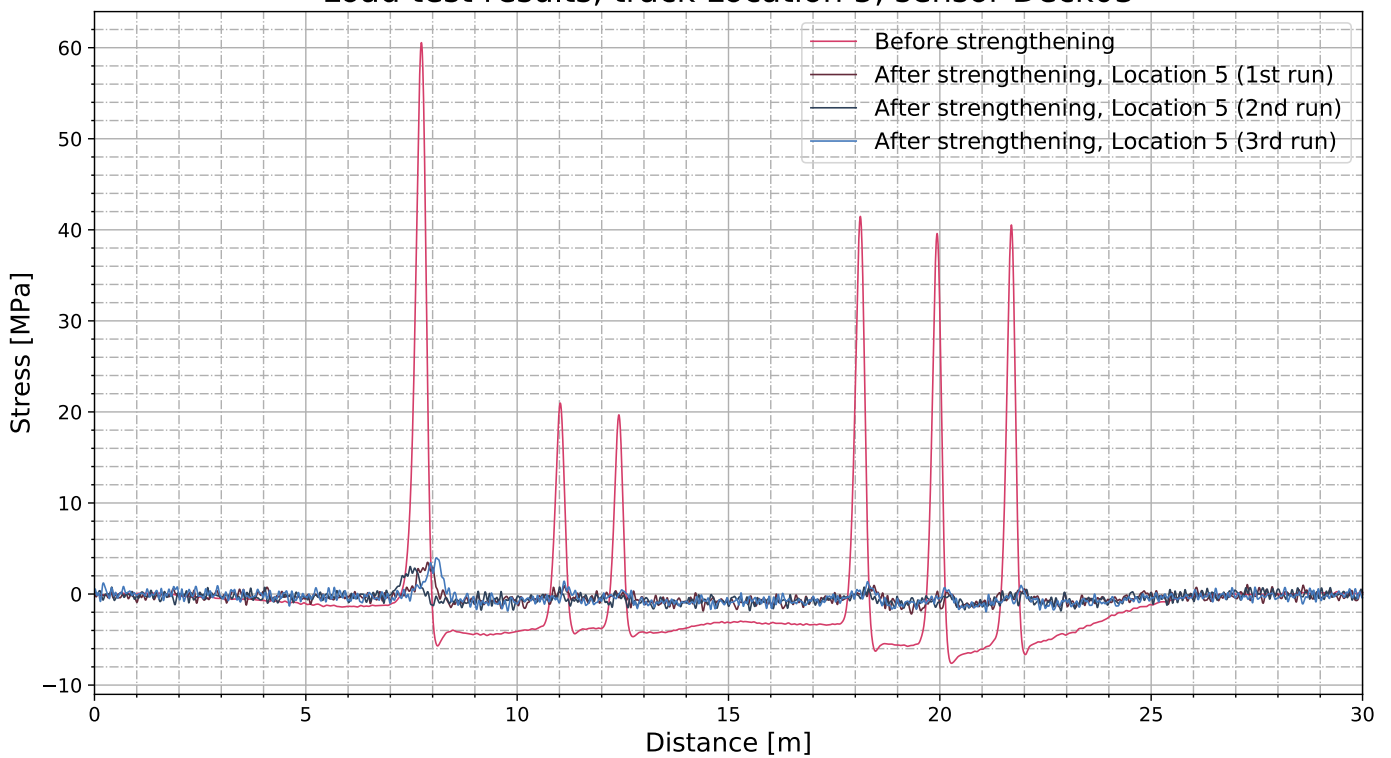


Figure 68: Comparison before and after strengthening, transverse bending of the deck plate at cross girder, sensor Deck03

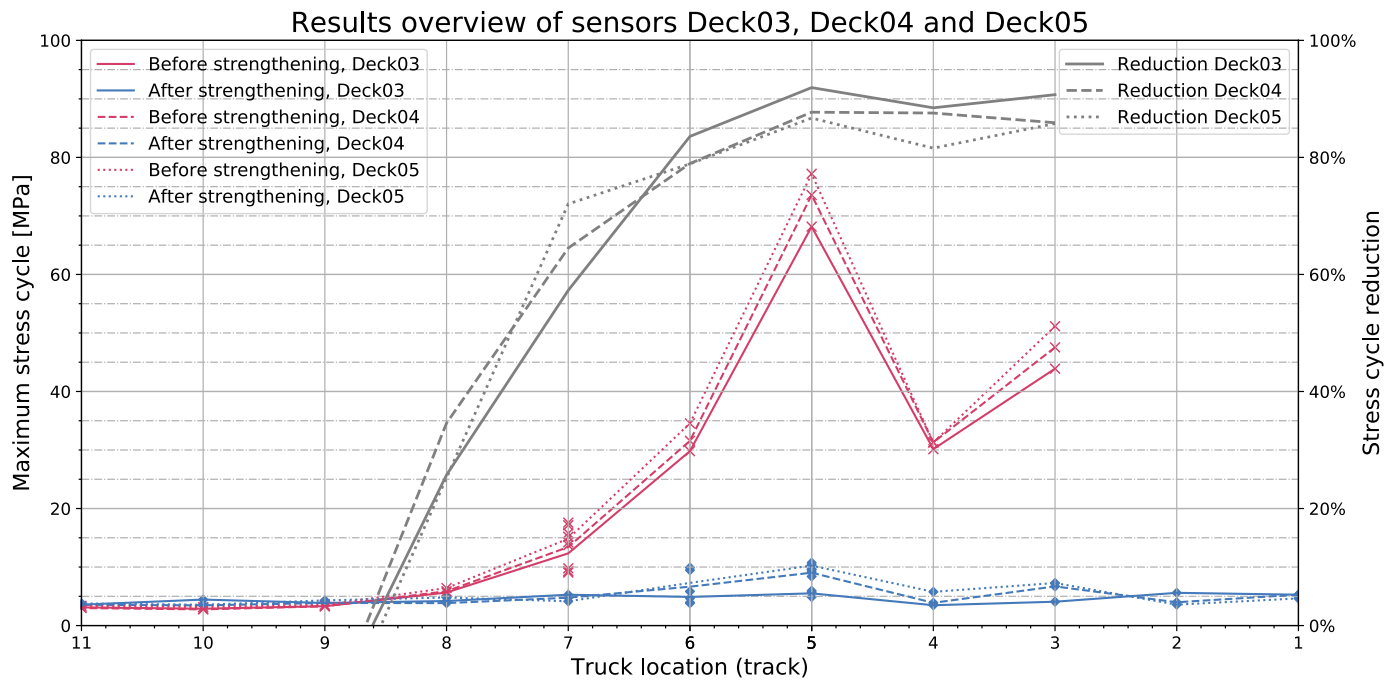


Figure 69: Overview results, transverse bending of the deck plate at cross girder

Firstly, it can be observed that the results of Deck01 and Deck03 match well, indicating that the load test has been performed accurately. Both sensors show a peak stress of around 60-65 MPa, which gets reduced by more than 90% due to the strengthening. Furthermore, the results of Deck03, Deck04 and Deck05 also match each other very closely and show no irregularities, indicating accurate results are obtained.

When examining Figure 69, it can be seen that both before and after strengthening, the stress cycle increases as the distance from the bolted connection increases (Deck03→Deck04→Deck05). It can be seen that the strengthening is more effective the closer the sensor is to the bolted connection. This is especially visible for sensors Deck01 and Deck03 that are positioned only 75mm next to the centre of the bolt. This clamps the deck plate to the strengthening plate and therefore locally stiffens the strengthened deck plate, almost entirely eliminating the stress cycles at the bottom of the deck plate.

To further investigate the behaviour of the bridge deck and the influencing factors, the results close to the cross-girder can be compared to the results at mid bay. This is illustrated below in Figure 70 and Figure 71, where transverse strains in the deck plate are compared.

Load test results before strengthening, track Location 5

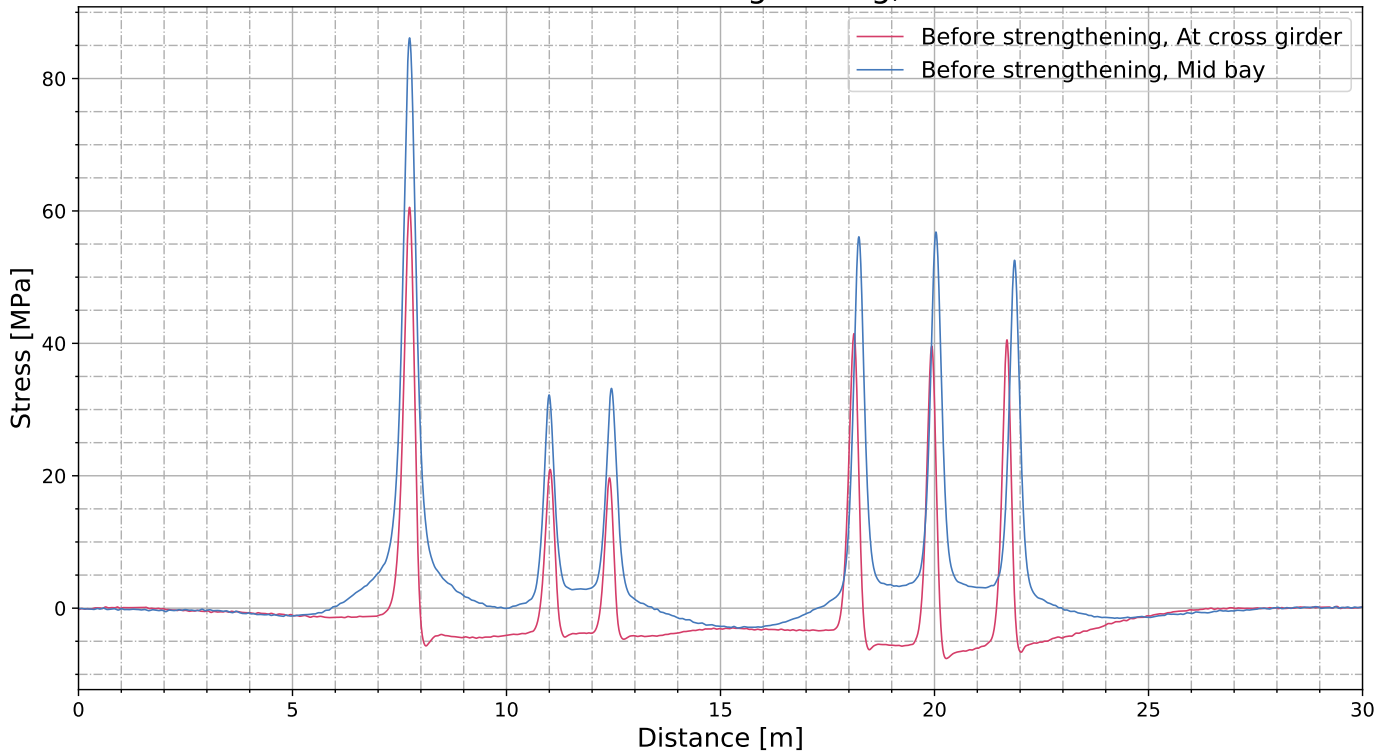


Figure 70: Comparison of transverse deck plate stresses at cross girder and mid bay, before strengthening, track 5

In Figure 70 it can be seen that at the cross-girder, the influence line has much sharper peaks than at mid bay. This is likely due to the deck plate and troughs being restrained by the cross-girder in this location. The same can be seen in Figure 71 for the strengthened bridge, with an even larger difference in peak values. This is in agreement with the previous results comparing sensors Deck03, Deck04 and Deck05, and it can be seen that beyond the first axle almost no relevant stress cycles are observed.

Load test results after strengthening, track location 5

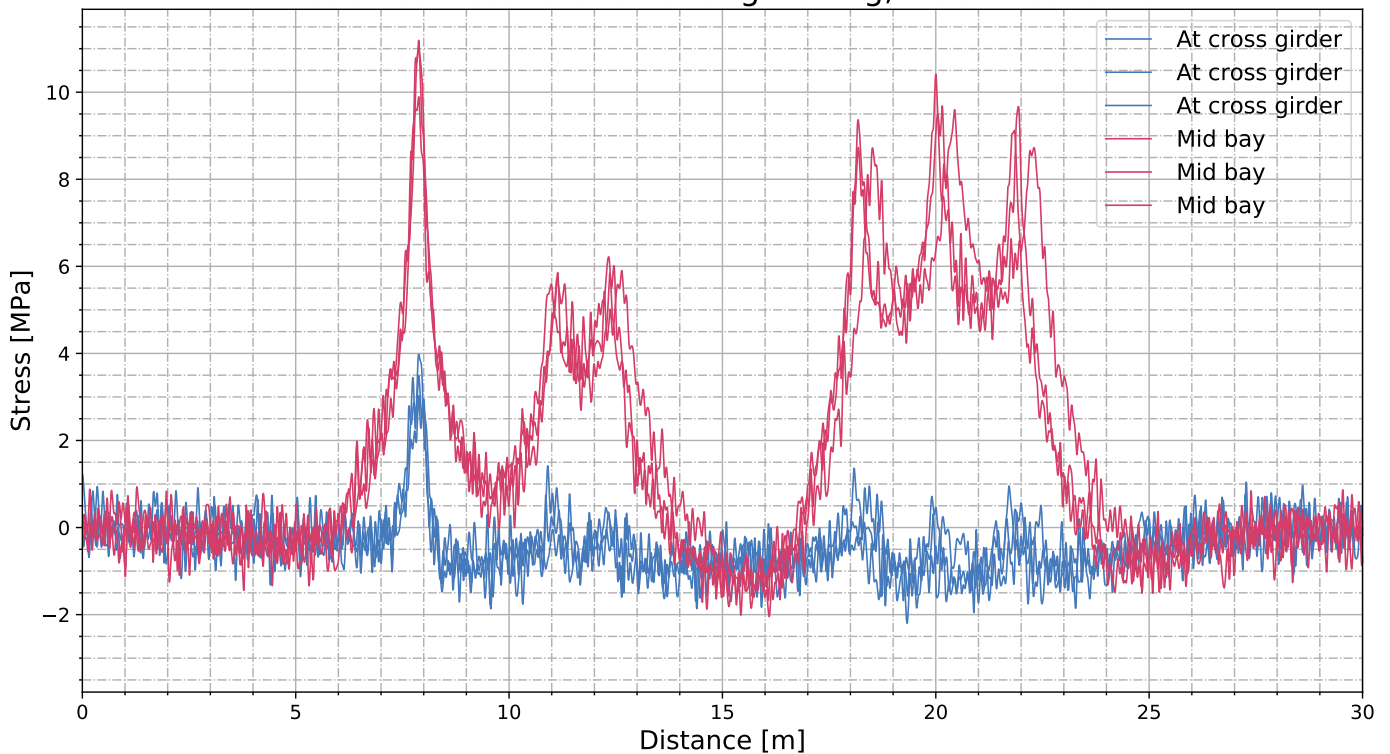


Figure 71: Comparison transverse stresses at cross girder and mid bay after strengthening, track 5

5.3.4. At cross girder, measuring longitudinal strain

Sensor Deck02 has been placed very close to the cross girder, at only 75 mm from the edge of the web, measuring longitudinal strain at the bottom of the deck plate. Figure 72 and Figure 73 present the results of this sensor.

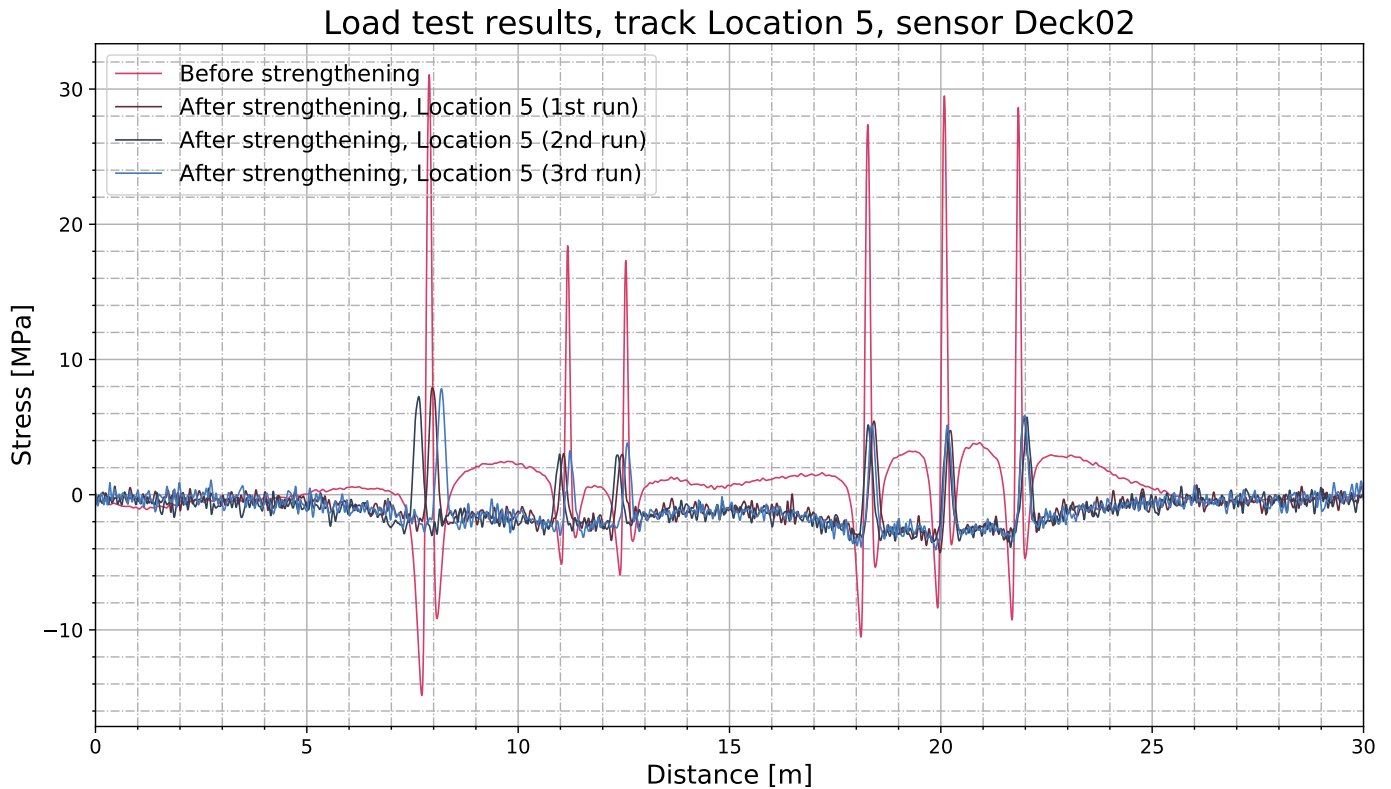


Figure 72: Comparison before and after strengthening, strain gauge Deck02, track 5

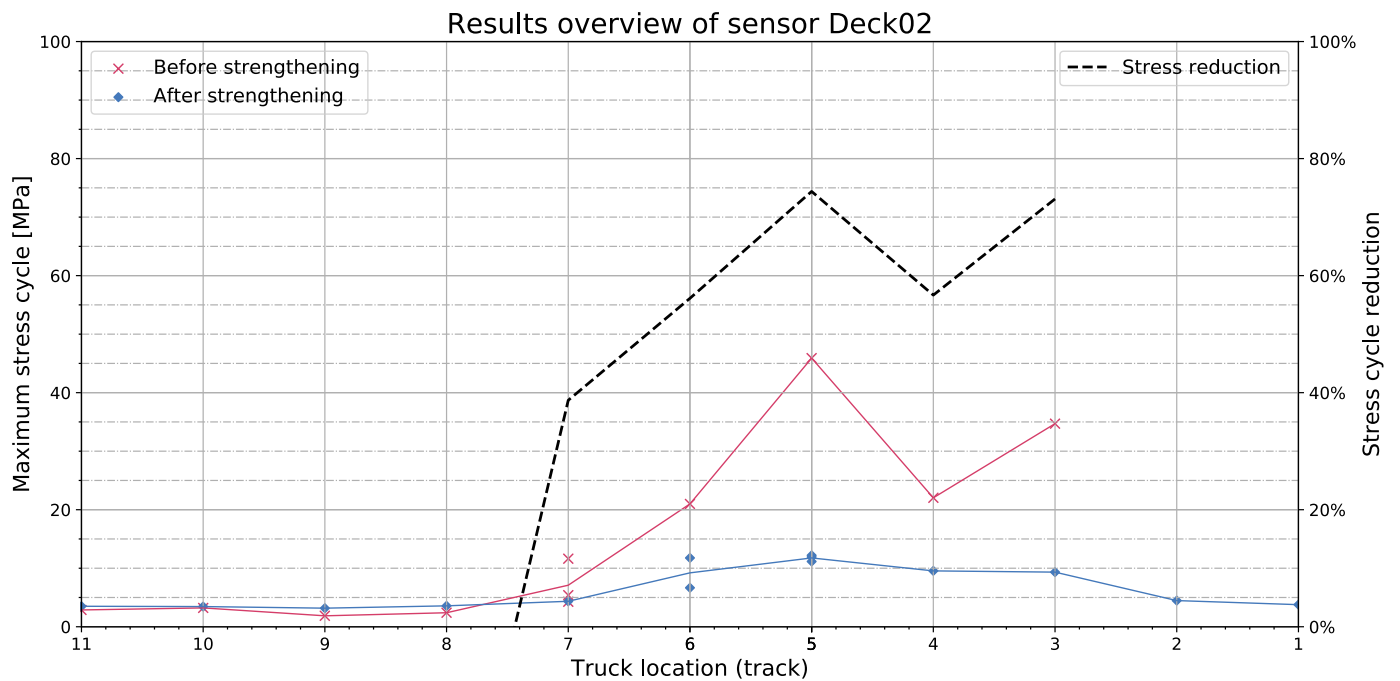


Figure 73: Overview results of Deck02

The results shown in Figure 72 show a few curious things. Before the strengthening, the observed behaviour was very local bending in the deck plate, similar to the sensor at mid bay. As expected, the strengthening does a good job reducing the large stress cycles due to this local bending. The overview in Figure 73 shows a reduction of around 75%, similar to the other types of sensors. However, the stresses observed in between

the truck axles is notably different between the two situations. Before strengthening, the bottom of the deck plate is in tension in between the truck axles, whereas it is in compression after strengthening.

The bottom of the deck plate being in compression means that the deck plate is bending upwards in longitudinal direction due to the strengthening. What this likely means is that due to the strengthening, the stiffer deck plate is exhibiting more global behaviour by bending over the stiff cross-girder, rather than bending downwards due to the local wheel loads.

5.4. Troughs

Lastly, four strain gauge sensors were installed on the trough bottoms. Two different types of trough sensors can be distinguished:

1. At mid bay
2. At cross girder

As with the deck plate sensors, the results will be presented and discussed per category:

5.4.1. At mid bay

At mid bay, sensor Trou03 measured longitudinal strain at the bottom of the trough. Since this location is at the bottom of the trough rather than on the deck plate, the strengthening is expected to have less impact than for the deck plate sensors.

First, Figure 74 and Figure 75 show the results of all tracks of both the unstrengthened and the strengthened bridge.

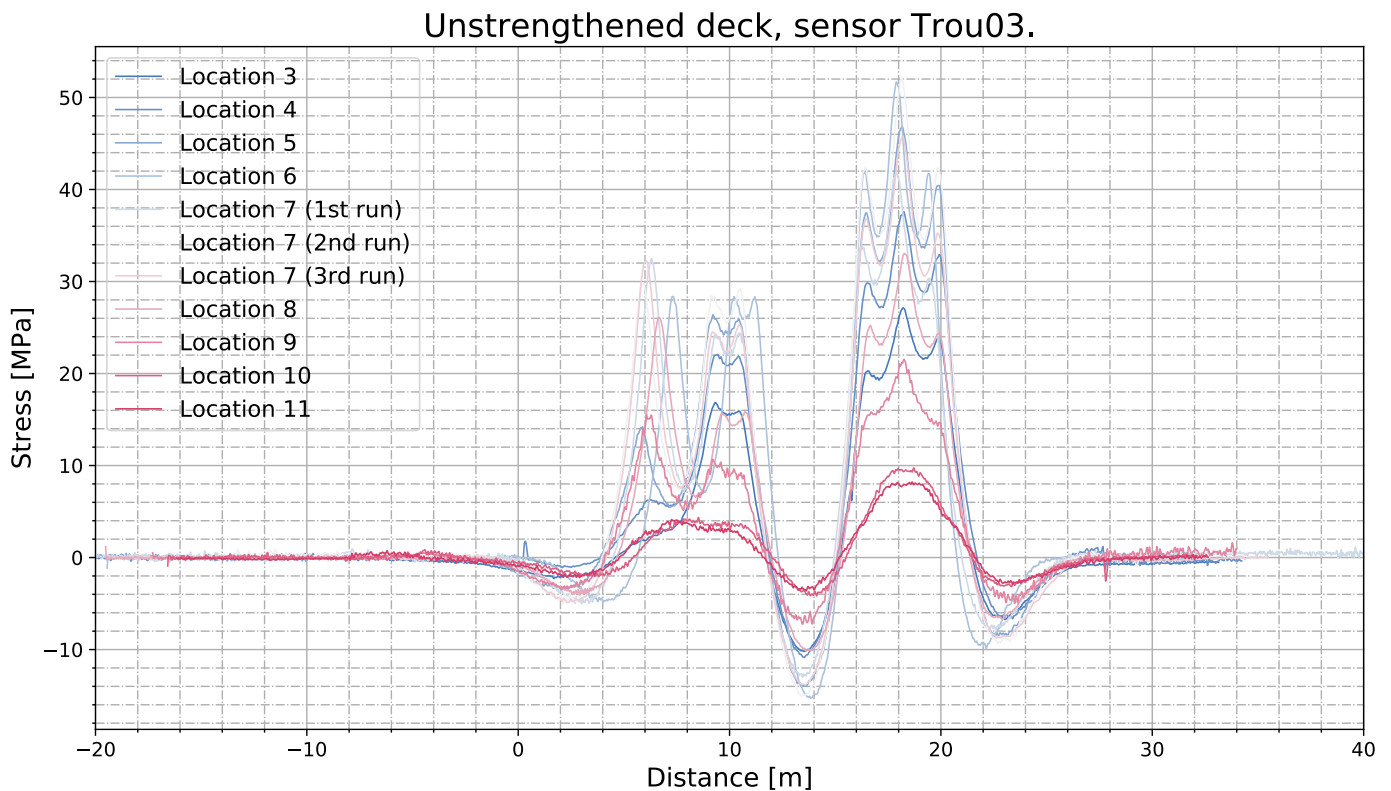


Figure 74: Results from the load test on the unstrengthened bride, trough at mid-bay

Strengthened deck, sensor Trou03.

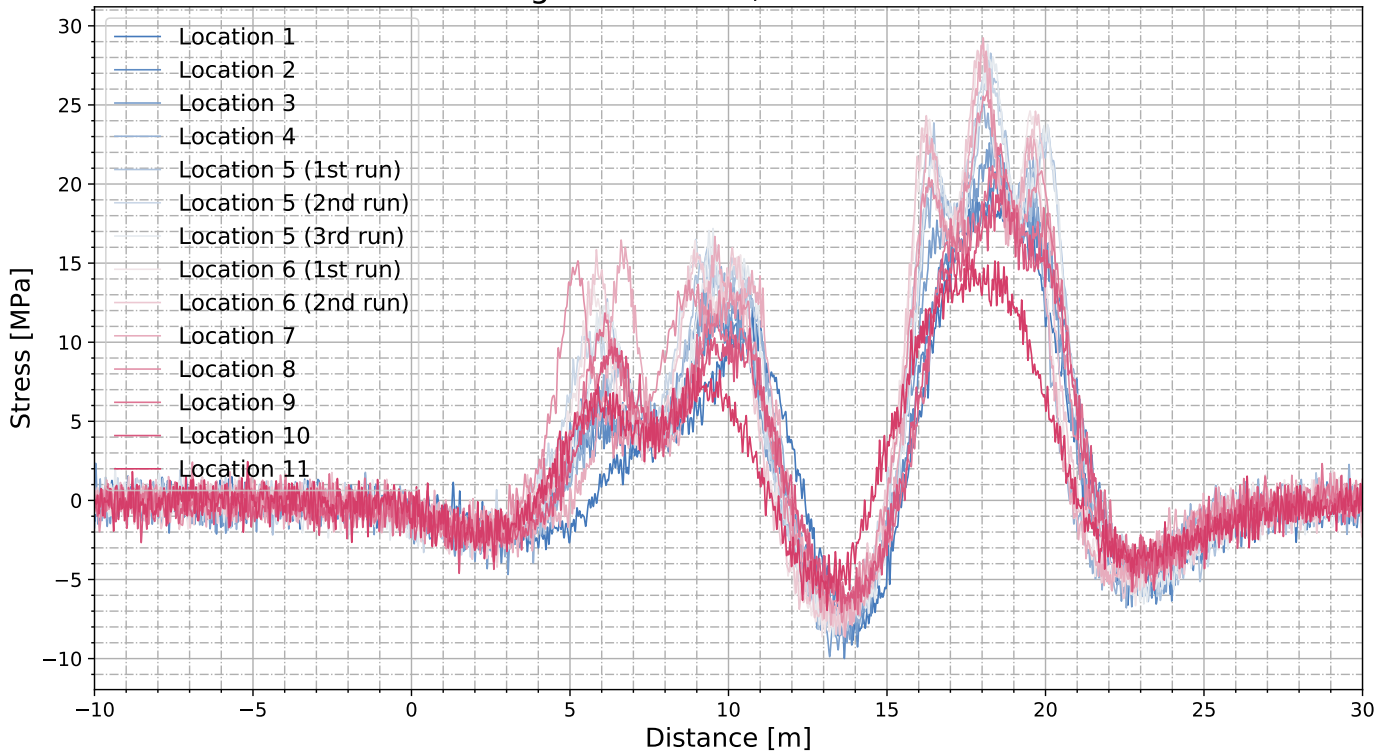


Figure 75: Results from the load test on the strengthened bridge, trough at mid-bay

From these first results, a couple of observations can be made. Firstly, bending at the bottom of the trough is less local than that in the deck plate. Individual peaks are still observed, but the trough is also activated in between the axles, carrying the load between the cross girders. Furthermore, it seems that the maximum stresses in the bottom of the trough are a result of the back three axles. This is more similar to the global behaviour shown by the cross girder rather than the deck plate, which experienced the highest peak due to the first axle.

It also seems that the increased stiffness of the strengthened bridge has a positive effect on the load spreading, with all 11 locations showing very similar results for the strengthened scenario. In Figure 76, a comparison is made before and after strengthening. Location 6 is used for this, since this is when most of the weight of the back three axles is located on top of the trough, causing the largest stress cycle. Figure 77 shows an overview of all the locations and an indication of the effectiveness of the strengthening for this sensor location.

Load test results, track Location 6, sensor Trou03

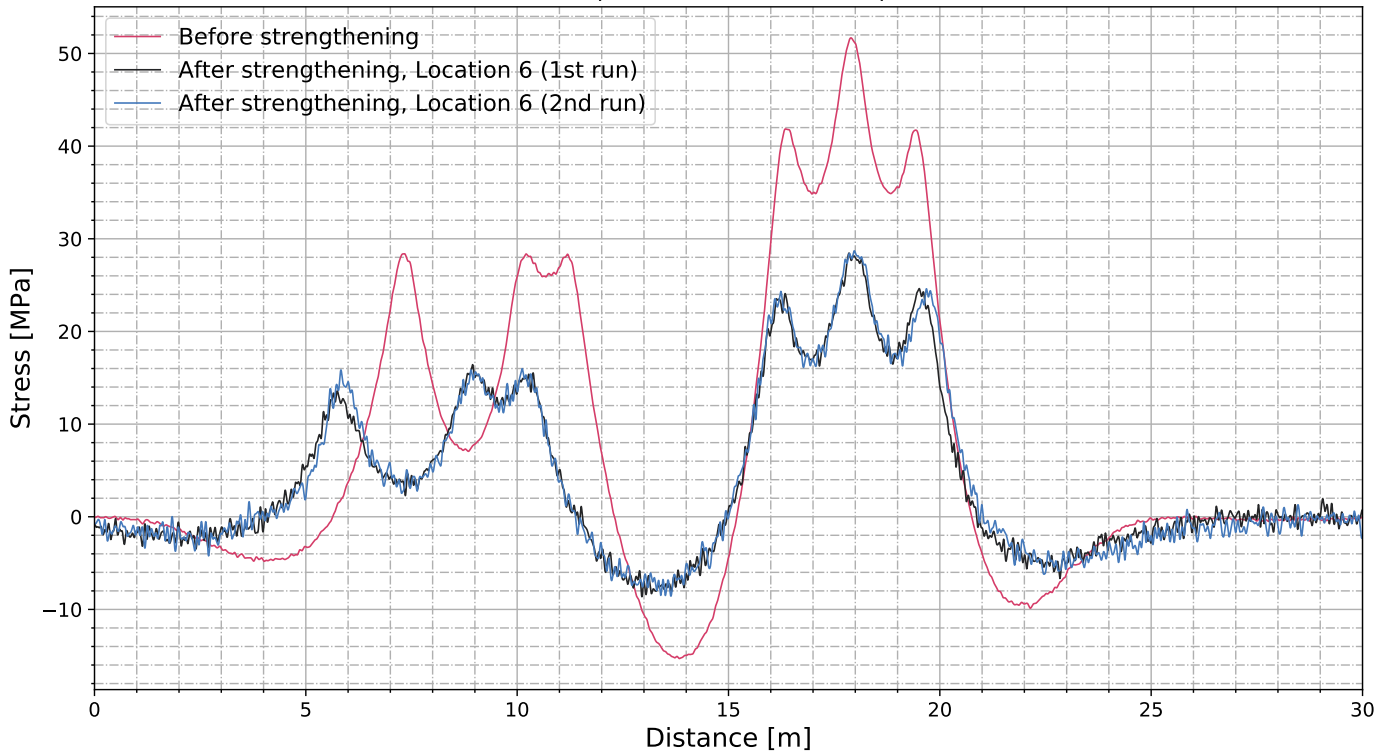


Figure 76: Comparison before and after strengthening, trough at mid-bay

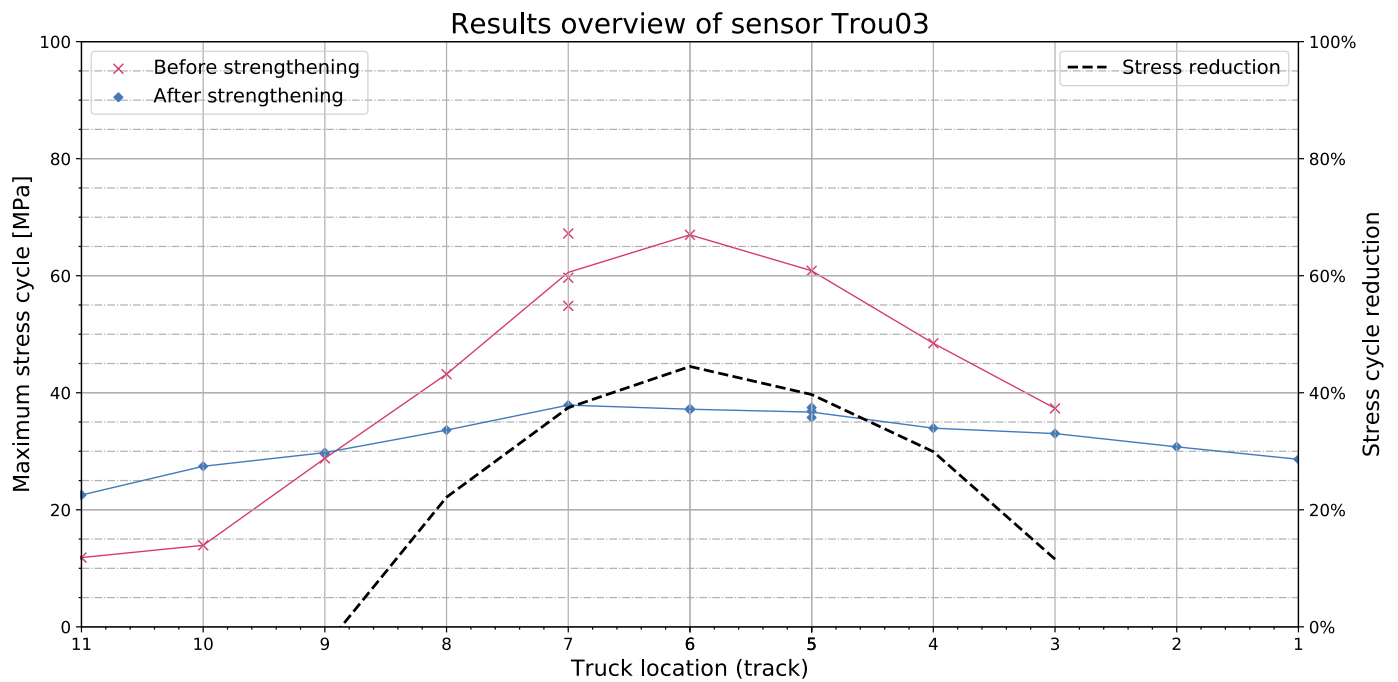


Figure 77: Overview results of trough at mid-bay

In Figure 77, it can clearly be seen that the strengthening has made the structure a lot stiffer and better at spreading the load. There is a lot more load spreading between troughs, which reduces the peak stresses that one trough has to carry. The strengthening manages to reduce the peak stresses in this location by around 45%. Even though the effectiveness decreases as the load moves to adjacent troughs, the stress cycles also become significantly smaller.

5.4.2. At cross girder

Lastly, the trough sensor at the cross girder will be discussed. This sensor is of particular interest since the fatigue detail between the trough and the cross girder is the most critical detail in this bridge, and this sensor

captures the stresses close to this location. Furthermore, it is also the most difficult sensor to interpret since the behaviour is a combination of bending of the trough and bending of the cross-girder. Firstly, Figure 78 and Figure 79 show the results of both the unstrengthened and the strengthened bridge. For the strengthened bridge, some selected tracks are chosen to keep the results clear and presentable.

Unstrengthened deck, sensor Trou01.

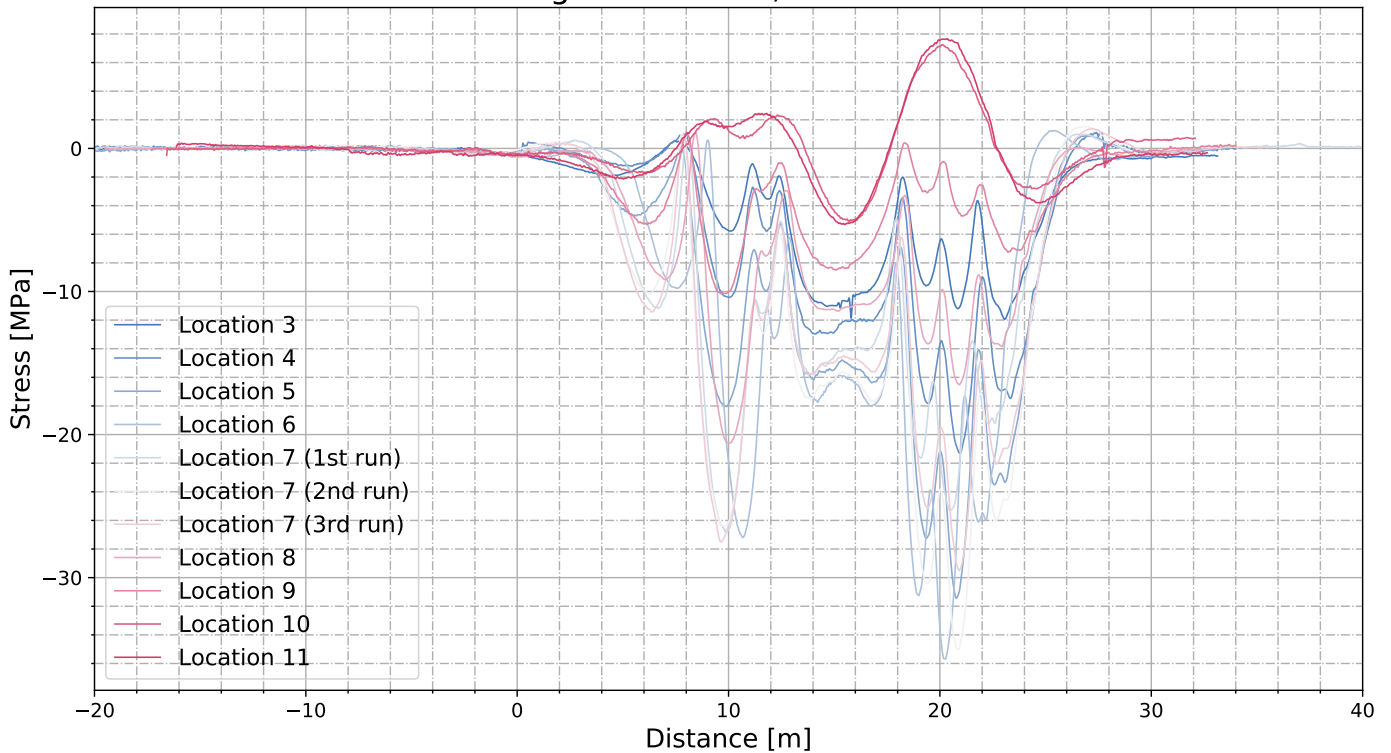


Figure 78: Results from the load test on the unstrengthened bride, trough at cross-girder

Strengthened deck, sensor Trou01.

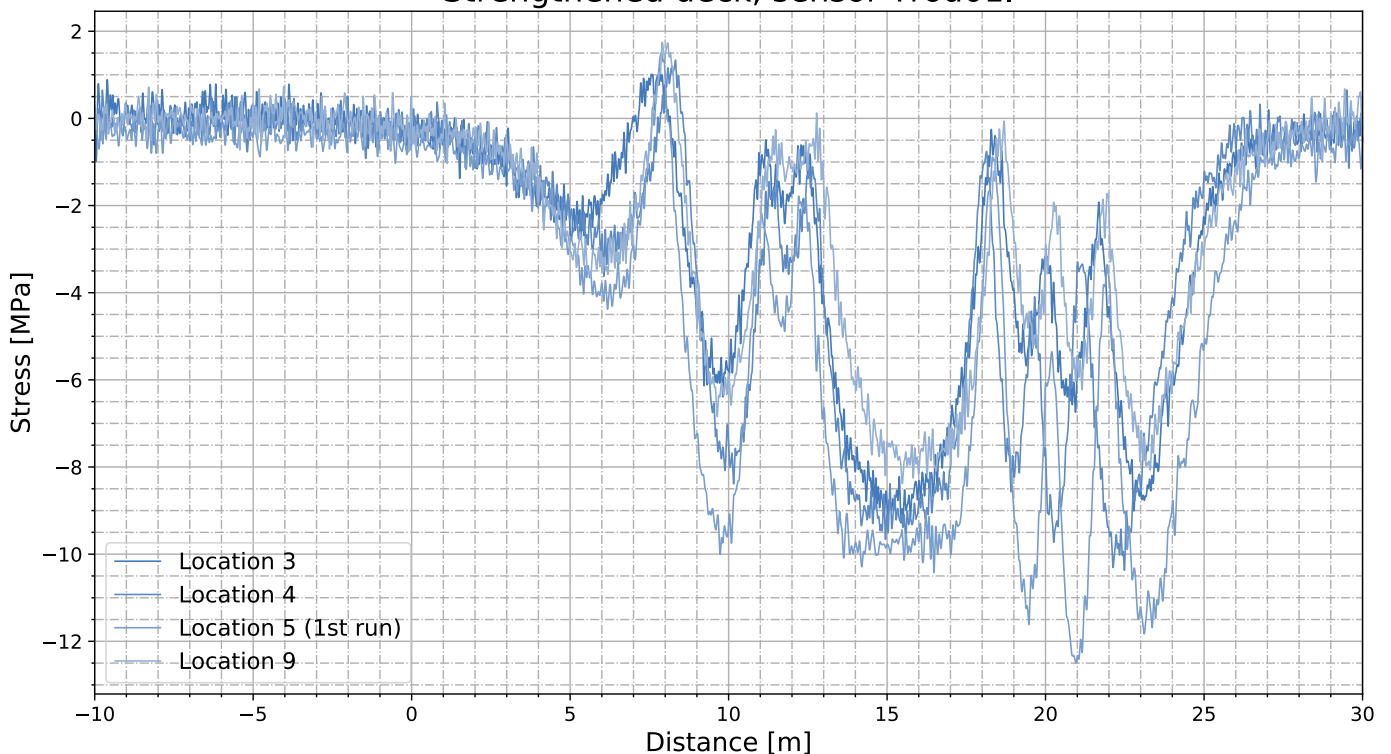


Figure 79: Results from the load test on the strengthened bride, trough at cross-girder

First of all, it can be seen that the behaviour of this sensor looks different than the one at mid bay. However, the behaviour is actually very similar on closer inspection. There are still six distinct tensile peaks visible, corresponding to the six axes. Also, in between the axes, the trough is transferring load to the cross girders. The difference is that since this sensor is located so close to the cross girder, the global behaviour is that the deck and troughs are bending upwards, causing compressive stresses in the bottom of the trough.

A comparison before and after strengthening is shown in Figure 80, and in Figure 81 an overview of the results is presented.

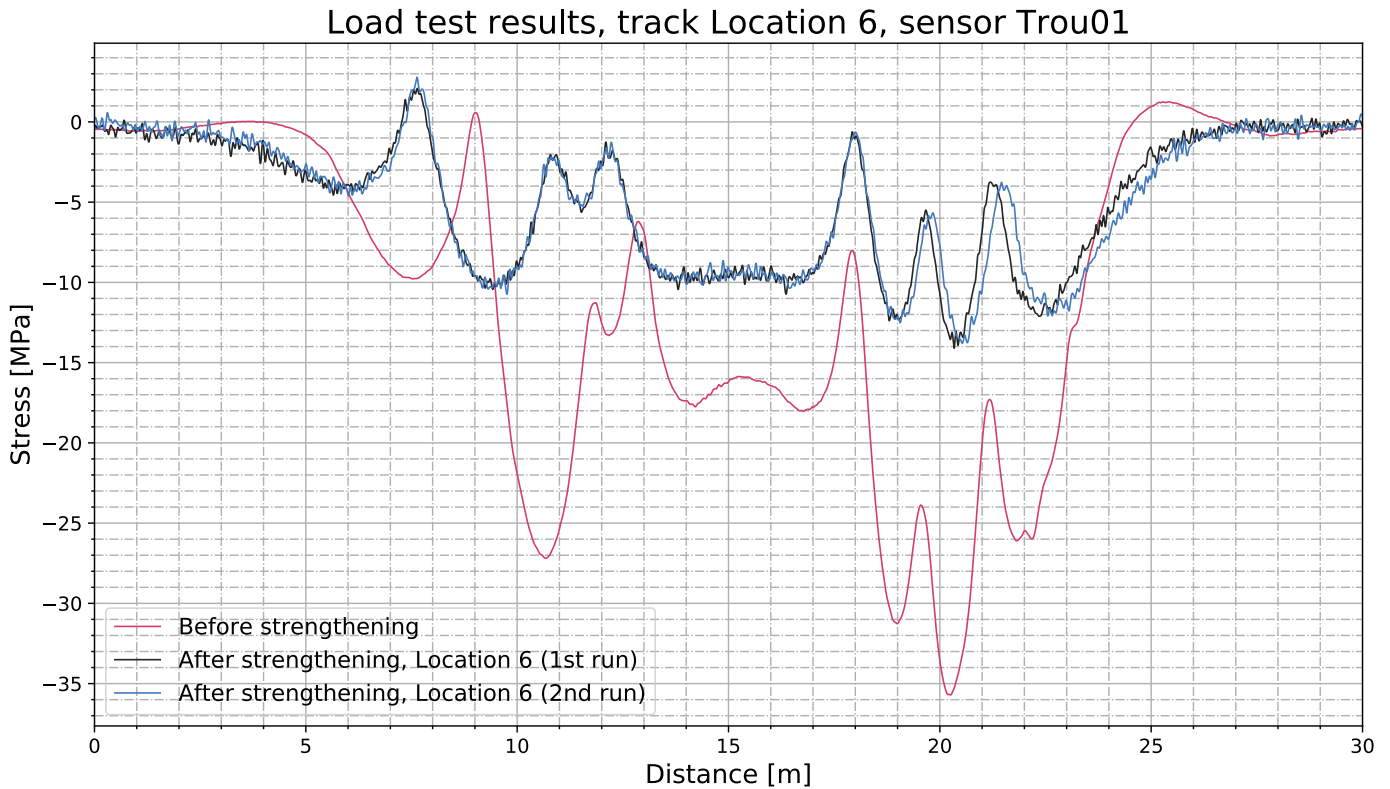


Figure 80: Comparison before and after strengthened bridge, trough at cross-girder

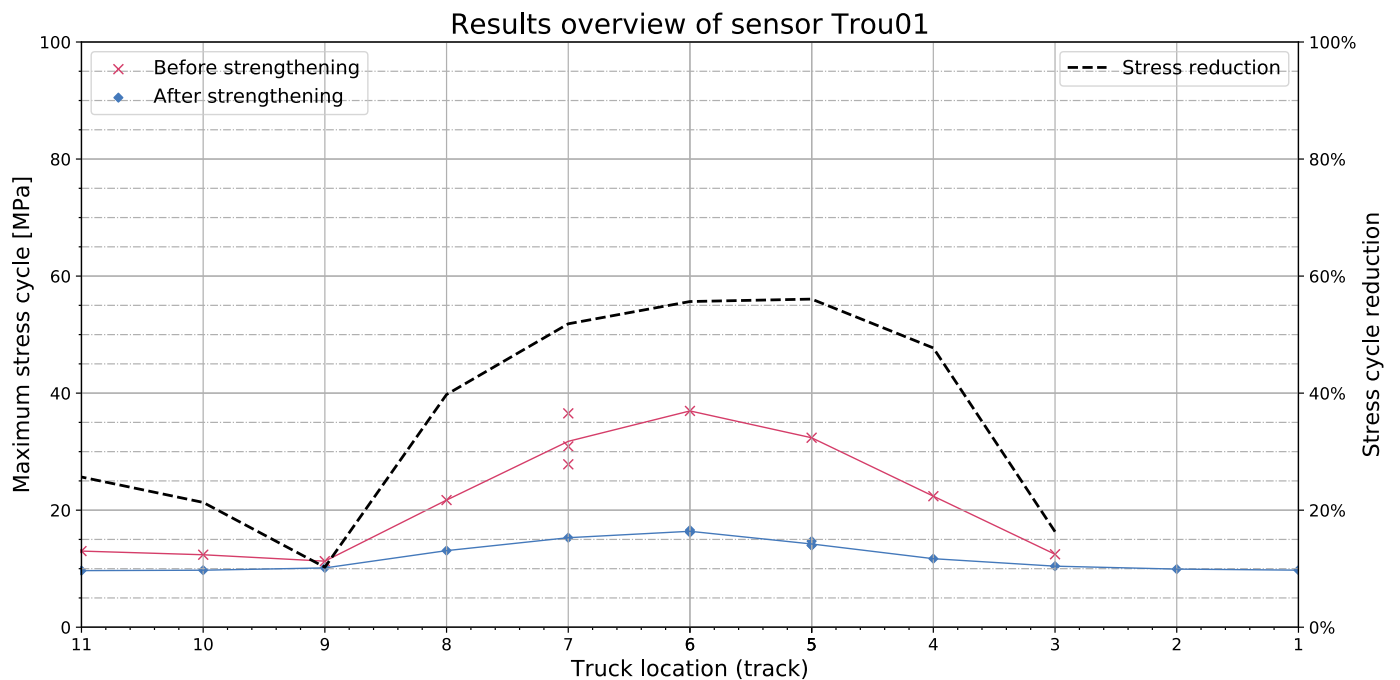


Figure 81: Overview results of trough at cross-girder

Figure 80 shows that the behaviour before and after strengthening stays very similar. The largest improvement seems to be made in the stresses experienced in between the axles. The bolted connections stiffen the deck structure and its connection to the cross girder significantly, relieving the troughs. From Figure 81 it can be seen that the effectiveness of the strengthening is higher at the cross girder than at mid bay. Moreover, it can be seen by the flatter transverse influence line that the strengthening helps distribute the load between different troughs at this location as well.

5.5. Summary

In this chapter, a lot of data has been presented and discussed. This section will give a short summary of the main findings and conclusions that can be made regarding the load test results.

First of all, it can be concluded that all the load tests have been carried out accurately. In comparisons between different sensors and in comparisons of data gained through repeating the same load test multiple times, no major deviations or unexplainable results have been obtained. For the load test on the unstrengthened bridge, some uncertainty is unavoidable due to the high sensitivity of the results on variables such as the exact transverse location of the wheel. This is simply due to the very flexible unstrengthened bridge deck, and this will have to be considered when comparing the load test results to the numerical results.

Secondly, it is concluded that the strengthening is behaving as expected, and that significant stress reductions are observed at the strain gauge locations. In Table 11, a summary is presented of the stress reduction that was observed in the load tests. For the cross girder, as expected, limited reduction is observed as the sensor is at the bottom of the bottom flange, far away from the strengthened area. For the deck plate, a stress reduction of 85-90% is observed for transverse stresses, both close to the cross girder and at mid bay. This location experienced high local stresses due to the wheel loading which get reduced massively due to the stiffened deck. Finally, a reduction of 45-55% is found for the trough bottom sensors. This location is further away from the stiffened deck, but due to the increased stiffness of the strengthened deck package more troughs are activated to carry traffic loading. Therefore, this stiffening also significantly reduces peak stresses in the bottom of the trough due to traffic loading.

Table 11: Summary of observed stress reduction in strain gauge locations

Sensor location	Observed stress reduction
Cross girder	5-10%
Deck plate (transverse stresses)	85-90%
Trough bottom (longitudinal stresses)	45-55%

6. FE modelling

This section will lay out the framework of the FE modelling that has been carried out. Firstly, in section 6.1, the used software is presented. Modelling choices and details such as the mesh size, material properties, contact definitions etc. are presented and explained for the unstrengthened bridge in section 6.2 and for the strengthened bridge in section 6.3. Finally, the load generation is discussed in section 6.4.

6.1. Software

A lot of powerful finite element software packages are available such as Abaqus, NASTRAN and LS-DYNA. Both offer various implicit and explicit solvers and option for dynamic and non-linear simulations. Furthermore, Arup has developed its own industry friendly FE software GSA, which focusses on linear analyses but has extensive options in practical areas such as load case definitions.

As a starting point for the finite element modelling in this project, a NASTRAN model of both the strengthened and unstrengthened bridge has been provided by Arup. Because of the complicated nature of the FE model and the necessity for non-linear analyses, GSA software was not a viable option for this thesis. Furthermore, it is not yet possible in the Arup Amsterdam office to run NASTRAN models due to licence and hardware limitations. Instead, Arup has a powerful cluster for running LS-DYNA models, as well as their own dedicated pre- and post-processing software (OASYS software). Therefore, the best solution for this thesis was deemed to export these models to the LS-DYNA environment. Therefore, all analyses in this work have been done the LS-DYNA environment.

Below, an overview of the used software is shown.

Software used:

Pre-processing:	Altair HyperMesh version 2020 Oasys Primer version 17.1
Analysis	LS-DYNA release R12
Post-processing	Oasys D3PLOT version 17.1 Python 3.6.5

6.2. Unstrengthened model

The unstrengthened model consists 100% of shell elements. In total, the model consists of around 750 000 shell elements, with a shell size in deck plate of around 80x80 mm. As can be seen in Figure 82, the region where the sensor are located is meshed in more detail, with the element size ranging from 40x40 mm all the way down to 4x4 mm elements. Besides for static analysis, the model was also used for fatigue verifications. The mesh is set up for the extraction of hot spot stresses at the welds connecting the deck plate to the trough, the deck plate to the cross-girder and the trough to the cross girder, as can be seen in Figure 83. The elements were defined so that the stress is extrapolated to a weld length from the intersection of the plates.

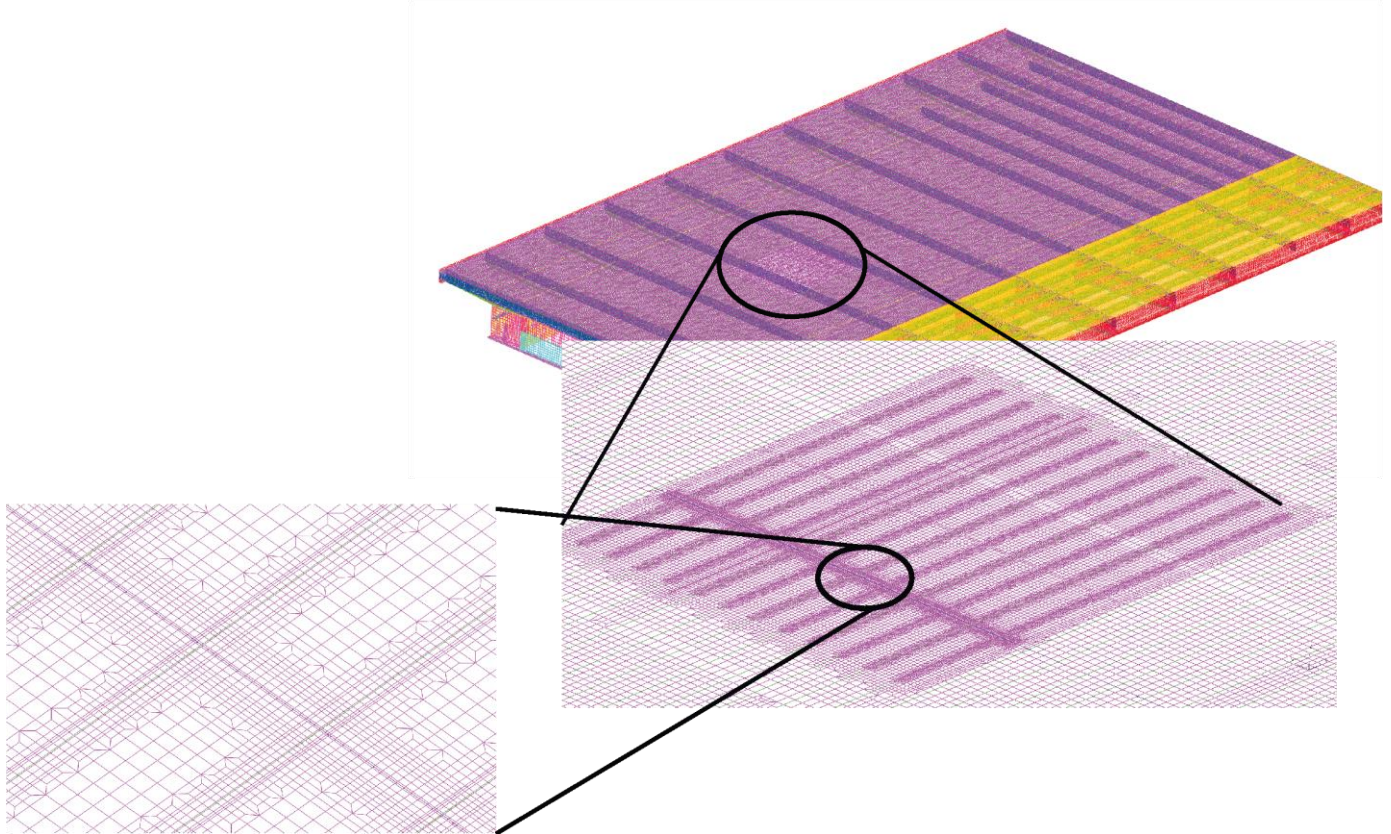


Figure 82: Unstrengthened FE model

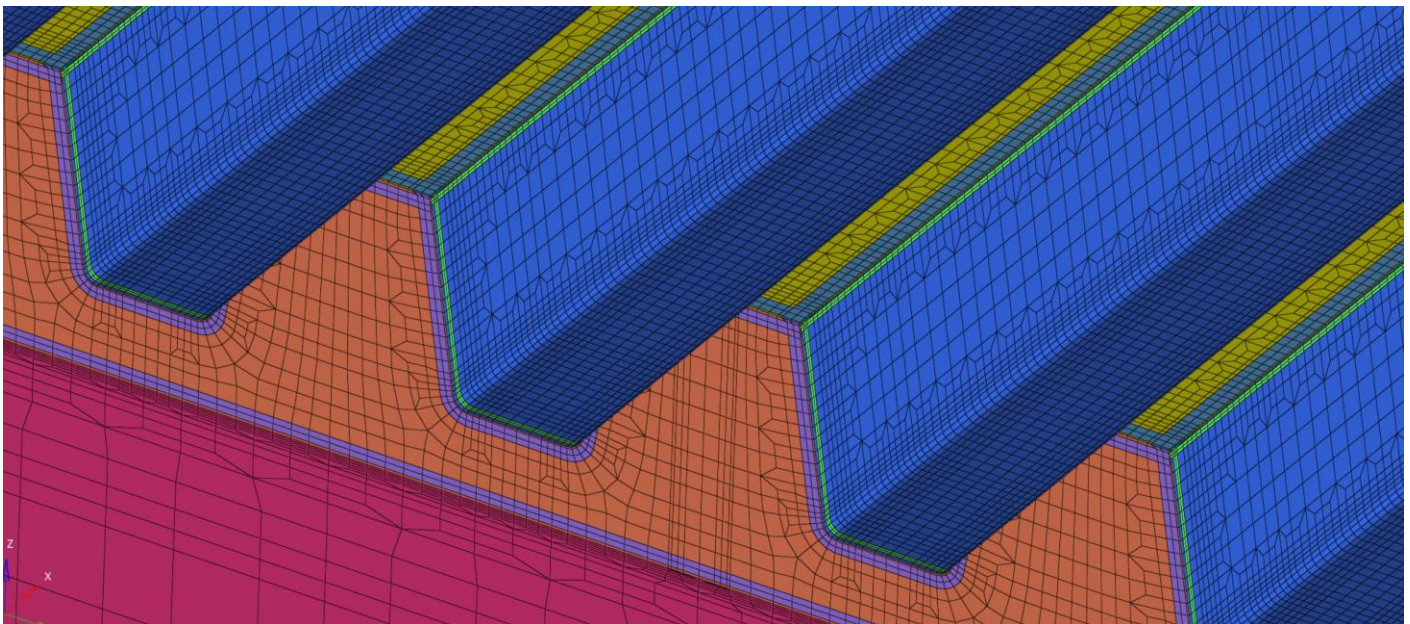


Figure 83: Close up of the detailed mesh with the elements used for the hot spot stress calculation

Shells are modelling using the default Belytschko-Lin-Tsay element formulation (ELFORM=2). This is based on the Reissner-Mindlin shell theory, which allows for shear deformation. It has one-point integration and is very efficient due to its use of velocity strains and Cauchy stresses (Haufe & Schweizerhof, 2013).

To verify the accuracy of this formulation, it has been compared with a more expensive fully integrated shell element (ELFORM=16) that has a 2x2 point integration. The different elements are depicted in Figure 84. Despite being 2-3 times more efficient, the results from the Belytschko-Lin-Tsay elements did not differ in any significant way from the fully integrated elements for the purposes of this thesis.

This element formulation was used in combination with hour glassing of the Belytschko-Bindeman viscosity type (IHQ=6) with a coefficient QH of 0.1. The hour glassing energy was extracted, together with the internal energy for each part. This nonphysical energy was verified to be well below any significant threshold

(10% of peak internal energy per part as a rule of thumb (DYNAmore GmbH, 2011)) and no hour glassing was observed during any of the simulation.

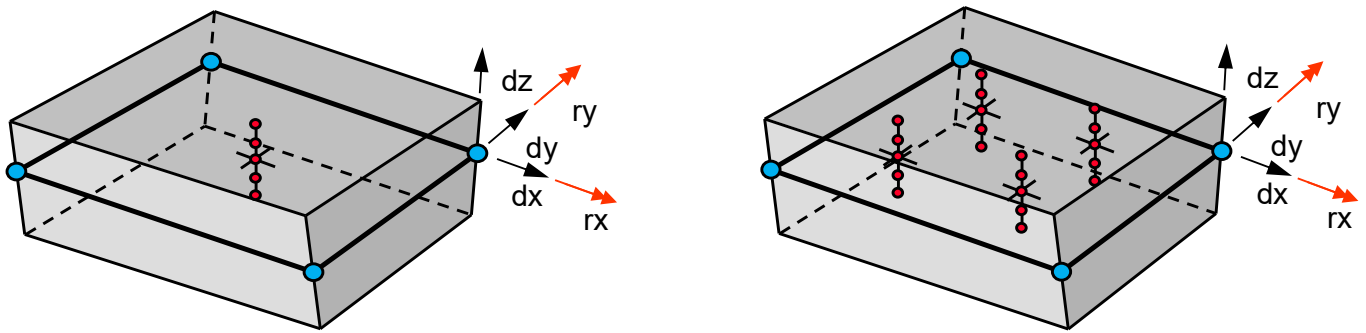


Figure 84: Belytschko-Lin-Tsay element formulation (left) and fully integrated shell formulation (right) (Haufe & Schweizerhof, 2013)

Linear elastic material properties are incorporated. The values of the steel material properties can be seen in Table 12 below.

Table 12: Material properties used in the unstrengthened FE model

	Youngs modulus	Poisson's ratio	Density
Steel	210 GPa	0.3	7850 kg/m ³

Boundary conditions

The boundary conditions are taken from the original model and shown in Figure 85. These correspond the physical situation and constrain the bridge at eight locations. The boundary conditions are implemented by combining a single point constrained to a nodal rigid body using *CONSTRAINED_NODAL_RIGID_BODY with the SPC option. This prevents unrealistic peak stresses and convergence issues. The locations are shown in Figure 85 and the corresponding directions are presenting in Table 13.

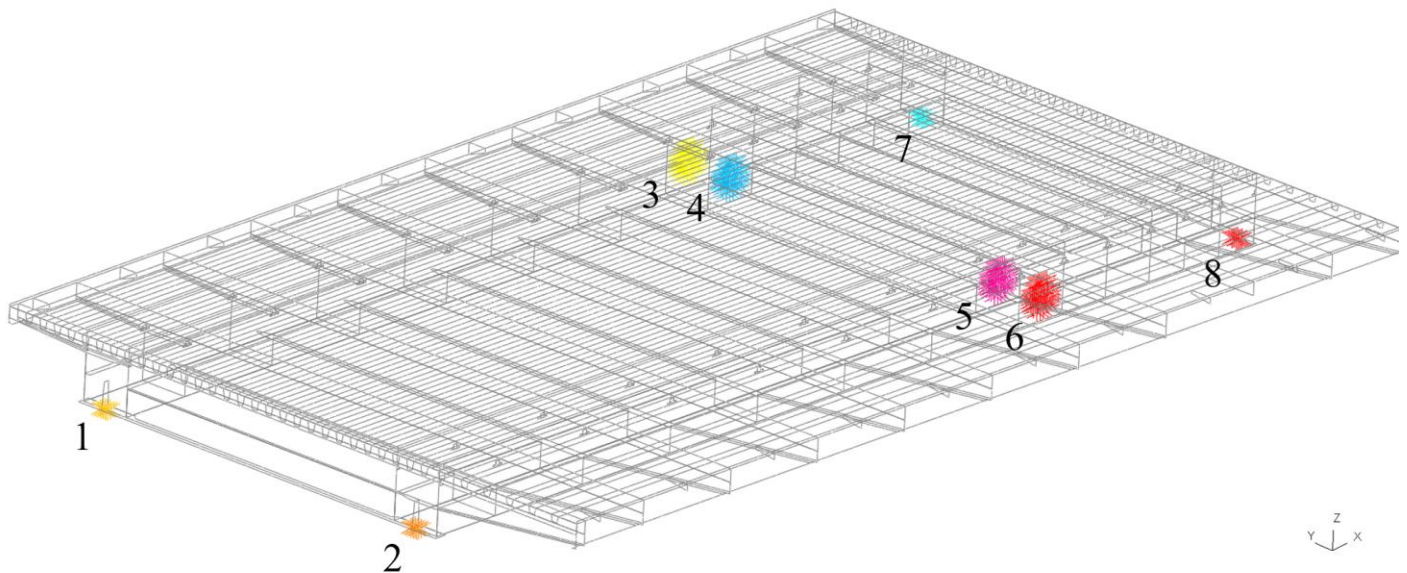


Figure 85: Local of boundary conditions of FE model

Table 13: FE model constraints

Constraint:	X-Direction	Y-Direction	Z-Direction
1	Free	Free	Fixed
2	Free	Free	Fixed
3	Fixed	Fixed	Fixed
4	Fixed	Fixed	Fixed
5	Fixed	Free	Fixed

6	Fixed	Free	Fixed
7	Free	Free	Fixed
8	Free	Free	Fixed

A single step implicit analysis was carried out with standard tolerance and iteration settings. To allow for replication of the simulations, details on the control parameters are presented in Annex B in the form of a reduced input file. This is a summary of the input file, excluding the loading, node and element information.

6.3. Strengthened model

The strengthened models adds all the strengthening elements to the unstrengthened model. The geometry and boundary conditions of the unstrengthened bridge are not altered. Added strengthening elements such as the filler plates, the strengthening plate, the epoxy and one of the backing strips are fully modelled in solid elements. A single element through thickness is used for the epoxy and filler plates, and two elements through thickness are used for the strengthening plate. During the design and from past experience, this has shown to provide a converged result. This amount to a total of more than 350 000 solid elements that are modelled in an effort to accurately simulate the behaviour of the strengthened bridge. Fatigue verifications of the strengthening elements is also partially done through this model. The exception for this is the epoxy layer, for which a model with a finer epoxy mesh is used, and the preloaded injection bolts, which tests have been carried out. The current model was not deemed accurate enough for verifying these elements. Using the model with the finer epoxy mesh for this thesis was investigated but could not be ran due to memory limitations of the LS-DYNA cluster present in the Amsterdam office. An overview of the different components of the strengthened model is presented in Figure 86 and Table 14.

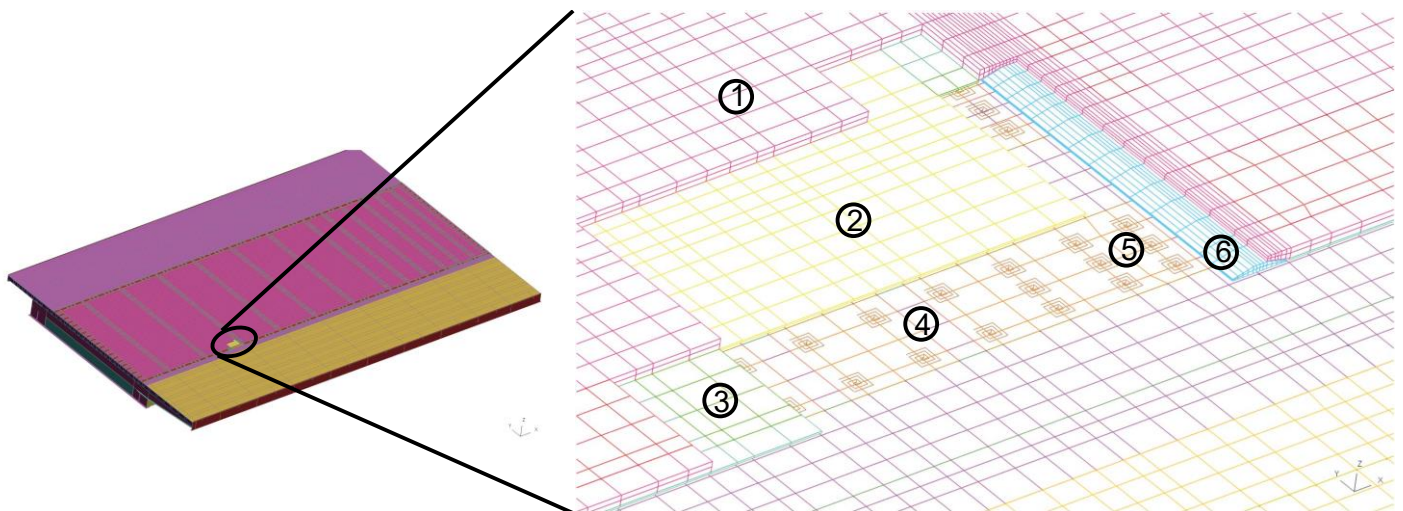


Figure 86: Overview of strengthened FE model components

Table 14: Description different components of the strengthened FE model

Description:	
Part 1:	Strengthening plate
Part 2:	Epoxy
Part 3:	Filler plates
Part 4:	Deck plate
Part 5:	Preloaded injection bolts (shear springs)
Part 6:	Backing plate

The bolts are modelled using springs in x and y direction, similar to what is done during the design process. Epoxy material properties have been taken conservatively as the tested properties at -20 degrees Celsius (remember the temperature dependency discussed in section 3.4). In Table 15, the used material properties are presented.

Table 15: Material properties used in strengthened finite element model

	Youngs modulus	Poisson's ratio	Density
Steel	210 GPa	0.3	7850 kg/m ³
Epoxy	3.639 GPa	0.364	1200 kg/m ³

Contacts

During the design phase of the strengthened deck, a lot of efforts was put into trying to prove that composite action can be achieved through the epoxy layer, i.e., that the shear stresses generated in the epoxy stay below the shear capacity of the epoxy layer. In the FE model that is used initially, composite action is assumed through the tied contact between the epoxy and the deck plate. This means that the nodes on the interface of the deck plate and epoxy are tied together and thus that shear stresses can be transferred through the interface. A constrained based contact that includes rotational degrees of freedom and is suitable for implicit analysis is chosen for this purpose (*TIED_SHELL_EDGE_TO_SURFACE_CONSTRAINED_OFFSET). The offset between the shell elements of the deck and the solid epoxy elements has accounted for through the optional _OFFSET card.

Besides the contact between the epoxy and the deck plate, there are more contacts that need to be resolved. For computational efficiency, the epoxy, the strengthening plate and the filler plates have shared nodes so that there is no need for any contact definition between these components. Between the deck plate and the filler plates, a general contact is applied to make sure there is no penetration. This is done by using the *AUTOMATIC_SURFACE_TO_SURFACE contact card. This is also used for the contacts of the backing strip with the deck plate and the strengthening plate. The *MORTAR card is used for the automatic contacts, which turns the contacts into segment-to-segment penalty-based contacts. This provides more accurate results for the contact, especially for higher order elements, since the individual shape function of the segments are considered when determining the contact forces (Livermore Software Technology Corporation, 2018). An illustration is shown in Figure 87.

The implicit accuracy flag (IACC = 1 ON *CONTROL_ACCURACY) is used in combination with these contacts to ensure an accurate simulation. This activates the strongly objective formulation for the contacts, which allows for accurate determination of forces and moments in a single implicit step.

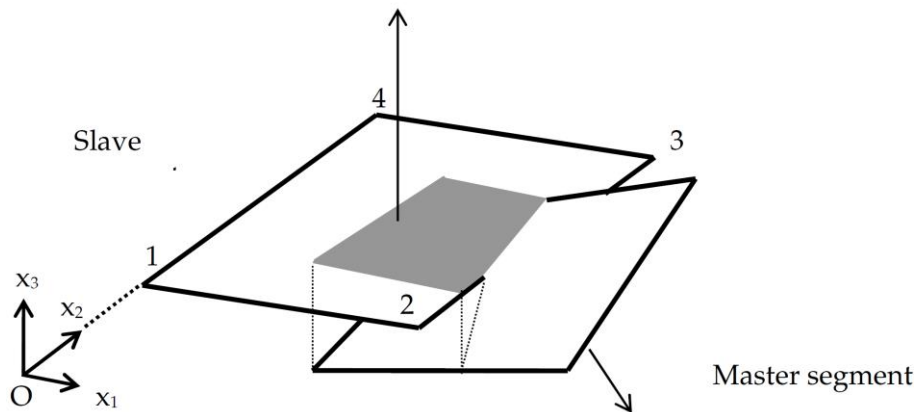


Figure 87: Illustration of a mortar segment to segment contact (Livermore Software Technology Corporation, 2018)

6.4. Load generation

This section will provide some notes on the load generation. A script which can generate pressure loading in a NASTRAN model has been provided by Arup as a starting point for this thesis. This is desirable to use when a large amount of loads cases is to be simulated to eliminate a lot of manual and time-consuming work. For this purpose, this script has been used and expanded for generating multiple load cases in an LS-DYNA environment. These loads will be generated as a *LOAD_SEGMENT. This keyword generates distributed pressure loads over segments that are defined by specifying a number of nodes. In practise, this provides identical results as the more common keyword *LOAD_SHELL, but this requires the input of shells ID's instead of nodes.

The workflow will now shortly be described step for step for those wishing to replicate the process. The Python code can be found in annex C:

1. Export the shell elements on which the pressure loads act

From the available NASTRAN models, the shell elements that will be loaded (the deck plate for the unstrengthened model and the load shells for the strengthened model) are exported in .dat format. This will serve as input data with which the script will generate the loads.

2. Set up a .csv file with all the relevant load information

A .csv file is set up that specifies all the specifics of the loading. This includes the axle dimensions, the desirable axle combinations, the load locations, and the different weaves that should be generated.

3. Run the loading script and merge loading back into full model

The script can now be run with the proper input data. This will generate loading in .dat format.

4. Export to LS-DYNA environment and set up load cases

In order for the loading to be recognized by PRIMER, the loading needs to be changed to a PLOAD4 format, which can be done very quickly in an editor such as Hypermesh. When exporting to LS-DYNA format, the option to write an additional comment line for every keyword needs to be checked. All information regarding the load collector and load case will be lost when exporting, so this option is necessary to retain this information. A script is written in Python which can recognize the load collector number written in the comment lines, and which will place all the loads in the proper load cases by appending the *CASE_BEGIN_XXX and *CASE_END_XXX keywords in the proper locations in the input file.

5. Merge loading into proper LS-DYNA model

The last step is to open this keyword file in a LS-DYNA pre-processing program (PRIMER in this case) and merge the loading into the main model. Before this is done, a script is run that sets up the matching master cases at the beginning of the main model so all the load cases can be run one by one.

7. Results FE modelling

This chapter will present the test results from FE models. Both the unstrengthened and the strengthened FE model results are presented and compared to the load test results in sections 7.1 and 7.2 respectively. In section 7.3, a critical reflection of the load tests is conducted, where the uncertainties and possible influencing variables are discussed. Finally, in section 7.4, the implications of the results will be discussed, with a focus on the fatigue performance of the renovated bridge.

7.1. Unstrengthened FE model load tests

This section will present a comparison between the unstrengthened FE model and the load test done on the unstrengthened bridge. To this end, track location 5 has been simulation with 119 load cases over the length of the bridge, i.e., the full truck has been simulated at 119 different longitudinal positions. The workflow to setup this analysis has been described in chapter 0. This track is chosen since it will result in the most relevant sensor information.

Besides simulating track 5, two weave locations at 5 cm from the centre of the track 5 have been simulated as well. These give an indication of the error of the results with regard to the uncertain truck position in the physical load tests. These weaves have been included as shaded areas around the FE results in all result plots shown in this section.

Stresses have been extracted at the locations of the strain gauges. The bottom layer of integration points have been used for extraction of the stresses. Non-averaged element results are used for the extraction of FE results. In case a strain gauge is located in the middle of two or four elements, the average of these elements is taken.

7.1.1. Cross-girder

In Figure 88, a comparison is presented for the stresses in the cross-girder bottom flange. It can be seen that a good match is obtained for the global behaviour of the structure. A small difference can be seen in between the two peaks, but after reviewing the load test results and the camera footage of the test it can be concluded that this is caused by traffic on the cantilever part of the bridge. This can be confirmed by looking back at Figure 55. In this comparison of all tracks, it can be seen that none of the other locations show this large dip at this location. Furthermore, a few other runs show other similar dips at other locations, indicating this error is indeed caused by traffic. Besides this small local difference, an almost exact match is obtained, meaning that the stiffness of the structure is simulated accurately.

During the second peak, a small sudden drop of the FE results can be observed around $x = 11.5\text{m}$. This is likely due to the fact that the first axle of the truck leaves the movable part of the bridge and enters the fixed bridge at this point. The FE model does not model any connection or interaction with the fixed bridge, while it seems that in reality there is a small amount of interaction which explains the small error observed in the global behaviour of the cross girder. All in all, it can be concluded that the global behaviour of the bridge matches very well.

Unstrengthened load test - FE comparison Stresses in the cross girder bottom flange

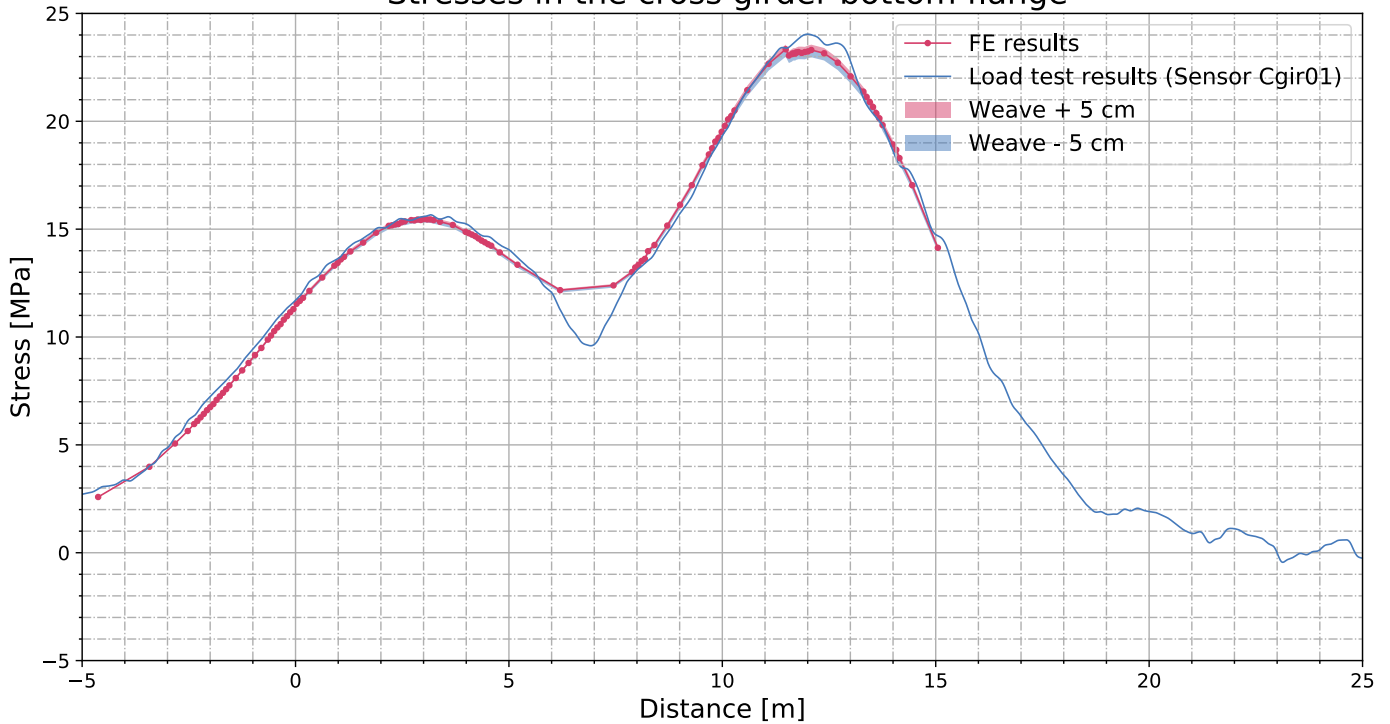


Figure 88: Unstrengthened load test – FE comparison, stresses in cross girder bottom flange

7.1.2. Deck plate

In Figure 89 and Figure 90, bending of the deck plate close to the cross girder is presented in transverse and longitudinal direction respectively. It can be seen that this very local behaviour is simulated very well. Enough load cases are defined to accurately capture the shape of the influence line and peak values. The close match also indicates that the wheel loading and tyre dimensions have been estimated fairly accurately.

Unstrengthened load test - FE comparison Transverse deck plate bending at the cross-girder

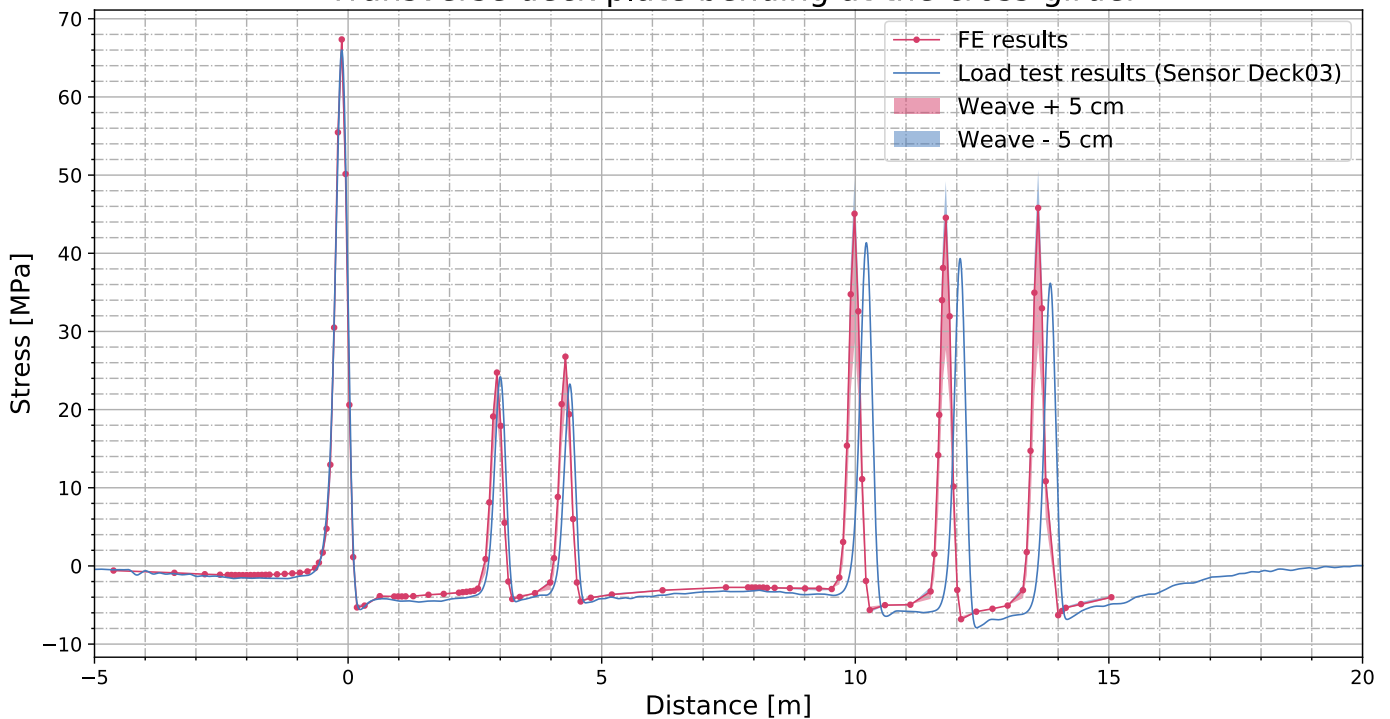


Figure 89: Unstrengthened load test – FE comparison, transverse deck plate bending at cross girder

Unstrengthened load test - FE comparison Longitudinal deck plate bending close to the cross girder

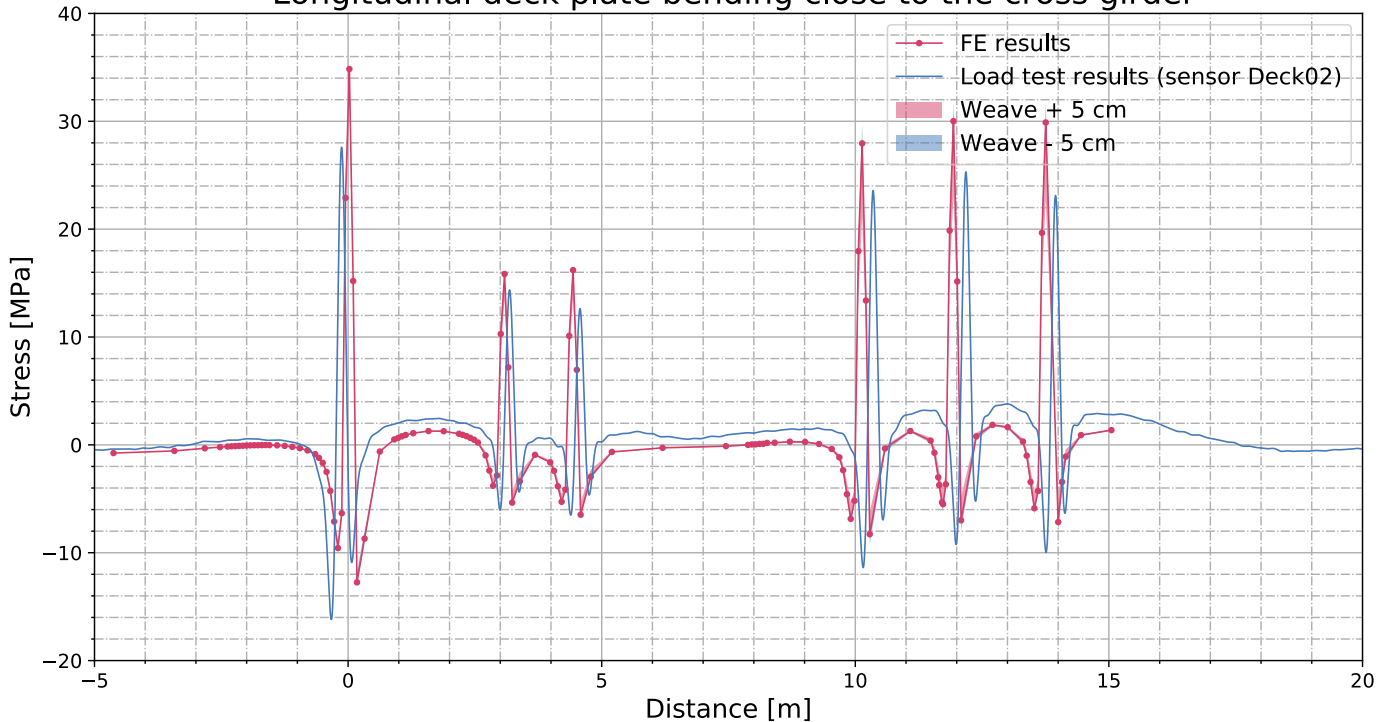


Figure 90: Unstrengthened load test – FE comparison, longitudinal deck plate bending at cross girder

Transverse bending at cross girder

For transverse bending of the deck plate, the accuracy of the results differs per axle. Whereas the first two axles match almost perfectly, a difference in peak value of 27% is observed for the last axle. However, it can be seen that the differences between the numerical and experimental results fall within the margin of error of the load position. Thus, it could be that the differences are due to a deviation of the load in the experimental investigation.

The difference in error between the axles that is observed conforms with this theory. It can be seen that the error is largest in the double wheel axles, especially the heavier back three axles. This is also where the largest uncertainty is in the model, thus where the largest error can be expected in case the truck did not drive directly in the centre of the track.

It can also be observed that the error is not symmetrical in this axle type, e.g., being off centre on one side results in much lower peak stresses in these axles while being off centre on the other side actually increases the peak stresses that are observed. This conforms with expectations of the local behaviour of the deck plate in between the trough, which can be understood when looking at the tyre geometry shown in Figure 50. The geometry of the first axle seems to align so well with the trough-to-trough distance that a 5 cm deviation does not impact the peak stresses in any significant way.

Longitudinal bending at cross girder

For longitudinal bending, a more or less constant overestimation of around 20-30% is observed. Whereas the transverse bending stresses in the deck plate lie largely within the margin of error, this is not entirely the case for the longitudinal bending stresses. In Figure 90 it can be seen that the results of the first three axles are overestimated beyond the margin of error due to the transverse truck position. Thus, while for transverse bending stresses the first three axles have the most accurate results, the opposite is true for longitudinal bending stresses.

A possible explanation could be the close proximity to the cross girder of this sensor location. The longitudinal stresses are measured 75 mm from the cross girder, whilst the transverse bending stresses compared in Figure 89 are taken at 225 mm from the cross girder. Since the behaviour close to the cross girder is very local and influenced by the stiffness of the connection between the deck plate to the cross girder, it can be theorized that a larger error can be expected here. For example, the welds are not explicitly modelled in the FE model, which could decrease the stiffness of the connection and thus overestimate the longitudinal bending stresses observed very close to the connection. However, this theory would mean that

the same overestimation should not be visible in the longitudinal bending stresses observed at midspan, while in Figure 92 it can be seen that more or less the same error is seen at midspan.

Furthermore, there is a striking difference between the sensitivity of the FE models to changes in the transverse position of the load. The margin of error due to the wheel position is significantly smaller for longitudinal stresses than it is for transverse stresses. This can be explained by the boundary condition of the local bending behaviour. Transverse stresses in the deck plate are due to deck plate bending between two troughs, which clearly act as boundary conditions. Thus, a change in transverse load position moves the load away from the centre, which affects the peak stresses significantly. For longitudinal stresses however, there are not such clear boundary conditions besides the deck to cross girder connection. This distance to this connection is however not influenced much by the transverse load position, explaining the smaller margin of error.

Transverse bending at mid bay

In Figure 91, the transverse bending stresses at mid-bay are shown. Generally, the results are similar to those at the cross girder. The fit with the numerical data is very good, with a maximum difference of around 12% for the first axle.

The numerical results at mid bay are less conservative compared to the experimental results than at the cross girder. Whereas the results were slightly overestimated at the cross girder, here the results seem to be slightly more similar or slightly underestimated. The uncertainty due to the weaves is very similar, with almost no change for the first axle and large differences for the back axles.

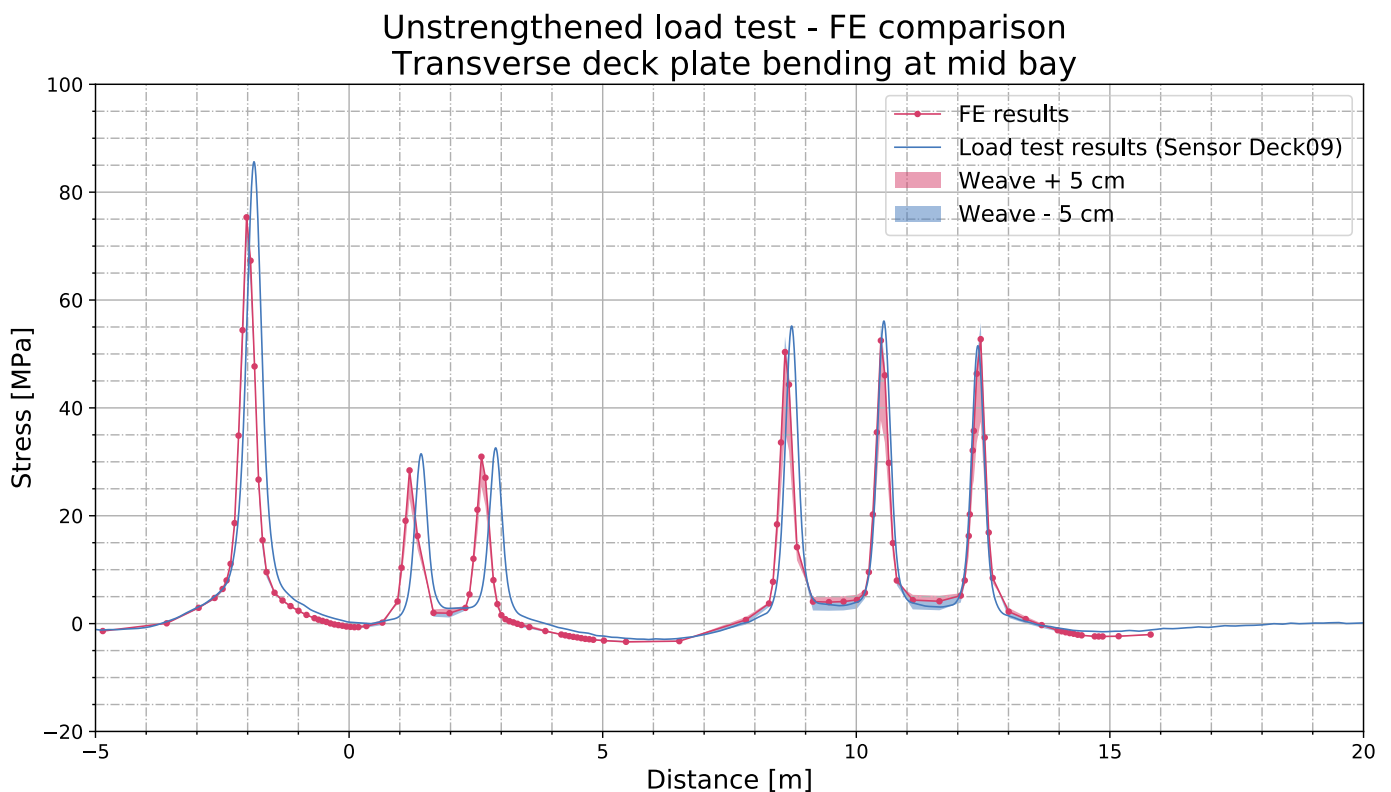


Figure 91: Unstrengthened load test – FE comparison, transverse deck plate bending at mid bay

Longitudinal bending at mid bay

Longitudinal bending of the deck plate at mid bay is shown in Figure 92. Results are very similar to those close to the cross girder shown in Figure 90. The negative stresses that occur right before the peaks are larger at midspan than at the cross girder, indicating that this location is less restrained. This very local behaviour is also underestimated by the numerical model which shows only limited negative stress peaks.

Peak stresses are overestimated up to 25%, which is outside of the uncertainty for the first axle. It is also interesting to observe the difference in numerical results between the second and third axle. Theoretically there should not be a significant difference between the two, so the difference between numerical results is likely a result of a mesh that is not fine enough to capture the local behaviour.

Unstrengthened load test - FE comparison Longitudinal deck plate bending at mid bay

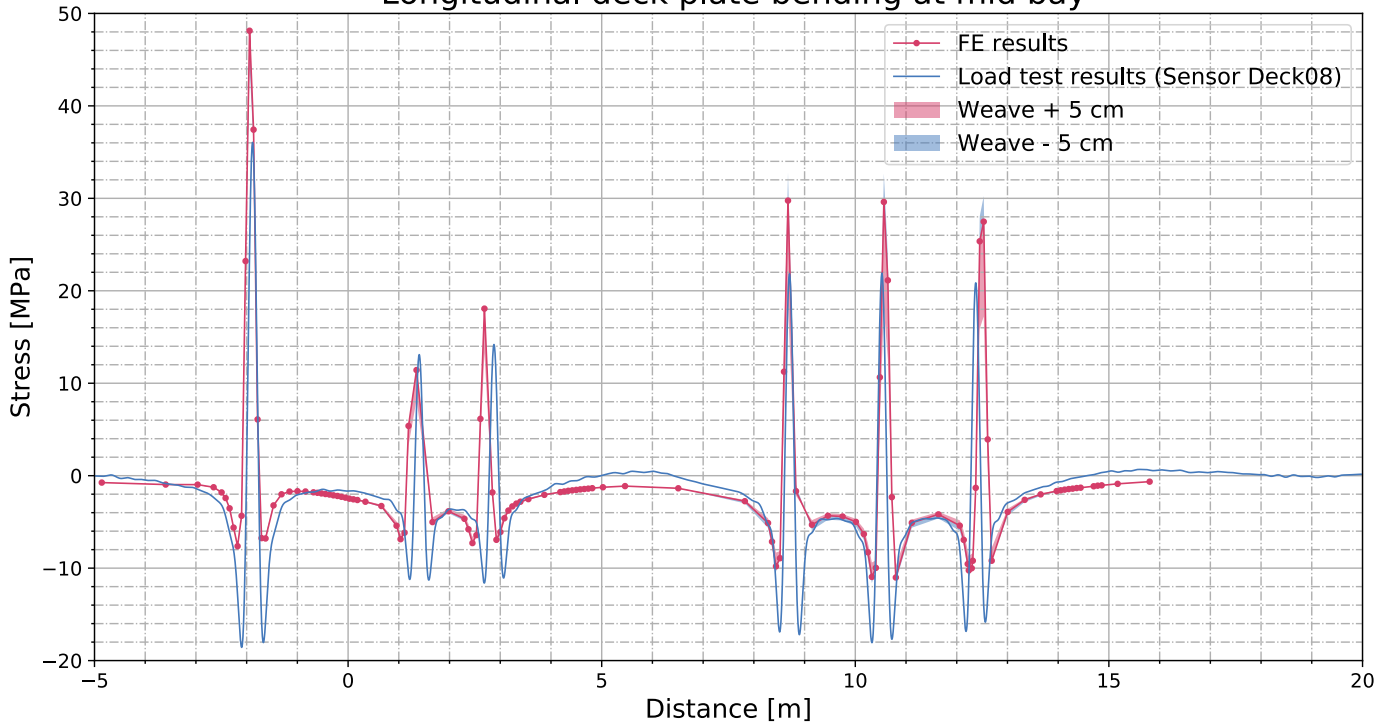


Figure 92: Unstrengthened load test – FE comparison, longitudinal deck plate bending at mid bay

7.1.3. Trough

In Figure 93, the response of the trough at mid bay is presented. It can be seen that the FE simulation matches the observed response very well. The shape of the influence lines is identical, and the peak values differ only a few percent between the two. The load on this trough is slightly higher in the experimental results. This can be due to a difference in stiffness, but the difference is too small for further investigation.

Unstrengthened load test - FE comparison Stresses in the trough bottom at mid bay

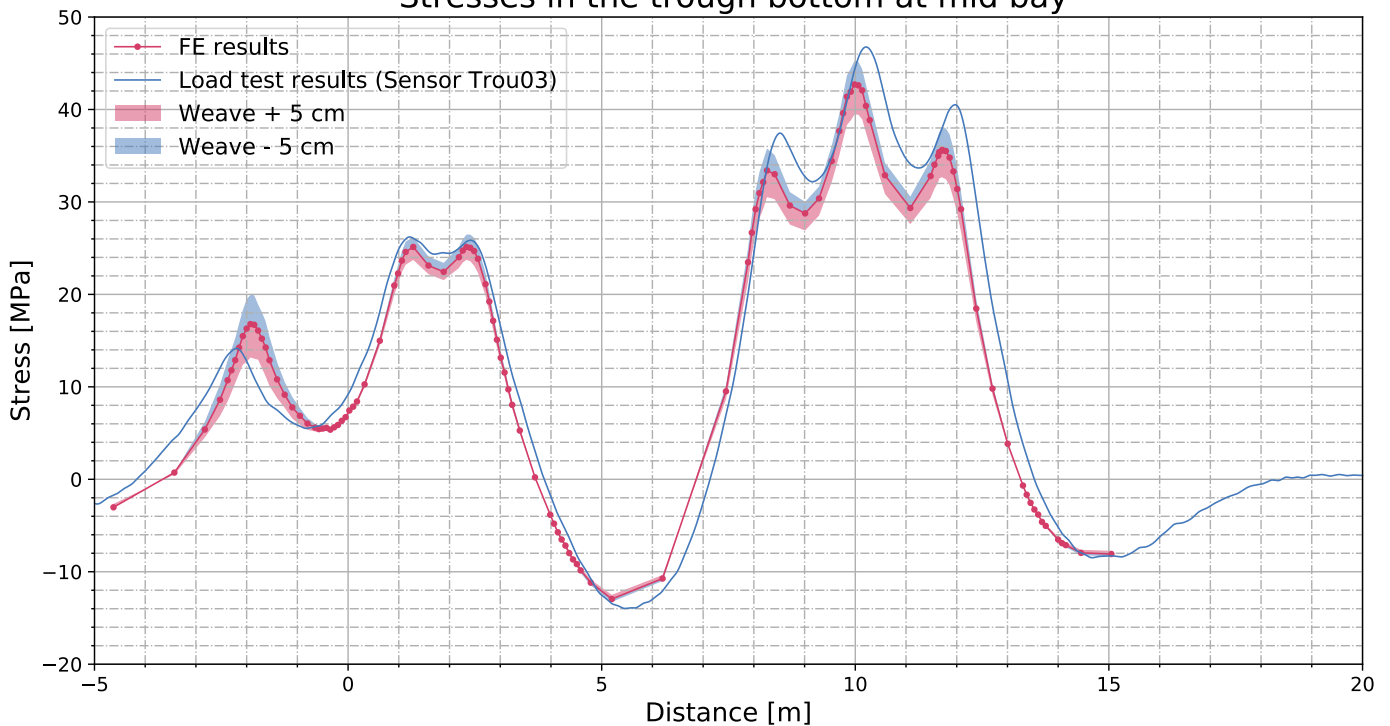


Figure 93: Unstrengthened load test – FE comparison, stresses in the trough bottom at mid bay

In Figure 94, the response of the trough close to the cross girder is shown. The general behaviour of the trough is similar, but the peak values, especially for the back axles, differ slightly more than for the mid bay results. It appears that the unstrengthened numerical model does not entirely capture the behaviour of the trough at this location.

The behaviour at this location of the trough is however also not very trivial and easy to interpret from the results. Longitudinal bending stresses as shown in Figure 94 show a combination of compressive and tensile peaks. It seems that the trough bottom is experiencing compressive stresses due to the global weight of the truck, but locally there are tensile peaks when the tyre is close to the sensor location. Compressive stresses in the trough bottom indicate that the trough is bending upwards over the cross girder, which is expected behaviour for the bridge deck. Locally, however, the tyre loading is causing the bridge deck to bend downwards instead of upwards, causing the tensile peaks.

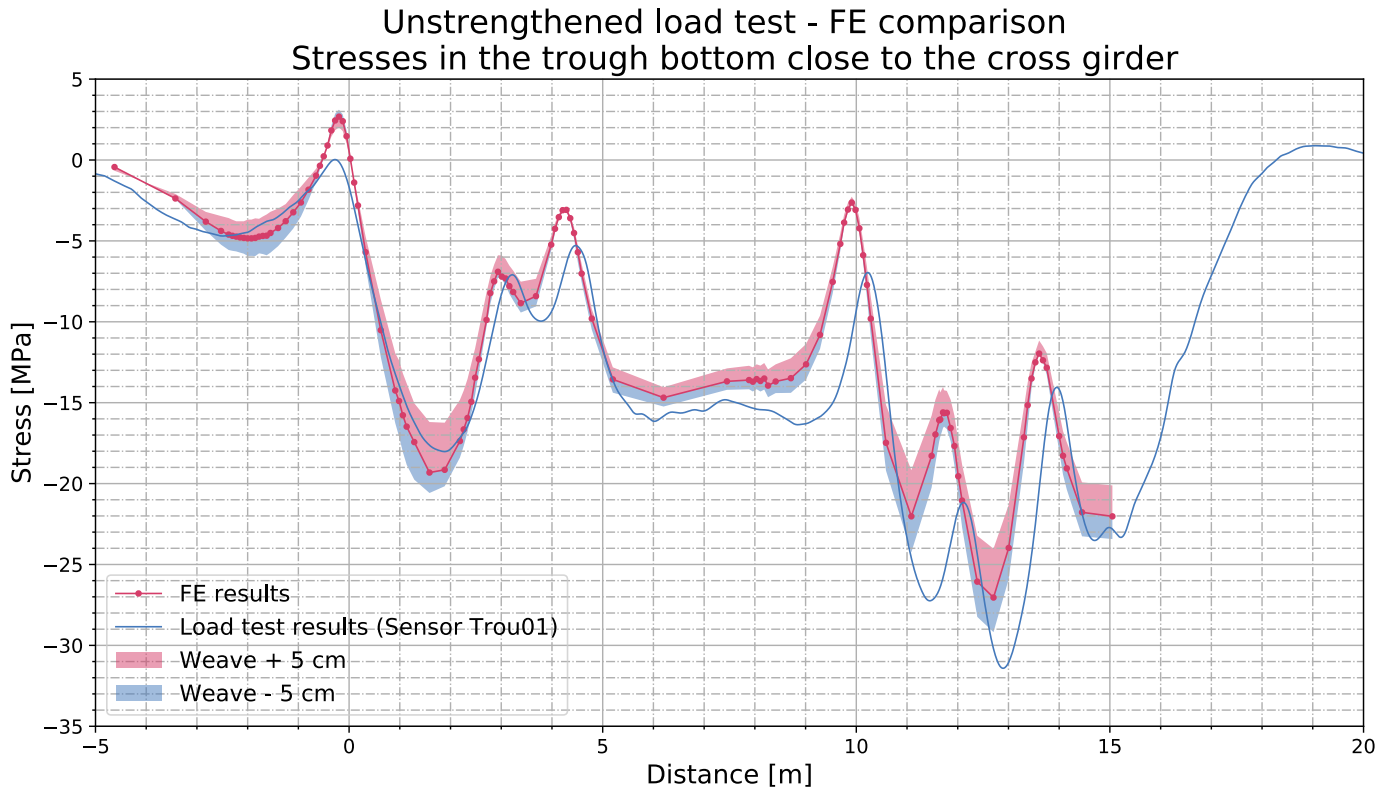


Figure 94: Unstrengthened load test – FE comparison, stresses in the trough bottom at cross girder

7.2. Strengthened FE model load tests

This section will present a comparison between the strengthened FE model and the load test done on the strengthened bridge. To this end, track location 5 has been simulated with 119 load cases over the length of the bridge, identical to the unstrengthened simulation. In this case, three experimental results are available to check against for more confidence in the results. The workflow to setup this analysis has been described in chapter 0. This track is chosen since it will result in the most relevant sensor information.

Stresses have been extracted at the locations of the strain gauges. The bottom layer of integration points have been used for extraction of the stresses. Non-averaged element results are used for the extraction of FE results.

7.2.1. Cross girder

In Figure 95, a comparison is presented for the stresses in bottom of the deck plate close to the cross girder. A small difference can be seen for the back axles, but on the whole the results correspond well with the experimental data.

Strengthened load test - FE comparison Stresses in the cross girder bottom flange

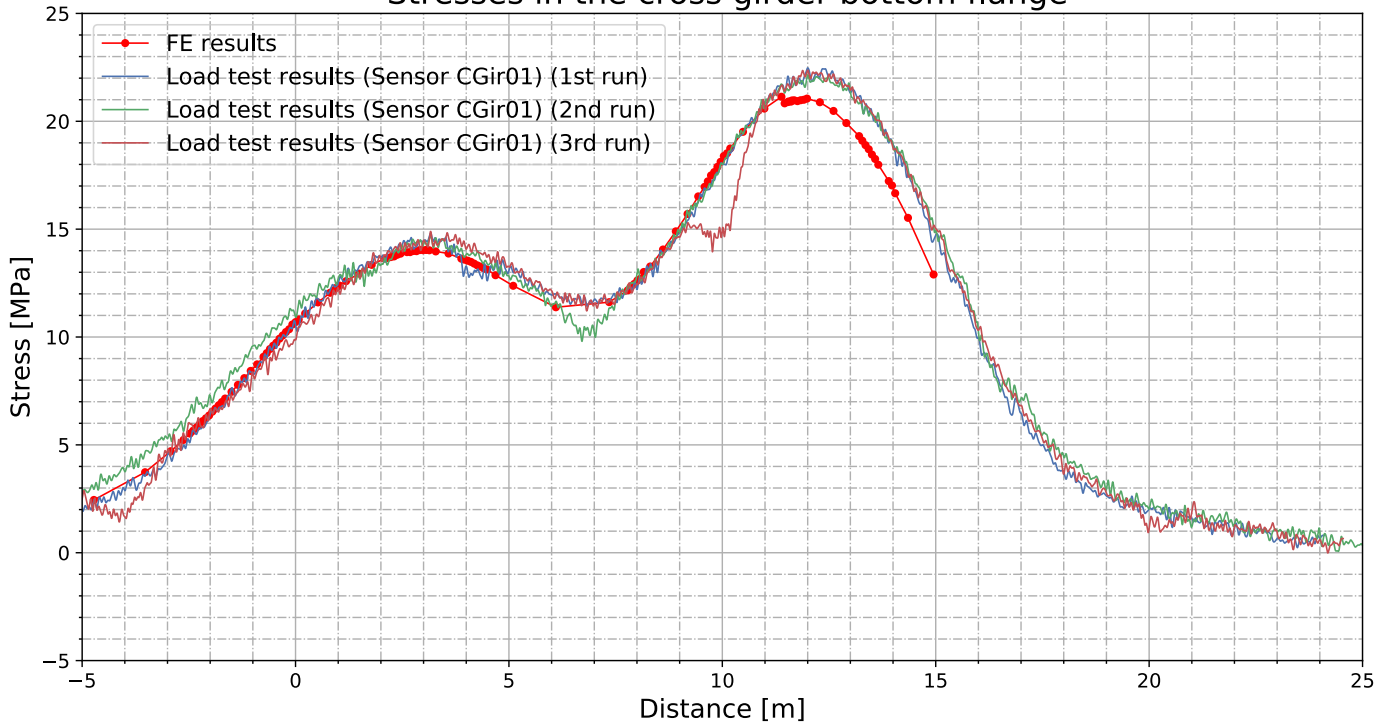


Figure 95: Strengthened load test – FE comparison, stresses in cross girder bottom flange

It can be seen that during the second peak, a slight sudden drop can again be seen, similar to the unstrengthened load test results (see Figure 88). This was theorised to be due to the truck moving onto the fixed bridge in reality, whilst in the FE model the load disappears when reaching the end of the movable bridge.

7.2.2. Deck plate

In this section, transverse bending of the deck plate close to the cross-girder is presented. Figure 96 shows the results of the sensor located very close to the added bolted connection (sensor Deck03, 75 mm from the bolted connection). In these results, clear differences can be observed between the experimental and numerical results. Due to the proximity to the bolt, very little stress peaks are observed in the strain gauge data. In the area around the bolt, the plates are pressed together due to the preloading of the bolt. This makes the package behave very compositely and stiff. This behaviour is not well captured in the numerical models, where the bolted connections are modelled using only a spring. Furthermore, the mesh around this spring element is not very refined, further decreasing the accuracy of the results in the immediate vicinity of the connection. The results are thus not unexpected, and the lower stresses that are observed in the experimental results are the 'correct' results. The larger stress cycles in the numerical model are a direct result of the simplified modelling choice, which is conservative in this area.

Strengthened load test - FE comparison Transverse deck plate bending close to the cross girder

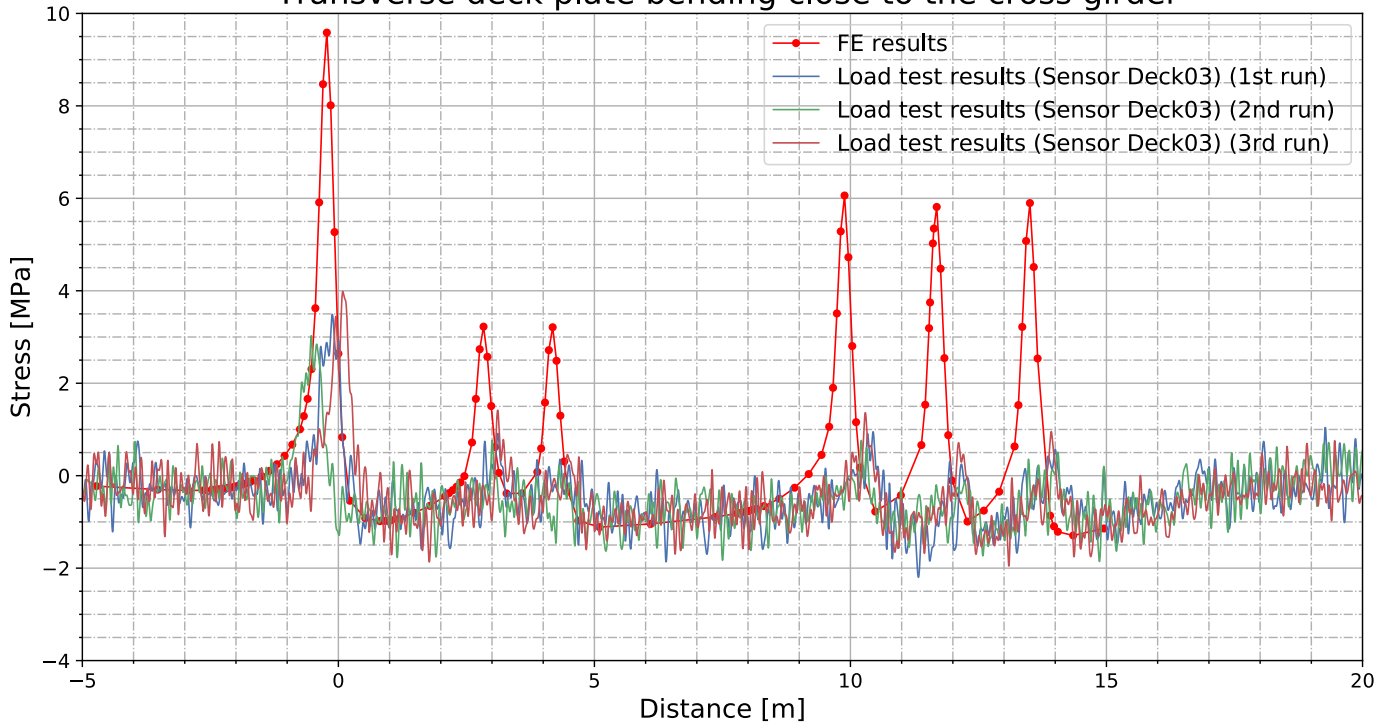


Figure 96: Strengthened load test – FE comparison, transverse deck plate bending at cross girder (Deck03)

In Figure 97 and Figure 98, the results of deck sensors Deck04 and Deck05 are shown. These are sensors at slightly larger distances from the bolt (150 mm and 225 mm respectively). In these graphs, it can clearly be seen that the error in the results is much smaller than what was observed from sensor Deck03. Much more distinct peaks are observed, and the results are more in line with the behaviour shown in the experimental results. At 150 mm from the bolted connection, the error has almost completely disappeared.

Strengthened load test - FE comparison Transverse deck plate bending close to the cross girder

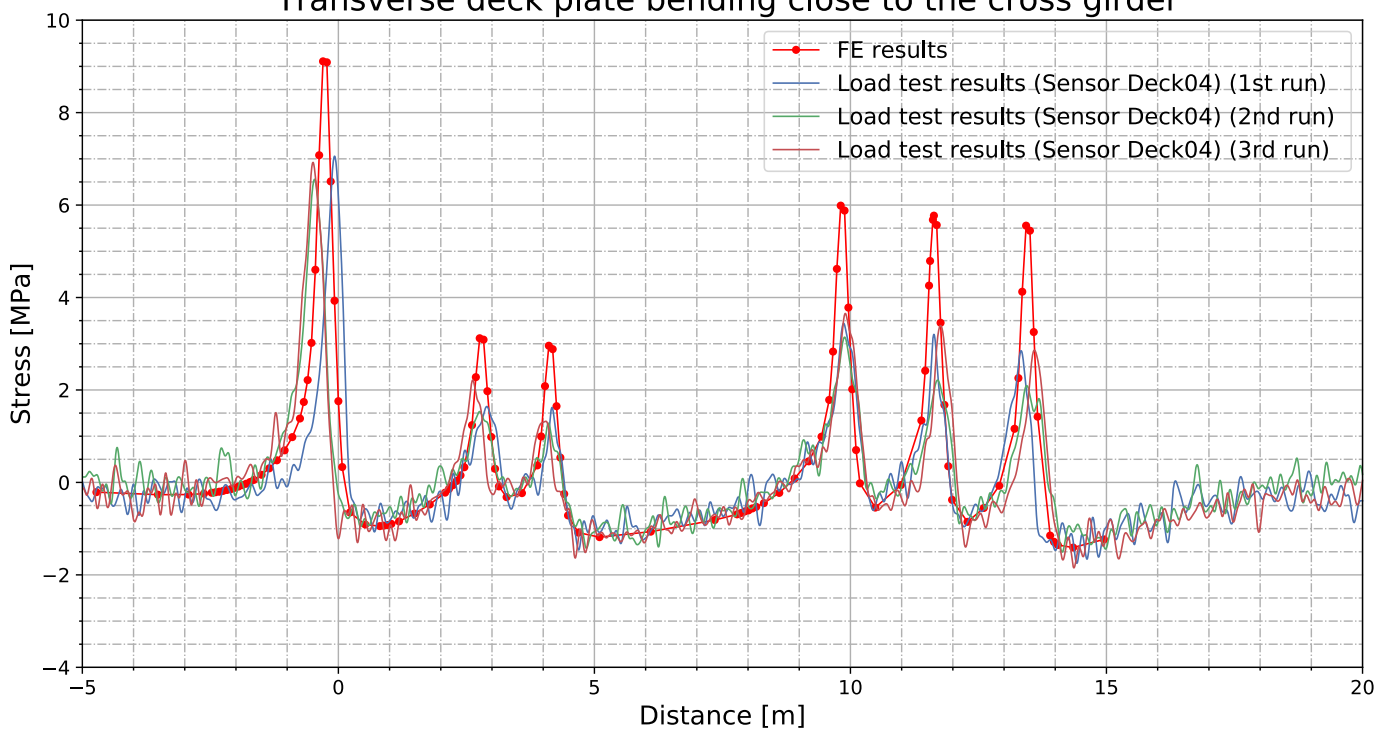


Figure 97: Strengthened load test – FE comparison, transverse deck plate bending at cross girder (Deck04)

Strengthened load test - FE comparison Transverse deck plate bending close to the cross girder

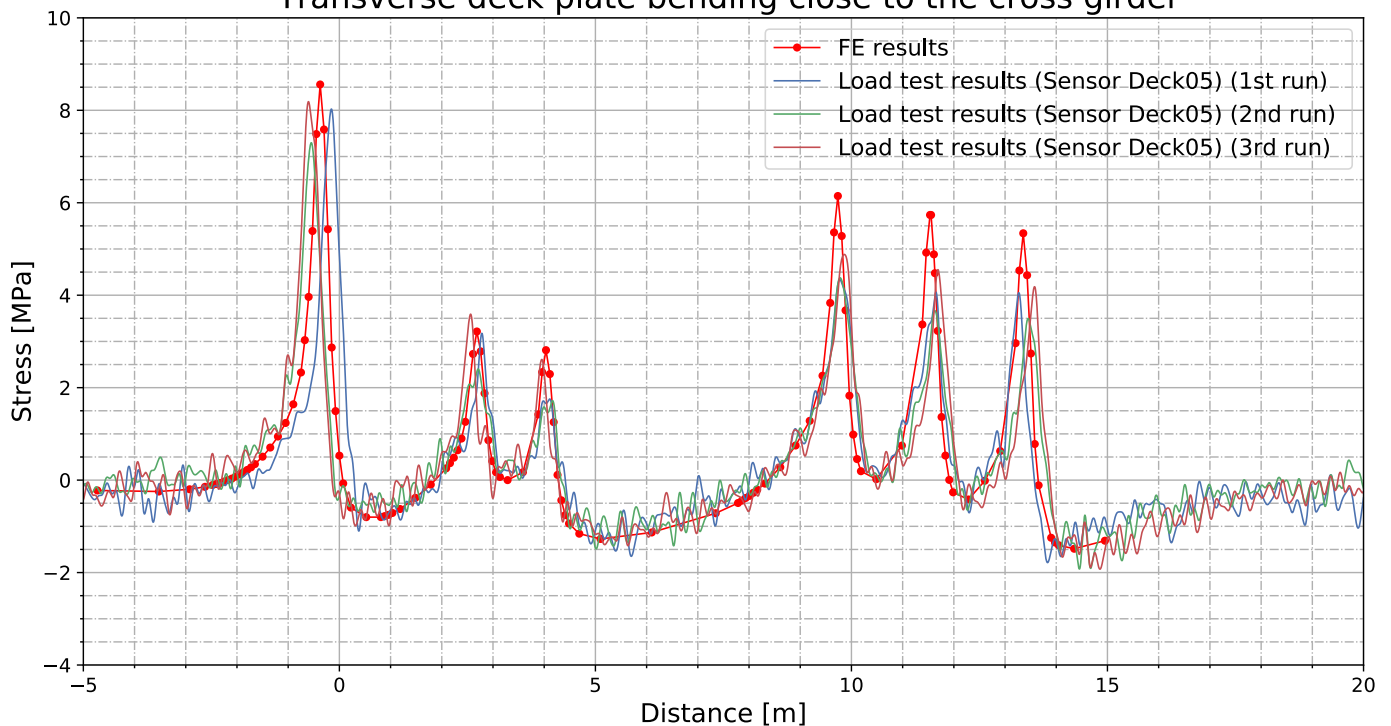


Figure 98: Strengthened load test – FE comparison, transverse deck plate bending at cross girder (Deck05)

In Figure 99, the longitudinal deck plate bending close to the cross girder is shown. Similar to the results shown in Figure 99, this strain gauge is located close to the bolted connection. It is therefore expected that there are discrepancies in local stresses around this area in the numerical results. It can be seen that the FE simulation predicts a larger amount of compressive stress in the bottom of the deck plate in between the axles. These compressive stresses are due to the OSD bending over the cross-girder. It can therefore be concluded that the bolted connections restrain the deck plate and prevent it from bending to the extent that the numerical simulation predicts. Nonetheless, the magnitude of the stress cycles due to the wheel loads is still predicted very accurately.

Another thing that can be noted is that the three different experimental runs show very similar results. This indicates that the experiment has been done accurately and/or that the strengthened bridge is less sensitive to deviations of the truck location.

Strengthened load test - FE comparison Longitudinal deck plate bending close to the cross girder

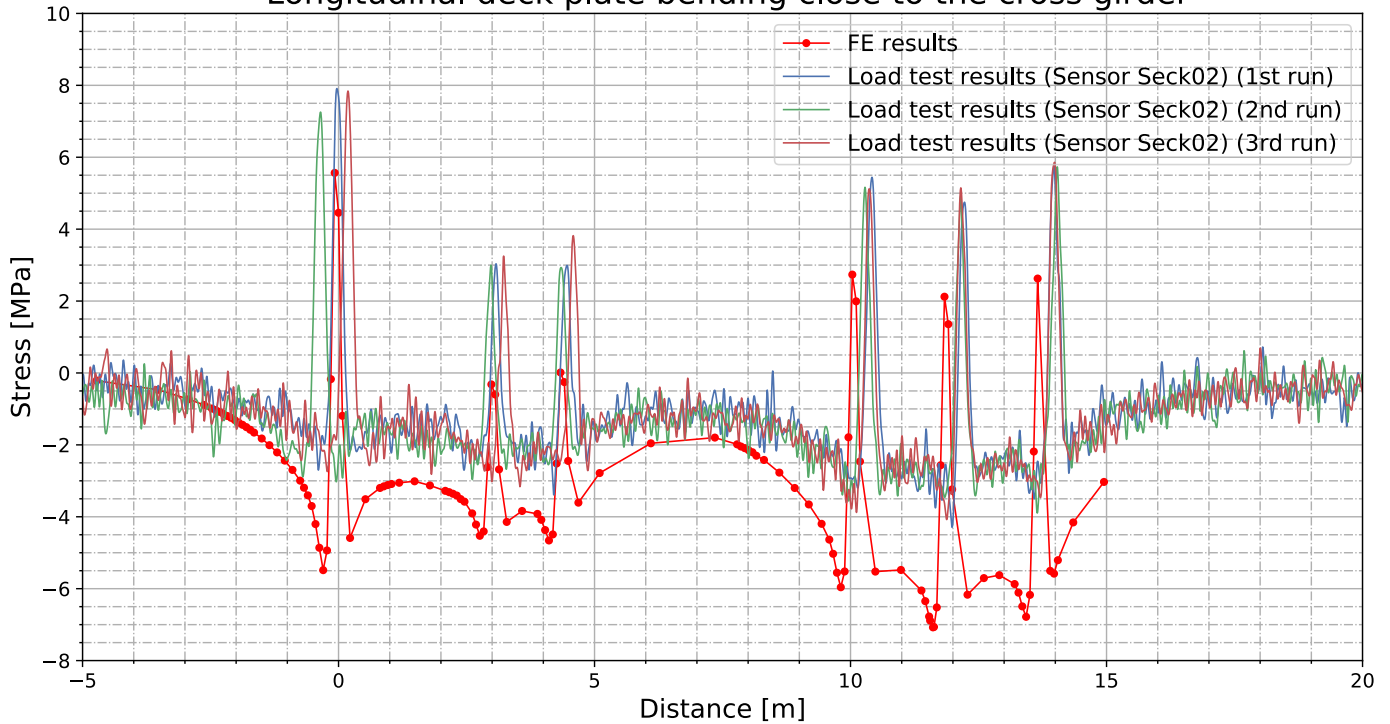


Figure 99: Strengthened load test – FE comparison, longitudinal deck plate bending at cross girder

In Figure 100, the transverse bending of the deck plate is shown at mid bay. In this case, there is no reason to expect significant deviations between the numerical and experimental results. As can be seen, this is also not observed. On the contrary, the results match very well, with no significant differences to speak of. This indicates that the local behaviour of the strengthened model is modelled accurately. This also means that composite interaction, which is for a large portion responsible for the stiffness of the strengthened deck plate, is achieved.

Strengthened load test - FE comparison Transverse deck plate bending at mid bay

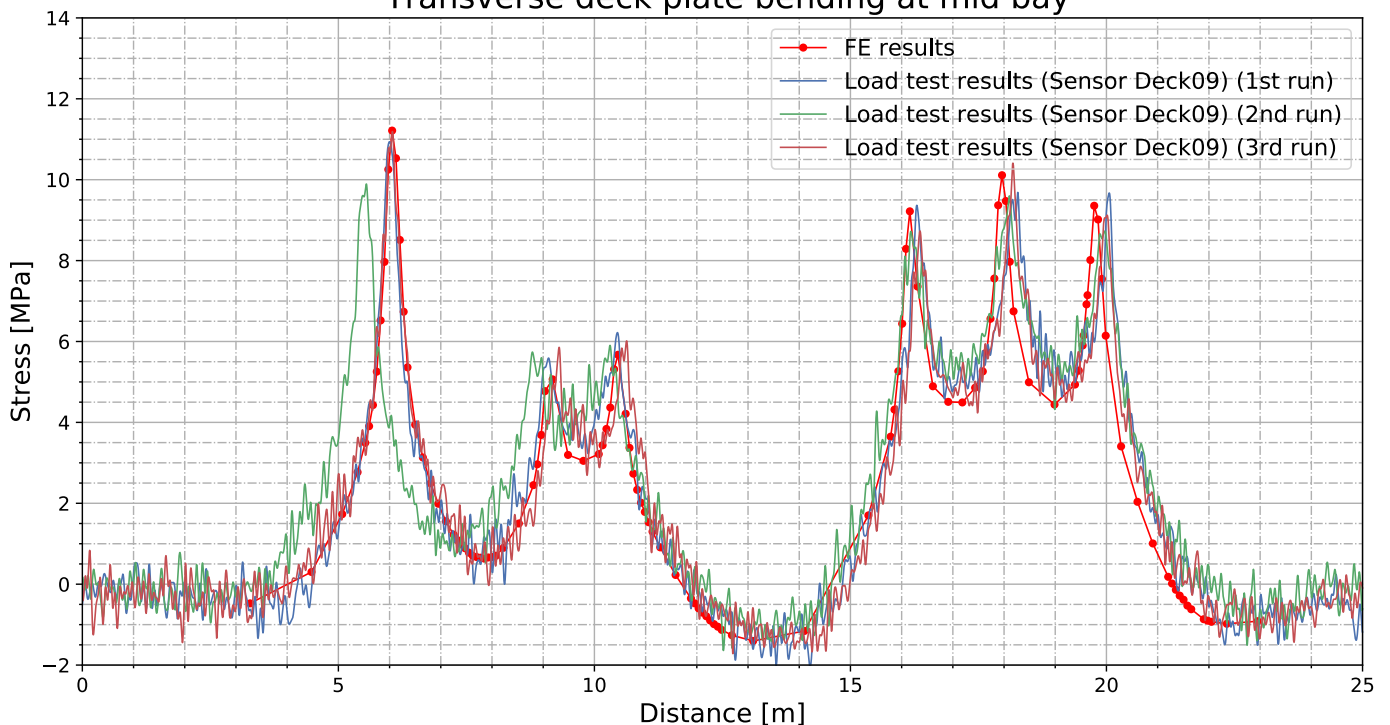


Figure 100: Strengthened load test – FE comparison, transverse deck plate bending at mid bay

In Figure 101, the longitudinal load test results at mid bay are presented. Again, the stress cycles are very well predicted. In between the axles, the FE models seems to predict slightly more flexible behaviour than what is observed in reality, especially between the back axles.

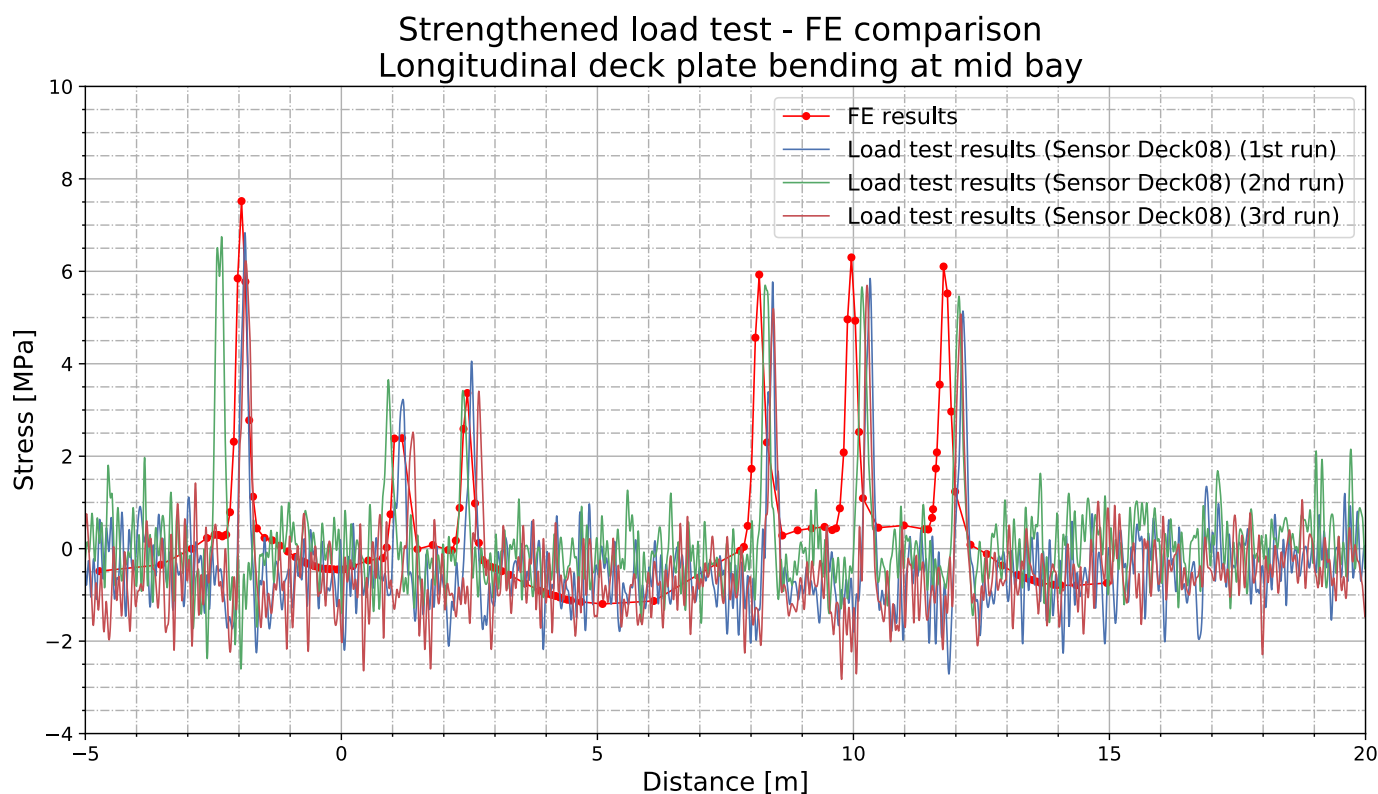


Figure 101: Strengthened load test – FE comparison, longitudinal deck plate bending at mid bay

7.2.3. Trough

In Figure 102 and Figure 103, the results from the trough bottom and mid bay and at the cross-girder are presented respectively. As can be seen in Figure 102, behaviour of the trough at mid bay is modelled very accurately. Similar to what was seen in the unstrengthened model, no real deviations to speak of are observed. More interesting is Figure 103, where the results for the trough bottom at the cross girder are presented. It can be seen that the numerical and experimental results match very well. In fact, the deviation is even smaller than what was observed in the unstrengthened comparison. This could be due to the fact that with the stiffer strengthening, the bending of the strengthened deck plate over the cross girder is now less pronounced.

Strengthened load test - FE comparison Stresses in the trough bottom at mid bay

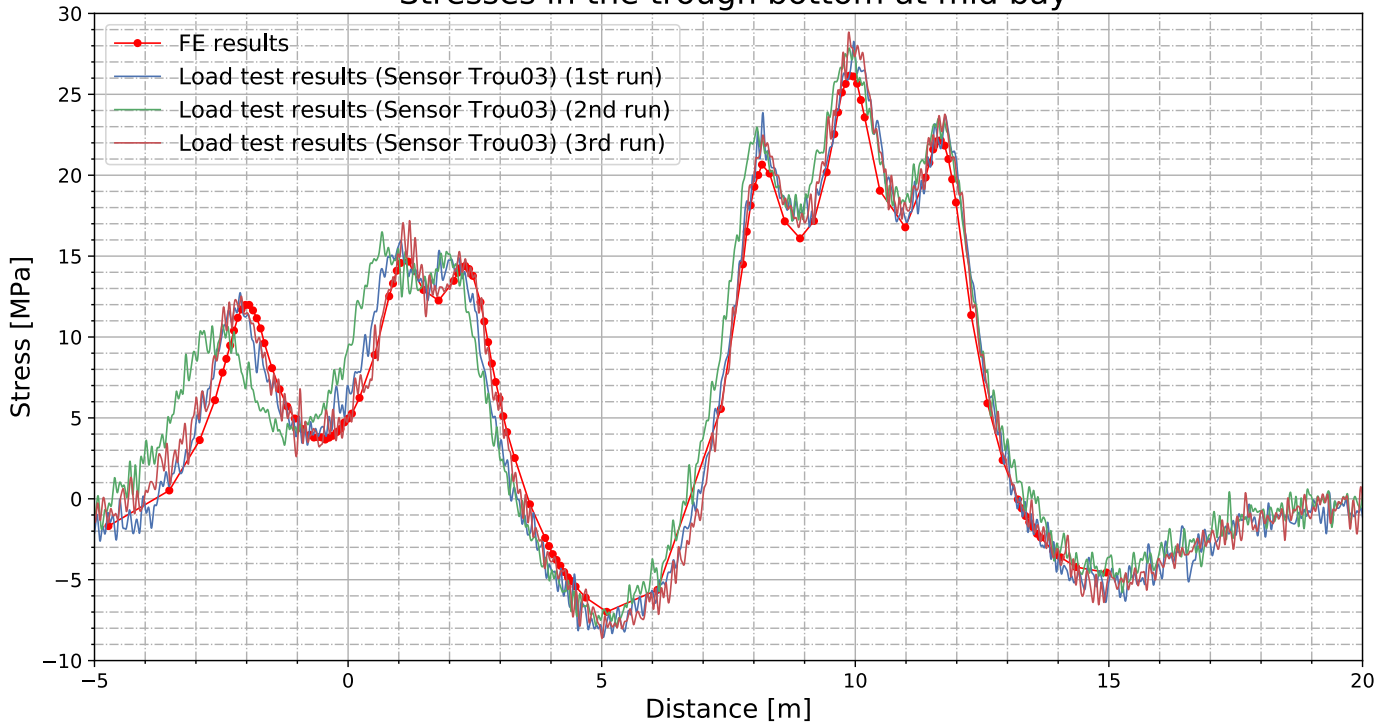


Figure 102: Strengthened load test – FE comparison, stresses in the trough bottom at mid bay

Strengthened load test - FE comparison Stresses in the trough bottom close to the cross girder

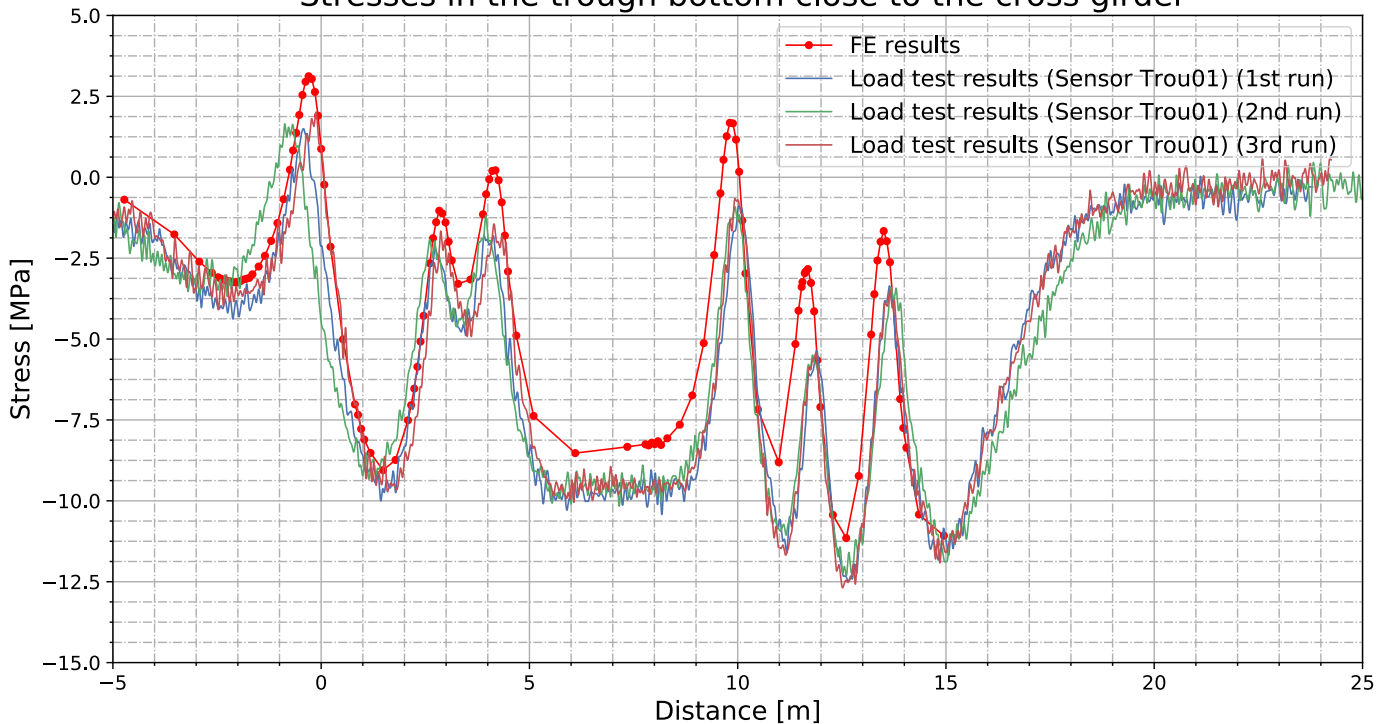


Figure 103: Strengthened load test – FE comparison, stresses in the trough bottom at cross girder

All in all, the numerical model has succeeded in capturing the behaviour of the bridge very accurately. Both globally and locally, stress peaks due to the truck loading can be predicted with sufficient accuracy. This implicates that the modelling techniques, i.e., the used contacts and methods of connecting the different strengthening elements, has been successful. Also, the design assumption of composite interaction corresponds with what is observed in reality. This however does not necessarily mean that the assumption

of composite interaction is always valid since the experimental results are from 1 observation soon after strengthening. Based on this research, no conclusions can be made regarding whether composite interaction will still be achieved after significant temperature on the epoxy. Lastly, it can be concluded that for the area around the bolted connections, the current modelling techniques are not accurate in predicted the behaviour of the bridge. They are however conservative, and for most applications this modelling technique will be sufficient. However, if stresses need to be extracted anywhere close to the bolted connection, more detailed modelling will be necessary.

7.3. Uncertainties

When comparing numerical with experimental data, there is always a limit to how many factors you can control and to how accurately the impacting variables can be measured. This section aims to give a quick discussion on possible influencing factors, their importance, and their possible impact on the results.

7.3.1. Transverse stiffness

So far, all FE analyses were carried out with the loading on track number 5, since this track provided the most information, and no differences were expected between the different locations. To check this assumption, another analysis was setup with the loading in different transverse positions. For this analysis, the truck was positioned such that the first axle is located at the longitudinal position of sensor Deck03. The transverse location of the truck is varied to cover 9 positions that were also executed during the experiments. The maximum stress due to the first axle is then plotted. The results at sensor location Deck03 can be seen in Figure 104.

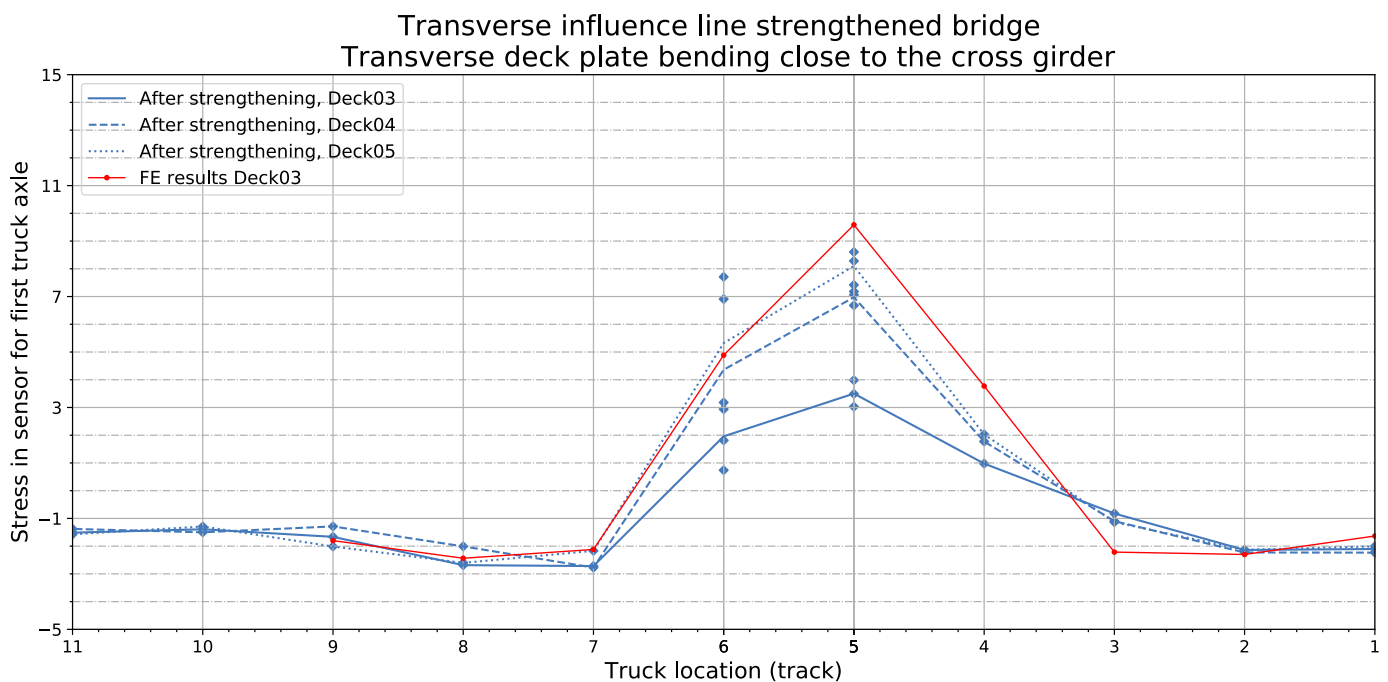


Figure 104: Transverse influence line for deck plate bending close to the cross girder

In Figure 104, it can be seen that the transverse behaviour is similar to the experimental results. The difference when the load is directly over the sensor was already discussed in section 7.2.2. Besides track 5, the numerical results match well with experimental data. This confirms that the results are accurate for different transverse location of the load.

7.3.2. Contact modelling

An important starting assumption of the analysis is that composite interaction with shear transfer between the steel plates is achieved. From the design report it can be observed that when assuming no composite interaction, stresses increase very significantly in all relevant areas. The cross section is a lot less effective in that case, with hot spot stresses increasing by more than 50% depending on the fatigue detail. When comparing the experimental results with the numerical results, no overestimation of that degree is observed. It can thus be theorised that, at least directly after the application, composite interaction is achieved. It is

deemed very unlikely that there is no composite interaction in reality, since much larger stresses would be observed in that case.

7.3.3. Truck location

It was expected that the exact truck location is one of the main influencing factors and source of uncertainty in the results. This was visualised in section 7.1 through the simulation of the different weaves. In these figures, it can be seen that the exact truck location indeed is a large source of uncertainty – a different of 5cm can make a different in observed stress cycle of almost 50% in certain cases. However, through redoing the same load test multiple times and by comparing data of similar strain gauges it can also be seen that the experiments have been carried out with reasonable accuracy. Especially for the strengthened bridge, the 3 different runs of track 5 rarely have any significant deviation between them.

7.3.4. Tyre size

One of the other unknowns is the dimension of the tyre load. The dimensions might be off and the simple uniform distribution might also be a simplification. As an quick study the transverse dimension of the front axle is varied (the pressure load is scaled to obtain the same total load). In Figure 105

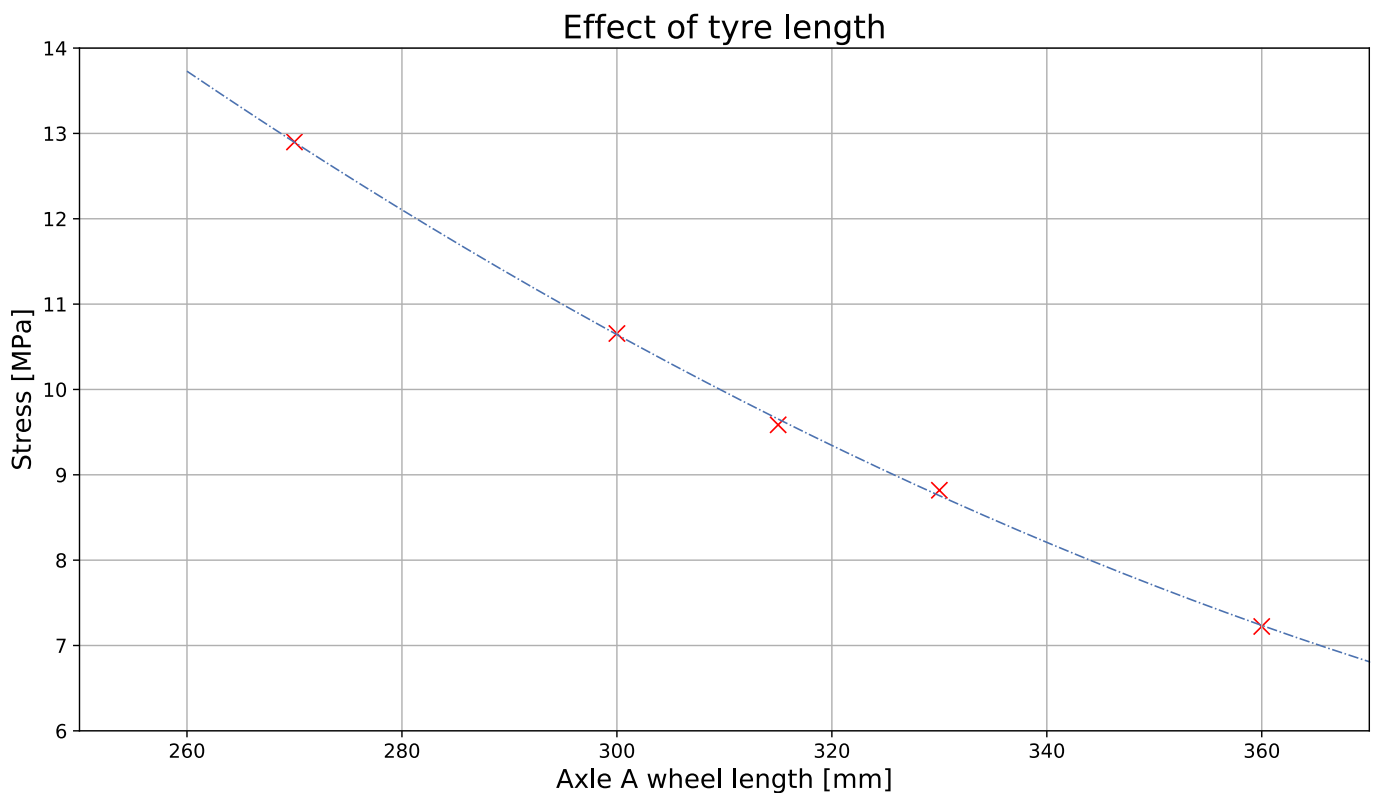


Figure 105: Influence of tyre length on the observed deck plate stress

Whilst it is impossible to check all possible variations, an error of 15mm in the width direction gives an error in the stress of around 10%. However, a systematic over or underestimation of the stresses would be expected if such an error was made. Since no such systematic over or underestimation was observed, it can be assumed that the tyre sizes were measured with sufficient accuracy.

7.4. Fatigue implications

With all the numerical and experimental results analysed, some conclusions can be made regarding the expected fatigue life of the bridge. In section 3.5, the fatigue design of the renovated bridge was discussed and proven. However, more knowledge on the used models is now available, which can be used to review the conclusions that were made. This section will shortly discuss the implications of the test results regarding the design fatigue life of the bridge.

Fatigue detail 1a and 1b

First, for fatigue detail 1a and 1b (crack in the deck plate to trough connection, originating from weld toe and root respectively), it was concluded that even the strengthened bridge with no composite action is sufficient to guarantee a sufficient fatigue life. With no composite action, stress factors of 0.20 and 0.23 were expected for fatigue details 1a and 1b respectively. When assuming composite interaction, these factors drop to 0.12 and 0.14.

In the discussing of the load test results, the stress reduction in the deck plate at mid-bay is predicted around 85-90%, corresponding to a stress factor of 0.10 - 0.15. It can however be questioned whether the stress factor in this location is comparable to the stress factor in the location of the fatigue detail. To this end, the stresses are also extracted in the deck plate shells directly next to the trough. Comparing the stresses before and after strengthening in this location, a stress factor of 0.16 is found. This closely relates to the found reduction at the strain gauge location, providing more confidence in the results. This comparison can be seen in Figure 106 and Figure 107.

Thus, the predictions in the design report match well with the experimental results. Using the results from this thesis, more confidence can thus be obtained that deck plate cracks are not expected during the design life of the renovated bridge.

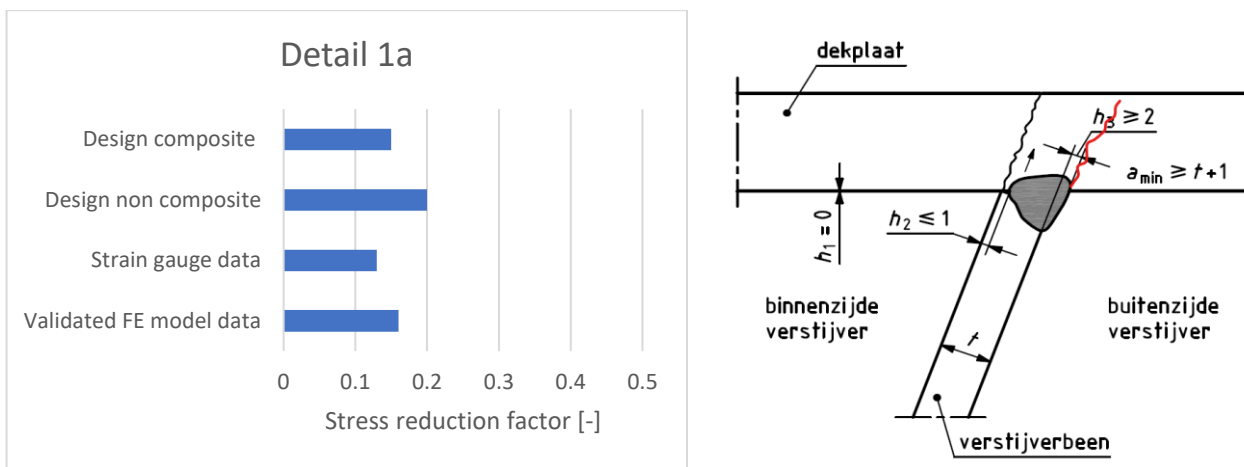


Figure 106: Stress reduction factor in fatigue detail 1a

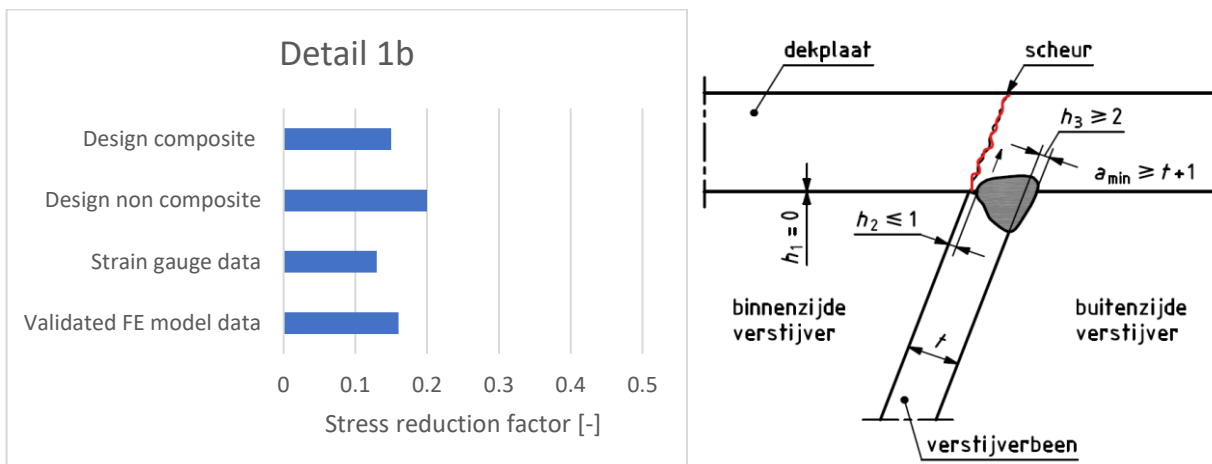


Figure 107: Stress reduction factor in fatigue detail 1b

Fatigue detail 2

Second, detail 2 (Crack in trough to deck plate connection propagating through the weld from the root) is discussed. In the design report, a stress reduction factor of 0.26 is observed here. Unfortunately, no strain gauge location is located close to this location. However, the numerical results of the trough lag can be compared. When assessing the stress reduction from the FE models at this location, a stress reduction factor of 0.30 is found. The comparison between the results is shown in Figure 108. Again, there is a good match with what is stated in the design report, reinforcing the conclusions made during the design.

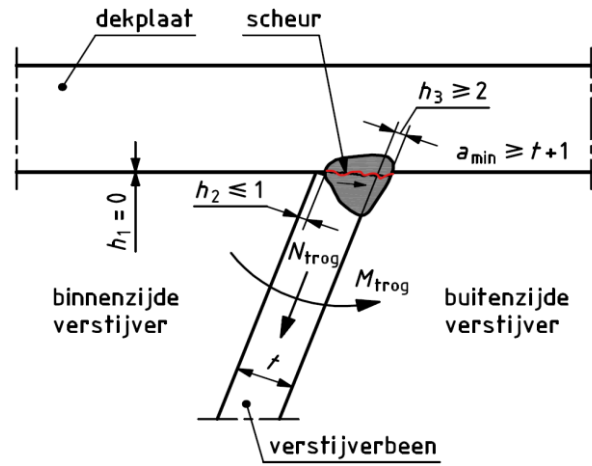
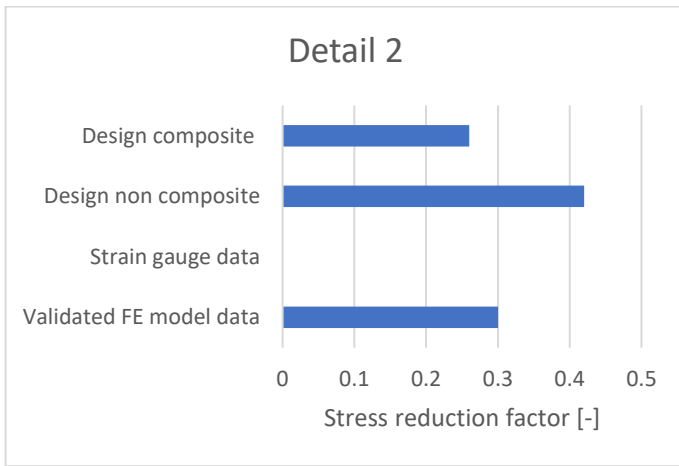


Figure 108: Stress reduction factor in fatigue detail 2

Fatigue detail 3

Lastly, fatigue detail 3 (trough to cross girder connection) is investigated. In the design report, a stress factor of 0.34 is found in this location. This initially meant that future trough to cross girder welds could not be ruled out. However, a RISK study verified the fatigue life of this connection with this stress factor, even when using a conservative stress factor of 0.57 for the bridge without composite interaction.

Looking at the experimental results at the bottom of the trough close to the cross girder, a stress factor of around 0.45 is found. This is close to, but slightly lower than the reported value in the design report, as shown in Figure 109. However, it is a larger stress reduction than what was accounted for in the design. Therefore, when repeating the RISK study with this stress factor, it can be concluded that no damage is expected in this connection until the end of service in 2036.

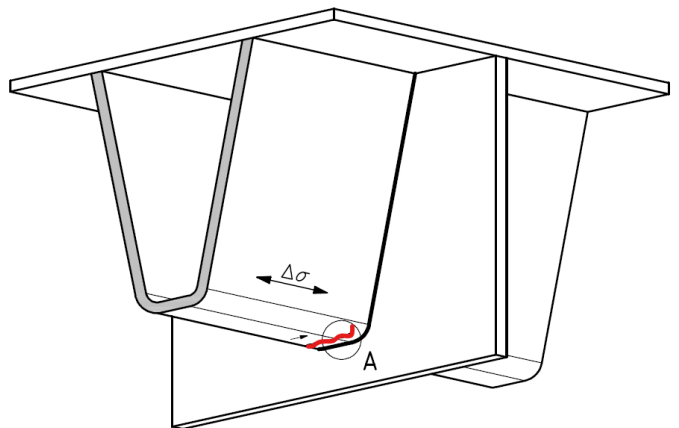
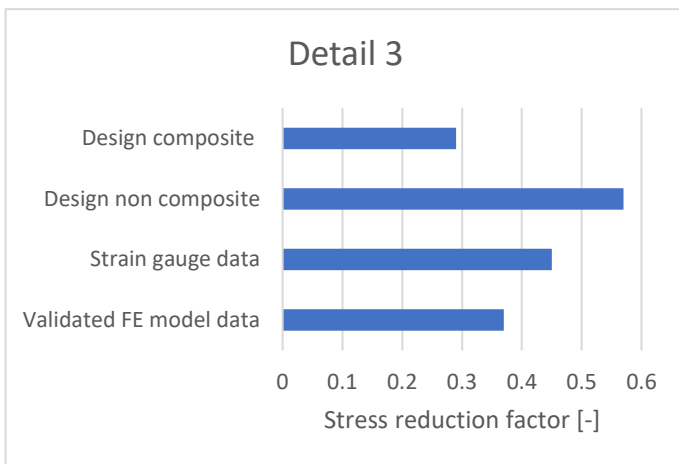


Figure 109: Stress reduction factor in fatigue detail 3

To summarise the findings in this section, it can be concluded that the conclusions made in the design report are verified by the experimental results.

8. Bolt modelling

This section provides an in-depth discussion of the results around the bolted connections. The implication of different modelling choices are discussed, with the aim of more accurately capturing the behaviour of the bridge deck in close proximity of the bolted connection.

The complexity of the modelling technique is increased incrementally. First, the impact of refining the mesh is discussed in section 8.1. Afterwards, the impact of the shear springs is discussed in section 8.2. In section 8.3, a simplified modelling adjustment is tested which could potentially simulate more realistically the boundary conditions experienced by the deck plate close to the bolt. Finally, in section 8.4, detailed model with an explicitly modelled bolt using solids is presented.

8.1. Mesh refinement

Before any changes can be made to the method of modelling the bolted connection, the issue of the mesh size is tackled. Due to high stress gradient that is expected in the location around the bolt, a crude mesh can give inaccurate results since the stress gradient cannot be simulated well. To provide more detailed results, a mesh refinement is made. An area of the model around the bolted connection is cut out and refined. This includes all components such as the deck plate, filler plate, epoxy and strengthening plate. In Figure 110 and Figure 111, the mesh refinement is shown.

In the area around the bolt, the mesh size is decreased from around 40 mm to 10 mm. The detailed area shared nodes with the rest of the model for full connectivity. The contact definitions are adjusted to include these detailed components. No through thickness refinements were made in the solid elements.

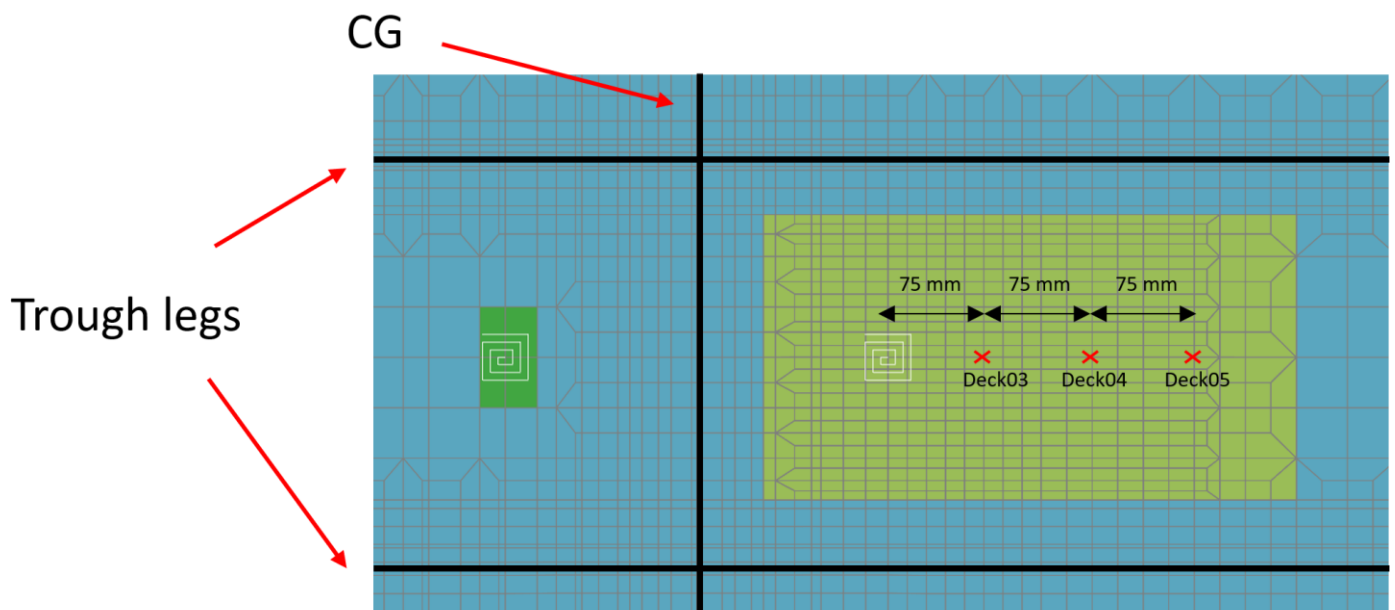


Figure 110: Top view of the refined FE model

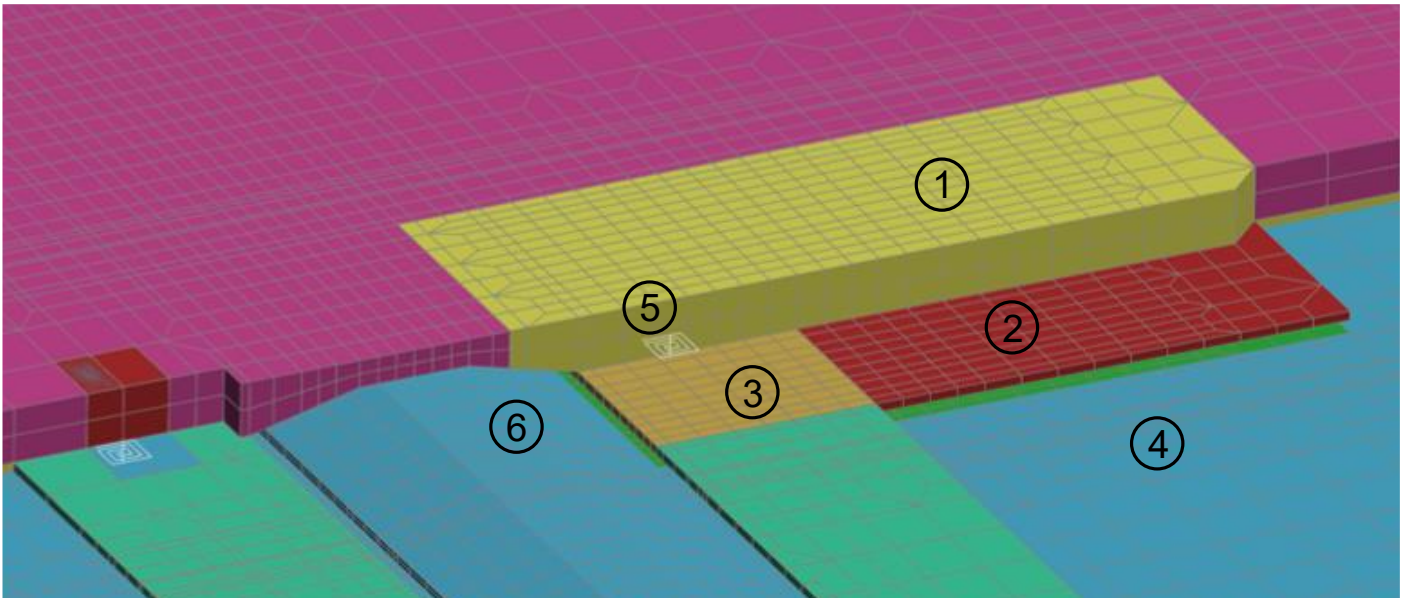


Figure 111: Isometric view of the detailed area showing all refined components.

In Table 16 below, the different components indicated in Figure 111 are labelled.

Table 16: Description different components of the strengthened FE model (similar to Table 14)

Part:	Description:
1	Strengthening plate
2	Epoxy
3	Filler plates
4	Deck plate
5	Preloaded injection bolts (shear springs)
6	Backing plate

On this refined model, a load case is simulated and compared to the original results of the strengthened model. In Figure 112, the results are presented. Only the refined area is shown for clarity. The load case where the front axle is located on top the sensor Deck03 is simulated since it allows for the best comparison with the experimental results.

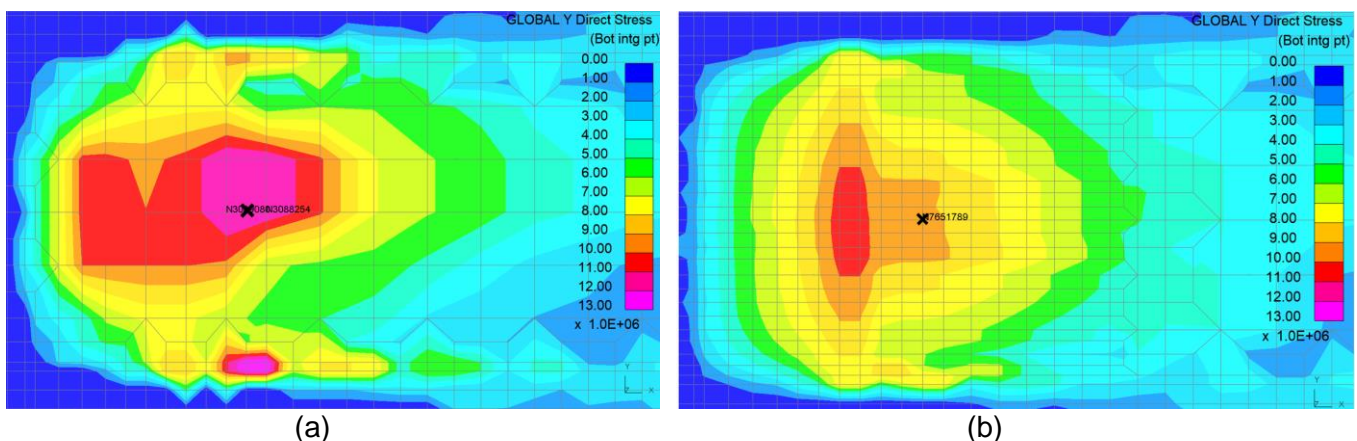


Figure 112: Tensile transverse stress distribution in the deck plate, before refinement (a) and after refinement (b) (stresses in MPa)

It can be seen that the in the crude model, the stress distribution is irregular, and the peak stresses are centred in only a few shell elements. On the other hand, in the refined model, the stress distribution looks better, with smoother stress gradients and the peak value in the expected place.

When taking the average of the adjacent shell elements, the stress at strain gauge location Deck03 does not differ significantly between the models (≈ 9.1 MPa). It can be seen that the coarser model has a larger peak stress than the more refined model. This might go against first intuition, since more refined models usually have larger peak values. The fact that this is not the case could be attributed to the influence of the contact definitions. Due to the larger elements, the deformation is concentrated in a fewer number of shell elements, which in turn experience a larger force to prevent any penetration of the elements.

Anyhow, from the figure it is fairly clear that the refined model gives a better representation of the true stress distribution. However, mesh refinement alone is not enough to better estimate stresses close to the bolted connection. Based on this refined FE model, further investigation into the behaviour of the bolted connection will now continue.

8.2. Spring stiffness

Now that the mesh refinement has been made, the first step in the investigation is to change the stiffness of the shear springs in the simplified model. This will give more insight into the importance of these connections and the impact they have on the global force transfer. It is however important to note that this investigation will be limited to the impact on the traffic loading. Whilst the spring connection can be theorised to have more impact on temperature loading, there is no test information available to confirm or investigate any possible effect on temperature loading.

First of all, the impact of the springs in the refined model is checked. The same load case is ran, with the first axle of the truck on sensor location Deck03. In this load case, the relative displacement between the nodes of the spring is only around $7.5 \cdot 10^{-8}$ m. With the chosen stiffness of 1449 kN/mm, this comes down to a spring force of 0.1kN. It is clear that this has a negligible effect on the load distribution through the system, and that thus most of the shear loading is thus transferred through the epoxy.

To check this assumption, a separate analysis is set up in which the springs are completely excluded. In Figure 113, a comparison between the analyses with and without the springs is presented. It can be seen that the exclusion of the springs does not actually significantly influence the transverse stress distribution in the deck plate due to traffic loading. From the full results, it can be confirmed that none of the other stress tensors is affected either.

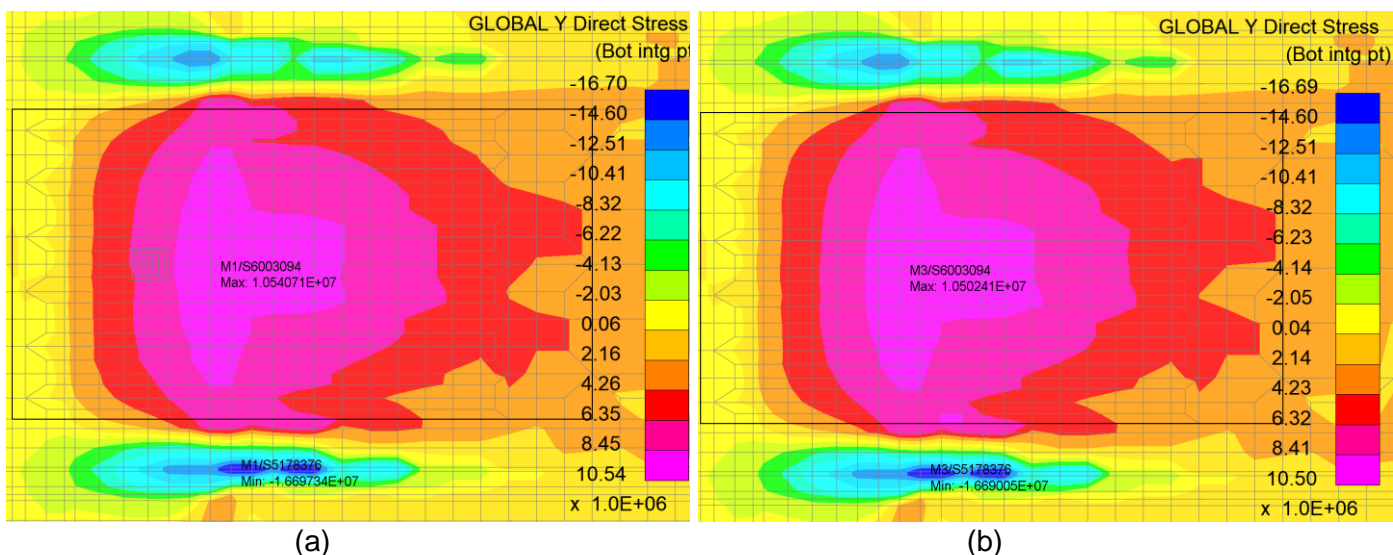


Figure 113: Refined model results with bolts included (a) and bolt excluded (b) (stresses in MPa)

On the other hand of the spectrum, the impact of a stiffer bolt connection is also investigated. In this comparison, that is shown in Figure 114 below, the bolt stiffness is increased by a factor 1000 to $1449 \cdot 10^3$ kN/mm.

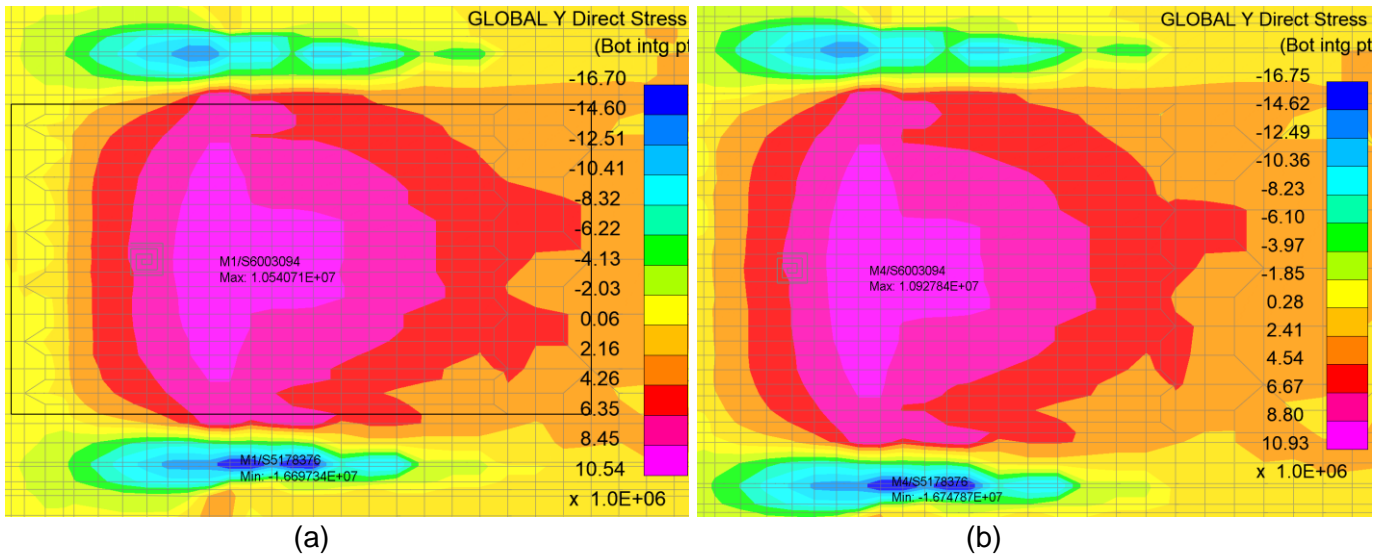


Figure 114: Comparison between normal bolt stiffness (a) and high bolt stiffness (x1000) (b) (stresses in MPa)

From the results, it can be seen that a very high stiffness again does not alter the stress distribution much. In this case, the peak stresses in the deck plate increase by around 5%. The forces in the springs increase by around 400% in longitudinal and 50% in transverse direction.

Based on these findings, it can be concluded that when investigating the behaviour of and stresses in the deck plate, the spring stiffness that is chosen to model the bolted connections does not matter significantly. Thus, it is not possible to improve the behaviour of the model around the bolts by altering the spring stiffness.

8.3. Spring with rotational restraints

In the previous section, it was shown that the spring stiffness does not alter the stress distribution in a significant way. In order to more accurately simulate the behaviour around the bolted connection, more changes in the model are needed besides simply changing the spring stiffness.

In this section, a relatively simply modelling change that could make the model behave more like reality is investigated. Rotational restraints are imposed on an area around the bolted connection to simulate the clamping effect due to the bolt preloading. Also, the restraints simulate the presence of the packer plate and the washer, restraining rotation of the deck plate locally. Through the use of nodal rigid bodies(*NODAL_RIGID_BODY), nodes closely located around the bolt are prescribed to have the same rotation. Thus, this means that there is no curvature possible at this location, which tries to replicate the very stiff deck package at this location.

Three analyses are set with different sizes of the nodal rigid bodies. A rectangular area of 2x2, 4x4 and 6x6 elements are restrained for the three different analyses. In Figure 115, the results are visualised. Furthermore, the stress values at the location of strain gauge Deck03 are extracted and compared in Table 17.

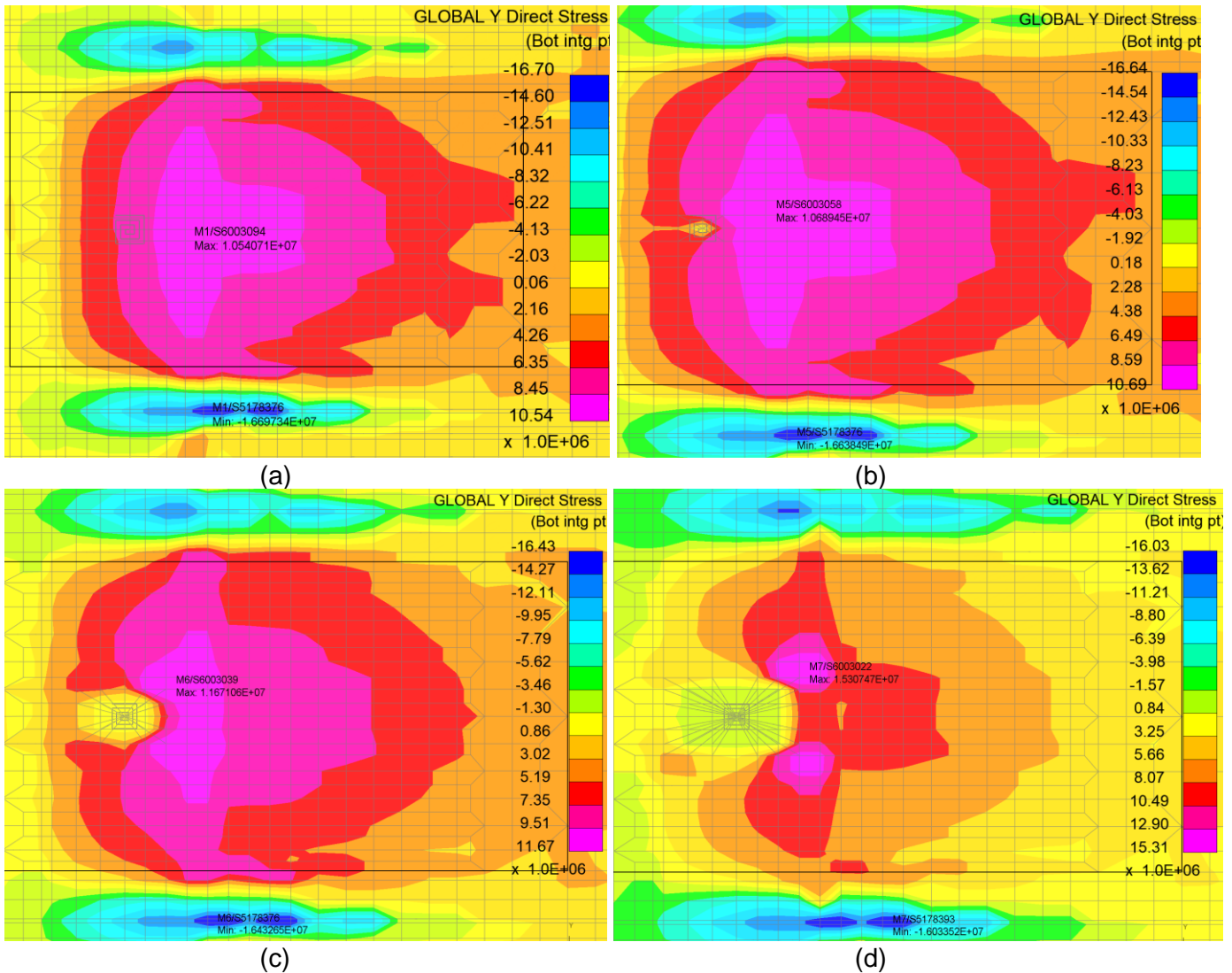


Figure 115: Comparison of the impact of rotational restraint around bolt area. Comparison between no restraints (a) with a restrained area of 2x2 (b), 4x4 (c) and 6x6 (d) elements. (stresses in MPa)

Table 17: Comparison of transverse stresses in strain gauge location Deck03

Model:	Transverse stress in Deck03:
Original refined model	9.14 MPa
2x2 Nodal rigid body	9.10 MPa
4x4 Nodal rigid body	8.86 MPa
6x6 Nodal rigid body	7.33 MPa
Experimental result	3.5 MPa

It can be seen that although there is a clear effect of the adjustment, the impact on the stresses remains very local and the modelling adjustment cannot lower the stresses to what was observed in the experiments. Also, the stress distribution becomes questionable when using a large NRB. In Figure 115 (d), peak stresses are no longer in the middle of the deck plate between the trough legs, but rather around the corners of the NRB. There is unfortunately no sensor placed in a different transverse position to compare this to reality, but it is deemed unlikely that this is the expected behaviour of the bridge deck.

In conclusion, adding a nodal rigid body does slightly lower the observed stresses. However, when making the nodal rigid body too large, an unrealistic stress distribution is obtained due to the stiffness jump at the edge of the NRB. In case of a 4x4 nodal rigid body, the stresses in sensor location are lowered by around 5%, which is not enough to call this modelling decision very successful.

8.4. Detailed modelling

From the previous sections it can be concluded that the complicated geometry and stress state due to the preloaded bolt is not easy to model and will require a higher level of complexity than what was done so far. In this step, the complexity is increased significantly, and the full geometry of the bolt is modelled with solids. This detailed representation will be compared to the simplified analyses and experimental results to conclude what the most optimal modelling technique is. In order to transition to this fully solid bolt with preloading, a number of modelling steps and choices were necessary. These will first be highlighted and explained. After this, the results are presented and discussed.

To insert the solid bolt into the model, first a bolt hole is meshed into the detailed model area. A nominal bolt hole of 26 mm is taken for the M24 bolt. The mesh can be seen in Figure 116.

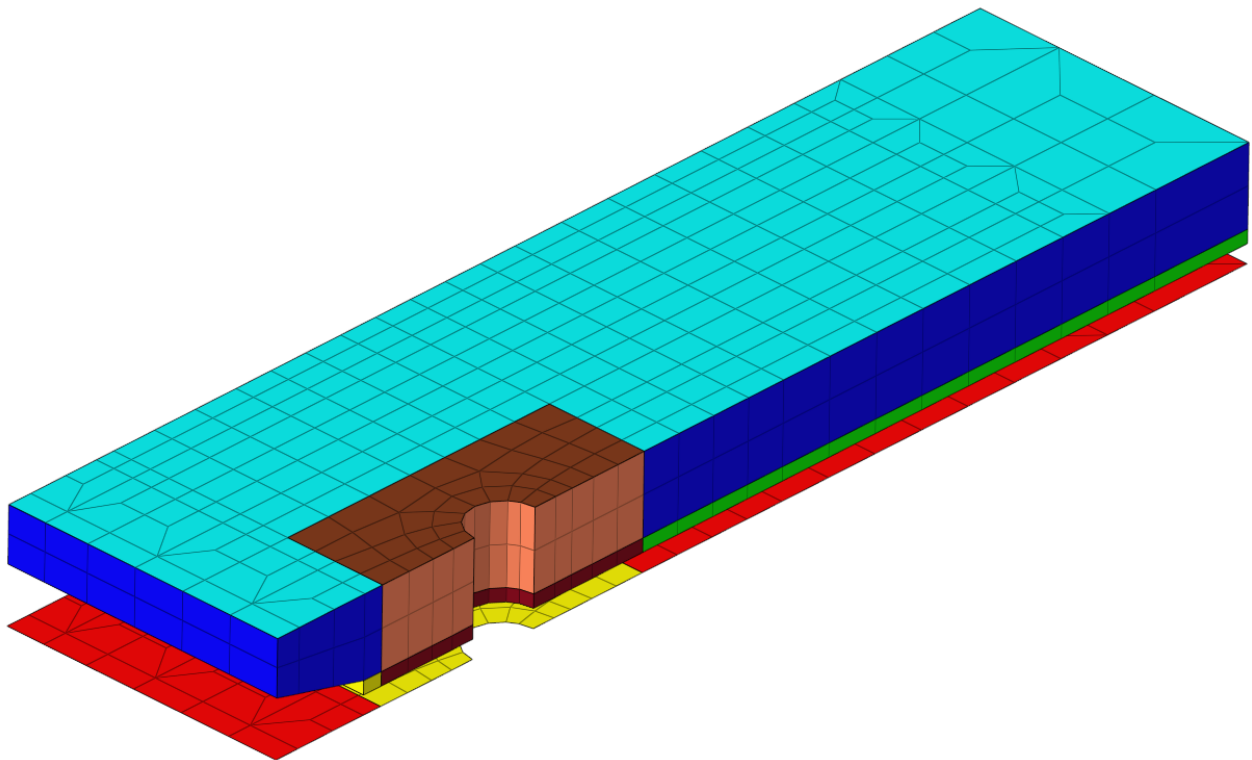


Figure 116: Meshed bolt hole

For the bolt, the M24 bolt shank is modelled without a thread. A 44 mm diameter washer and a nut with a width across flats of 36mm are modelled according to nominal dimensions. No countersunk geometry is considered, and no influence of epoxy injection is taken into account, i.e., all the load transfer is through friction and none through bearing of the bolt shank. The mesh of the bolt can be seen in Figure 117.

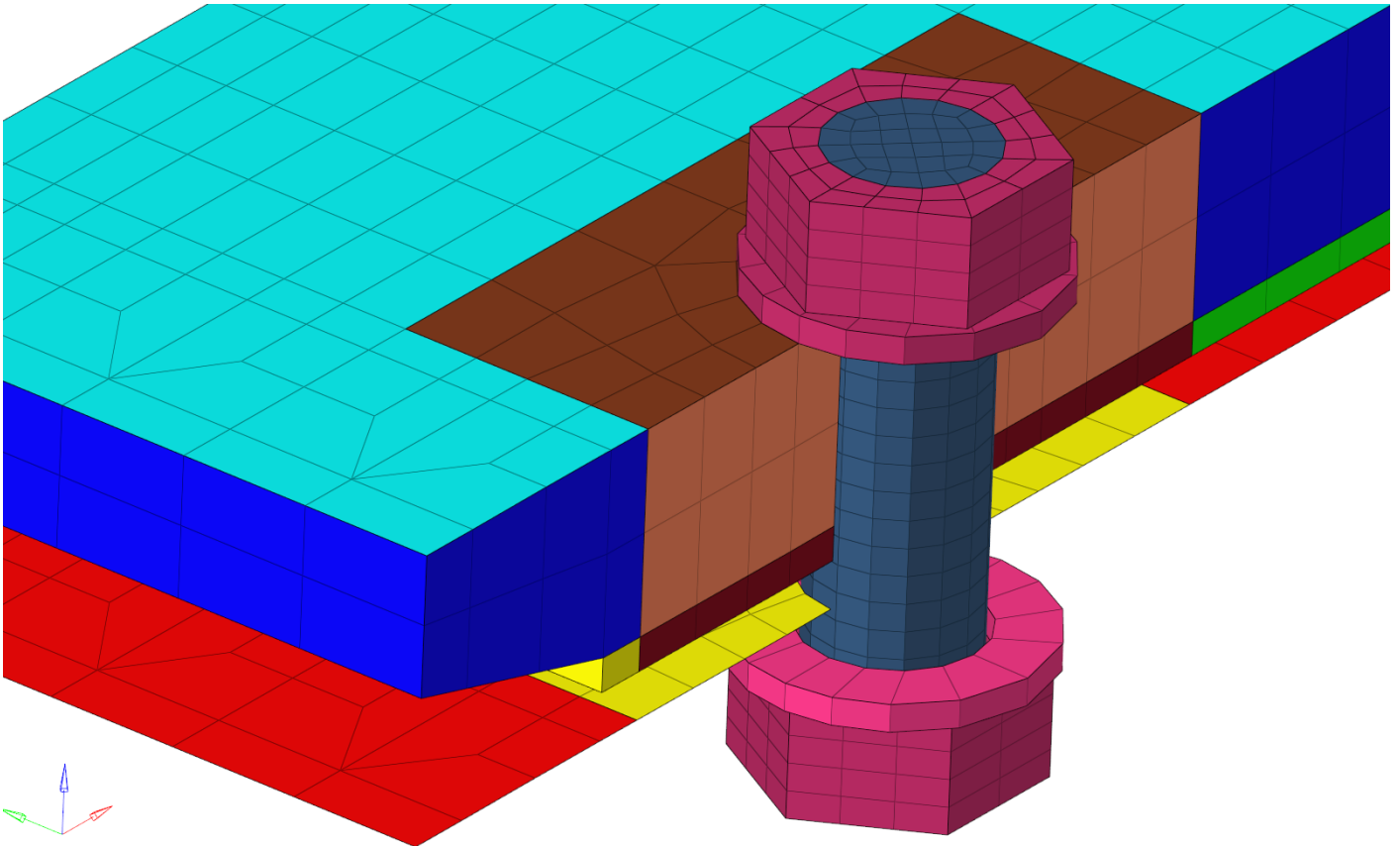


Figure 117: Fully solid mesh of the bolt

In order for the preload to be modelled accurately, the deck plate will also have to be modelled by solid elements around the bolt. This is in order to transfer stresses through the thickness (z) direction, which is not included in shell elements. Two solid elements are modelled through thickness, shown in Figure 118. The solid mesh is connected to the shells by the LS-DYNA card `*CONSTRAINED_SHELL_IN_SOLID`. This defines a constraint-based coupling between the shells and the solids, ensuring proper connectivity. An automatic surface to surface contact is added between the solid elements and the filler plates since the shell edge to solid contact that is defined for the rest of the deck plate is not applicable for solid-to-solid contacts. The local solid mesh is presented in Figure 118.

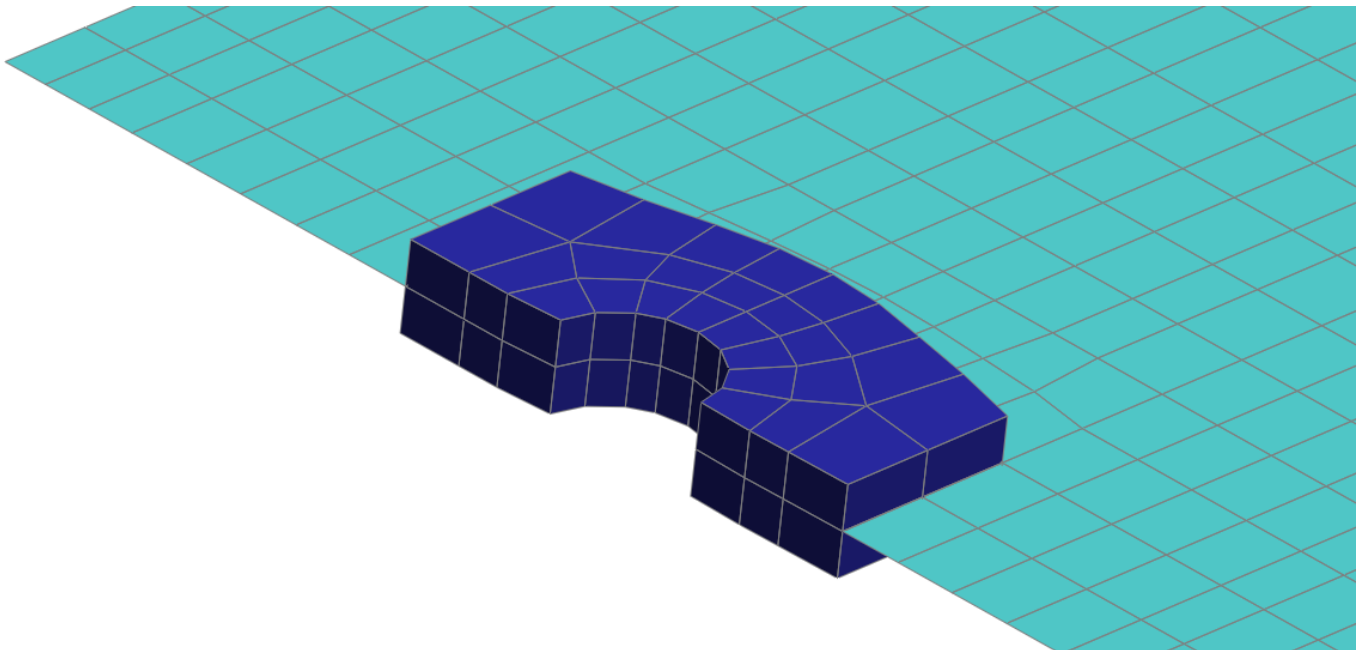


Figure 118: Solid part of the deck plate

To ensure proper behaviour of the model and achieve convergence, a number of contact definitions need to be added to the advanced model. Tied surface to surface contacts are chosen as these ensure easier convergence and are not expected to negatively influence the model behaviour. Contacts are added between the following elements:

- Bolt to washer
- Washer to deck plate
- Washer to strengthening plate
- Bottom nut to shank
- Nut to washer

Furthermore, the friction is activated in the interface between the steel plates. A friction coefficient of 0.5 is assumed, corresponding with the thermally sprayed aluminium used in the strengthening, as stated in the design report.

In order to initiate the preload, a so-called dynamic relaxation analysis is executed. This happens in so-called pseudo-time, which is a fictitious time that occurs before the actual analysis. In this analysis, the bolt shank is preloaded using the LS-DYNA card *INITIAL_STRESS_SECTION to the nominal preload of 700 MPa. This makes it possible to have this preloaded bolt in combination with an implicit analysis which is very time efficient compared to an explicit analysis. In the current case, the dynamic relaxation phase takes about 20 minutes to execute, which roughly doubles the total time needed for the analysis. However, this initial preloaded state can be exported and used in all consequent load cases through the use of a stress initialization file. When doing this, the dynamic relaxation phase will only have to be executed once, so the increase in computation time when running multiple load cases is very small.

When assessing the results, it is important to realise that when comparing stresses to experimental results, the stresses after preloading will have to be seen as the baseline. Remember that during the load tests, the average stress after strengthening but within any loading was seen as the '0' measurement. In Figure 119, the stress plots of the results of the analysis are presented.

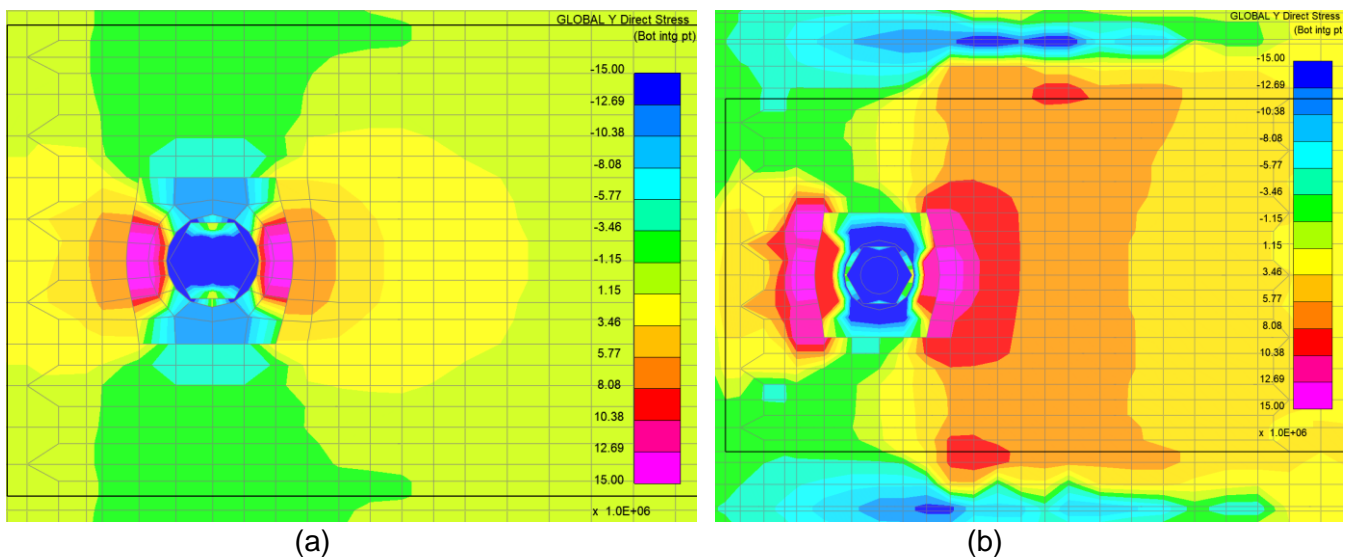


Figure 119: Transverse stresses after preloading (a) and during loading (b), fully solid bolt (stresses in MPa)

From the results above, the results in strain gauge location Deck03 can be extracted. A transverse bending stress of 3.9 MPa is observed during the preloading, and a stress of 10.1 MPa during the truck loading. This means that the truck is causing a stress cycle of 6.2 MPa. While this is not yet 100% in agreement with the experimental results, it is a lot closer than any of the simplified modelling techniques. The stress plots are more realistic, making this approach a good solution for a detailed analysis of a local region.

The same analysis has been repeated, but with the loading at 75 and 150 mm further away from the bolt, i.e., at stain gauge location Deck04 and Deck05. In section 7.2.2, it was observed that the error was very local and that the results at sensor location Deck05 were close to the experimental results again. This same

comparison is made with the refined FE model. A comparison between the numerical and experimental results is plotted in Figure 120 for the stress observed due to the first truck axle.

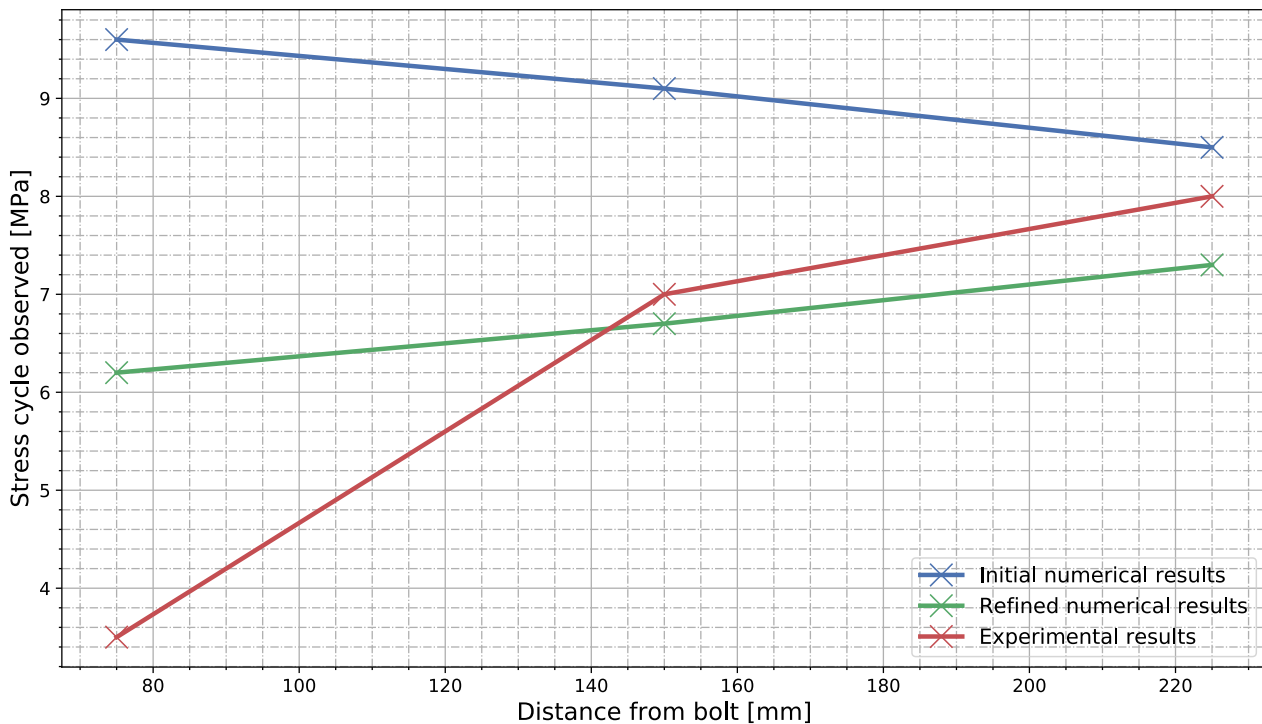


Figure 120: Comparison of deck plate results close to the bolted connection

A number of interesting observations can be made. First of all, the refined model does a better job at capturing the magnitude of the transverse stresses around the bolted connection. The stress gradient is also better captured. Although close to the bolt the improvement is big, there is still a relatively large discrepancy to the experimental results. Especially for fatigue purposes, in case results close to the bolts were needed, a closer match is desirable.

Model optimisations

In a final attempt to improve the refined FE model, some final model adjustments are proposed. First, the 20 mm packer plate is added to the model. This packer plate makes the geometry more realistic and could increase the stiffness of the deck plate locally to further decrease transverse bending stresses. Four elements are modelled through thickness. The contacts between the washer and the packer plate is added and the packer plate shares nodes with the solid part of the deck plate. The same mesh as for the deck plate is used. Figure 121 shows the geometry of the packer plate.

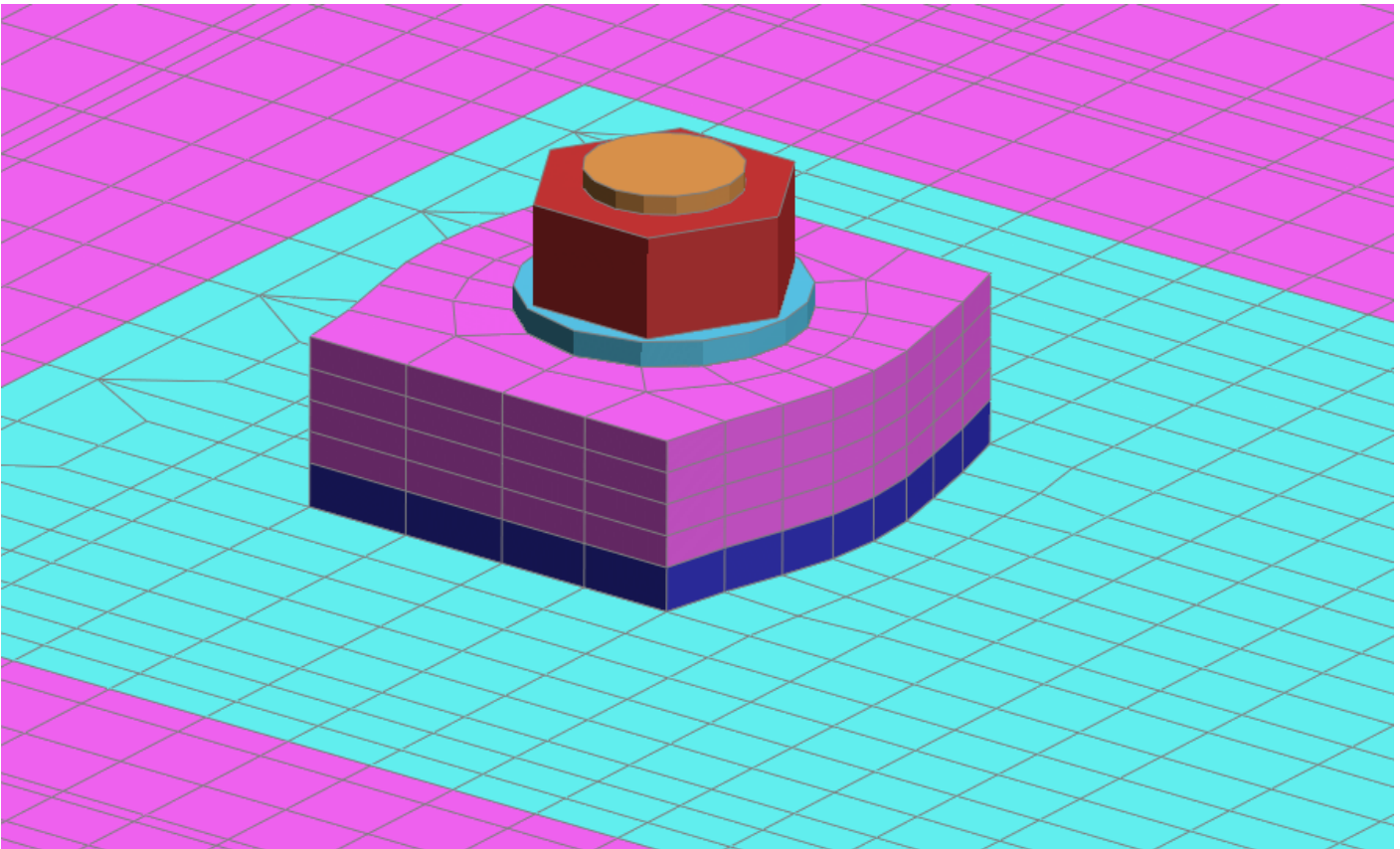


Figure 121: Packer plate seen from the bottom of the deck plate

In Figure 122, the stress plots of the results are presented.

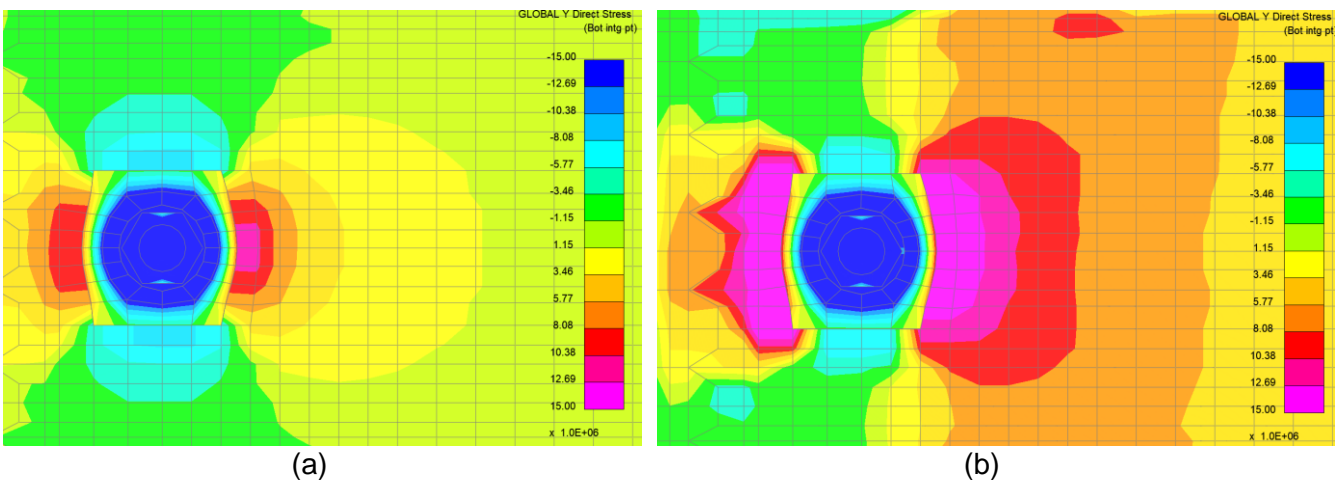


Figure 122: Transverse stresses after preloading (a) and during loading (b), added packer plate (stresses in MPa)

Again, the results at the strain location are extracted. In this case, a stress of 4.9 MPa is observed during preloading and a stress of 10.7 MPa is observed during the truck loading. With the packer plate included, it is curious that the stresses due to preloading have increased rather than decreased. While it could be theorised that the increased stiffness should distribute the stresses more, it seems that the sudden drop in stiffness at the edge of the packer plate increases peak stresses observed around the packer plate. With the added packer plate, a stress cycle of 5.8 MPa is observed for this model due to truck loading, which is slightly more in line with the experimental results compared to the original model.

The last model optimisation has to do with the deck plate. Because of the importance of the vertical stresses due to the bolt, it can be theorised that the solid deck plate has been meshed in a too small area to properly simulate the stress distribution. Especially with the packer plate included, z stresses can be expected in the area around the packer plate, which was not modelled in solids in that analysis. Therefore, another analysis has been set up with the entire refined deck plate area has been modelled in solids. Again, the

*SHELL_IN_SOLID card has been used to connect the area to the adjacent shells. The deck plate to epoxy and deck plate to filler plate contacts have been updated to be compatible with solid-to-solid connections (also restraining rotational degrees of freedom of the nodes). The region meshed with solids can be seen in Figure 123. In order to extract stresses in the bottom fibre of the deck plate, the solids have been coated with a thin shell layer.

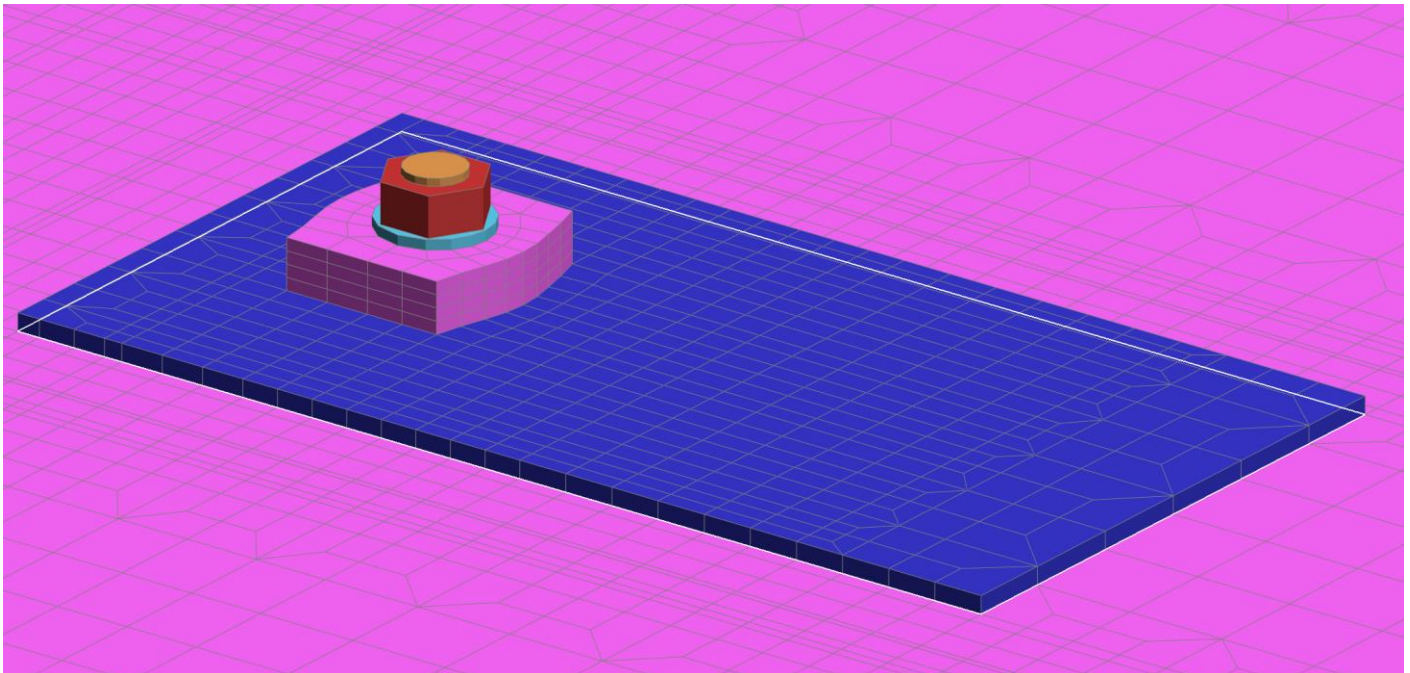


Figure 123: Geometry of the fully solid deck plate in the detailed region

Again, the same analysis is set up and executed. Firstly, to verify the assumption that the stress distribution was not ideal in the previous analysis, Figure 124 shows a comparison of the Z-stress distribution in both analyses. It can clearly be seen that solids are needed around the packer plate, since significant z stresses are observed at this location.

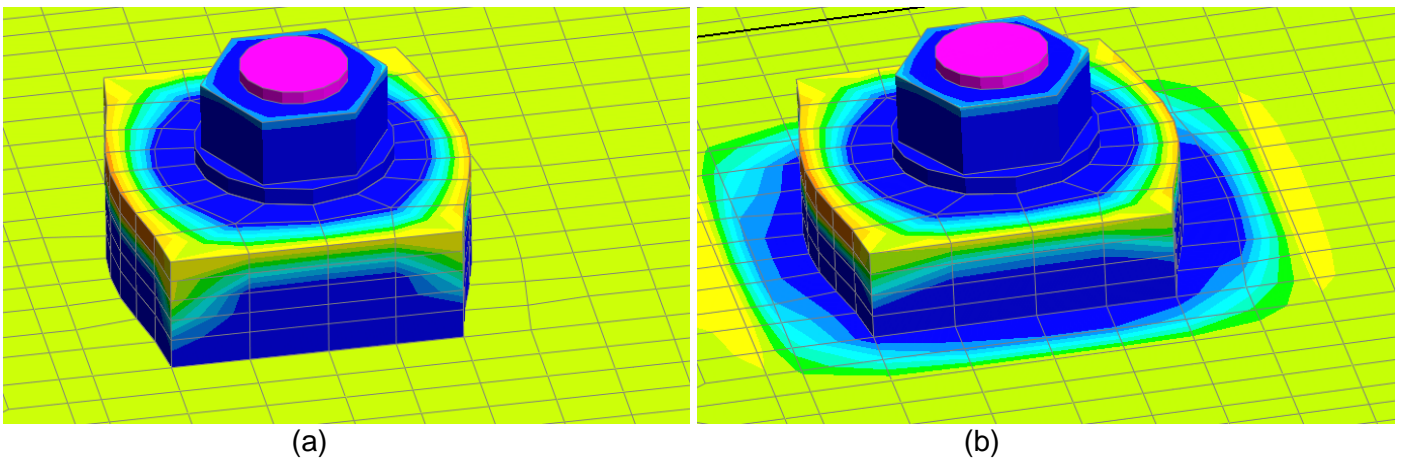


Figure 124: Comparison of Z-stress distribution between model with small solid region (a) and more extensive solid region (b)

With this suspicion confirmed, the results of the analysis are presented in Figure 125.

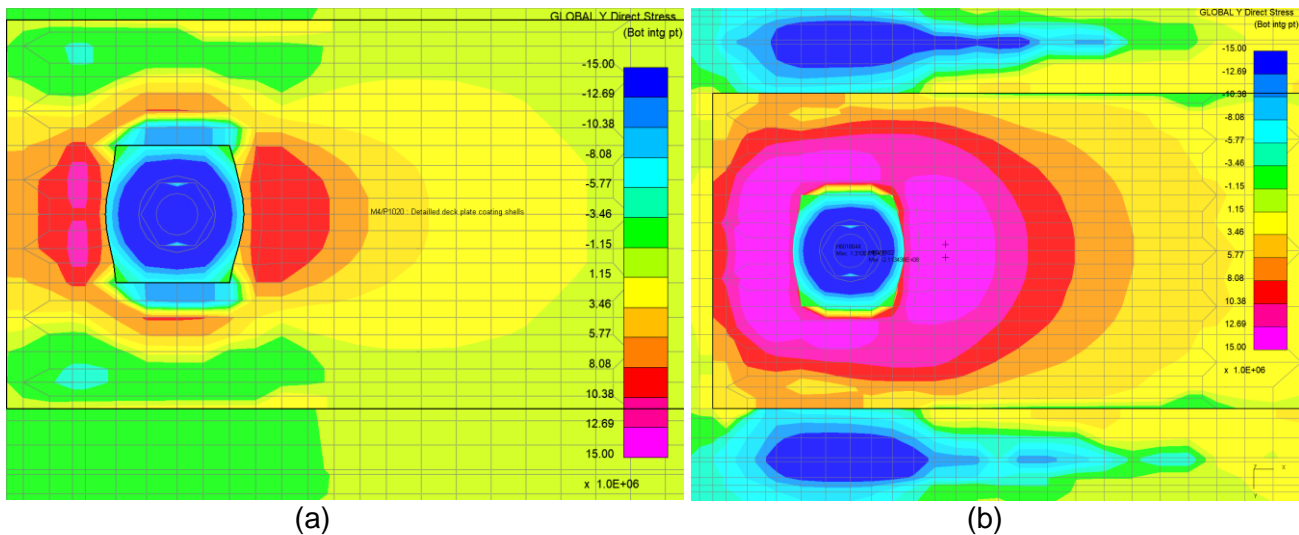


Figure 125: Transverse stresses after preloading (a) and during loading (b), solid deck plate (stresses in MPa)

Some interesting observations can be made from the stress plots above. The stress distribution is significantly different from the previous results, with larger stresses in y-direction around the bolts. Especially in transverse direction from the bolts there are large differences, with larger stresses in the deck plate but also at the trough intersection. At the location of strain gauge Deck03, A stress of 9.4 MPa is observed due to preloading, increasing to 16.3 MPa during the truck loading. Again, the force due to the preloading has increased significantly compared to the previous analyses. However, the stress cycle of 6.9 MPa is slightly larger than the analysis without the packer plate and solid deck plate, so this added realism did not result in better matching results.

To conclude this section, it can be stated that the detailed bolt modelling seems to give a much better representation of the stress distribution close to the bolted connection. The added steel elements add a lot of stiffness locally, which is of large importance to stresses in the deck plate close to this location. Furthermore, a method has been laid out in which these detailed bolt representations can be present directly in the global FE model of the bridge. An implicit analysis is still possible, and the added part do not add a very significant increase in computational costs.

However, when comparing the results of the analyses, it also has to be concluded that the present study has not been able to 100% match the experimental results. Despite cutting the error in half and proving that the error only exists in the first 150 mm around the bolt, no perfect match could be obtained.

Multiple reasons for this unresolved difference can be thought of. First of all, the countersunk geometry of the bolt has not been taken into account. It can be expected that when the bolt is countersunk, the smaller thickness of the clamped package results in less distribution of the clamping force. Furthermore, no impact of the injection is taken into account. Whilst the injection material can significantly increase the slip capacity of the connection, its stiffness at very small relative displacements between the plates. Therefore, the expected error due to this omission is limited. Lastly, preloading the bolt induces large, localized stresses in the plate package. Prescribing non-linear material properties could significantly influence the stress and strain distribution around the bolt. However, too much non-linearity will limit the application of implicit analyses, and this will come at the cost of computational power.

A short overview and summary of the different bolt modelling options that were investigated in this chapter are shown in Table 18,

Table 18: Overview of different modelling results

Modelling technique:	Stress cycle in deck plate sensor	Error with experimental results
Experimental result	3.5 MPa	-
Original model	9.1 MPa	160%
Mesh refinement	9.1 MPa	160%
Spring stiffness	9.1 MPa	160%
Rotational restraints	9.1 – 7.3 MPa	160 – 108%
Solid bolt modelling	6.9 – 5.8 MPa	97 – 66%

9. Conclusions & recommendations

In this thesis, the effectiveness of strengthening an orthotropic steel deck using a bonded & bolted strengthening plate is investigated. This was done using a monitoring programme involving 16 strain gauges installed on the deck plate, troughs and cross girder. Quasi static load tests were carried out both before and after strengthening to determine the stress reduction in relevant areas. Furthermore, the numerical models used during the design were validated using these experimental results. Lastly, an attempt was made to improve these numerical models in areas where any discrepancy between the results was observed.

9.1. Conclusions

From the research done in this thesis, the following conclusions are drawn:

Monitoring & load test results

- The load tests were successfully carried out and provide accurate results. Video footage shows that the position of the wheel stays within 5 cm of the intended track throughout the load tests.
- In the trough bottom, a stress reduction of 45% was observed at mid-bay and a stress reduction of 55% was observed close to the cross girder.
- Transverse and longitudinal stresses in the deck plate, in the middle between two troughs, are reduced by 85% at midspan and 90% close to the cross girder.

FE validation

- The full influence line found during the load tests has been simulated in an FE model by positioning the truck at 119 longitudinal positions. This was needed to accurately obtain the influence line at all sensor locations since the local behaviour results in very 'peaky' influence lines.
- Numerical modelling was able to accurately predict the shape and magnitude of the influence line in all sensor locations for the unstrengthened bridge.
- A difference in peak value between experimental and numerical results of up to 30% was observed in the unstrengthened bridge. Comparison of the results of similar sensors show that there is no systematic deviation between the numerical and experimental results. Further sensitivity analyses, done by rerunning the full influence line with the wheel loading 5 cm off the centre of the trough, show that the error can in most cases be explained by the uncertainty in the exact location of the wheel.
- For the strengthened bridge, a difference of no more than 10% is observed when not considering the area very close to the added bolts. The lower error compared to the unstrengthened bridge is attributed to the increased stiffness of the strengthened deck structure. This allows for more stress redistribution and a corresponding lower sensitivity to the load location.
- Close to the added bolted connections (± 200 mm), no accurate results can be obtained with a simplified modelling approach. The current modelling technique using shear springs does not accurately represent the local stress state and bending behaviour. However, the obtained numerical results are conservative compared to the experimental results, and the global behaviour is not impacted by the simplified modelling choice.

Fatigue life

- Even though the strain gauge sensors are not located in the position of the fatigue details, they confirm that the FE models that are used to predict the fatigue life of the bridge are accurate and behave similar to the real bridge.
- For further confirmation, stresses are extracted in the element pairs used for hot spot stress calculations. These are compared to the stress factors that are reported in the design report so that a conclusion can be made regarding the fatigue life that is predicted.
- In fatigue details 1a (crack in the deck plate outside trough) and 1b (crack in the deck plate inside trough), a stress factor of 0.16 is found in the FE model. This matches closely with the factor of 0.14 stated in the design report.

- In fatigue detail 2 (connection of the trough leg with the deck plate, crack originating in the weld root), a stress factor of 0.30 is found in the FE model. This matches closely with the factor of 0.26 stated in the design report.
- In fatigue detail 3 (Trough to cross girder connection, crack in weld or trough), a stress factor of 0.45 is found in the FE model. This is smaller than the factor of 0.34 found in the design report when assuming composite action, but it is larger than the factor 0.57 that was used for the design. Thus, the design is conservative, but a closer look is needed at this discrepancy for future applications of the strengthening scheme.
- It can be concluded that the results from the calibrated FE model match well with the values provided in the design report. Where there are small differences, the design report is conservative. Therefore, this thesis strengthens the conclusions regarding the fatigue design life stated in the design report.

Bolt modelling

- Different simplified modelling techniques have attempted to improve the stress state of the FE model in the region around the bolted connection. Changes made to the mesh density and spring stiffness, as well as local rotational restraints have been applied. These have however been unable to make significant improvement to the stress state around the bolt.
- A detailed modelling approach has successfully been applied in which a fully solid bolt has been modelled. The detailed modelling has been implemented without any relevant increase in computation time so this can be applied in global FE models.
- This detailed modelling technique is more accurate compared to the simplified modelling technique and reduces the error by more than 50%. However, stresses close to the bolt are still overestimated even with this advanced modelling approach as no perfect match has been obtained yet.
- For a better match, a more detailed geometric representation of the connection and/or incorporation of non-linear material behaviour might be necessary.

Strengthening design

- The innovative strengthening scheme shows much potential and has clear advantages with regard to the alternative solutions.
- The weight and execution time is significantly lower than the HSC alternative. Furthermore, the strengthening is applicable on larger bridge and has lower risks compared to using only a bonded plate.
- The conclusions made in this thesis allows for more confidence in the strengthening design and reinforces the potential of the strengthening scheme for future applications.
- With more research and time investment, there is a lot of potential for improving the current design with regard to weight, costs and effectiveness.

9.2. Recommendations

To build on the current research and further improve the knowledge of the strengthening scheme, the following recommendations are laid out:

- The current strengthening scheme shows a lot of potential but was designed in a conservative way to reduce risks. Using data from this pilot application and by carrying out additional testing, a more optimised design can be made for future applications. This can include an optimisation in the bolt layout, as well as a thinner strengthening plate.
- A critical aspect for the strengthening scheme is the temperature loading. A more long-term testing scheme including temperature sensors is desirable to reduce the conservative temperature loading, and thus, further optimise the design.
- Despite the efforts of the current research, local stresses close to the bolted connections were unable to be accurately predicted. These local stresses are however necessary in some possible fatigue strengthening applications. A more extensive research and detailed FE model can be setup to solve these issues.

Bibliography

- Abaqus FEA. (2021, 05 18). *Contact formulations in Abaqus/Standard*. Retrieved from Abaqus documentation: <https://abaqus-docs.mit.edu/2017/English/SIMACAEITNRefMap/simaitn-c-contactpairform.htm>
- Apostolidis, P., Liu, X., Erkens, S., & Scarpas, A. (2020). Use of Epoxy Asphalt as Surfacing and Tack Coat Material for Roadway Pavements. *Construction and Building Materials*, 250. doi:<https://doi.org/10.1016/j.conbuildmat.2020.118936>
- Arup. (2012). *Strain gauge comparison Muider bridge*. Arup.
- Arup. (2021, 20 4). *Circular Economy inspires renovation of Netherlands busiest bridge, extending lifespan by another 100 years*. Retrieved from Arup: <https://www.arup.com/projects/van-brienoord-bridge-renovation>
- Bouters, T., Braam, R., Kolstein, H., & Romeijn, A. (2009). Concrete Overlay of Movable Steel Orthotropic Bridge Decks. *Steel Construction*, 2(2), 104-108. doi:<https://doi.org/10.1002/stco.200910014>
- Buitelaar, P., Braam, R., & Kaptijn, N. (2004). Reinforced High Performance Concrete Overlay System for Rehabilitation and Strengthening of Orthotropic Steel bridge decks. *2004 Orthotropic Bridge Conference*, (pp. 384-401). Sacramento, California, USA.
- Crocco, D., de Agostinis, M., & Vincenzi, N. (2011). Failure Analysis of bolted joints: Effect of friction coefficients in torque-preloading relationship. *Engineering Failure Analysis*, 18(1), 364-373. doi:<https://doi.org/10.1016/j.engfailanal.2010.09.015>
- Cui, C., Zhang, Q., Hao, H., Li, J., & Bu, Y. (2018). Influence of Asphalt Pavement Conditions on Fatigue Damage of Orthotropic Steel Decks: Parametric Analysis. *Journal of Bridge Engineering*, 23(12). doi:[https://doi.org/10.1061/\(ASCE\)BE.1943-5592.0001313](https://doi.org/10.1061/(ASCE)BE.1943-5592.0001313)
- de Backer, H. (2015). Chapter 22: Orthotropic Steel Decks. In *Innovative Bridge Design Handbook* (pp. 597-613). doi:<https://doi.org/10.1016/B978-0-12-800058-8.00022-0>
- de Freitas, S. (2012). *Steel Plate Reinforcement of Orthotropic Bridge Decks*. TU Delft.
- de Freitas, S. T., Kolstein, H., & Bijlaand, F. (2013). Lightweight Reinforcement System for Fatigue-Cracked Orthotropic Bridge Decks. *Structural Engineering International*, 23(4), 458-467. doi:<https://doi.org/10.2749/101686613X13627347100356>
- de Freitas, S., Kolstein, H., & Bijlaard, F. (2010). Sandwich system for renovation of Orthotropic Steel Bridge Decks. *Journal of Sandwich Structures & Materials*, 13(3), 279-301. doi:[doi:10.1177/1099636210386848](https://doi.org/10.1177/1099636210386848)
- de Freitas, S., Kolstein, H., & Bijlaard, F. (2012). Structural monitoring of a strengthened orthotropic steel bridge deck using strain data. *Structural Health Monitoring*, 11(5), 558-576. doi:<https://doi.org/10.1177/1475921712449507>
- de Freitas, S., Kolstein, H., & Bijlaard, F. (2017). Fatigue Assessment of Full-Scale Retrofitted Orthotropic Bridge Decks. *Journal of Bridge Engineering*, 22(11), 04017092. doi:[https://doi.org/10.1061/\(ASCE\)BE.1943-5592.0001115](https://doi.org/10.1061/(ASCE)BE.1943-5592.0001115)
- de Jong, F. (2006). *Renovation Techniques for Fatigue Cracked Orthotropic Steel Bridge Decks*. TU Delft.
- de Jong, F., & Kolstein, M. (2004). Strengthening a Bridge Deck with High Performance Concrete. *2004 Orthotropic Bridge Conference*, (pp. 328-347). Sacramento, California, USA.
- DeWolf, J. T., Lauzon, R. G., & Culmo, M. P. (2002). Monitoring Bridge Performance. *Structural Health Monitoring*, 1(2), 129-138. doi:<https://doi.org/10.1177/1475921702001002001>
- DYNAmore GmbH. (2011, 11 11). *Hourglass*. Retrieved from LS-DYNA Support: <https://www.dynasupport.com/howtos/element/hourglass>
- DYNAmore GmbH. (2021, 05 18). *Preload general*. Retrieved from LS-DYNA support: <https://www.dynasupport.com/howtos/general/preload-general>
- Epotek. (2011). *Tech Tip 19: Understanding Mechanical Properties of Epoxies For Modeling, Finite Element Analysis (FEA)*. Billerica: Epoxy Technology Inc. Retrieved from www.epotek.com.
- ESDEP. (n.d.). *Lecture 11.3.2: Connections with Preloaded Bolts*.
- European Committee for Standardization. (2005). *NEN-EN 1993-1-9 Eurocode 3: Design of steel structures - Part 1-9: Fatigue*.
- European Committee for Standardization. (2011). *NEN-EN 1993-1-8: Eurocode 3: Design of Steel Structures - Part 1-8: Design of Joints*. Delft: Nederlands Normalisatie Instituut.

- European Committee for Standardization. (2011). *NEN-En 1993-2+C1/NB*. Delft: Nederlands Normalisatie-instituut.
- European Committee for Standardization. (2011). *NEN-EN 1993-2+C1/NB: Eurocode 3: Design of Steel Structures - Part 2: Steel bridges*. Delft: Nederlands Normalisatie Instituut.
- European Committee for Standardization. (2018). *NEN-EN 1090-2: Execution of Steel and Aluminium Structures - Part 2: Technical requirements for Steel Structures*.
- European Convention for Constructural Steelwork. (2000). *Good design practise - A guideline for fatigue design*. Brussels.
- European Convention for Constructural Steelwork. (1994). *European Recommendations for Bolted Connections with Injection Bolts*. ECCS Technical Committee 10: Structural Connections.
- European Research Commission. (2018). *Execution and reliability of slip-resistant connections for steel structures using CS and SS (SIROCO)*.
- European Research Commission. (2018). *SIROCO task 3.2: Use of injection bolts*. Delft.
- European Steel Design Education Programme. (2021, 07 26). *Lecture 15B.3: Bridge Decks. - 2. HISTORICAL DEVELOPMENT*. Retrieved from ESDEP WG 15B: <http://fgg-web.fgg.uni-lj.si/~pmoze/ESDEP/master/wg15b/10300.htm>
- Feldmann, M., Sedlacek, G., & Geßler, A. (2007). A System of Steel-Elastomer Sandwich Plates for Strengthening Orthotropic Bridge Decks. *Mechanics of Composite Materials*, 43(2), 183-190. doi:<https://doi.org/10.1007/s11029-007-0018-y>
- Gibson, R., Rus, L., Gration, D., Vonk, E., Hajar, Z., & Nagtegaal, G. (2014). Prefabricated UHPFRC Slabs as a Strengthening Alternative for Ewijk Bridge. *IABSE Madrid Symposium Report*, (pp. 2207-2214). Madrid, Spain.
- Gresnigt, N., Beg, D., & Bijlaard, F. (2012). Injection bolts in steel structures with short duration high loads. *Seventh international workshop on Connections in Steel Structures*, (pp. 423-435). Timisoara, Romania.
- Gurney, T. (1992). *Fatigue of Steel Bridge Decks*. (D. o. Transport Research Laboratory, Ed.) London, England: HMSO Publication Centre.
- Hadjoannou, M., Stevens, D., & Barsotti, M. (2016). Development and Validation of Bolted Connection Modeling in LS-DYNA for Large Vehicle Models. *14th international LS-DYNA Users Conference*. Detroit.
- Haibach, E., & Plasil, I. (1983). *Untersuchungen zur Betriebsfestigkeit von Stahlleichtfahrbahnen mit Trapezhohlsteifen in Eisenbahnbrueckenbau (Investigation on the strength of ligheweight railways with trapezoidal stiffeners in railway bridge construction)*. Der Stahlbau, Wilhelm Ernst und Sohn.
- Haufe, A., & Schweizerhof, K. (2013). Properties & Limits: Review of Shell Element Formulation. *LS DYNA Developer Forum 2013*. Filderstadt, Germany.
- Hedayat, A., Afzadi, E., & Iranpour, A. (2017). Prediction of the Bolt Fracture in Shear Using Finite Element Method. *Structures*, 12, 188-210. doi:<https://doi.org/10.1016/j.istruc.2017.09.005>
- Hirt, M., Bez, R., & Nussbaumer, A. (2006). *Construction Métallique - Notions fondamentales et méthodes de dimensionnement*. PPUR Lausanne.
- Huurman, M., Voskuilen, J., van Dijk, P., & Molenaar, J. (2008). *Het belang van hechtlagen in tweelaags asfalt constructies op orthotrope stalen brugdekken*. Delft - Ede: CROW Infradagen.
- Infra Inspectie B.V. (2021, 07 09). *TOFD (Time OF Flight Diffraction)*. Retrieved from Diensten: <http://infrainspectie.nl/tofd.php>
- Inter-Composite. (2021). *Gelcoat Resin: Araldite® SW 404 Resin with HY 2404 Hardener*. Retrieved 05 07, 2021, from <https://inter-composite.com/wp-content/uploads/2012/12/Araldite-SW-404-a-HY-2404.pdf>
- International Organization for Standardization. (2007). *NEN-EN-ISO 8501:2007: Preparation of steel substrates before application of paints and related products - Visual assessment of surface cleanliness*. Delft: Nederlands Normalisatie Instituut.
- Johnson, G., & Cook, W. (1983). A Constitutive Model and Data for Metals Subjected to Large Strains, Hight Strain Rates and High Temperatures. *Proceedings of the Seventh International Symposium on Ballistics*, (pp. 541-548). The Hague.
- Karajan, N., Schenke, M., Borrvall, T., & Pydimarry, K. (2018). Modeling bolts in LS-DYNA using explicit and implicit time integration. *15th German LS-DYNA forum*. Bamberg, Germany. Retrieved from <https://www.dynamore.de/de/download/papers/dynamore/de/download/papers/2018-ls-dyna-forum/papers-2018/mittwoch-17.-oktober-2018/simulation-bolts-and-delamination/modeling-bolts-in-ls-dyna-using-explicit-and-implicit-time-integration>
- Koper, A. (2017). *Assessment of Epoxy Resins for Injection Bolted Shear Connection*. Delft: TU Delft.

- Kortis, J. (2011). The Numerical Solution of the Bolted Connection with the Low-Quality Injected Bolts. *9th international conference on new trends in statics and dynamics of buildings*. Bratislava.
- Krolo, P., Grandić, D., & Bulić, M. (2016). The Guidelines for Modelling the Preloading Bolts in the Structural Connections Using Finite Element Methods. (M. Krawczuk, Ed.) *Journal of Computational Engineering*. doi:<https://doi.org/10.1155/2016/4724312>
- Kulak, G., Fisher, J., & Struik, J. (2001). *Guide to design criteria for bolted and riveted joints: Second edition*. Chicago : American Institute of Steel Construction Inc.
- Lebet, J., & Hirt, M. (2013). *Steel Bridges: Conceptual and Structural Design of Steel and Steel-Concrete Composite Bridges*. Lausanne, Switzerland: EFPL Press.
- Li, J., Liu, X., Scarpas, A., & Tzimiris, T. (2013). Finite Element Study of Multilayer Surfacing Systems on Orthotropic Steel Bridges. *2013 International Highway Technology Summit*, (pp. 1457-1469).
- Livermore Software Technology Corporation. (2018). *LS-DYNA R11 Keyword User's Manual: Volume 1*.
- Lu, Q., & Bors, J. (2015). Alternate uses of Epoxy Asphalt on Bridge Decks and Roadways. *Construction and Building Materials*, 78, 18-25. doi:<https://doi.org/10.1016/j.conbuildmat.2014.12.125>
- Marzahn, G., & Hamme, M. (2008). Strengthening of Orthotropic Bridge Decks by SPS technology. *Structural Congress 2008: Crossing borders*, (pp. 1-9). doi:[doi:10.1061/41016\(314\)25](https://doi.org/10.1061/41016(314)25)
- Matuschek, J., Stihl, T., & Bild, S. (2007). Verstärkung der orthotropen Stahlfahrbahn der Schönwasserparkbrücke mittels Stahl-Elastomer-Sandwich (SPS). *Stahlbau*, 76(7), 465-471. doi:<https://doi.org/10.1002/stab.200710050>
- MC Renovatie Bruggen. (2021). *Existing Suurhoff Bridge - Lifting bridge deck strengthening V2.0*. Arup.
- Medani, T. (2006). *Design Principles of Surfacing on Orthotropic Steel Bridge Decks*. Delft: Road and Railway Engineering Seciton, Faculty of Civil Engineering and Geosciences, TU Delft.
- Michigan Scientific Corporation. (2021, 12 16). *What is a Strain Gauge and How Does it Work?* Retrieved from <https://www.michsci.com/what-is-a-strain-gauge/>
- Miner, M. (1945). Cumulative damage in fatigue. *Journal of applied mechanics*, 12(3), 159-164. doi:<https://doi.org/10.1115/1.4009458>
- MISTRAS. (2021, 07 08). *Pulsed Eddy Current (PEC) & PEC Array (PECA) Inspection Services*. Retrieved from Field Inpsections: <https://www.mistrasgroup.com/how-we-help/field-inspections/advanced-ndt/pulsed-eddy-current-pec/>
- Može, P. (2018). Bearing strength at bolt holes in connections with large end distance and bolt pitch. *Journal of Constructional Steel Research*, 147, 132-144. doi:<https://doi.org/10.1016/j.jcsr.2018.04.006>
- Može, P., & Beg, D. (2011). Investigation of high strength steel connections with several bolts in double shear. *Journal of Constructional Steel Research*, 67(3), 333-347. doi:<https://doi.org/10.1016/j.jcsr.2010.10.007>
- Narkhede, S., Lokhande, N., & Gadekar, G. (2010). Bolted Joint Representation in LS-DYNA to Model Bolt Pre-stress and Bolt Failure Characteristics in Crash Simulation. *11th International LS-DYNA Users Conference*. Detroit.
- Nijgh, M. (2017). *New Materials for Injected Bolted Connection*. TU Delft (MSc Thesis).
- Nijgh, M. (2021). *A multi-scale approach towards reusable steel-concrete composite floor systems*. TU Delft (PhD Thesis). doi:<https://doi.org/10.4233/uuid:983b06e7-c30b-465c-a032-2439a7e9863f>
- Nijgh, M., Xin, H., & Veljkovic, M. (2019). Mechanical properties of (steel-reinforced) resins used in injection bolted connections. *Proceedings of the 22nd International Conference on Composite Materials*. Melbourne: Australia International Committee on Composite Materials.
- Nussbaumer, A., Borges, L., & Davaine, L. (2011). *Fatigue Design of Steel and Composite Structures*. Berlin: ECCS - European Convention for Constructional Steelwork.
- Palmgren, A. (1924). Die Lebensdauer von Kugellagern. *VDI-Zeitschrift*, 68, 339-341.
- Partov, D., Pasternak, H., Petkov, M., Nikolov, R., & Dimitrova, A. (2018). About the history of Orthotropic Bridge Decks. *Annual of the University of Architecture, Civil Engineering and Geodesy, Volume 51 (4)*, (pp. 295-311). Sofia, Bulgaria.
- Pavlovic, M., Markovic, Z., Veljkovic, M., & Budevaca, D. (2013). Bolted shear connectors vs. headed studs behaviour in push-out tests. *Journal of Constructional Steel Research*, 88, 134-149. doi:<https://doi.org/10.1016/j.jcsr.2013.05.003>
- Pedrosa, B., Correia, J., Rebelo, M., Veljkovic, M., & Gervásio, H. (2021). Fatigue experimental characterization of preloaded injection bolts in a metallic bridge strengthening scenario. *Engineering Structures*, Vol 234(112005). doi:<https://doi.org/10.1016/j.engstruct.2021.112005>
- Pelikan, W., & Eßlinger, M. (1957). *Die stahlfahrbahn - Berechnung und Konstruktion*. Germany: M.A.N.-Forschungsheft Nr. 7.

- Pouget, S., Sauzéat, C., Benedetto, D., & Olard, F. (2012). Modeling of viscous bituminous wearing course materials on orthotropic steel deck. *Material and Structures*, 45, 1115-1125. doi:<https://doi.org/10.1617/s11527-011-9820-z>
- Rijkswaterstaat. (2007). *Inventarisatie Kunstwerken (bruggen, tunnels en viaducten)*. Ministerie van Verkeer en Waterstaat.
- Rijkswaterstaat. (2021, 11 29). *A15: renovatie en nieuwbouw Suurhoffbrug*. Retrieved from <https://www.rijkswaterstaat.nl/wegen/projectenoverzicht/a15-renovatie-en-nieuwbouw-suurhoffbrug>
- Rijkswaterstaat. (2021, 4 20). *Projecten*. Retrieved from Rijkswaterstaat: <https://www.rijkswaterstaat.nl/wegen/projectenoverzicht/samen-werken-aan-een-bereikbaar-zuid-holland/projecten>
- Rijkswaterstaat. (2021). *Richtlijnen Ontwerp Kunstwerken: ROK 2.0 (concept version)*.
- Romeijn, A. (2006). *Steel Bridges Dictaat deel 1*. Delft: TU Delft, Faculty of Civil Engineering and Geosciences.
- Rugelj, T. (2008). *Uporaba injektiranih vijakov v jeklenih konstrukcijah (Use of injection bolts in steel structures)*. Univerza v Ljubljani.
- Schijve, J. (2003). Fatigue of Structures and Materials in the 20th Century and the State of the Art. *International Journal of Fatigue*, 679-702. doi:[https://doi.org/10.1016/S0142-1123\(03\)00051-3](https://doi.org/10.1016/S0142-1123(03)00051-3)
- Schijve, J. (2009). *Fatigue of Structures and Materials*, (Vols. Second Edition with CD-ROM). Dordrecht: Springer. doi:<https://doi-org.tudelft.idm.oclc.org/10.1007/978-1-4020-6808-9>
- Schumacher, A., & Blanc, A. (1999). *Stress measurements and fatigue analysis on the new bridge at Aarwangen, Report ICOM 386*. EPFL, Lausanne: ICOM-steel structures.
- Schütz, W. (1996). A history of fatigue. *Engineering fracture mechanics*, 54(2), 263-300. doi:[https://doi.org/10.1016/0013-7944\(95\)00178-6](https://doi.org/10.1016/0013-7944(95)00178-6)
- Sonnenschein, U. (2008). Modelling of bolts under dynamic loads. *7th LS-DYNA Anwerderform*. Bamberg, Germany.
- Stam, T. (2008). *UIT Behandelingsrapport laskrimp testen*.
- Stihl, T., Chassard, C., & Feldmann, M. B. (2013). Neue Technologie Für die Hängebrücke über die Saar in Mettlach - Brückenfahrbahn aus Sandwich Plate System (SPS). *Stahlbau*, 82(3), 179-187. doi:<https://doi-org.tudelft.idm.oclc.org/10.1002/stab.201310029>
- Stopel, M., Cichański, A., & Skibicki, D. (2017). Modeling of Prestressed bolt Connection in LS-DYNA Crash Test Analysis of Road Infrastructure. *23rd international conference of engineering mechanics*, (pp. 922-925). Svatka, Czech Republic.
- TNO. (2010). *Kennisdocument inspecties en reparaties van orthotrope rijdekken*. TNO Bouw en Ondergrond.
- TNO. (2017). *Startdocument voor NEN commissie 3510010204 Bestaande Staalbouw voor het opstellen van NEN 8703*. Delft: TNO.
- TNO. (2017). *TNO 2019 R10914 Deck plate crack detail category derived from fracture mechanics*.
- van der Laan, H. (2021). *Structural Optimization of Stiffened Plates: Application on an Orthotropic Steel Bridge Deck*. Delft: TU Delft.
- van Dooren, F. (2018, 06 05). Renovation of Steel bridges: Static and fatigue strenghtening Muiden bridge and Galecopperbridge. *CIE5125: Steel Bridges Lecture 4.1*. Delft: TU Delft, Rijkswaterstaat.
- van Dooren, F., Gratton, D., den Blanken, S., Nagtegaal, G., Ashurst, D., & Kunst, P. (2010). Orthotropic Deck Fatigue: Renovation of 8 Bridges in The Netherlands. *Structural Faults and Repair*. doi:10.13140/RG.2.1.1571.1200
- Vardanega, P. J., Webb, G. T., Ridles, P. R., & Middleton, C. R. (2015). Chapter 29: Bridge Monitoring. In A. Pipinato, *Innovative Bridge Design Handbook* (pp. 759-775). Elsevier. doi:<https://doi.org/10.1016/B978-0-12-800058-8.00029-3>
- Vincent, R., & Ferro, A. (2004). A New Orthotropic Bridge Deck: Design Fabrication and Construction of the Shenley Bridge Incorporating an SPS Orthotropic Bridge Deck. *2004 Orthotropic bridge Conference*. Sacramento, CA.
- Voermans, J., Souren, W., & Bosselaar, M. (2018). Strengthening the Orthotropic Steel Deck Structure of the Movable Bridge across the hartelkanaal, The Netherlands. *Structural Engineering International*, 23(3), 420-424. doi:<https://doi.org/10.2749/101686614X13844300210434>
- Wang, S., Ke, Z., Gao, Y., & Zhang, Y. (2019). Long-Term In Situ Performance Investigation of Orthotropic Steel Bridge Deck Strengthened by SPS and RPC solution. *Journal of Bridge Engineering*, 24(6), 04019054. doi:[https://doi.org/10.1061/\(ASCE\)BE.1943-5592.0001421](https://doi.org/10.1061/(ASCE)BE.1943-5592.0001421)
- Webb, G., & Middleton, C. (2014). *Structural Health Monitoring of Bridges*. Cambridge, UK: Univeristy of Cambridge.

- Webb, G., Vardanega, P., & Middleton, C. (2015). Capabilities, Categories of SHM Deployments: Technologies and Capabilities. *Journal of Bridge Engineering* , 20(11), Art. no. 04014118. doi:10.1061/(ASCE)BE.1943-5592.0000735
- Yuan, Y., Wu, C., & Jiang, X. (2019). Experimental study on the fatigue behaviour of the orthotropic steel deck rehabilitated by UHPC overlay. *Journal of Constructional Steel Research*, 157, 1-9. doi:https://doi.org/10.1016/j.jcsr.2019.02.010
- Zhang, D., Li, Y., & Cui, C. (2011). A retrofitted case study of orthotropic steel bridge decks strengthened with sandwich plate system. *Advanced materials research*, 255-260, 866-870. doi:https://doi.org/10.4028/www.scientific.net/AMR.255-260.866

Annex A: Reduced input file with analysis details

```

1  *KEYWORD
2  $>
3  $> Primer17.1 created on: Tue Mar 15 09:39:23 2022
4  $> LS-DYNA version: R12.0
5  $>
6  $> model title: M4 + M6
7  $>
8  $$ HM_OUTPUT_DECK created 10:20:44 02-03-2022 by HyperMesh Version 2020.1.1-HWDesktop
9  $$ Ls-dyna Input Deck Generated by HyperMesh Version : 2020.1.1-HWDesktop
10 $> Generated using HyperMesh-Ls-dyna 971_R11.1 Template Version :
    2020.1.1_hotfix-HWDesktop
11 $> end_saved_comments
12 $
13 $PR_MODEL_UNITS: METRES
14 $
15 $ =====
16 $ CONTROL cards
17 $ =====
18 $
19 *CONTROL_ACCURACY
20     0          0          0          1          0.0
21 *CONTROL_CONTACT
22     0.0        0.0        0          2          0          0          0          0
23     0          0          0          0          0.0        0          0          0
24     0.0        0.0        0.0        0.0        0.0        0.0        0.0        0.0
25     2          0          0          0          0          0          0.0
26 *CONTROL_DYNAMIC_RELAXATION
27     0          0.0        0.0        0.0        0.0        0.0        0          0.0
28 *CONTROL_ENERGY
29     2          0          0          0          0
30 *CONTROL_HOURLASS
31     6          0.1
32 *CONTROL_IMPLICIT_DYNAMICS_DYN
33     0          0.6        0.38        0.0        0.0        0.0        0          0.0
34 *CONTROL_IMPLICIT_EIGENVALUE
35     0          0.0        0          0.0        0          0.0        0          0.0
36     0          0          2          0          0          0          0.0
37 *CONTROL_IMPLICIT_GENERAL
38     1          1.0        0          0          0          0          0          0
39 *CONTROL_IMPLICIT_SOLUTION
40     12         6          12        0.0        0.0        0.0        0.9        0.0
41     1          1          1          3          2          1          0
42     0          0          0.0        1          2          0.0        0.0        0.0
43 *CONTROL_IMPLICIT_SOLVER
44     6          2          0          0          0          0.0        0          0.0
45 *CONTROL_MPP_IO_NODUMP
46 *CONTROL_RIGID
47     0          0          0          0          0          0          1          0
48 *CONTROL_SHELL
49     0.0        1          0          0          0          0          0          0
50     0.0        1          0          0          0
51 *CONTROL_SOLID
52     1          0          0          0          0          0.0        0          0
53 *CONTROL_TERMINATION
54     1.0        0          0.0        0.0        0.0        0
55 $
56 $
57 $ =====
58 $ DATABASE cards
59 $ =====
60 $
61 *DATABASE_BNDOUT
62     0.001      1          0          0
63 *DATABASE_DEFORC
64     0.001      1          0          0
65 *DATABASE_GLSTAT
66     0.01       1          0          0
67 *DATABASE_MATSUM
68     0.01       1          0          0
69 *DATABASE_NODOUT
70     0.01       1          0          0          0.0        0
71 *DATABASE_RBDOUT
72     0.001      1          0          0

```

```

73 *DATABASE_SECFORC
74   0.001      1      0      0
75 *DATABASE_RCFORC
76   0.001      1      0      0
77 *DATABASE_SPCFORC
78   0.001      1      0      0
79 *DATABASE_BINARY_D3PLOT
80   1.0        0      0      0      0
81 *DATABASE_EXTENT_BINARY
82     0        0      3      11      1      1      1      1
83     0        0      0      0      0      0      2      1
84     1        0      1.0    0      0      0
85     0        0      0      0      0
86 *DATABASE_CROSS_SECTION_PLANE_ID
87     1
88     20145 0.2084955-.50842702      0.022 0.2084955-.50842702      1.022      0.5
89     0.20849550.49157298      0.022      0.1      0.2      0      0
90 $
91 $: Cross-reference summary for SET_PART 20145
92 $:-----
93 $: DATABASE_CROSS_SECTION 1
94 $: INITIAL_STRESS_SECTION 1
95 $: INITIAL_STRESS_SECTION 2
96 $
97 *SET_PART LIST
98     20145      0.0      0.0      0.0      0.0
99     1013
100 $
101 $
102 $
103 $ =====
104 $ MAT (Material) cards
105 $ =====
106 $
107 *MAT_ELASTIC_TITLE
108 $HMNAME MATS      1Steel
109 Steel
110     1      7850.0      2.1E11      0.3      0.0      0.0      0.0
111 $
112 *MAT_ELASTIC_TITLE
113 $HMNAME MATS      3Epoxy
114 Epoxy
115     3      1200.0      4.3E9      0.34      0.0      0.0      0.0
116 $
117 *MAT_SPRING_ELASTIC
118     5      1.449E9
119 $
120 *MAT_SPRING_ELASTIC
121     6      1.449E9
122 $
123 *MAT_ELASTIC_TITLE
124 Material created by Primer for implicit analysis
125     7      7850.0      2.1E11      0.3      0.0      0.0      0.0
126 $
127 *MAT_ELASTIC_TITLE
128 Material created by Primer for implicit analysis
129     9      1200.0      3.639E9      0.364      0.0      0.0      0.0
130 $
131 *MAT_SPRING_ELASTIC_TITLE
132 Material created by Primer for implicit analysis
133     11      1.0E11
134 $
135 *MAT_SPRING_ELASTIC_TITLE
136 Material created by Primer for implicit analysis
137     12      1.0E11
138 $
139 *MAT_ELASTIC_TITLE
140 Material created by Primer for implicit analysis
141     13      7850.0      2.1E11      0.3      0.0      0.0      0.0
142 $
143 *MAT_SPOTWELD_TITLE
144 bolt spotweld
145     14      8750.0      2.1E9      0.3      1.0E9      0.0      0.0      0.0

```

146	0.0	0.0	0.0	0.0	0.0	0.0	0.0	0.0
147	\$							
148	*MAT_ELASTIC_TITLE							
149	Material created by Primer for implicit analysis							
150	15	7850.0	2.1E11	0.3	0.0	0.0	0.0	
151	\$							
152	\$							
153	\$							
154	\$ =====							
155	\$ SECTION cards							
156	\$ =====							
157	\$							
158	*SECTION DISCRETE							
159	1004	0	0.0	0.0	0.0	0.0		
160	0.0	0.0						
161	\$							
162	*SECTION_SHELL_TITLE							
163	\$HMNAME PROPS	2	transverse beam bottom flange cantilever					
164	transverse beam bottom flange cantilever							
165	2	2	1.0	3	0.0	0.0	0	0
166	0.016	0.016	0.016	0.016	0.0	0.0	0.0	0
167	\$							
168	\$HMNAME PROPS	3	trough support plate					
169	trough support plate							
170	3	2	1.0	3	0.0	0.0	0	0
171	0.01	0.01	0.01	0.01	0.0	0.0	0.0	0
172	\$							
173	\$HMNAME PROPS	5	deck plate					
174	deck plate							
175	5	2	1.0	3	0.0	0.0	0	0
176	0.014	0.014	0.014	0.014	0.0	0.0	0.0	0
177	\$							
178	\$HMNAME PROPS	6	main girder web					
179	main girder web							
180	6	2	1.0	3	0.0	0.0	0	0
181	0.014	0.014	0.014	0.014	0.0	0.0	0.0	0
182	\$							
183	\$HMNAME PROPS	7	transverse beam web					
184	transverse beam web							
185	7	2	1.0	3	0.0	0.0	0	0
186	0.01	0.01	0.01	0.01	0.0	0.0	0.0	0
187	\$							
188	\$HMNAME PROPS	8	main girder bottom flange					
189	main girder bottom flange							
190	8	2	1.0	3	0.0	0.0	0	0
191	0.014	0.014	0.014	0.014	0.0	0.0	0.0	0
192	\$							
193	\$HMNAME PROPS	10	transverse beam top flange					
194	transverse beam top flange							
195	10	2	1.0	3	0.0	0.0	0	0
196	0.016	0.016	0.016	0.016	0.0	0.0	0.0	0
197	\$							
198	\$HMNAME PROPS	11	main girder outstands					
199	main girder outstands							
200	11	2	1.0	3	0.0	0.0	0	0
201	0.012	0.012	0.012	0.012	0.0	0.0	0.0	0
202	\$							
203	\$HMNAME PROPS	14	side plates					
204	side plates							
205	14	2	1.0	3	0.0	0.0	0	0
206	0.01	0.01	0.01	0.01	0.0	0.0	0.0	0
207	\$							
208	\$HMNAME PROPS	15	troughs					
209	troughs							
210	15	2	1.0	3	0.0	0.0	0	0
211	0.005	0.005	0.005	0.005	0.0	0.0	0.0	0
212	\$							
213	\$HMNAME PROPS	17	load shells					
214	load shells							
215	17	2	1.0	3	0.0	0.0	0	0
216	1.0E-6	1.0E-6	1.0E-6	1.0E-6	0.0	0.0	0.0	0
217	\$							
218	\$HMNAME PROPS	22	transverse beam end attachment					


```

292         1002         -1         0
293 $
294 $HMNAME PROPS      1003filler plates NEAR BOLTS
295 filler plates NEAR BOLTS
296         1003         -1         0
297 $
298 Beam spotweld
299         1006         -1         0
300 $
301 $HMNAME PROPS      1007Str plate around bolt detailed
302 Str plate around bolt detailed
303         1007         -1         0
304 $
305 $HMNAME PROPS      1009filler plate detailed around bolt
306 filler plate detailed around bolt
307         1009         -1         0
308 $
309 $HMNAME PROPS      1013bolt elements
310 bolt elements
311         1013         -1         0
312 $
313 Solid deck plate
314         1014         -1         0
315 $
316 $HMNAME PROPS      1015bolt elements_1
317 bolt elements
318         1015          2         0
319 $
320 $
321 $
322 $ =====
323 $ PART cards
324 $ =====
325 $
326 *PART
327 $HMNAME COMPS      2transverse beam bottom flange cantilever
328 transverse beam bottom flange cantilever
329          2          2          7          0          0          0          0          0
330 $
331 *PART
332 $HMNAME COMPS      3trough support plate coarse
333 trough support plate welds
334          3          3          7          0          0          0          0          0
335 $
336 *PART
337 $HMNAME COMPS      5deck plate coarse
338 deck welds
339          5          5          7          0          0          0          0          0
340 $
341 *PART
342 $HMNAME COMPS      6main girder web coarse
343 main girder web coarse
344          6          6          7          0          0          0          0          0
345 $
346 *PART
347 $HMNAME COMPS      7transverse beam web
348 transverse beam web
349          7          7          7          0          0          0          0          0
350 $
351 *PART
352 $HMNAME COMPS      8main girder bottom flange
353 main girder bottom flange
354          8          8          7          0          0          0          0          0
355 $
356 *PART
357 $HMNAME COMPS      10transverse beam top flange coarse
358 bottom plate
359          10         10          7          0          0          0          0          0
360 $
361 *PART
362 $HMNAME COMPS      11main girder outstands
363 main girder outstands
364          11         11          7          0          0          0          0          0

```

365	\$								
366	*PART								
367	\$HMNAME COMPS	14	side plates						
368	side plates								
369	14	14	7	0	0	0	0	0	0
370	\$								
371	*PART								
372	\$HMNAME COMPS	15	troughs coarse						
373	trough welds								
374	15	15	7	0	0	0	0	0	0
375	\$								
376	*PART								
377	\$HMNAME COMPS	17	load shells						
378	load shells								
379	17	17	7	0	0	0	0	0	0
380	\$								
381	*PART								
382	\$HMNAME COMPS	22	transverse beam end attachment						
383	transverse beam end attachment								
384	22	22	7	0	0	0	0	0	0
385	\$								
386	*PART								
387	\$HMNAME COMPS	23	cantilever deck handrail stiffener						
388	cantilever deck handrail stiffener								
389	23	23	7	0	0	0	0	0	0
390	\$								
391	*PART								
392	\$HMNAME COMPS	30	end plate						
393	end plate								
394	30	30	7	0	0	0	0	0	0
395	\$								
396	*PART								
397	\$HMNAME COMPS	31	end plate bottom flange						
398	end plate stiffener								
399	31	31	7	0	0	0	0	0	0
400	\$								
401	*PART								
402	\$HMNAME COMPS	32	epoxy						
403	epoxy								
404	32	32	9	0	0	0	0	0	0
405	\$								
406	*PART								
407	\$HMNAME COMPS	33	strengthening plate						
408	strengthening plate tapered								
409	33	33	7	0	0	0	0	0	0
410	\$								
411	*PART								
412	\$HMNAME COMPS	34	deck plate cycle lane						
413	deck plate cycle lane								
414	34	34	7	0	0	0	0	0	0
415	\$								
416	*PART								
417	\$HMNAME COMPS	35	strengthening plate shells						
418	strengthening plate shells								
419	35	35	7	0	0	0	0	0	0
420	\$								
421	*PART								
422	\$HMNAME COMPS	36	filler plates						
423	filler plates								
424	36	36	7	0	0	0	0	0	0
425	\$								
426	*PART								
427	\$HMNAME COMPS	37	Shear Springs X						
428	Shear Springs X								
429	37	1004	11	0	0	0	0	0	0
430	\$								
431	*PART								
432	\$HMNAME COMPS	38	Shear Springs Y						
433	Shear Springs Y								
434	38	1004	12	0	0	0	0	0	0
435	\$								
436	*PART								
437	\$HMNAME COMPS	39	Backing strip						


```

511 *PART
512 $HNAME COMPS 1020Detailed deck plate coating shells
513 Detailed deck plate coating shells
514 1020 35 7 0 0 0 0 0
515 $
516 $
517 $
518 $ =====
519 $ NODE cards removed
520 $ =====
521 $
522 $ =====
523 $ ELEMENT cards removed
524 $ =====
525 $
526 $ =====
527 $ DEFINE cards
528 $ =====
529 $
530 $
531 *DEFINE_BOX
532 1-.590034010.42142749 -5.9008 6.7500138 -0.1 0.1
533 $
534 *DEFINE_COORDINATE_SYSTEM
535 1 0.0 0.0 0.0 1.0 0.0 0.0 0
536 1.0 1.0 0.0
537 2 0.0 0.0 0.0 0.0 1.0 0.0 0
538 1.0 1.0 0.0
539 $
540 $
541 *DEFINE_CURVE
542 $:
543 $: Cross-reference summary for Load-curve 1
544 $: -----
545 $:
546 $: Child Case 193 : Segment pressure vs time
547 $: X axis : Time (Units: Time)
548 $: Y axis : Segment pressure (Units: Pressure)
549 $:
550 $: Child Case 192 : Segment pressure vs time
551 $: X axis : Time (Units: Time)
552 $: Y axis : Segment pressure (Units: Pressure)
553 $:
554 $: Load segment definition <No label>: Segment pressure vs time
555 $: X axis : Time (Units: Time)
556 $: Y axis : Segment pressure (Units: Pressure)
557 $: :
558 $: (To a total of 808 unlabelled Load segment definition entries)
559 $:
560 $: Usage: Transient analysis
561 $:
562 1 0 0.0 0.0 0.0 0.0 0 0
563 0.0 0.0
564 1.0 1.0
565 $
566 $
567 *DEFINE_CURVE
568 $:
569 $: Cross-reference summary for Load-curve 2
570 $: -----
571 $:
572 $: Initial stress section 1 : Stress vs time
573 $: X axis : Time (Units: Time)
574 $: Y axis : Preload stress (Units: Stress)
575 $:
576 $: Usage: Stress initialization
577 $:
578 2 1 0.0 1.0E9 0.0 0.0 0 0
579 0.0 0.0
580 1.0 0.5
581 2.0 1.0
582 $
583 $

```

```

584 *DEFINE_CURVE
585 $:
586 $: Cross-reference summary for Load-curve 3
587 $: -----
588 $:
589 $: Initial stress section 2 : Stress vs time
590 $: X axis : Time (Units: Time)
591 $: Y axis : Preload stress (Units: Stress)
592 $:
593 $: Usage: Transient analysis
594 $:
595 3 0 0.0 1.0E9 0.0 0.0 0 0
596 0.0 1.0
597 1.0 1.0
598 $
599 *DEFINE_SD_ORIENTATION
600 1 0 1.0 0.0 0.0
601 2 0 0.0 1.0 0.0
602 $
603 $
604 $ =====
605 $ DAMPING cards
606 $ =====
607 $
608 *DAMPING_PART_STIFFNESS
609 2 0.05
610 3 0.05
611 5 0.05
612 6 0.05
613 7 0.05
614 8 0.05
615 10 0.05
616 11 0.05
617 14 0.05
618 15 0.05
619 17 0.05
620 22 0.05
621 23 0.05
622 30 0.05
623 31 0.05
624 32 0.05
625 33 0.05
626 34 0.05
627 35 0.05
628 36 0.05
629 37 0.05
630 38 0.05
631 39 0.05
632 1000 0.05
633 1001 0.05
634 1002 0.05
635 1003 0.05
636 1006 0.05
637 1007 0.05
638 1009 0.05
639 1010 0.05
640 1012 0.05
641 1013 0.05
642 1014 0.05
643 1015 0.05
644 1017 0.05
645 1019 0.05
646 1020 0.05
647 $
648 $
649 $ =====
650 $ CONSTRAINED cards
651 $ =====
652 $
653 *CONSTRAINED_NODAL_RIGID_BODY_SPC
654 194118 0 116116 0 1 0 0
655 1.0 6 0
656 $

```

```

657 $: Cross-reference summary for SET_NODE 116116
658 $:-----
659 $: NODAL_RIGID_BODY 194118
660 $
661 *SET_NODE_LIST
662   116116      0.0      0.0      0.0      0.0
663   1899821   1899645   1899649   1899651   1899657   1899658   1899659   1899660
664   1899661   1899666   1899772   1899774   1899776   1899777   1899779   1899781
665   1899782   1899783   1899784   1899786   1899787   1899788   1899789   1899790
666   1899792   1899793   1899795   1899796   1899800   1899801   1899803   1899805
667   1899806   1899807   1899808   1899809   1899810   1899811   1899813   1899814
668   1899816   1899818   1899820   1899824   1899828   1899830   1899832   1899833
669   1899838   1899846   1899876   1899878   1899879   1899883   1899885   1899888
670   1899893   1899894   1899895   1899896   1899897   1899899   1899901   1899902
671   1899904   1920108   1920114   1920121   1920125   1920179   1920190   1920191
672 $
673 *CONSTRAINED_NODAL_RIGID_BODY_SPC
674   194119      0      116187      0      1      0      0
675     1.0      6      0
676 $
677 $: Cross-reference summary for SET_NODE 116187
678 $:-----
679 $: NODAL_RIGID_BODY 194119
680 $
681 *SET_NODE_LIST
682   116187      0.0      0.0      0.0      0.0
683   1899290   1899099   1899103   1899106   1899112   1899113   1899114   1899117
684   1899118   1899130   1899236   1899239   1899242   1899243   1899245   1899247
685   1899248   1899249   1899250   1899252   1899253   1899254   1899255   1899256
686   1899258   1899259   1899261   1899262   1899266   1899267   1899269   1899271
687   1899272   1899273   1899274   1899275   1899276   1899277   1899279   1899280
688   1899282   1899285   1899289   1899296   1899300   1899302   1899304   1899305
689   1899310   1899326   1899372   1899374   1899375   1899379   1899381   1899384
690   1899389   1899390   1899391   1899392   1899393   1899395   1899397   1899398
691   1899400   1919814   1919820   1919827   1919831   1919885   1919899   1919900
692 $
693 *CONSTRAINED_NODAL_RIGID_BODY_SPC
694   194120      0      116258      0      1      0      0
695     1.0      7      0
696 $
697 $: Cross-reference summary for SET_NODE 116258
698 $:-----
699 $: NODAL_RIGID_BODY 194120
700 $
701 *SET_NODE_LIST
702   116258      0.0      0.0      0.0      0.0
703   1895008   1894668   1894709   1894712   1894718   1894719   1894720   1894723
704   1894724   1894736   1894954   1894957   1894960   1894961   1894963   1894965
705   1894966   1894967   1894968   1894970   1894971   1894972   1894973   1894974
706   1894976   1894977   1894979   1894980   1894984   1894985   1894987   1894989
707   1894990   1894991   1894992   1894993   1894994   1894995   1894997   1894998
708   1895000   1895003   1895007   1895014   1895018   1895020   1895022   1895023
709   1895028   1895044   1895092   1895174   1895175   1895179   1895181   1895184
710   1895189   1895190   1895191   1895192   1895193   1895195   1895197   1895198
711   1895200   1917317   1917323   1917330   1917334   1917451   1917464   1917465
712 $
713 *CONSTRAINED_NODAL_RIGID_BODY_SPC
714   194121      0      116329      0      1      0      0
715     1.0      7      0
716 $
717 $: Cross-reference summary for SET_NODE 116329
718 $:-----
719 $: NODAL_RIGID_BODY 194121
720 $
721 *SET_NODE_LIST
722   116329      0.0      0.0      0.0      0.0
723   1898348   1898172   1898176   1898178   1898184   1898185   1898186   1898187
724   1898188   1898193   1898299   1898301   1898303   1898304   1898306   1898308
725   1898309   1898310   1898311   1898313   1898314   1898315   1898316   1898317
726   1898319   1898320   1898322   1898323   1898327   1898328   1898330   1898332
727   1898333   1898334   1898335   1898336   1898337   1898338   1898340   1898341
728   1898343   1898345   1898347   1898351   1898355   1898357   1898359   1898360
729   1898365   1898373   1898403   1898405   1898406   1898410   1898412   1898415

```

```

730      1898420  1898421  1898422  1898423  1898424  1898426  1898428  1898429
731      1898431  1919306  1919312  1919319  1919323  1919377  1919388  1919389
732  $
733  *CONSTRAINED_NODAL_RIGID_BODY_SPC
734      194122      0  116400      0      1      0      0
735      1.0      3      0
736  $
737  $: Cross-reference summary for SET_NODE 116400
738  $:-----
739  $: NODAL_RIGID_BODY 194122
740  $
741  *SET_NODE_LIST
742      116400      0.0      0.0      0.0      0.0
743      2413952  1256493  1256679  1261740  1261747  1261758  1261762  2413953
744      2413954  2413998
745  $
746  *CONSTRAINED_NODAL_RIGID_BODY_SPC
747      194123      0  116409      0      1      0      0
748      1.0      3      0
749  $
750  $: Cross-reference summary for SET_NODE 116409
751  $:-----
752  $: NODAL_RIGID_BODY 194123
753  $
754  *SET_NODE_LIST
755      116409      0.0      0.0      0.0      0.0
756      2414038  1251577  1255745  1262277  1262283  1262291  1262298  2414039
757      2414040  2414061
758  $
759  *CONSTRAINED_NODAL_RIGID_BODY_SPC
760      194124      0  116418      0      1      0      0
761      1.0      3      0
762  $
763  $: Cross-reference summary for SET_NODE 116418
764  $:-----
765  $: NODAL_RIGID_BODY 194124
766  $
767  *SET_NODE_LIST
768      116418      0.0      0.0      0.0      0.0
769      2165618  2168094  2231507  2231529  2231541  2231544  2231591  2231593
770      2231600  2231601
771  $
772  *CONSTRAINED_NODAL_RIGID_BODY_SPC
773      194125      0  116428      0      1      0      0
774      1.0      3      0
775  $
776  $: Cross-reference summary for SET_NODE 116428
777  $:-----
778  $: NODAL_RIGID_BODY 194125
779  $
780  *SET_NODE_LIST
781      116428      0.0      0.0      0.0      0.0
782      2168676  2168839  2231552  2231572  2231581  2231584  2231606  2231613
783      2231616  2231617
784  $
785  *CONSTRAINED_SHELL_IN_SOLID_ID
786      1
787      5      1017      1      1
788      0.0      0.0
789  $
790  $
791  $ =====
792  $ INITIAL cards
793  $ =====
794  $
795  *INITIAL_STRESS_SECTION
796      1      1      2      20145      0      2      0
797      2      1      3      20145      0      2      0
798  $
799  $
800  $ =====
801  $ LOAD cards removed
802  $ =====

```

```

803 $
804 $ =====
805 $ CONTACT cards
806 $ =====
807 $
808 *CONTACT_TIED_SHELL_EDGE_TO_SURFACE_ID_CONSTRAINED_OFFSET
809   1Deck_to_epoxy
810     20141     20143         2         2         0         0         0         0
811     0.0     0.0         0.0     0.0         0.2         0         0.0     0.0
812     0.0     0.0         0.0     0.0         0.0         0.0     0.0     0.0
813 $
814 $
815 $: Cross-reference summary for SET_PART 20141
816 $:-----
817 $: CONTACT 1
818 $: CONTACT 2
819 $: CONTACT 4
820 $
821 *SET_PART_LIST_TITLE
822 Deck_plate
823     20141         0.0         0.0         0.0         0.0
824         5         1000
825 $
826 $
827 $: Cross-reference summary for SET_PART 20143
828 $:-----
829 $: CONTACT 1
830 $
831 *SET_PART_LIST
832     20143         0.0         0.0         0.0         0.0
833         32
834 $
835 *CONTACT_TIED_SHELL_EDGE_TO_SURFACE_ID_CONSTRAINED_OFFSET
836   2Deckplate_to_backing_strip
837     20141     39         2         3         1         0         0         0
838     0.5     0.5         0.0     0.0         0.2         0         0.0     0.0
839     0.0     0.0         0.0     0.0         0.0         0.0     0.0     0.0
840 $
841 *CONTACT_AUTOMATIC_SURFACE_TO_SURFACE_MORTAR_ID
842   4Deckplate_to_filler_plates
843     20141     20142         2         2         0         0         0         0
844     0.5     0.5         0.0     0.0         0.2         0         0.0     0.0
845     2.5     2.5         0.0     0.0         0.0         0.0     0.0     0.0
846     0         0.0         0         0.0         0.0         0         0         0
847     0.0     1         2         0         0         0         0.0     0.0
848     10     2         0.0     0.0
849     0.0         0
850 $
851 $: Cross-reference summary for SET_PART 20142
852 $:-----
853 $: CONTACT 4
854 $
855 *SET_PART_LIST_TITLE
856 Filler plates
857     20142         0.0         0.0         0.0         0.0
858     36         1003         1009
859 $
860 *CONTACT_AUTOMATIC_SURFACE_TO_SURFACE_MORTAR_ID
861   5Backing strip to strengthening plate
862     39     20144         3         2         0         1         0         0
863     0.5     0.5         0.0     0.0         0.2         0         0.0     0.0
864     2.5     2.5         0.0     0.0         0.0         0.0     0.0     0.0
865     0         0.0         0         0.0         0.0         0         0         0
866     0.0     1         2         0         0         0         0.0     0.0
867     5         2         0.0     0.0         0.0         0
868 $
869 $
870 $: Cross-reference summary for SET_PART 20144
871 $:-----
872 $: CONTACT 5
873 $
874 *SET_PART_LIST
875     20144         0.0         0.0         0.0         0.0

```

876	33	1002	1007						
877	\$								
878	*CONTACT_TIED_SURFACE_TO_SURFACE_ID_OFFSET								
879	6Bolt to washer								
880	1014	1013	3	3	0	0	1	1	
881	0.5	0.5	0.0	0.0	0.2	0	0.0	0.0	
882	2.5	2.5	0.0	0.0	0.0	0.0	0.0	0.0	
883	\$								
884	*CONTACT_TIED_SURFACE_TO_SURFACE_ID_OFFSET								
885	7Washer to str plate								
886	1014	1007	3	3	0	0	1	1	
887	0.5	0.5	0.0	0.0	0.2	0	0.0	0.0	
888	2.5	2.5	0.0	0.0	0.0	0.0	0.0	0.0	
889	\$								
890	*CONTACT_TIED_SURFACE_TO_SURFACE_ID_OFFSET								
891	8Washer to packer plate								
892	1014	1019	3	3	0	0	1	1	
893	0.5	0.5	0.0	0.0	0.2	0	0.0	0.0	
894	2.5	2.5	0.0	0.0	0.0	0.0	0.0	0.0	
895	\$								
896	*CONTACT_TIED_SURFACE_TO_SURFACE_ID_OFFSET								
897	9Bottom nut to shank								
898	1015	1013	3	3	0	0	1	1	
899	0.0	0.0	0.0	0.0	0.2	0	0.0	0.0	
900	0.0	0.0	0.0	0.0	0.0	0.0	0.0	0.0	
901	\$								
902	*CONTACT_TIED_SURFACE_TO_SURFACE_ID_OFFSET								
903	10Bottom nut to washer								
904	1015	1014	3	3	0	0	1	1	
905	0.5	0.5	0.0	0.0	0.2	0	0.0	0.0	
906	2.5	2.5	0.0	0.0	0.0	0.0	0.0	0.0	
907	\$								
908	*CONTACT_AUTOMATIC_SURFACE_TO_SURFACE_MORTAR_ID								
909	11solid deck plate to filler plate								
910	1017	1009	3	3	0	0	1	1	
911	0.5	0.5	0.0	0.0	0.2	0	0.0	0.0	
912	2.5	2.5	0.0	0.0	0.0	0.0	0.0	0.0	
913	0	0.0	0	0.0	0.0	0	0	0	
914	0.0	1	2	0	0	0	0.0	0.0	
915	10	2	0.0	0.0			0.0	0	
916	\$								
917	*CONTACT_TIED_SURFACE_TO_SURFACE_ID_OFFSET								
918	12Solid deck plate to epoxy								
919	1017	32	3	3	0	0	1	1	
920	0.0	0.0	0.0	0.0	0.2	0	0.0	0.0	
921	0.0	0.0	0.0	0.0	0.0	0.0	0.0	0.0	
922	\$								
923	\$								
924	\$								
925	\$ =====								
926	\$ SET cards								
927	\$ =====								
928	\$								
929	\$								
930	\$: <No cross-references to SET_PART 20140 found>								
931	\$								
932	*SET_PART_LIST_TITLE								
933	Strengthening plate + Filler plates								
934	20140	0.0	0.0	0.0	0.0				
935	33	1002	36	1003					
936	\$								
937	\$								
938	\$: <No cross-references to SET_SHELL 1 found>								
939	\$								
940	*SET_SHELL_LIST								
941	1	0.0	0.0	0.0	0.0				
942	5378505	5378506	5378507	5378508	5380427	5380435	5380437	5380438	
943	5380439	5380440	5380457	5380458	5380459	5380460	5380477	5380484	
944	5380485	5380486	5380487	5380488	5380493	5380494	5380495	5380496	
945	5380497	5380498	5381401	5381402	5381403	5381404	5383007	5383008	
946	5383009	5383010	5383521	5383529	5383531	5383532	5383533	5383534	
947	5383551	5383552	5383553	5383554	5383571	5383578	5383579	5383580	
948	5383581	5383582	5383587	5383588	5383589	5383590	5383591	5383592	

949	5384648	5384649	5384650	5384651	5385604	5385608	5385616	5385624
950	5385626	5385839	5386167	5386535	5386651	5386790	5386963	5387203
951	5387381	5387608	5389404	5389660	5389865	5389869	5389873	5390002
952	5390010	5395221	5395285	5398021	5398229	5398537	5398547	5398558
953	5398690	5398772	5398869	5399012	5399022	5399114	5399180	5399255
954	5403293	5403473	5403474	5403479	5403480	5403484	5403485	5403488
955	5403489	5403721	5403722	5403727	5403728	5403732	5403733	5403736
956	5403737	5403796	5406826	5406895	5406921	5407481	5407643	5407736
957	5407737	5407808	5408959	5408961	5408963	5408971	5409191	5409192
958	5409193	5409194	5409199	5409200	5409201	5409202	5409266	5409463
959	5409600	5409849	5409850	5409851	5409852	5409861	5409862	5409863
960	5409864	5410333	5410343	5410345	5411185	5412290	5412889	5412893
961	5413039	5413040	5413908	5433819	5433826	5433827	5433838	5433842
962	5433844	5433886	5433887	5433894	5433895	5433907	5433914	5433926
963	5433930	5433931	5433938	5433943	5433950	5433954	5433955	5433961
964	5433972	5433974	5433982	5433983	5433991	5434108	5434109	5434112

965 \$
966 \$
967 \$: <No cross-references to SET_SHELL 2 found>
968 \$

969 *SET_SHELL_LIST
970 2 0.0 0.0 0.0 0.0
971 5386297 5386387 5387113 5387205 5387216 5387303 5387305 5387415
972 5387451 5387607 5389393 5391107 5391110 5391194 5391202 5391220
973 5391294 5391295 5391431 5391436 5391440 5391588 5391589 5391736
974 5392062 5392670 5393353 5393354 5393366 5393373 5393374 5393384
975 5393385 5393386 5393387 5393416 5393418 5393455 5393589 5393591
976 5393827 5393831 5395664 5395665 5395666 5395667 5395692 5395693
977 5395694 5395695 5396279 5396282 5396294 5396295 5396298 5396310
978 5396311 5396312 5396313 5396319 5396324 5396325 5396326 5396329
979 5396331 5396332 5396333 5396334 5396346 5396347 5396348 5396349
980 5396352 5396353 5396354 5396356 5396357 5396358 5396911 5396912
981 5396913 5396914 5396927 5396928 5396929 5396930 5397292 5397295
982 5397307 5397308 5397311 5397323 5397324 5397325 5397326 5397332
983 5397337 5397338 5397339 5397342 5397344 5397345 5397346 5397347
984 5397359 5397360 5397361 5397362 5397365 5397366 5397367 5397369
985 5397370 5397371 5399096 5399118 5399184 5399207 5399245 5399503
986 5399509 5433928 5433929 5433932 5434031 5434035 5434040 5434041
987 5434042 5434043 5434045 5434047 5434050 5434053 5434054 5434056
988 5434058 5434059 5434065 5434066 5434067 5434068 5434069 5434070

989 \$
990 \$
991 \$: <No cross-references to SET_SHELL 3 found>
992 \$

993 *SET_SHELL_LIST
994 3 0.0 0.0 0.0 0.0
995 5393659 5393660 5393667 5393672 5393673 5393674 5393675 5393676
996 5393677 5393682 5393723 5393725 5393732 5393733 5393734 5393735
997 5393736 5393737 5393738 5393739 5393742 5393743 5393744 5393785
998 5393786 5393787 5393792 5393807 5393810 5393811 5393816 5393821
999 5393822 5393823 5393824 5393825 5393848 5393849 5393851 5393854
1000 5393856 5393858 5393948 5393949 5393954 5393955 5393958 5393979
1001 5393980 5393981 5393990 5393991 5393992 5393993 5393997 5394085
1002 5394086 5394088 5394089 5394090 5394091 5394092 5394171 5394172
1003 5394173 5394174 5394181 5394182 5394183 5394184 5394195 5394196
1004 5394303 5394304 5394305 5394306 5394311 5394312 5394313 5394314
1005 5394317 5394319 5394321 5394323 5394324 5394326 5394331 5394333
1006 5394340 5394342 5394343 5394345 5394347 5394348 5394350 5394351
1007 5394352 5394353 5394354 5394355 5394356 5394357 5394358 5394359
1008 5394361 5394365 5394366 5394382 5394399 5394401 5394409 5394411
1009 5394438 5394446 5394451 5394457 5394459 5394461 5394463 5394465
1010 5394516 5394518 5394532 5394533 5394535 5394537 5394539 5394540
1011 5394541 5394542 5394543 5394556 5394558 5394560 5394561 5394565
1012 5394566 5394670 5394719 5394736 5394737 5394748 5394750 5394752
1013 5394754 5394780 5394800 5394824 5394827 5394938 5394940 5394950
1014 5394951 5394959 5394960 5394963 5394964 5394965 5394966 5394967
1015 5394968 5394970 5394971 5394972 5394979 5394980 5394981 5394982
1016 5394989 5394990 5394991 5394993 5394995 5394996 5394999 5395001
1017 5395338 5395340 5395342 5395344 5395346 5395397 5395398 5395399
1018 5395400 5395401 5395402 5395403 5395404 5395477 5395478 5395594
1019 5395595 5395596 5395597 5395598 5395599 5395600 5395601 5395618
1020 5395619 5395620 5395621 5395622 5395623 5395624 5395625 5395626
1021 5395627 5395628 5395629 5395939 5395940 5395941 5395954 5395955

1022	5395956	5395957	5395958	5395959	5395960	5395961	5395962	5395963	
1023	5395964	5395965	5395967	5395968	5395969	5395970	5395971	5395972	
1024	5395973	5395974	5395975	5395976	5395977	5395978	5395979	5395980	
1025	5395981	5395982	5395983	5395984	5396005	5396006	5396007	5396008	
1026	5396009	5396010	5396011	5396012	5396015	5396016	5396017	5396018	
1027	5396019	5396020	5396021	5396022	5406595	5406612	5406613	5406614	
1028	5406615	5406639	5406640	5406645	5406646	5406662	5406665	5406686	
1029	5406753	5406757	5406758	5406759	5406760	5406778	5406791	5406793	
1030	5406819	5406820	5406822	5406831	5406832	5406833	5406881	5406882	
1031	5406892	5406893	5406896	5407085	5407086	5407087	5407088	5407089	
1032	5407090	5407091	5407092	5407093	5412068	5412082	5412083	5412084	
1033	5412085	5412088	5412089	5412090	5412091	5412092	5412093	5412094	
1034	5412114	5412115	5412116	5412117	5412160	5412161	5412162	5412163	
1035	5412172	5412173	5412174	5412175	5412176	5412177	5412178	5412179	
1036	5412180	5412181	5412182	5412183	5412207	5412208	5412209	5412210	
1037	5412212	5412214	5412216	5412218	5412238	5412326	5412327	5412328	
1038	5412329	5412334	5412335	5412336	5412337	5412348	5412349	5412350	
1039	5412495	5412496	5412497	5412498	5412499	5412500	5412501	5412502	
1040	5412507	5412508	5412509	5412510	5412515	5412516	5412517	5412518	
1041	5412519	5412520	5412521	5412522	5412523	5412524	5412525	5412526	
1042	5412527	5412528	5412529	5412530	5394731	5394732	5394784	5394942	
1043	5394946	5394949	5406877	5406885	5412321	5412322	5394899	5394975	
1044	5394978	5412331	5412332						
1045	\$								
1046	\$								
1047	\$:	<No cross-references to SET_SHELL 4 found>							
1048	\$								
1049	*SET_SHELL_LIST								
1050	4	0.0	0.0	0.0	0.0				
1051	5378110	5378112	5378114	5378174	5378182	5378184	5378188	5378190	
1052	5378192	5378194	5378613	5378627	5378629	5378631	5378652	5378653	
1053	5378793	5378794	5378832	5378833	5378834	5378835	5378916	5378918	
1054	5378926	5378928	5378930	5378932	5378942	5378943	5378953	5378954	
1055	5378970	5378972	5378975	5378977	5378979	5378981	5378991	5379057	
1056	5379058	5379059	5379060	5379061	5379062	5379063	5379064	5379065	
1057	5379099	5379100	5379101	5379102	5379103	5379104	5379105	5379106	
1058	5379329	5379330	5379331	5379332	5379334	5379335	5379336	5379337	
1059	5379340	5379341	5379477	5379478	5379479	5379480	5380957	5380958	
1060	5380965	5380970	5380971	5380972	5380973	5380974	5380975	5380980	
1061	5381044	5381045	5381046	5381047	5381054	5381056	5381057	5381058	
1062	5381059	5381060	5381061	5381063	5381066	5381067	5381069	5381132	
1063	5381133	5381134	5381139	5381154	5381163	5381180	5381181	5381182	
1064	5381183	5381184	5381232	5381233	5381236	5381239	5381241	5381243	
1065	5381359	5381360	5381365	5381366	5381369	5381437	5381534	5381535	
1066	5381537	5381672	5381674	5381857	5381859	5381861	5381862	5381866	
1067	5381867	5381868	5381869	5381870	5381871	5381872	5381873	5381876	
1068	5381877	5381879	5381897	5381928	5381930	5381962	5381967	5381982	
1069	5381984	5381986	5381988	5381989	5382037	5382038	5382039	5382047	
1070	5382052	5382053	5382055	5382057	5382059	5382060	5382062	5382074	
1071	5382076	5382078	5382079	5382082	5382083	5382100	5382204	5382269	
1072	5382297	5382298	5382309	5382311	5382313	5382315	5382511	5382513	
1073	5382523	5382524	5382530	5382531	5382534	5382535	5382536	5382537	
1074	5382538	5382539	5382560	5382561	5382562	5382564	5382566	5382567	
1075	5382570	5382571	5383117	5383118	5383119	5383120	5383121	5383122	
1076	5383123	5383124	5383125	5383126	5383954	5383955	5383956	5383969	
1077	5383970	5383971	5383972	5383973	5383974	5383975	5383976	5383977	
1078	5383978	5383979	5383980	5383982	5383983	5383984	5383985	5383986	
1079	5383987	5383988	5383989	5383990	5383991	5383992	5402896	5402898	
1080	5402899	5402900	5403061	5403062	5403076	5403078	5403079	5403080	
1081	5403081	5403094	5403095	5403120	5403121	5403139	5403140	5403141	
1082	5403142	5403161	5403163	5403164	5403165	5403166	5403167	5403200	
1083	5403201	5403233	5403234	5403239	5403240	5403276	5403277	5403390	
1084	5403391	5403394	5403399	5403400	5403401	5403402	5403811	5403828	
1085	5403829	5403830	5403831	5403855	5403856	5403862	5403863	5403880	
1086	5403883	5403904	5403975	5403979	5403980	5403981	5403982	5404000	
1087	5404013	5404015	5404043	5404044	5404046	5404055	5404056	5404057	
1088	5404107	5404108	5404118	5404119	5404122	5404313	5404314	5404315	
1089	5404316	5404317	5404318	5404319	5404320	5404321	5409301	5409315	
1090	5409316	5409317	5409318	5409321	5409322	5409324	5409328	5409329	
1091	5409331	5409332	5409380	5409381	5409382	5409383	5409492	5409493	
1092	5409494	5409495	5409497	5409499	5409501	5409503	5409531	5409636	
1093	5409637	5409638	5409639	5409658	5409659	5409660	5409939	5409940	
1094	5409941	5409942	5409943	5409944	5409945	5409946	5378577	5378578	

```

1095      5378620   5378621   5378623   5378625   5378906   5378908   5379000   5379001
1096      5379156   5379157   5379358   5379361   5380133   5380134   5380150   5380151
1097      5380160   5380161   5378648   5378713   5403083   5403117   5378636   5382280
1098      5382281   5382350   5382515   5382519   5382522   5404103   5404111   5409631
1099      5409632
1100      $
1101      $
1102      $: <No cross-references to SET_SHELL 5 found>
1103      $
1104      *SET_SHELL_LIST
1105          5          0.0          0.0          0.0          0.0
1106      5378639   5382521   5378796   5378798   5382272   5382276   5383613   5383615
1107      5383617   5383619   5383635   5383637   5383639   5383641   5383643   5383645
1108      5383647   5382305
1109      $
1110      $
1111      $: <No cross-references to SET_SHELL 6 found>
1112      $
1113      *SET_SHELL_LIST
1114          6          0.0          0.0          0.0          0.0
1115      5394744   5394898   5395479   5395480   5395616   5395617   5394727   5394948
1116      $
1117      $
1118      $: <No cross-references to SET_SHELL 7 found>
1119      $
1120      *SET_SHELL_LIST
1121          7          0.0          0.0          0.0          0.0
1122      5393755   5393756   5393761   5393768   5393769   5393778   5393780   5393781
1123      5393782   5393783   5393784   5393789   5393790   5393923   5393924   5393925
1124      5393926   5393927   5393928   5393929   5393932   5393933   5393934   5393935
1125      5393936   5393937   5393938   5393939   5393940   5393941   5393942   5393943
1126      5393944   5393945   5393946   5393947   5393950   5393951   5393952   5393953
1127      5394048   5394049   5394050   5394055   5394060   5394061   5394064   5394065
1128      5394068   5394069   5394072   5394073   5394078   5394083   5394084   5394087
1129      5394495   5394496   5394501   5394502   5394503   5394504   5394510   5394513
1130      5394514   5394515   5394519   5394520   5394525   5394843   5394844   5394845
1131      5394846   5394847   5394852   5394867   5394868   5394869   5394870   5394871
1132      5394877   5394879   5394880   5394881   5394882   5394883   5394884   5394885
1133      5394886   5394889   5394890   5394891   5394892   5394893   5394894   5394895
1134      5394933   5394935   5394937   5394939   5394941   5394943   5394944   5395233
1135      5395235   5395237   5395239   5395241   5395648   5395649   5395650   5395651
1136      5395652   5395653   5395654   5395655   5395656   5395657   5395678   5395679
1137      5395680   5395681   5395682   5395683   5395684   5395685   5395686   5395687
1138      5396261   5396262   5402509   5402510   5402511   5402512   5402513   5402514
1139      5402515   5402516   5402517   5402518   5402519   5402520   5402521   5402522
1140      5402525   5402526   5402527   5402528   5402529   5402530   5402531   5402532
1141      5402533   5402534   5402535   5402536   5402537   5402538   5402539   5402540
1142      5402541   5402542   5402543   5402544   5402545   5402546   5402547   5402552
1143      5402557   5402558   5402561   5402562   5402565   5402566   5402569   5402570
1144      5402575   5402580   5402581   5402582   5402591   5402592   5402593   5402594
1145      5402595   5402596   5402597   5402598   5402599   5402600   5402601   5402602
1146      5402603   5402604   5402605   5402606   5402607   5402608   5402609   5402610
1147      5402613   5402614   5402615   5402616   5402617   5402618   5402619   5402620
1148      5402621   5402622   5402623   5402624   5402625   5402626   5402636   5402637
1149      5402638   5402639   5402640   5402641   5402642   5402643   5402644   5402645
1150      5402646   5402647   5402648   5402649   5402650   5402651   5402652   5402653
1151      5402654   5402655   5406623   5406624   5406625   5406628   5406629   5406653
1152      5406658   5406659   5406660   5406661   5406676   5406685   5406788   5406845
1153      5406846   5406850   5406851   5406864   5406874   5406875   5412072   5412073
1154      5412074   5412075   5412098   5412099   5412102   5412103   5412106   5412107
1155      5412108   5412109   5412122   5412123   5412124   5412125   5412126   5412127
1156      5412128   5412129   5412249   5412250   5412295   5412296   5412297   5412299
1157      5412310   5412311   5412314   5412315   5414081   5414082   5414083   5414088
1158      5414089   5414090   5414091   5414092   5414101   5414102   5414103   5414104
1159      5414105   5414110   5414111   5414112   5414273   5414274   5414277   5414278
1160      5414281   5414282   5414283   5414284   5414285   5414286   5414287   5414288
1161      5414289   5414290   5414291   5414292   5414293   5414294   5414295   5414296
1162      5414299   5414300   5414303   5414304   5396276   5396277   5396284   5396300
1163      5396302   5396321   5407179   5407187   5412587   5412594   5396306   5396309
1164      5396317   5412597   5394498   5394499   5394509   5412080   5412100   5412101
1165      5412104   5412105   5412246   5412247   5412248   5412308   5412309   5412312
1166      5412313   5414275   5414276   5414279   5414280   5414297   5414298   5414301
1167      5414302   5412596   5393767   5393770   5393773   5393774   5393776   5394524

```

```

1168      5406627   5406789   5412077   5412078
1169 $
1170 $
1171 $: <No cross-references to SET_SHELL 8 found>
1172 $
1173 *SET_SHELL_LIST
1174      8          0.0          0.0          0.0          0.0
1175      5378495   5378496   5378497   5378498   5378499   5378500   5378501   5378502
1176      5378503   5378504   5378604   5378661   5378662   5378837   5379176   5379177
1177      5379178   5379179   5379181   5379182   5379183   5379184   5379187   5379188
1178      5379191   5379192   5379195   5379196   5379199   5379200   5379201   5379202
1179      5379204   5379205   5379206   5379207   5379259   5379260   5379370   5379387
1180      5379389   5379390   5379391   5379392   5380411   5381092   5381099   5381100
1181      5381109   5381127   5381128   5381129   5381130   5381131   5381136   5381137
1182      5381325   5381326   5381327   5381342   5381343   5381345   5381346   5381347
1183      5381348   5381349   5381350   5381361   5381362   5381363   5381364   5381493
1184      5381494   5381495   5381500   5381509   5381511   5381517   5381518   5381527
1185      5381532   5381533   5381536   5382014   5382015   5382034   5382035   5382036
1186      5382040   5382041   5382045   5382411   5382412   5382413   5382414   5382415
1187      5382419   5382433   5382434   5382435   5382436   5382437   5382442   5382466
1188      5382467   5382468   5382506   5382508   5382510   5382512   5382514   5382516
1189      5382517   5383011   5383012   5383013   5383014   5383015   5383016   5383017
1190      5383018   5383019   5383020   5384276   5384277   5401940   5401941   5401942
1191      5401943   5401944   5401945   5401946   5401947   5401948   5401963   5401964
1192      5401988   5401989   5401990   5401991   5401993   5401994   5401995   5401996
1193      5401999   5402000   5402003   5402004   5402007   5402008   5402011   5402012
1194      5402013   5402014   5402016   5402017   5402018   5402019   5402043   5402044
1195      5402059   5402077   5402078   5402079   5402080   5402081   5402082   5402083
1196      5402084   5402085   5402086   5402101   5402102   5402103   5402104   5402105
1197      5402106   5402107   5402108   5402109   5402110   5402111   5402112   5402113
1198      5402114   5402115   5402120   5402129   5402130   5402133   5402134   5402143
1199      5402148   5402149   5402150   5402151   5402152   5402153   5402154   5402155
1200      5402156   5402157   5402158   5402159   5402160   5402161   5402162   5402177
1201      5402178   5402179   5402180   5402181   5402182   5402183   5402184   5402185
1202      5402186   5402196   5402197   5402198   5402199   5402200   5402201   5402202
1203      5402203   5403085   5403086   5403087   5403088   5403130   5403131   5403204
1204      5403205   5403206   5403207   5403208   5403209   5403210   5403211   5403220
1205      5403221   5403222   5403223   5403248   5403249   5403839   5403840   5403841
1206      5403844   5403845   5403871   5403876   5403877   5403878   5403879   5403894
1207      5403903   5404010   5404070   5404071   5404075   5404076   5404090   5404100
1208      5404101   5409305   5409306   5409307   5409308   5409372   5409373   5409374
1209      5409375   5409388   5409389   5409390   5409391   5409392   5409393   5409394
1210      5409395   5409605   5409606   5409607   5409609   5413956   5413957   5413958
1211      5413959   5413965   5413966   5413967   5413968   5413969   5413970   5413971
1212      5413972   5413978   5413979   5413980   5413981   5413985   5413986   5413987
1213      5413992   5413993   5413994   5413995   5413996   5414005   5414006   5414007
1214      5414008   5414009   5414014   5414015   5414016   5414185   5414186   5414187
1215      5414188   5414189   5414190   5414191   5414192   5414193   5414194   5414195
1216      5414196   5414197   5414198   5414199   5414200   5380434   5380443   5380461
1217      5403469   5403478   5378855   5379384   5379396   5403133   5403464   5381098
1218      5381101   5381104   5381105   5381107   5382044   5403843   5404011   5409310
1219      5409311   5384291   5384292   5384299   5384315   5384317   5384336   5404407
1220      5404415   5410031   5410038
1221 $
1222 $
1223 $: <No cross-references to SET_SHELL 9 found>
1224 $
1225 *SET_SHELL_LIST
1226      9          0.0          0.0          0.0          0.0
1227      5378509   5378510   5380433   5383005   5383006   5384335   5382032   5378493
1228      5378494   5383021   5383022   5379385   5382042   5384342   5383667   5383669
1229      5383671   5383673   5383675   5383677   5383681   5402205   5402207   5402209
1230      5402211
1231 $
1232 $
1233 $: <No cross-references to SET_SHELL 10 found>
1234 $
1235 *SET_SHELL_LIST
1236      10         0.0          0.0          0.0          0.0
1237      5395229   5396320   5395243   5394511   5394521   5395658   5395659   5395676
1238      5395677   5394507   5396316   5395662   5395663   5395696   5395697   5396327
1239 $
1240 $

```

```

1241 $: <No cross-references to SET_SHELL 11 found>
1242 $
1243 *SET_SHELL_LIST
1244     11      0.0      0.0      0.0      0.0
1245     6003611 6003612 6003613 6003614 6003615 6003616 6003617 6003618
1246     6003619 6003620 6003621 6003622 6003623 6003624 6003625 6003626
1247     6003627 6003628 6003629 6003630 6003631 6003632 6003633 6003634
1248     6003635 6003636 6003637 6003638 6003639 6003640 6003641 6003642
1249     6003643 6003644 6003645 6003646 6003647 6003648 6003649 6003650
1250     6003651 6003652 6003653 6003654 6003655 6003656 6003657 6003658
1251     6003659 6003660 6003661 6003662 6003663 6003664 6003665 6003666
1252     6003667 6003668 6003669 6003670 6003671 6003672 6003673 6003674
1253     6003675 6003676 6003677 6003678 6003679 6003680 6003681 6003682
1254     6003683 6003684 6003685 6003686 6003687 6003688 6003689 6003690
1255     6003691 6003692 6003693 6003694 6003695 6003696 6003697 6003698
1256     6003699 6003700 6003701 6003702 6003703 6003704 6003705 6003706
1257     6003707 6003708 6003709 6003710 6003711 6003712 6003713 6003714
1258     6003715 6003716 6003717 6003718 6003719 6003720 6003721 6003722
1259     6003723 6003724 6003725 6003726 6003727 6003728 6003729 6003730
1260     6003731 6003732 6003733 6003734 6003735 6003736 6003737 6003738
1261     6003739 6003740 6003741 6003742 6003743 6003744 6003745 6003746
1262     6003747 6003748 6003749 6003750 6003751 6003752 6003753 6003754
1263     6003755 6003756 6003757 6003758 6003759 6003760 6003761 6003762
1264     6003763 6003764 6003765 6003766 6003767 6003768 6003769 6003770
1265     6003771 6003772 6003773 6003774 6003775 6003776 6003777 6003778
1266     6003779 6003780 6003781 6003782 6003783 6003784 6003785 6003786
1267     6003787 6003788 6003789 6003790 6003791 6003792 6003793 6003794
1268     6003795 6003796 6003797 6003798 6003799 6003800 6003801 6003802
1269     6003803 6003804 6003805 6003806 6003807 6003808 6003809 6003810
1270     6003811 6003812 6003813 6003814 6003815 6003816 6003817 6003818
1271     6003819 6003820 6003821 6003822 6003823 6003824 6003825 6003826
1272     6003827 6003828 6003829 6003830 6003831 6003832 6003833 6003834
1273     6003835 6003836 6003837 6003838 6003839 6003840 6003841 6003842
1274     6003843 6003844 6003845 6003846 6003847 6003848 6003849 6003850
1275     6003851 6003852 6003853 6003854 6003855 6003856 6003858 6003859
1276     6003860 6003862 6003863 6003864 6003865 6003866 6003867 6003868
1277     6003869 6003870 6003871 6003872 6003873 6003874 6003875 6003876
1278     6003877 6003878 6003884 6003886 6003887 6003888 6003889 6003890
1279     6003891 6003892 6003893 6003894 6003895 6003896 6003897 6003898
1280     6003899 6003900 6003908 6003910 6003911 6003912 6003913 6003914
1281     6003915 6003916 6003917 6003918 6003919 6003920 6003921 6003922
1282     6003923 6003924 6003935 6003936 6003937 6003938 6003939 6003940
1283     6003941 6003942 6003943 6003944 6003945 6003946 6003961 6003962
1284     6003963 6003964 6003965 6003966 6003967 6003968 6003987 6003988
1285     6003989 6003990 6015863 6015871 6015892 6015896 6015904 6015906
1286     6015915 6015941
1287 $
1288 $
1289 *END
1290

```

Annex B: Python code for data analysis

Script for visualizing the results of the loadtests done on the movable Suurhoff bridge renovation

First few code blocks are for importing all the data etc.

```
In [ ]: #Importing relevant packages

import matplotlib.pyplot as plt
import matplotlib as mpl
import pandas as pd
import numpy as np
import seaborn as sns
import os
from scipy.signal import argrelextrema
from scipy.signal import savgol_filter
from scipy.signal import butter
from scipy.signal import sosfilt
from scipy.signal import filtfilt
from scipy.fftpack import fft
from scipy.stats import linregress
from IPython.display import display

%matplotlib inline

import ipywidgets as widgets
from ipywidgets import interact
from ipywidgets import interactive_output
```

```
In [ ]: #General plotting settings used to ensure all plots look the same
plt.style.use('seaborn-deep')
plt.rcParams['axes.grid'] = 'True'
plt.rcParams['axes.facecolor'] = 'none'
plt.rcParams['figure.facecolor'] = 'white'
plt.rcParams['figure.figsize'] = (12,7)
plt.rcParams['lines.linewidth'] = 1
plt.rcParams['axes.titlesize'] = 20
plt.rcParams['axes.labelsize'] = 16
plt.rcParams['xtick.major.size'] = 4
plt.rcParams['ytick.major.size'] = 4
plt.rcParams['xtick.labelsize'] = 12
plt.rcParams['ytick.labelsize'] = 12
plt.rcParams['legend.fontsize'] = 14
```

```
In [ ]: # Cell in which the data is loaded in and filtered
# Make sure this notebook is in the a folder with all the xlsx/csv results in a subf
# This cell takes a few minutes to run, especially on lower-end pc's

files1 = ['2021-07-12-fast_010.csv',
          '2021-07-12-fast_012.csv',
          '2021-07-12-fast_013.csv',
          '2021-07-12-fast_014.csv',
          '2021-07-12-fast_016.csv',
          '2021-07-12-fast_019.csv',
          '2021-07-12-fast_020.csv',
          '2021-07-12-fast_021.csv',
```

```

'2021-07-12-fast_023.csv',
'2021-07-12-fast_024.csv',
'2021-07-12-fast_025.csv']

files2 = ['2021-08-18-fast_033.csv',
'2021-08-18-fast_034.csv',
'2021-08-18-fast_035.csv',
'2021-08-18-fast_036.csv',
'2021-08-18-fast_037.csv',
'2021-08-18-fast_038.csv',
'2021-08-18-fast_039.csv',
'2021-08-18-fast_040.csv',
'2021-08-18-fast_041.csv',
'2021-08-18-fast_042.csv',
'2021-08-18-fast_043.csv',
'2021-08-18-fast_044.csv',
'2021-08-18-fast_045.csv',
'2021-08-18-fast_046.csv']

#Locs = ['SG001', 'SG002', 'SG003', 'SG004', 'SG005', 'SG006', 'SG007', 'SG008', 'SG009', 'SG0
#sensors = ['Deck01', 'Deck02', 'Deck03', 'Deck04', 'Deck05', 'Deck06', 'Deck07', 'D

locs1 = ['Location 7 (1st run)', 'Location 7 (2nd run)', 'Location 8', 'Location 9',
locs2 = ['Location 1', 'Location 2', 'Location 3', 'Location 4', 'Location 5 (1st ru

list1 = []

# Loading in csv files
for i in files1:
    if(os.path.exists(f'./data/{i}')) == True:
        list1.append(pd.read_csv(f'./data/{i}'))

list2 = []

for i in files2:
    if(os.path.exists(f'./data/{i}')) == True:
        temp = pd.read_csv(f'./data/{i}', sep = ';', skiprows=1)
        temp = temp.drop(0,0)
        temp.Time = pd.to_numeric(temp.Time)
        list2.append(temp)

vis1 = list1[5]
vis2 = list2[4]

print('Part 1/6 done')

#First number loc1-11, second optional run 1-3, Last number load test 1 or 2
locations1 = [loc7_1_1, loc7_2_1, loc8_1, loc9_1, loc6_1, loc5_1, loc4_1, loc3_1, lo
locations2 = [loc1_2, loc2_2, loc3_2, loc4_2, loc5_1_2, loc5_2_2, loc5_3_2, loc6_1_2

print('Part 2/6 done')

# Set up noise filter
fs = 1000 # Sample frequency
fc = 5 # Cut-off frequency of the filter
w = fc / (fs / 2) # Normalize the frequency
b, a = butter(5, w, 'low') # Set up butter filter

for i in locations1:
    for j in i.columns:
        if j[0:2] == 'SG' and j[-1] != 'M':
            i['delta'] = np.average(i[j][0:10000]) # Set average of first 10 second
            i[j + 'M'] = (i[j] - i['delta']) * 0.21 # Factor 0.21 to convert from mi
            i[j + 'M'] = filtfilt(b, a, i[j + 'M']) # Apply noise filter

```

```

i['Time [s]'] = i['Time'] - i['Time'][50]
i = i.reset_index(drop = True)

print('Part 3/6 done')

for i in locations2:
    for j in i.columns:
        if j[0:2] == 'SG' and j[-1] != 'M':
            i['delta'] = np.average(pd.to_numeric(i[j])[0:10000]) # Set average of f
            i[j + 'M'] = (pd.to_numeric(i[j]) - i['delta']) * 0.21 # Factor 0.21 to
            i[j + 'M'] = filtfilt(b, a, i[j + 'M']) # Apply noise filter

    i['Time [s]'] = pd.to_numeric(i['Time']) - pd.to_numeric(i['Time'][51]) # Remove
    i = i.reset_index(drop = True)

print('Part 4/6 done')

# Making some dictionaries for easy access to all results
match1 = {'Location 3': loc3_1, 'Location 4': loc4_1, 'Location 5': loc5_1, 'Locatio
match2 = {'Location 1': loc1_2, 'Location 2': loc2_2, 'Location 3': loc3_2, 'Locatio
sensors = {'Deck01': 'SG001M', 'Deck02': 'SG002M', 'Deck03': 'SG003M', 'Deck04': 'SG

# Coincide peaks for comparing multiple runs
for i in locs1:
    location = match1[i]
    maxima = location.SG016M[argrelextrema(location.SG016M.values, np.greater_equal,
    maxima_sorted = maxima.sort_values(ascending = False)
    location['counter'] = location.index - maxima_sorted.index[0]
    diff = maxima_sorted.index[0] - maxima_sorted.index[1] # Determine amount of mea
    location['counter'] = (location['counter'] * 10 * 0.883636 / diff) + 20 # With t

print('Part 5/6 done')

for i in locs2:
    location = match2[i]
    maxima = location.SG016M[argrelextrema(location.SG016M.values, np.greater_equal,
    maxima_sorted = maxima.sort_values(ascending = False)
    location['counter'] = location['Time [s]'] - location['Time [s]'][maxima_sorted.
    diff = location['Time [s]'][maxima_sorted.index[0]] - location['Time [s]'][maxim
    location['counter'] = (location['counter'] * 10 * 0.883636 / diff) + 20 # With

print('Ready')

```

In []:

```

#Function for interactive plotting of unstrenghtened Load test results
def plot_line3(a, b, c, d, e, f, g, h, i, j, k, z, y, x):

    track = sensors[z]

    with sns.diverging_palette(250, 0, l = 50, center = "light", n = 11):

        if a: plt.plot(match1['Location 3'].counter, match1['Location 3'][track], la
        if b: plt.plot(match1['Location 4'].counter, match1['Location 4'][track], la
        if c: plt.plot(match1['Location 5'].counter, match1['Location 5'][track], la
        if d: plt.plot(match1['Location 6'].counter, match1['Location 6'][track], la
        if e: plt.plot(match1['Location 7 (1st run)'].counter, match1['Location 7 (1
        if f: plt.plot(match1['Location 7 (2nd run)'].counter, match1['Location 7 (2
        if g: plt.plot(match1['Location 7 (3rd run)'].counter, match1['Location 7 (3
        if h: plt.plot(match1['Location 8'].counter, match1['Location 8'][track], la
        if i: plt.plot(match1['Location 9'].counter, match1['Location 9'][track], la
        if j: plt.plot(match1['Location 10'].counter, match1['Location 10'][track],
        if k: plt.plot(match1['Location 11'].counter, match1['Location 11'][track],

```

```

plt.minorticks_on()
plt.ylabel('Stress [MPa]')
plt.xlabel('Distance [m]')
plt.grid(axis = 'x', which = 'minor', linestyle = '-.', linewidth=0.2)
plt.grid(axis = 'y', which = 'minor', linestyle = '-.', linewidth=0.2)
plt.title(f"Unstrengthened deck, sensor {z}.")
plt.legend(loc = 'upper left')
if z == 'Trou01' or z == 'Trou02':
    plt.legend(loc = 'lower left')
plt.xlim(-10,30)
plt.tight_layout()
#plt.savefig(f"./results_figures/Results_Test1_{z}.svg") #uncomment to save

# Widget definition and layout

a = widgets.Checkbox(value = True, description = 'Location 3')
b = widgets.Checkbox(value = True, description = 'Location 4')
c = widgets.Checkbox(value = True, description = 'Location 5')
d = widgets.Checkbox(value = True, description = 'Location 6')
e = widgets.Checkbox(value = True, description = 'Location 7 (1st run)')
f = widgets.Checkbox(value = True, description = 'Location 7 (2nd run)')
g = widgets.Checkbox(value = True, description = 'Location 7 (3rd run)')
h = widgets.Checkbox(value = True, description = 'Location 8')
i = widgets.Checkbox(value = True, description = 'Location 9')
j = widgets.Checkbox(value = True, description = 'Location 10')
k = widgets.Checkbox(value = True, description = 'Location 11')

z = widgets.Dropdown(options = sensors.keys(), value = 'Cgir01', description = 'Sensor')
y = widgets.FloatSlider(min = 0, max = 1, step = 0.01, value = 0, description = 'Stress')
x = widgets.FloatSlider(min = 0, max = 1, step = 0.01, value = 1, description = 'Distance')

hb1 = widgets.VBox((a, b, c, d, e, f, g))
hb2 = widgets.VBox((h, i, j, k))
hb3 = widgets.VBox((z, y, x))
hb4 = widgets.HBox((hb3, hb1, hb2))

ip = interactive_output(plot_line3, {'a': a,
                                     'b': b,
                                     'c': c,
                                     'd': d,
                                     'e': e,
                                     'f': f,
                                     'g': g,
                                     'h': h,
                                     'i': i,
                                     'j': j,
                                     'k': k,
                                     'z': z,
                                     'y': y,
                                     'x': x})

display(hb4, ip);

```

In []:

```

#Function for interactive plotting of the strengthened Load test results
def plot_line4(a, b, c, d, e, f, g, h, i, j, k, l, m, n, z, y, x):

    track = sensors[z]

    with sns.diverging_palette(250, 0, l = 50, center = "light", n = 14):

        if a: plt.plot(match2['Location 1'].counter, match2['Location 1'][track], la
        if b: plt.plot(match2['Location 2'].counter, match2['Location 2'][track], la

```

```

if c: plt.plot(match2['Location 3'].counter, match2['Location 3'][track], la
if d: plt.plot(match2['Location 4'].counter, match2['Location 4'][track], la
if e: plt.plot(match2['Location 5 (1st run)'].counter, match2['Location 5 (1
if f: plt.plot(match2['Location 5 (2nd run)'].counter, match2['Location 5 (2
if g: plt.plot(match2['Location 5 (3rd run)'].counter, match2['Location 5 (3
if h: plt.plot(match2['Location 6 (1st run)'].counter, match2['Location 6 (1
if i: plt.plot(match2['Location 6 (2nd run)'].counter, match2['Location 6 (2
if j: plt.plot(match2['Location 7'].counter, match2['Location 7'][track], la
if k: plt.plot(match2['Location 8'].counter, match2['Location 8'][track], la
if l: plt.plot(match2['Location 9'].counter, match2['Location 9'][track], la
if m: plt.plot(match2['Location 10'].counter, match2['Location 10'][track],
if n: plt.plot(match2['Location 11'].counter, match2['Location 11'][track],

```

```

plt.minorticks_on()
plt.ylabel('Stress [MPa]')
plt.xlabel('Distance [m]')
plt.grid(axis = 'x', which = 'minor', linestyle = '-.', linewidth=0.2)
plt.grid(axis = 'y', which = 'minor', linestyle = '-.', linewidth=0.2)
plt.title(f"Strengthened deck, sensor {z}.")
plt.legend(loc = 'upper left')
if z == 'Trou01' or z == 'Trou02':
    plt.legend(loc = 'lower left')
plt.xlim(-10,30)
plt.tight_layout()
##plt.savefig(f"./results_figures/Results_Test2_{z}.svg") #Uncomment to save

```

Widget definition and layout

```

a = widgets.Checkbox(value = True, description = 'Location 1')
b = widgets.Checkbox(value = True, description = 'Location 2')
c = widgets.Checkbox(value = True, description = 'Location 3')
d = widgets.Checkbox(value = True, description = 'Location 4')
e = widgets.Checkbox(value = True, description = 'Location 5 (1st run)')
f = widgets.Checkbox(value = True, description = 'Location 5 (2nd run)')
g = widgets.Checkbox(value = True, description = 'Location 5 (3rd run)')
h = widgets.Checkbox(value = True, description = 'Location 6 (1st run)')
i = widgets.Checkbox(value = True, description = 'Location 6 (2nd run)')
j = widgets.Checkbox(value = True, description = 'Location 7')
k = widgets.Checkbox(value = True, description = 'Location 8')
l = widgets.Checkbox(value = True, description = 'Location 9')
m = widgets.Checkbox(value = True, description = 'Location 10')
n = widgets.Checkbox(value = True, description = 'Location 11')

z = widgets.Dropdown(options = sensors.keys(), value = 'Cgir01', description = 'Sens
y = widgets.FloatSlider(min = 0, max = 1, step = 0.01, value = 0, description = 'Sta
x = widgets.FloatSlider(min = 0, max = 1, step = 0.01, value = 1, description = 'Sto

hb1 = widgets.VBox((a, b, c, d, e, f, g))
hb2 = widgets.VBox((h, i, j, k, l, m, n))
hb3 = widgets.VBox((z, y, x))
hb4 = widgets.HBox((hb3, hb1, hb2))

ip = interactive_output(plot_line4, {'a': a,
                                     'b': b,
                                     'c': c,
                                     'd': d,
                                     'e': e,
                                     'f': f,
                                     'g': g,
                                     'h': h,
                                     'i': i,
                                     'j': j,
                                     'k': k,
                                     'l': l,

```

```

        'm': m,
        'n': n,
        'z': z,
        'y': y,
        'x': x})

display(hb4, ip);

```

In []:

```

#Function for Interactive plot for selected sensors per run for strenghtened bridge

def plot_line5(q, z, y, x):

    if z == 'Overview':
        sensor = q
        tlist1 = []
        xlist1 = []
        tlist2 = []
        xlist2 = []

    for i in match1: #Loop trough the different Locations for the unstrenghtened
        xlist1.append(np.int(i[9:11])) #Get the Location number to put on the x-
        maxima1 = np.amax(match1[i][sensors[sensor]][100:]) #Find the maximum of
        if sensor == 'Cgir01':
            minima1 = 0 #In case of sensorCGir01, this value is set to 0 to prev
        else:
            minima1 = np.amin(match1[i][sensors[sensor]][100:]) #In case of sens
        diff1 = np.amax(maxima1) - np.amax(minima1)
        tlist1.append(diff1) #Append the maximum stress cycle experienced by the

    for i in match2: # Same thing but for the strengthened scenario (code could
        xlist2.append(np.int(i[9:11]))
        maxima2 = np.amax(match2[i][sensors[sensor]][100:])
        if sensor == 'Cgir01':
            minima2 = 0
        else:
            minima2 = np.amin(match2[i][sensors[sensor]][100:])
        diff2 = np.amax(maxima2) - np.amax(minima2)
        tlist2.append(diff2)

    #Remove duplicates from x coordinates (for the Locations where more than 1 r
    xlist3 = list(dict.fromkeys(xlist1))
    xlist4 = list(dict.fromkeys(xlist2))

    #Average out the duplicate values (for the Locations where more than 1 run w
    tlist3 = 1 * tlist1
    del tlist3[4:7]
    tlist3.insert(4, np.average(tlist1[4:7]))

    tlist4 = 1 * tlist2
    del tlist4[4:7]
    tlist4.insert(4, np.average(tlist2[4:7]))
    del tlist4[5:7]
    tlist4.insert(5, np.average(tlist2[7:9]))

    tlist5 = []

    #Effectiveness:
    for i in range(len(tlist3)):
        tlist5.append(-100 * ((tlist4[i+2] - tlist3[i]) / tlist3[i]))

    #Plotting
    fig, ax1 = plt.subplots(figsize = (14,7))

```

```

ax1.plot(xlist3,tlist3, color = sns.diverging_palette(0, 250, l = 50, center
ax1.scatter(xlist1,tlist1, marker = 'x', s = 50, label = 'Before strengthen

ax1.plot(xlist4,tlist4, color = sns.diverging_palette(0, 250, l = 50, center
ax1.scatter(xlist2,tlist2, marker = 'D', s = 20, label = 'After strengtheni

ax1.set_xlim(1,11)
ax1.set_ylim(bottom = 0, top = 100)
ax1.set_xticks(xlist2)
ax1.set_xlabel('Truck location (track)')
ax1.set_ylabel('Maximum stress cycle [MPa]')
ax1.minorticks_on()
ax1.grid(axis = 'y', which = 'minor', linestyle = '-.', linewidth=0.2)
ax1.invert_xaxis() #Swap location 1-11 to 11-1 to match other figures

#Secondary y axis for plotting effectiveness:
ax2 = ax1.twinx()
ax2.set_ylim(0, 100)
labels = [0, 20, 40, 60, 80, 100]
#Labels = [0, 4, 8, 12, 16, 20]
ax2.set_yticks(labels)
ax2.set_yticklabels(f'{x}%' for x in labels)
ax2.set_ylabel('Stress cycle reduction')
ax2.grid(axis = 'y', which = 'minor', linestyle = '-.', linewidth=0.2)

ax2.plot(xlist3,tlist5, '--', color = 'black', linewidth = 2, label = 'Stres

plt.title(f'Results overview of sensor {sensor}')

fig.tight_layout()

#Align the gridlines and tick labels of y-axes:
l1 = len(ax1.get_yticks())
l2 = len(ax2.get_yticks())

a = ax2
b = ax1
l = l2

b_ticks = np.linspace(b.get_yticks()[0],b.get_yticks()[-1], l)

b.set_yticks(b_ticks)

ax1.legend(loc = 'upper left')
ax2.legend(loc = 'upper right')

elif z == '345': #Comparison plot deck03, 04 and 05
    with sns.diverging_palette(0, 250, l = 50, center = "dark", n = 4):
        fig, ax1 = plt.subplots(figsize = (14,7))
        ax2 = ax1.twinx()
        for j, style in zip(['Deck03', 'Deck04', 'Deck05'],['-', '--', ':']):

            sensor = j
            tlist1 = []
            xlist1 = []
            tlist2 = []
            xlist2 = []

            for i in match1: #Loop trough the different locations for the unstre
                xlist1.append(np.int(i[9:11])) #Get the location number to put o
                maxima1 = np.amax(match1[i][sensors[sensor]][100:]) #Find the ma
                if sensor == 'Cgir01':
                    minima1 = 0 #In case of sensorCGir01, this value is set to 0
                else:

```

```

        minima1 = np.amin(match1[i][sensors[sensor]][100:]) #In case
diff1 = np.amax(maxima1) - np.amax(minima1)
tlist1.append(diff1) #Append the maximum stress cycle experience

for i in match2: # Same thing but for the strengthened scenario (cod
xlist2.append(np.int(i[9:11]))
maxima2 = np.amax(match2[i][sensors[sensor]][100:])
if sensor == 'Cgir01':
    minima2 = 0
else:
    minima2 = np.amin(match2[i][sensors[sensor]][100:])
diff2 = np.amax(maxima2) - np.amax(minima2)
tlist2.append(diff2)

#Remove duplicates from x coordinates (for the Locaitons where more
xlist3 = list(dict.fromkeys(xlist1))
xlist4 = list(dict.fromkeys(xlist2))

#Average out the duplicate values (for the Locations where more than
tlist3 = 1 * tlist1
del tlist3[4:7]
tlist3.insert(4, np.average(tlist1[4:7]))

tlist4 = 1 * tlist2
del tlist4[4:7]
tlist4.insert(4, np.average(tlist2[4:7]))
del tlist4[5:7]
tlist4.insert(5, np.average(tlist2[7:9]))

tlist5 = []

#Effectiveness:
for i in range(len(tlist3)):
    tlist5.append(-100 * ((tlist4[i+2] - tlist3[i]) / tlist3[i]))

#Plotting

ax1.plot(xlist3, tlist3, style, label = f'Before strengthening, {j}')
ax1.scatter(xlist1, tlist1, marker = 'x', s = 50, color = sns.diverg

ax1.plot(xlist4, tlist4, style, label = f'After strengthening, {j}',
ax1.scatter(xlist2, tlist2, marker = 'D', s = 20, color = sns.diverg

ax2.plot(xlist3,tlist5, style, label = f'Reduction {j}', color = 'gr

ax1.set_xlim(1,11)
ax1.set_ylim(bottom = 0, top = 100)
ax1.set_xticks(xlist2)
ax1.set_xlabel('Truck location (track)')
ax1.set_ylabel('Maximum stress cycle [MPa]')
ax1.minorticks_on()
ax1.grid(axis = 'y', which = 'minor', linestyle = '-.', linewidth=0.2)
ax1.invert_xaxis() #Swap Location 1-11 to 11-1 to match other figures

#Secondary y axis for plotting effectiveness:

ax2.set_ylim(0, 100)
labels = [0, 20, 40, 60, 80, 100]
ax2.set_yticks(labels)
ax2.set_yticklabels(f'{{x}}%' for x in labels)

```

```

#ax2.yaxis.Label.set_color('orange')
#ax2.tick_params(axis='y', colors='orange')

ax2.set_ylabel('Stress cycle reduction')
ax2.grid(axis = 'y', which = 'minor', linestyle = '-.', linewidth=0.2)

#Align the gridlines and tick labels of y-axes:
l1 = len(ax1.get_yticks())
l2 = len(ax2.get_yticks())

a = ax2
b = ax1
l = l2

b_ticks = np.linspace(b.get_yticks()[0],b.get_yticks()[-1], l)

b.set_yticks(b_ticks)

ax1.legend(loc = 'upper left', fontsize = '13')
ax2.legend(loc = 'upper right', fontsize = '13')

plt.title('Results overview of sensors Deck03, Deck04 and Deck05')
fig.tight_layout()

elif z == 'Location 1' or z == 'Location 2': #Plotting of Loc 1 and 2: Only stre
    with sns.diverging_palette(0, 250, l = 50, center = "dark", n = 1):
        location2 = match2[z]
        plt.plot(location2['counter'], location2[sensors[q]], label = 'After str

elif z == 'Location 5': #Location 5: 3 x strengthened runs, 1 x unstrengthened
    with sns.diverging_palette(0, 250, l = 50, center = "dark", n = 4):
        location1 = match1[z]
        plt.plot(location1['counter'], location1[sensors[q]], label = 'Before st
        for z in 'Location 5 (1st run)', 'Location 5 (2nd run)', 'Location 5 (3r
            location2 = match2[z]
            plt.plot(location2['counter'], location2[sensors[q]], label = f'Afte
        z = 'Location 5'

elif z == 'Location 6': #Location 6: 2 x strengthened run, 1 x unstrengthened
    with sns.diverging_palette(0, 250, l = 50, center = "dark", n = 3):
        location1 = match1[z]
        plt.plot(location1['counter'], location1[sensors[q]], label = 'Before st
        for z in 'Location 6 (1st run)', 'Location 6 (2nd run)':
            location2 = match2[z]
            plt.plot(location2['counter'], location2[sensors[q]], label = f'Afte
        z = 'Location 6'

elif z == 'Location 7': #Location 7: 1 x strengthened run, 3 x unstrengthened
    with sns.diverging_palette(0, 250, l = 50, center = "dark", n = 4):
        for z in 'Location 7 (1st run)', 'Location 7 (2nd run)', 'Location 7 (3r
            location1 = match1[z]
            plt.plot(location1['counter'], location1[sensors[q]], label = f'Befo
        z = 'Location 7'

        location2 = match2[z]
        plt.plot(location2['counter'], location2[sensors[q]], label = 'After str

else: #all other runs: 1 x strengthened, 1 x unstrengthened

```

```

with sns.diverging_palette(0, 250, l = 50, center = "dark", n = 2):

    location1 = match1[z]
    location2 = match2[z]

    plt.plot(location1['counter'], location1[sensors[q]], label = 'Before str
    plt.plot(location2['counter'], location2[sensors[q]], label = 'After str

if z != 'Overview' and z != '345':
    print('test')
    plt.minorticks_on()
    plt.ylabel('Stress [MPa]')
    plt.xlabel('Distance [m]')
    plt.grid(axis = 'x', which = 'minor', linestyle = '-.', linewidth=0.2)
    plt.grid(axis = 'y', which = 'minor', linestyle = '-.', linewidth=0.2)
    plt.title(f'Load test results, track {z}, sensor {q}')
    plt.legend(loc = 'best')
    plt.xlim(0 + y, 30 + (x-30))

plt.tight_layout()

#plt.savefig(f"./results_figures/Results_{z}_{q}.svg")

q = widgets Dropdown(options = sensors.keys(), value = 'Deck09', description = 'Sele
z = widgets Dropdown(options = ['Overview', '345', 'Location 1', 'Location 2', 'Loca

y = widgets.IntSlider(min = 0, max = 30, step = 1, value = 0, description = 'Start v
x = widgets.IntSlider(min = 0, max = 30, step = 1, value = 30, description = 'Stop v

hb2 = widgets.VBox((y, x))
hb3 = widgets.VBox((z, q))
hb4 = widgets.HBox((hb2, hb3))

ip = interactive_output(plot_line5, {'q': q,
                                     'z': z,
                                     'y': y,
                                     'x': x})

display(hb4, ip);

```

In []:

```

#Comparison of behaviour of the deck plate at midspan & cross girder
temp = 0
xshift = 0
count = 0
z = 'Location 5'
for q in 'Deck02', 'Deck08':
    if q == 'Deck08':
        label = 'Mid bay'
    if q == 'Deck02':
        label = 'At cross girder'

with sns.diverging_palette(0, 250, l = 50, center = "dark", n = 2):
    location1 = match1[z]
    if q == 'Deck08':
        xshift = temp - location1['counter'][np.argmax(location1[sensors[q]])]
        print(xshift)
    plt.plot(location1['counter'] + xshift, location1[sensors[q]], label = f'Bef
    temp = location1['counter'][np.argmax(location1[sensors[q]])]
    print(np.argmax(location1[sensors[q]]))

```

```

print(location1['counter'][np.argmax(location1[sensors[q]])])

print('test')
plt.minorticks_on()
plt.ylabel('Stress [MPa]')
plt.xlabel('Distance [m]')
plt.grid(axis = 'x', which = 'minor', linestyle = '-.', linewidth=0.2)
plt.grid(axis = 'y', which = 'minor', linestyle = '-.', linewidth=0.2)
plt.title(f'Load test results before strengthening, track {z}')
plt.legend(loc = 'upper right')

plt.xlim(0 , 30)
plt.tight_layout()

##plt.savefig(f"./results_figures/Results_02_08_compare.svg")
plt.show()

```

In []:

```

temp = 0
xshift = 0
count = 0
z = 'Location 5'
for q in 'Deck02', 'Deck08':
    if q == 'Deck08':
        label = 'Mid bay'
        color = sns.diverging_palette(0, 250, 1 = 50, center = "dark", n = 6)[0]
    if q == 'Deck02':
        label = 'At cross girder'
        color = sns.diverging_palette(0, 250, 1 = 50, center = "dark", n = 6)[-1]
    for z in 'Location 5 (1st run)', 'Location 5 (2nd run)', 'Location 5 (3rd run)':
        location2 = match2[z]
        if count != 0:
            xshift = temp - location2['counter'][np.argmax(location2[sensors[q]])]
            plt.plot(location2['counter'] + xshift, location2[sensors[q]], color = color)
        if count == 0:
            temp = location2['counter'][np.argmax(location2[sensors[q]])]
            count += 1

plt.minorticks_on()
plt.ylabel('Stress [MPa]')
plt.xlabel('Distance [m]')
plt.grid(axis = 'x', which = 'minor', linestyle = '-.', linewidth=0.2)
plt.grid(axis = 'y', which = 'minor', linestyle = '-.', linewidth=0.2)
plt.title(f'Load test results after strengthening, track location 5')
plt.legend(loc = 'upper right')

plt.xlim(0 , 30)
plt.tight_layout()

#plt.savefig(f"./results_figures/Results_02_08_compare2.svg")
plt.show()

```

In []:

```

# Reload some data in order to visualise unfiltered-filtered results

list3 = []
for i in files1:
    if(os.path.exists(f'./data/{i}')) == True:
        list3.append(pd.read_csv(f'./data/{i}'))

```

```

list4 = []
for i in files2:
    if(os.path.exists(f'./data/{i}')) == True:
        temp = pd.read_csv(f'./data/{i}', sep = ';', skiprows=1)
        temp = temp.drop(0,0)
        temp.Time = pd.to_numeric(temp.Time)
        list4.append(temp)

vis1 = list3[5]
vis2 = list4[4]

print('Part 1/6 done')

#First number Loc1-11, second optional run 1-3, Last number Load test 1 or 2
locations3 = [loc7_1_1, loc7_2_1, loc8_1, loc9_1, loc6_1, loc5_1, loc4_1, loc3_1, lo
locations4 = [loc1_2, loc2_2, loc3_2, loc4_2, loc5_1_2, loc5_2_2, loc5_3_2, loc6_1_2

```

In []:

```

#Visualisation of effectiveness of the noise filter that is used
with sns.diverging_palette(0, 250, l = 50, center = "light", n = 14):

    plt.rcParams['figure.figsize'] = (8,5.6)

    count = 0
    for i in locations4:
        plt.plot(pd.to_numeric(i.SG003), label = locs2[count])    #CHANGED FROM SG01
        count +=1
        plt.title('Unfiltered data')
        plt.minorticks_on()
        plt.ylabel('Microstrain')
        plt.xlabel('Measurement')
        plt.grid(axis = 'x', which = 'minor', linestyle = '-.', linewidth=0.2)
        plt.grid(axis = 'y', which = 'minor', linestyle = '-.', linewidth=0.2)
        plt.legend(loc = 'upper left', fontsize = 'small')
        # plt.xlim(10000,70000)
        # plt.ylim(0,160)
        plt.tight_layout()
        # #plt.savefig('./results_figures/Unfiltered.svg')

    plt.show()

    count = 0

    for i in locations2:
        plt.plot(pd.to_numeric(i.counter), pd.to_numeric(i.SG003M), label = locs2[co
        count +=1
        plt.title('Filtered data')
        plt.minorticks_on()
        plt.ylabel('Stress [MPa]')
        plt.xlabel('Distance [m]')
        plt.grid(axis = 'x', which = 'minor', linestyle = '-.', linewidth=0.2)
        plt.grid(axis = 'y', which = 'minor', linestyle = '-.', linewidth=0.2)
        plt.legend(loc = 'upper left', fontsize = 'small')
        # plt.xlim(-10,30)
        # plt.ylim(-5,25)
        plt.tight_layout()
        # #plt.savefig('./results_figures/Filtered.svg')

    plt.rcParams['figure.figsize'] = (12,7)

```

In []:

```

plt.rcParams['figure.figsize'] = (14,7) #8,5.6

fs = 1000 #Sample frequency
fc = 5 # Cut-off frequency of the filter
w = fc / (fs / 2) # Normalize the frequency
b, a = butter(5, w, 'lowpass')

plt.plot(list3[5]['Time'], list3[5]['SG009'] * 0.21, label = 'Unfiltered', color = s
plt.plot(list3[5]['Time'], savgol_filter(list3[5]['SG009'],151, 2) * 0.21, label =
plt.plot(list3[5]['Time'], filtfilt(b, a, list3[5]['SG009']) * 0.21, label = 'Low-pa
plt.legend(loc = 'upper left', fontsize='x-large')

plt.title('Noise filter compare test 1')
plt.minorticks_on()
plt.grid(axis = 'y', which = 'minor', linestyle = '-.', linewidth=0.2)
plt.grid(axis = 'x', which = 'minor', linestyle = '-.', linewidth=0.2)
#plt.xticks([])
plt.ylabel('Stress [MPa]')
plt.xlim(21.5,22.5)
#plt.ylim(0,80)
plt.xlabel('Distance [m]')
plt.tight_layout()
##plt.savefig("./results_figures/Filter_compare_1.svg")
plt.show()

plt.plot(pd.to_numeric(list4[4]['Time']), pd.to_numeric(list4[4]['SG009']) * 0.21, l
plt.plot(pd.to_numeric(list4[4]['Time']), savgol_filter(pd.to_numeric(list4[4]['SG00
plt.plot(pd.to_numeric(list4[4]['Time'])[50:]), filtfilt(b, a, pd.to_numeric(list4[4]
plt.legend(loc = 'upper left', fontsize='x-large')
plt.title('Noise filter compare test 2')
plt.minorticks_on()
plt.grid(axis = 'y', which = 'minor', linestyle = '-.', linewidth=0.2)
plt.grid(axis = 'x', which = 'minor', linestyle = '-.', linewidth=0.2)
#plt.xticks([])
plt.ylabel('Stress [MPa]')
plt.xlabel('Distance [m]')
plt.xlim(29,30.25)
plt.tight_layout()
plt.show()
#plt.ylim(0,80)
##plt.savefig("./results_figures/Filter_compare_2.svg");

plt.rcParams['figure.figsize'] = (12,7)

```

From here individual graphs are made, comparing the test results with FE results, which are imported.

In []:

```

output = pd.DataFrame()
output = output.append(pd.read_csv('./fe_results/Deck03_remesh.csv', names= ['1', '2
wheels_fe = pd.read_csv('./fe_results/Wheel loads FE_V4.csv')
wheels_fe = wheels_fe['Unnamed: 11']
output['Deck03'] = (output['2'] + output['4'] ) / 2

output2 = pd.DataFrame()
output2 = output2.append(pd.read_csv('./fe_results/Deck03_weaves_unstr.csv', names=
output2['weave1'] = (output2['2'] + output2['4'] ) / 2
output2['weave2'] = (output2['6'] + output2['8'] ) / 2

```


In []:

```
z = 'Location 5'
q = 'Deck09'
with sns.diverging_palette(0, 250, l = 50, center = "dark", n = 2):
    fig, ax = plt.subplots()
    location1 = match1[z]
    shift = 1.875 + location1['counter'][np.argmax(location1[sensors[q]])]
    #plt.plot(wheels_fe*-1, output['Deck09']* 10**-6, marker= '.', Label = 'FE resul

    output = pd.DataFrame()
    output = output.append(pd.read_csv('./fe_results/Deck09_remesh.csv', names= ['1'
wheels_fe = pd.read_csv('./fe_results/Wheel loads FE_V4.csv')
wheels_fe = wheels_fe['Unnamed: 11']
output['Deck09'] = (output['2'] + output['4'] + output['6'] + output['8']) / 4

    output2 = pd.DataFrame()
    output2 = output2.append(pd.read_csv('./fe_results/Deck09_weaves_unstr.csv', nam
output2['weave1'] = (output2['2'] + output2['4'] + output2['6'] + output2['8'])
output2['weave2'] = (output2['10'] + output2['12'] + output2['14'] + output2['16

    plt.plot(wheels_fe*-1.05, output['Deck09']* 10**-6, marker= '.', label = 'FE res
    plt.plot(location1['counter'] - shift, location1[sensors[q]], label = 'Load test

    ax.fill_between(wheels_fe*-1.05, output2['weave1'] * 10**-6, output['Deck09']* 1
    ax.fill_between(wheels_fe*-1.05, output2['weave2'] * 10**-6, output['Deck09']* 1

plt.minorticks_on()
plt.ylabel('Stress [MPa]')
plt.xlabel('Distance [m]')
plt.grid(axis = 'x', which = 'minor', linestyle = '-.', linewidth=0.2)
plt.grid(axis = 'y', which = 'minor', linestyle = '-.', linewidth=0.2)
plt.title(f'Unstrengthened load test - FE compare, sensor Deck09')
plt.title(f'Unstrengthened load test - FE comparison \n Transverse deck plate bendin
plt.legend(loc = 'upper right')

plt.xlim(-5 , 20)
plt.ylim(-20,100)
plt.tight_layout()
#plt.savefig("./results_figures/FE_Test_Compare_Deck09_unstr.svg");
```

In []:

```
output = pd.DataFrame()
output = output.append(pd.read_csv('./fe_results/Trou_mid_remesh.csv', names= ['1',
wheels_fe = pd.read_csv('./fe_results/Wheel loads FE_V4.csv')
wheels_fe = wheels_fe['Unnamed: 11']
output['Trou'] = (output['2'] + output['4'] + output['6'] + output['8']) / 4

    output2 = pd.DataFrame()
    output2 = output2.append(pd.read_csv('./fe_results/Trou_mid_weaves_unstr.csv', names
output2['weave1'] = (output2['2'] + output2['4'] + output2['6'] + output2['8']) / 4
output2['weave2'] = (output2['10'] + output2['12'] + output2['14'] + output2['16'])

z = 'Location 5'
q = 'Trou03'
with sns.diverging_palette(0, 250, l = 50, center = "dark", n = 2):
    fig, ax = plt.subplots()
    location1 = match1[z]
    shift = 8 #+ location1['counter'][np.argmax(location1[sensors[q]])]
    plt.plot(wheels_fe*-1, output['Trou']* 10**-6, marker= '.', label = 'FE results
    plt.plot(location1['counter'] - shift, location1[sensors[q]], label = 'Load test

    ax.fill_between(wheels_fe*-1, output2['weave1'] * 10**-6, output['Trou']* 10**-6
    ax.fill_between(wheels_fe*-1, output2['weave2'] * 10**-6, output['Trou']* 10**-6
```

```

plt.minorticks_on()
plt.ylabel('Stress [MPa]')
plt.xlabel('Distance [m]')
plt.grid(axis = 'x', which = 'minor', linestyle = '-.', linewidth=0.2)
plt.grid(axis = 'y', which = 'minor', linestyle = '-.', linewidth=0.2)
plt.title(f'Unstrengthened load test - FE compare, sensor {q}')
plt.title(f'Unstrengthened load test - FE comparison \n Stresses in the trough botto

plt.legend(loc = 'upper left')

plt.xlim(-5 , 20)
plt.ylim(-20,50)
plt.tight_layout()
#plt.savefig("./results_figures/FE_Test_Compare_Trou03_unstr.svg");

```

In []:

```

output = pd.DataFrame()
output = output.append(pd.read_csv('./fe_results/Trou_cgir_remesh.csv', names= ['1',
wheels_fe = pd.read_csv('./fe_results/Wheel loads FE_V4.csv')
wheels_fe = wheels_fe['Unnamed: 11']
output['Trou'] = (output['2'] + output['4'] + output['6'] + output['8']) / 4

output2 = pd.DataFrame()
output2 = output2.append(pd.read_csv('./fe_results/Trou_cgir_weaves_unstr.csv', name
output2['weave1'] = (output2['2'] + output2['4'] + output2['6'] + output2['8']) / 4
output2['weave2'] = (output2['10'] + output2['12'] + output2['14'] + output2['16'])

z = 'Location 5'
q = 'Trou01'
with sns.diverging_palette(0, 250, l = 50, center = "dark", n = 2):
    fig, ax = plt.subplots()
    location1 = match1[z]
    shift = 8 #+ location1['counter'][np.argmax(location1[sensors[q]])]
    plt.plot(wheels_fe*-1, output['Trou']* 10**-6, marker= '.', label = 'FE results
    plt.plot(location1['counter'] - shift, location1[sensors[q]], label = 'Load test

    ax.fill_between(wheels_fe*-1, output2['weave1'] * 10**-6, output['Trou']* 10**-6
    ax.fill_between(wheels_fe*-1, output2['weave2'] * 10**-6, output['Trou']* 10**-6

plt.minorticks_on()
plt.ylabel('Stress [MPa]')
plt.xlabel('Distance [m]')
plt.grid(axis = 'x', which = 'minor', linestyle = '-.', linewidth=0.2)
plt.grid(axis = 'y', which = 'minor', linestyle = '-.', linewidth=0.2)
plt.title(f'Unstrengthened load test - FE compare, sensor {q}')
plt.title(f'Unstrengthened load test - FE comparison \n Stresses in the trough botto

plt.legend(loc = 'lower left')

plt.xlim(-5,20)
plt.ylim(-35,5)
plt.tight_layout()
#plt.savefig("./results_figures/FE_Test_Compare_Trou01_unstr.svg");

```

In []:

```

output = pd.DataFrame()
output = output.append(pd.read_csv('./fe_results/Deck08_remesh.csv', names= ['1', '2
wheels_fe = pd.read_csv('./fe_results/Wheel loads FE_V4.csv')
wheels_fe = wheels_fe['Unnamed: 11']
output['Deck08'] = (output['2'] + output ['4'] ) / 2

```

```

output2 = pd.DataFrame()
output2 = output2.append(pd.read_csv('./fe_results/Deck08_weaves_unstr.csv', names=
output2['weave1'] = (output2['2'] + output2['4'] ) / 2
output2['weave2'] = (output2['6'] + output2['8'] ) / 2

z = 'Location 5'
q = 'Deck08'
with sns.diverging_palette(0, 250, l = 50, center = "dark", n = 2):
    fig, ax = plt.subplots()
    location1 = match1[z]
    shift = 7.7 #+ location1['counter'][np.argmax(location1[sensors[q]])]
    plt.plot(wheels_fe*-1.05, output['Deck08']* 10**-6, marker= '.', label = 'FE re
    plt.plot(location1['counter'] - shift, location1[sensors[q]], label = 'Load test

    ax.fill_between(wheels_fe*-1.05, output2['weave1'] * 10**-6, output['Deck08']* 1
    ax.fill_between(wheels_fe*-1.05, output2['weave2'] * 10**-6, output['Deck08']* 1

plt.minorticks_on()
plt.ylabel('Stress [MPa]')
plt.xlabel('Distance [m]')
plt.grid(axis = 'x', which = 'minor', linestyle = '-.', linewidth=0.2)
plt.grid(axis = 'y', which = 'minor', linestyle = '-.', linewidth=0.2)
plt.title(f'Load test - FE compare, track {z}, sensor {q}')
plt.title(f'Unstrengthened load test - FE comparison \n Longitudinal deck plate bend
plt.legend(loc = 'upper right')

plt.xlim(-5 , 20)
plt.ylim(-20,50)
plt.tight_layout()

#plt.savefig("./results_figures/FE_Test_Compare_deck08_unstr.svg");

```

In []:

```

output = pd.DataFrame()
output = output.append(pd.read_csv('./fe_results/Deck02_remesh.csv', names= ['1', '2
wheels_fe = pd.read_csv('./fe_results/Wheel loads FE_V4.csv')
wheels_fe = wheels_fe['Unnamed: 11']
output['Deck02'] = (output['2'] + output['4'] + output['6'] + output['8']) / 4

output2 = pd.DataFrame()
output2 = output2.append(pd.read_csv('./fe_results/Deck02_weaves_unstr.csv', names=
output2['weave1'] = (output2['2'] + output2['4'] + output2['6'] + output2['8']) / 4
output2['weave2'] = (output2['10'] + output2['12'] + output2['14'] + output2['16'])

z = 'Location 5'
q = 'Deck02'
with sns.diverging_palette(0, 250, l = 50, center = "dark", n = 2):
    fig, ax = plt.subplots()
    location1 = match1[z]
    shift = 8
    plt.plot(wheels_fe*-1.02, output['Deck02']* 10**-6, marker= '.', label = 'FE res
    plt.plot(location1['counter'] - shift, location1[sensors[q]], label = 'Load test

    ax.fill_between(wheels_fe*-1.02, output2['weave1'] * 10**-6, output['Deck02']* 1
    ax.fill_between(wheels_fe*-1.02, output2['weave2'] * 10**-6, output['Deck02']* 1

plt.minorticks_on()
plt.ylabel('Stress [MPa]')
plt.xlabel('Distance [m]')
plt.grid(axis = 'x', which = 'minor', linestyle = '-.', linewidth=0.2)
plt.grid(axis = 'y', which = 'minor', linestyle = '-.', linewidth=0.2)
plt.title(f'Unstrengthened load test - FE comparison \n Longitudinal deck plate bend
plt.legend(loc = 'upper right')

```

```
plt.xlim(-5, 20)
plt.ylim(-20,40)
plt.tight_layout()

#plt.savefig("./results_figures/FE_Test_Compare_deck02_unstr.svg");
```

Strengthened compare:

```
In [ ]: with sns.color_palette():

        output = pd.DataFrame()
        output = output.append(pd.read_csv('./fe_results/Deck03_FE_str.csv', names= ['1'
        wheels_fe = pd.read_csv('./fe_results/Wheel loads FE_V5.csv')
        wheels_fe = wheels_fe['Unnamed: 11']
        output['Deck02'] = (output['2'] + output['4']) / 2
        plt.plot(wheels_fe*-1, output['Deck02']* 10**-6, marker= '.', markersize='8', col

        for z in 'Location 5 (1st run)', 'Location 5 (2nd run)', 'Location 5 (3rd run)':

            q = 'Deck03'
            location2 = match2[z]
            shift = 8
            plt.plot(location2['counter'] - shift, location2[sensors[q]], label = f'Load

        plt.minorticks_on()
        plt.ylabel('Stress [MPa]')
        plt.xlabel('Distance [m]')
        plt.grid(axis = 'x', which = 'minor', linestyle = '-.', linewidth=0.2)
        plt.grid(axis = 'y', which = 'minor', linestyle = '-.', linewidth=0.2)
        plt.title(f'Strengthened load test - FE compare, sensor {q}')
        plt.title(f'Strengthened load test - FE comparison \n Transverse deck plate bend
        plt.legend(loc = 'upper right')

        plt.xlim(-5 , 20)
        plt.ylim(-4,10)
        plt.tight_layout()
        #plt.savefig("./results_figures/FE_Test_Compare_deck03_str.svg");
```

```
In [ ]: with sns.color_palette():

        output = pd.DataFrame()
        output = output.append(pd.read_csv('./fe_results/deck09_2_str.csv', names= ['1',
        wheels_fe = pd.read_csv('./fe_results/Wheel loads FE_V5.csv')
        wheels_fe = wheels_fe['Unnamed: 11']
        output['Deck09'] = output['2']
        plt.plot(wheels_fe*-1 + 8, output['Deck09']* 10**-6, marker= '.', markersize='8'

        for z in 'Location 5 (1st run)', 'Location 5 (2nd run)', 'Location 5 (3rd run)':
            q = 'Deck09'
            location2 = match2[z]
            plt.plot(location2['counter'] , location2[sensors[q]], label = f'Load test r

        plt.minorticks_on()
        plt.ylabel('Stress [MPa]')
        plt.xlabel('Distance [m]')
        plt.grid(axis = 'x', which = 'minor', linestyle = '-.', linewidth=0.2)
        plt.grid(axis = 'y', which = 'minor', linestyle = '-.', linewidth=0.2)
        plt.title(f'Strengthened load test - FE compare, sensor {q}')
        plt.title(f'Strengthened load test - FE comparison \n Transverse deck plate bending
        plt.legend(loc = 'upper right')
```

```
plt.xlim(-0, 25)
plt.ylim(-2,14)
plt.tight_layout()
#plt.savefig("./results_figures/FE_Test_Compare_deck09_str.svg");
```

In []:

```
with sns.color_palette():

    output = pd.DataFrame()
    output = output.append(pd.read_csv('./fe_results/Deck08_str.csv', names= ['1', '
wheels_fe = pd.read_csv('./fe_results/Wheel loads FE_V5.csv')
wheels_fe = wheels_fe['Unnamed: 11']
output['Deck08'] = (output['2'] + output['4']) / 2
plt.plot(wheels_fe*-1, output['Deck08']* 10**-6, marker= '.', markersize='8', co

    for i in 'Location 5 (1st run)', 'Location 5 (2nd run)', 'Location 5 (3rd run)':
        q = 'Deck08'
        location2 = match2[i]
        shift = 8
        plt.plot(location2['counter'] - shift, location2[sensors[q]], label = f'Load

plt.minorticks_on()
plt.ylabel('Stress [MPa]')
plt.xlabel('Distance [m]')
plt.grid(axis = 'x', which = 'minor', linestyle = '-.', linewidth=0.2)
plt.grid(axis = 'y', which = 'minor', linestyle = '-.', linewidth=0.2)

plt.title(f'Strengthened load test - FE comparison \n Longitudinal deck plate bendin
plt.legend(loc = 'upper right')

plt.xlim(-5 , 20)
plt.ylim(-4,10)
plt.tight_layout()
#plt.savefig("./results_figures/FE_Test_Compare_Deck08_str.svg");
```

In []:

```
with sns.color_palette():

    output = pd.DataFrame()
    output = output.append(pd.read_csv('./fe_results/Deck02_3_str.csv', names= ['1', '
wheels_fe = pd.read_csv('./fe_results/Wheel loads FE_V5.csv')
wheels_fe = wheels_fe['Unnamed: 11']
output['Deck02'] = (output['2'] + output['4']) / 2
plt.plot(wheels_fe*-1, output['Deck02']* 10**-6, marker= '.', markersize='8', co

    for i in 'Location 5 (1st run)', 'Location 5 (2nd run)', 'Location 5 (3rd run)':
        q = 'Deck02'
        location2 = match2[i]
        shift = 8
        plt.plot(location2['counter'] - shift, location2[sensors[q]], label = f'Load

plt.minorticks_on()
plt.ylabel('Stress [MPa]')
plt.xlabel('Distance [m]')
plt.grid(axis = 'x', which = 'minor', linestyle = '-.', linewidth=0.2)
plt.grid(axis = 'y', which = 'minor', linestyle = '-.', linewidth=0.2)

plt.title(f'Strengthened load test - FE comparison \n Longitudinal deck plate bendin
plt.legend(loc = 'upper right')

plt.xlim(-5 , 20)
plt.ylim(-8,10)
plt.tight_layout()
#plt.savefig("./results_figures/FE_Test_Compare_Deck02_str.svg");
```

```
In [ ]: with sns.color_palette():
        output = pd.DataFrame()
        output = output.append(pd.read_csv('./fe_results/Cgir_2_fe_str.csv', names= ['1'
        wheels_fe = pd.read_csv('./fe_results/Wheel loads FE_V5.csv')
        wheels_fe = wheels_fe['Unnamed: 11']
        output['Deck02'] = (output['2'] + output['4']) / 2
        plt.plot(wheels_fe*-1, output['Deck02']* 10**-6, marker= '.', markersize='8', co

        for i in 'Location 5 (1st run)', 'Location 5 (2nd run)', 'Location 5 (3rd run)':
            q = 'Cgir01'
            location2 = match2[i]
            shift = 8
            plt.plot(location2['counter'] - shift, location2[sensors[q]], label = f'Load

        plt.minorticks_on()
        plt.ylabel('Stress [MPa]')
        plt.xlabel('Distance [m]')
        plt.grid(axis = 'x', which = 'minor', linestyle = '-.', linewidth=0.2)
        plt.grid(axis = 'y', which = 'minor', linestyle = '-.', linewidth=0.2)

        plt.title(f'Strengthened load test - FE comparison \n Stresses in the cross girder b
        plt.legend(loc = 'upper left')

        plt.xlim(-5 , 25)
        plt.ylim(-5,25)
        plt.tight_layout()
        #plt.savefig("./results_figures/FE_Test_Compare_cgir01_str.svg");
```

```
In [ ]: output = pd.DataFrame()
        output = output.append(pd.read_csv('./fe_results/Trou01_FE_str.csv', names= ['1', '2
        wheels_fe = pd.read_csv('./fe_results/Wheel loads FE_V5.csv')
        wheels_fe = wheels_fe['Unnamed: 11']
        output['Deck02'] = output['2']
        plt.plot(wheels_fe*-1, output['Deck02']* 10**-6, marker= '.', markersize='8', color

        for i in 'Location 5 (1st run)', 'Location 5 (2nd run)', 'Location 5 (3rd run)':
            q = 'Trou01'
            with sns.diverging_palette(0, 250, l = 50, center = "light", n = 16):
                location2 = match2[i]
                shift = 8.3
                plt.plot(location2['counter'] - shift, location2[sensors[q]], label = f'Load

        plt.minorticks_on()
        plt.ylabel('Stress [MPa]')
        plt.xlabel('Distance [m]')
        plt.grid(axis = 'x', which = 'minor', linestyle = '-.', linewidth=0.2)
        plt.grid(axis = 'y', which = 'minor', linestyle = '-.', linewidth=0.2)
        plt.title(f'Strengthened load test - FE comparison \n Stresses in the trough bottom
        plt.legend(loc = 'upper right')

        plt.xlim(-5 , 25)
        plt.ylim(-15,5)
        plt.tight_layout()
        #plt.savefig("./results_figures/FE_Test_Compare_trou01_str.svg");
```

```
In [ ]: output = pd.DataFrame()
        output = output.append(pd.read_csv('./fe_results/Trou03_FE_str.csv', names= ['1', '2
        wheels_fe = pd.read_csv('./fe_results/Wheel loads FE_V5.csv')
        wheels_fe = wheels_fe['Unnamed: 11']
        output['Deck02'] = output['2']
```

```

plt.plot(wheels_fe*-1, output['Deck02']* 10**-6, marker= '.', markersize='8', color

for i in 'Location 5 (1st run)', 'Location 5 (2nd run)', 'Location 5 (3rd run)':
    q = 'Trou03'
    with sns.diverging_palette(0, 250, l = 50, center = "light", n = 16):
        location2 = match2[i]
        shift = 8.3
        plt.plot(location2['counter'] - shift, location2[sensors[q]], label = f'Load

plt.minorticks_on()
plt.ylabel('Stress [MPa]')
plt.xlabel('Distance [m]')
plt.grid(axis = 'x', which = 'minor', linestyle = '-.', linewidth=0.2)
plt.grid(axis = 'y', which = 'minor', linestyle = '-.', linewidth=0.2)
plt.title(f'Strengthened load test - FE comparison \n Stresses in the trough bottom
plt.legend(loc = 'upper left')

plt.xlim(-5 , 20)
plt.ylim(-10,30)
plt.tight_layout()
#plt.savefig("./results_figures/FE_Test_Compare_trou03_str.svg");

```

Other:

In []:

```

with sns.diverging_palette(0, 250, l = 50, center = "dark", n = 4):
    fig, ax1 = plt.subplots(figsize = (14,7))

    for j, style in zip(['Deck03', 'Deck04', 'Deck05'], ['- ', '- - ', ':']):
        sensor = j
        tlist2 = []
        xlist2 = []
        test = []

        for i in match2: # Same thing but for the strengthened scenario (code could
            xlist2.append(np.int(i[9:11]))
            maxima2 = np.amin(match2[i][sensors[sensor]][30000:36000])
            test2 = np.argmin(match2[i][sensors[sensor]][30000:36000])

            if i == 'Location 4' or i == 'Location 5 (1st run)' or i == 'Location 5
                maxima2 = np.amax(match2[i][sensors[sensor]][30000:36000])
                test2 = np.argmax(np.amax(match2[i][sensors[sensor]][30000:36000]))

            minima2 = 0
            diff2 = np.amax(maxima2) - np.amax(minima2)
            tlist2.append(diff2)
            test.append(test2)

        #Remove duplicates from x coordinates (for the Locaitons where more than 1 r
        xlist4 = list(dict.fromkeys(xlist2))

        #Average out the duplicate values (for the Locations where more than 1 run w
        tlist4 = 1 * tlist2
        del tlist4[4:7]
        tlist4.insert(4, np.average(tlist2[4:7]))
        del tlist4[5:7]
        tlist4.insert(5, np.average(tlist2[7:9]))
        tlist5 = []

        #Plotting
        ax1.plot(xlist4, tlist4, style, label = f'After strengthening, {j}', color =
        ax1.scatter(xlist2, tlist2, marker = 'D', s = 20, color = sns.diverging_pale

ax1.set_xlim(1,11)

```

```

ax1.set_ylim(bottom = -5, top = 15)
ax1.set_xticks(xlist2)
ax1.set_xlabel('Truck location (track)')
ax1.set_ylabel('Stress in sensor for first truck axle')
ax1.minorticks_on()
ax1.grid(axis = 'y', which = 'minor', linestyle = '-.', linewidth=0.2)
ax1.invert_xaxis() #Swap Location 1-11 to 11-1 to match other figures

output = pd.DataFrame()
output = output.append(pd.read_csv('./fe_results/Deck03_transverse_original.csv')
output['adjusted'] = (output['2'] + output['4']) / 2
ax1.plot(np.arange(9,0,-1), output['adjusted']* 10**-6, marker= '.', color = 're

#Align the girdlines and tick labels of y-axes:
l1 = len(ax1.get_yticks())
b = ax1
b_ticks = np.linspace(b.get_yticks()[0],b.get_yticks()[-1], l1)
b.set_yticks(b_ticks)
ax1.legend(loc = 'upper left', fontsize = '13')
plt.title('Results overview of sensors Deck03, Deck04 and Deck05, trans')
plt.title(f'Transverse influence line strengthened bridge \n Transverse deck pla
fig.tight_layout()

#plt.savefig("./results_figures/FE_sensitivity_transverse_str.svg");

```

In []:

```

output = pd.DataFrame()
output = output.append(pd.read_csv('./fe_results/Deck03_tyre.csv', names= ['1', '2',
wheels_fe = pd.read_csv('./fe_results/Wheel loads FE_V5.csv')
wheels_fe = wheels_fe['Unnamed: 11']
output['adjusted'] = (output['2'] + output['4']) / 2
plt.scatter([315,300,270,330,360], output['adjusted']* 10**-6, marker= 'x', color =

x = np.linspace(260,380,150)
b = np.polyfit(np.array([315,300,270,330,360]), np.array(output['adjusted']* 10**-6)

plt.plot(x, b[0]* x **2 + b[1] * x + b[2], '-. ')
plt.ylabel('Stress [MPa]')
plt.xlabel('Axle A wheel length [mm]')
plt.xlim(250,370)
plt.ylim(6,14)
plt.title('Effect of tyre length')
plt.tight_layout()
#plt.savefig("./results_figures/FE_influence_tyre_size.svg");

```

Remesh:

In []:

```

with sns.color_palette():

output = pd.DataFrame()
output = output.append(pd.read_csv('./fe_results/Deck04_FE_str.csv', names= ['1'
wheels_fe = pd.read_csv('./fe_results/Wheel loads FE_V5.csv')
wheels_fe = wheels_fe['Unnamed: 11']
output['Deck02'] = (output['2'] + output['4']) / 2
plt.plot(wheels_fe*-1, output['Deck02']* 10**-6, marker= '.', markersize='8', col

for z in 'Location 5 (1st run)', 'Location 5 (2nd run)', 'Location 5 (3rd run)':

    q = 'Deck04'
    location2 = match2[z]
    shift = 8
    plt.plot(location2['counter'] - shift, location2[sensors[q]], label = f'Load

```

```

plt.minorticks_on()
plt.ylabel('Stress [MPa]')
plt.xlabel('Distance [m]')
plt.grid(axis = 'x', which = 'minor', linestyle = '-.', linewidth=0.2)
plt.grid(axis = 'y', which = 'minor', linestyle = '-.', linewidth=0.2)
plt.title(f'Strengthened load test - FE compare, sensor {q}')
plt.title(f'Strengthened load test - FE comparison \n Transverse deck plate bend')
plt.legend(loc = 'upper right')

plt.xlim(-5 , 20)
plt.ylim(-4,10)
plt.tight_layout()
#plt.savefig("./results_figures/FE_Test_Compare_deck04_str.svg");

```

In []:

```

with sns.color_palette():

output = pd.DataFrame()
output = output.append(pd.read_csv('./fe_results/Deck05_FE_str.csv', names= ['1'
wheels_fe = pd.read_csv('./fe_results/Wheel loads FE_V5.csv')
wheels_fe = wheels_fe['Unnamed: 11']
output['Deck02'] = (output['2'] + output['4']) / 2
plt.plot(wheels_fe*-1, output['Deck02']* 10**-6, marker= '.', markersize='8', col

for z in 'Location 5 (1st run)', 'Location 5 (2nd run)', 'Location 5 (3rd run)':

    q = 'Deck05'
    location2 = match2[z]
    shift = 8
    plt.plot(location2['counter'] - shift, location2[sensors[q]], label = f'Load

plt.minorticks_on()
plt.ylabel('Stress [MPa]')
plt.xlabel('Distance [m]')
plt.grid(axis = 'x', which = 'minor', linestyle = '-.', linewidth=0.2)
plt.grid(axis = 'y', which = 'minor', linestyle = '-.', linewidth=0.2)
plt.title(f'Strengthened load test - FE compare, sensor {q}')
plt.title(f'Strengthened load test - FE comparison \n Transverse deck plate bend')
plt.legend(loc = 'upper right')

plt.xlim(-5 , 20)
plt.ylim(-4,10)
plt.tight_layout()
# plt.savefig("./results_figures/FE_Test_Compare_deck05_str.svg");

```